Mathematical modeling and simulation of the spatial dynamics of voles populations in eastern France

Thi Nhu Thao Nguyen

Modélisation mathématique et simulation de la dynamique spatiale de populations de campagnols dans l'est de la France

Thèse de doctorat de l'Université Bourgogne Franche-Comté
préparée à l'Université de Franche-Comté

École doctorale CARNOT-PASTEUR

présentée et soutenue publiquement le 20 novembre 2020
en vue de l'obtention du grade de

Docteur en Mathématiques
de l'Université Bourgogne Franche-Comté

par

Thi Nhu Thao NGUYEN

Composition du jury :

Rapporteurs :	M. Mauro GARAVELLO	University of Milano Bicocca
	M. Nicolas VAUCHELET	Université Paris 13
Président :	M. Frédéric LAGOUTIÈRE	Université Claude Bernard Lyon 1
Examinateurs :	Mme Raluca EFTIMIE	University of Dundee
	Mme Magali RIBOT	Université d'Orléans
Directeurs de thèse :	M. Giuseppe Maria COCLITE	Polytechnic University of Bari
	Mme Carlotta DONADELLO	Université Bourgogne Franche-Comté
	M. Ulrich RAZAFISON	Université Bourgogne Franche-Comté

Acknowledgments

I would like to express my sincere gratitude to the people who have given me their assistance and who have contributed to the development of this thesis.

First of all, I would like to warmly thank my thesis supervisors Mr. Ulrich RAZAFISON, Mrs. Carlotta DONATELLO, and Mr. Giuseppe Maria COCLITE for believing, enthusiastic supervision, encouraging, and supporting me in the thesis. I am infinitely grateful to them for the sincere and wise advice which they lavished on me throughout the last three years.

Other thanks to Simon LABARTHE, Béatrice LAROCHE, Bastien POLIZZI, and Magali RIBOT for their interesting project during the summer school I had the opportunity to participate in.

I really thank Professors Mauro GARAVELLO and Nicolas VAUCHELET for the honor they have done me for having accepted to be the reviewers of this thesis. I express my gratitude to them for the precious time they devoted to reading the thesis and preparing the reports.

Plus, I would also like to thank Professors Frédéric LAGOUTIÈRE , Magali RIBOT, and Raluca EFTIMIE for having accepted to be part of my thesis jury.

Furthermore, a big thank to Professor Frédéric LAGOUTIÈRE and Mr. Martin MEYER for setting up my thesis monitoring committee for the past three years.

I would like to express additional thanks to all the members of the Besançon Mathematics Laboratory who helped me to integrate quickly and accomplish my work in a happy and friendly atmosphere.

My last thanks go to my lovely parents, sister, and friends for all of their constant support, encouragement as well as sharing with me in the difficult times.

Résumé

L'objectif principal de la thèse est de proposer et d'analyser des modèles mathématiques basés sur des équations aux dérivées partielles (EDP) afin de décrire la dynamique spatiale de deux espèces de campagnols (Microtus arvalis et Arvicola terrestris), qui sont particulièrement surveillés dans l'est de la France. Les modèles que nous avons proposés reposent sur des EDP qui décrivent l'évolution de la densité de la population de campagnols en fonction du temps, de l'âge et de la position dans l'espace. Nous avons suivi deux approches complémentaires pour représenter la dynamique. Dans la première approche, nous avons proposé un premier modèle qui consiste en une EDP scalaire en structurée en temps, en âge, et en espace. Elle est complétée par une condition au bord non locale. Le flux est linéaire à coefficient constant dans la direction de l'âge mais contient un terme non local dans les directions de l'espace. De plus, l'équation contient un terme de second ordre par rapport aux variables spatiales. Nous avons démontré l'existence et la stabilité de solutions faibles entropiques pour le modèle en utilisant, la compacité par compensation établie par Panov et un argument du type doublement de variables. Dans la deuxième approche, nous nous sommes inspirés du modèle Multi Agents introduit par Marilleau-Lang-Giraudoux, où la dynamique spatiale des juvéniles est découplée de l'évolution locale dans chaque parcelle. Pour mettre en place ce deuxième modèle, nous avons introduit un graphe orienté dont les nœuds sont les parcelles (ou colonies). Dans chaque nœud, l'évolution de la colonie est décrite par une équation de transport structurée en temps et en âge, et les mouvements de dispersion dans l'espace sont représentés par les passages d'un nœud à un autre. Nous avons proposé une discrétisation du modèle, par des schéma volumes finis, et, grâce à des simulations numériques, nous avons pu illustrer le fait que le modèle est capable de reproduire certaines caractéristiques qualitatives de la dynamique spatiale observée dans la nature. Nous avons ensuite proposé un troisième modèle qui est un système proie-prédateur constitué d'une équation hyperbolique pour les prédateurs et d'une équation parabolique-hyperbolique pour les proies analogue à celle proposée dans le premier modèle. Le terme de force dans l'équation des prédateurs dépend de manière non localement de la densité des proies et les deux équations sont également couplées via des termes sources classiques de type Lotka-Volterra. Nous avons établi l'existence de solutions en appliquant la méthode de la viscosité évanescente, et nous avons établi un résultat de stabilité par un argument de type doublement de variables. Enfin nous avons pro-

posé et validé un schéma de type volumes finis pour le premier modèle.

La dernière partie de mes travaux de recherche est dédiée à un projet auquel j'ai participé lors d'une école d'été CEMRACS. Il concerne un sujet de biomathématiques différent du thème principal de la thèse et porte sur un modèle épidémiologique pour la salmonellose. Nous avons proposé un nouveau cadre de modélisation générique multi-échelles de la transmission hétérogène d'agents pathogènes dans une population animale. Au niveau intra-hôte, le modèle décrit l'interaction entre le microbiote commensal, le pathogène et la réponse inflammatoire. Des fluctuations aléatoires de la dynamique écologique du microbiote individuel et de la transmission à l'échelle inter-hôte sont ajoutées pour obtenir un modèle EDP de la distribution des agents pathogènes au niveau de la population. Une extension du modèle a, par ailleurs, été développé pour représenter la transmission entre plusieurs populations. Le comportement asymptotique ainsi que l'impact des stratégies de contrôle, y compris le nettoyage et l'administration d'antimicrobiens, sont étudiés par des simulations numériques.

Mots-clés : Méthode des volumes finis, Équation parabolique – hyperbolique, Compacité par compensation, Problème aux limites non locales, Systèmes proie-prédateur, Équations de transport.

Abstract

The main objective of the thesis is to propose and analyze mathematical models based on partial differential equations (PDE) to describe the spatial dynamics of two species of voles (Microtus arvalis and Arvicola terrestris), which are particularly monitored in Eastern France. The models that we have proposed are based on PDE which describe the evolution of the density of the population of voles as a function of time, age and position in space. We have two complementary approaches to represent the dynamics. In the first approach, we propose a first model that consists of a scalar PDE depending on time, age, and space supplemented with a non-local boundary condition. The flux is linear with constant coefficient in the direction of age but contains a non-local term in the directions of space. Moreover, the equation contains a second order term in the spatial variables only. We have demonstrated the existence and stability of weak entropy solutions for the model by using, respectively, the Panov's theorem of the multidimensional compensated and a doubling of the variables type argument. In the second approach we were inspired by a Multi Agent model proposed by Marilleau-Lang-Giraudoux, where the spatial dynamics of juveniles is decoupled from local evolution in each plot. To apply this model, we have introduced a directed graph whose nodes are the plots. In each node, the evolution of the colony is described by a transport equation with two variables, time and age, and the movements of dispersion, in space, are represented by the passages from one node to the other. We have proposed a discretization of the model, by finite volume methods, and noticed that this approach manages to reproduce the qualitative characteristics of the spatial dynamics observed in nature. We also proposed to consider a predator-prey system consisting of a hyperbolic equation for predators and a parabolic-hyperbolic equation for preys, where the prey's equation is analogous to the first model of the vole populations. The drift term in the predators' equation depends nonlocally on the density of prey and the two equations are also coupled via classical source terms of Lotka-Volterra type. We establish existence of solutions by applying the vanishing viscosity method, and we prove stability by a doubling of variables type argument. Moreover, concerning the numerical simulation of the first model in one-dimensional space, we obtain a finite volume discretization by using the upwind scheme and then validate the numerical scheme.

The last part of my thesis work is a project in which I participated during a Summer school

CEMRACS. The project was on a subject of biomathematics different from that of the thesis (an epidemiological model for salmonellosis). A new generic multi-scale modeling framework for heterogeneous transmission of pathogens in an animal population is suggested. At the intra-host level, the model describes the interaction between the commensal microbiota, the pathogen and the inflammatory response. Random fluctuations in the ecological dynamics of the individual microbiota and transmission at the inter-host scale are added to obtain a PDE model of drift-diffusion of pathogen distribution at the population level. The model is also extended to represent transmission between several populations. Asymptotic behavior as well as the impact of control strategies, including cleaning and administration of antimicrobials, are studied by numerical simulation.

Keywords : Finite volumes method, Parabolic–hyperbolic equation, Compensated compactness, Nonlocal Boundary value problem, Prey-predator systems, Transport equations.

Contents

Introduction

Small rodents, as voles, are cornerstone species in most temperate ecosystems as their presence is necessary for the survival of a variety of predators. At the same time, they can be vectors of serious diseases transmissible to humans and lead to significant losses in agricultural production and storage. Hence, the control of populations of voles is a major problem for ecologists and socio-ecologists.

From 1989, Patrick Giraudoux and collaborators monitored these vole populations in the Alps (Massif des Ecrins) and in eastern France, in particular within the framework of the Zone Atelier Arc Jurassien and the Zone Atelier Alpes, see in [21, 4, 23]. Direct observations, realized in different countries and ecosystems, show that density variations of voles are due to multiple driving factors: climate, topography, the proportion between farmland and forest, different kinds of predators, and so on (see [17] and references therein). In more detail, as described in the papers [21, 23, 41, 29], voles are herbivores rodents, who dig underground tunnels where they breed and stay most of the time. Their ideal environment is grassland, where both food and shelter are easily available, but they can also settle in woodlands and in laboured fields. In each of these landscapes, the density and the kind of predators vary, leading to different mortality rates. Voles' reproduction season lasts typically from April to October, but variations are possible due to weather conditions and, of course, depending on the landscape characteristics. Mortality is everywhere high during the winter season because of starvation. The population of voles can be structured into three age classes: babies, juveniles, and adults. Observations show that babies and juveniles have larger mortality rates than adults, and that only juveniles and adults reproduce. Moreover, while most individuals always remain in a small neighborhood of the nest, juveniles can exhibit much more significant spatial dynamics. Indeed, under specific stress conditions, some of the juveniles disperse to initiate new settlements. The mechanism triggering dispersal is still not completely understood and it is most probably related to the interaction of several factors. However, for modeling purposes, it is reasonable to link stress conditions to overcrowding, and say that dispersal begins when the total number of individuals in a colony reaches a threshold value, fixed as a fraction of the carrying capacity of the environment. New colonies most often appear in a radius of a few hundreds meters around the original one, but individuals might disperse further

than 5 Km from the initial colony. Topography, especially height, drives the dispersal direction, and during this phase voles' mortality is very high. Since most voles die out of predation, disease, or starvation, as a first approximation we can neglect aging when describing the adult population: in particular, it is not necessary to consider a decline of fertility over age. Sex ratio at birth is 1-1, so that it is enough to model the female population.

Moreover, the results of these ecologists also revealed that outbreaks of vole populations occurred as a wave, and dispersal spread over more than 2500 km^2. For example, paper [21] investigates the effect of land use, landscape composition and structure on the population dynamics of voles from 1989 to 1994 in the Doubs department, France, by using index methods. They divided the Doubs into four different agroclimatic zones due to the characterized geomorphological features of the department. Data used were collected every year by the technicians of the Regional Crop Protection Service, Ministry of Agriculture of the communes in the department to record vole colonies. Land-use patterns were studied based on agriculture and forestry data from the French Ministry of Agriculture, collected over several years. In [4] they provide empirical evidence showing that the wave-like profile detected for the vole population, adds to the list of empirical examples supporting the theory that periodic Travelling Wave solutions do occur in natural populations undergoing multi-year cycles.

Extensive literature is devoted to the mathematical modeling of such populations, see [38, 45] and the references therein, in which the focus is on a two variables dynamics (time and age or time and space) while the observations suggest that the evolution depends on the three of them. The paper [47], monograph [46] studied the dynamic population with three variables, but we do not find in the literature a satisfactory model including the dynamics of dispersal.

Therefore, it is interesting to propose and analyze mathematical models with three variables (age, time, and space), based on partial differential equations to describe all of the behaviors of the vole population, which include population behavior (vole population growth dynamics) and individual behavior (vole movements), with the hope that the obtained results match the available collected data from the biologists. This work is the first step of collaboration with biologists aiming to find the way to control the population of voles, a subject of many surveys and investigations over multiples years.

In the thesis, we study the modeling of the spatial dynamics of these vole populations, from two different points of view. Firstly, we propose and study a macroscopic PDE model to describe the spatial dynamics of a vole population structured in age where we use a nonlinear flux to describe the dispersal of voles (since it regarded as a travelling wave). We suppose that the dispersal motion of juvenile individuals in space starts when the total density of voles reaches a threshold value. This dispersal direction depends on the topography. We obtained the well-posedness of the model under some suitable assumptions on the parameters, detailed in [9]. The qualitative behaviour of the solutions to this PDE model is not straightforward and we still need to calibrate our parameters to fit the observations. Also, our ultimate

goal is to produce effective tools toward the monitoring and management of voles, available to researchers with no particular PDE background. For these reasons, on the one hand we develop a numerical discretization of the model; on the other hand, we introduce another approach (in the second part of the thesis), where the spatial dynamics of juveniles is decoupled from local evolution in each colony, inspired by the Multi-Agent Model in [29].

In the second part of the thesis, we introduce a directed graph whose nodes are the settlements. In each node, the evolution of the density of voles living inside that place is described by a transport equation of two variables: time and age. The traveling of juvenile individuals between nodes represents the voles dispersal. The numerical discretization is easier and still adapted to describe these movements in space, especially in the future work when we will consider a significantly large area, combining hundreds of colonies. Furthermore, since the equations in each node are classical, the existence and uniqueness of the solutions are available. Then this method is a simple but efficient way to illustrate the evolution of the vole populations in space.

In the attempt to translate into the PDE formalism the essential characters of the evolution of a vole population, in the first part of this thesis we consider the following initial boundary value problem

$$\begin{cases} \partial_t \rho + \partial_a \rho + \mathrm{div}_x \left(\rho \chi_1(a) \mathbf{v}(x) Y_\theta(\phi - R) \right) = \mu \Delta_x \rho - \mathfrak{d}(t,a,x)\rho, \\ \rho(t,0,x) = \mathscr{A}(\phi) \left(\int_{A_1}^{T} \rho(t,a,x) \mathrm{d}a \right) \omega(t,x), \\ \rho(0,a,x) = \rho_0(a,x), \end{cases} \tag{0.0.1}$$

where $\rho = \rho(t,a,x)$ represents the density of voles of age $a \in (0,T)$, at the time $t \in (0,T)$, at $x \in \mathbb{R}^2$, and $T > 0$ is given. In the first equation, $\phi = \phi(t,x)$ is the total density of voles at time t and position x, $\chi_1(a)$ is a smooth approximation of the indicator function of the interval $[A_1, A_2]$, where A_1 is the limit age of babies, A_2 is the limit age of juveniles, R is a fraction of capacity of the environment where the colony is located, Y_θ is an approximation of the Heaviside function. The flux includes a linear term in the age direction and a nonlocal term, so that when the total population, ϕ, reaches a certain value, R, the juveniles start to disperse with a velocity $\mathbf{v}(x)$ which depends on the topography. The coefficient $\mu > 0$ in the parabolic term (a diffusion coefficient) represents the foraging activity of voles, and $\mathfrak{d}(t,a,x)$ is the mortality rate. In addition, in the boundary condition at $a = 0$, $\omega(t,x)$ is the reproduction rate of voles, which depends on the seasons of the year and the landscape in which the voles are settled, and $\mathscr{A}(\phi)$ is a positive real function, representing the Allee's effect. This means that if the total population of voles, ϕ, falls below a certain threshold, the reproduction rate diminishes and might become too small to compensate for the mortality. This boundary condition at $a = 0$ takes into account the fact that only juvenile and adult voles can reproduce. In the last equation, $\rho_0(a,x)$ is the initial condition at $t = 0$.

Since our model has the form of a hyperbolic-parabolic equation we use the compensated

compactness to study it. This approach has been used extensively to prove the existence of entropy solutions of the equations, see [44, 18, 35, 43, 7, 8, 10]. Indeed, as this equation includes a nonlocal boundary condition on a and a flux term nonlocal in space, the estimates on its approximations are a challenge. A priori estimates are impossible to do with the original model because of the two difficult parts mentioned above. For example, to take the limit of the approximation parabolic sequence, we need at least the boundedness of the sequence, ρ_ε. However, when we integrate on $(0,T)$, there are two terms that cannot be estimated. The first term is from the boundary condition at $a = 0$, whose boundedness is unknown because its definition depends on ρ_ε. The other one comes from the derivative with respect to x of $Y_\theta(\phi)$. To avoid those problems, we used cut-off functions to modify the equation before the computations. We rewrite our equations for $t \in (0,\infty)$, $a \in (0,\infty)$ where the cut-off functions will be used to neglect the newborn babies at $a = 0$ and the presence of individuals of age larger than T. Moreover, the BV estimates on t, and on x can not be obtained. We use the lemma of compensated compactness of Panov in [35] for multi-dimension space, to overcome that difficulty. This model is introduced and analyzed in the published paper [9], in collaboration with my supervisors Giuseppe M. Coclite and Carlotta Donadello.

Recently, there have been two different approaches to consider the spatial population of voles, introduced by Berthier in [4], and Giraudoux et al in [29]. They are the first endeavors in understanding the spatial dimension of the vole population dynamics. In [4], ecologists showed that dispersal can be seen as a traveling wave (TW), by analyzing 16-year time series of cyclic vole populations collected at 314 localities covering 2500 km² in France, using appropriate statistical analyses. The detected TW emerges and spreads from the edge of the Jura Plateaus, an area with a high ratio of permanent grasslands favoured by voles. Moreover, the direction of the wave's movement is influenced by landscape obstacles, for example, the significant high mountains and large lakes. Paper [29] leads to the conception of a hybrid ODE-Multi Agent model, in which they propose to couple two modelling methods of ecology in studying spatial dynamics (ABM and EBM). ABM (agent-based modelling), is a spatially explicit paradigm that models space as a heterogeneous environment in which individuals move and are represented as 'agents'. EBM (equation-based models) is a purely mathematical technique where the model is a set of equations (this paper uses a simple logistic ODE). More in detail, in [29], Marilleaux, Lang and Giraudoux reproduced the first colonization dynamics observed from 1998 to 2010 in the Romanche Valley (Hautes Alpes, France) by a hybrid ODE-Multi Agents model structured as follows : the valley area is decomposed into squared cells of side length 100m, so that, at a first approximation, the evolution of the population inside each of the cells can be described by an ODE (no spatial dynamics). As soon as the total population in a cell reaches a fixed threshold value, which is a fraction of the cell capacity, dispersal occurs, i.e. some of the juvenile voles "leave" the cell, and aggregate into a migrating vole agent with a specific dynamics also depending on the topography and landscape characteristics of the neighbouring cell agents. In the following we refer to this model as MLG. The advantage of this approach over the purely PDE one is that simulations are fast and their results are visualized in a format which is accessible to a non specialized audience. At the same time, the description of the population dynamics inside cells is relatively rough, and the set

of parameters for which computational results match empirical observations is not organized in a continuum, which makes it difficult to predict the behaviour of the model under perturbations. Both approaches need a system of collected data, then analyze these data, and run simulations to reproduce the ecological result of vole populations in space.

Thus, in the second part of the thesis, we exploit the idea of decoupling the local population evolution from its spatial dynamics to construct two simple but effective PDE models structured on a graph whose nodes correspond to the cells in the MLG model. The nodes of the graph represent uniform landscape areas of relatively small size, where voles can settle. Edges are used to model the main feature of voles' macroscopic spatial dynamics, which is the dispersal of juvenile individuals whenever the total population at one node reaches a threshold number. This is supposed to be a gradual process in the first model while it takes place instantaneously in the second model. We assume that a dispersal occurs inside the node (or a cell) whenever its total population reaches a threshold value, R. The first model is a model with gradual dispersal (GD), which means that the dispersal lasts for a time $\eta > 0$ after the moment at which the total population of voles in the node passes again below R and the departure rate of juveniles during dispersal is $\frac{c}{\eta}$, where $c > 0$ is chosen. The second model is an instantaneous dispersal (ID), which means that whenever the total population at a node reaches its threshold value, the departure of dispersers takes place instantaneously. As a consequence, all the voles who left their node heading for another node will reach that node at the same time. Although the second model describes less precisely the dynamics, it should be easier to implement on large graphs in the view of a hybrid PDE-Multi Agent model similar to the MLG, with several hundreds of nodes, for instance. For both models, we validate the implementation by comparing them with their exact solution, which was obtained by using the characteristic method, and then collect some numerical simulations on simple graphs, which show that the models reproduce the qualitative features of the population dynamics at the different landscapes and in different seasons of the year. We propose their discretization by using the upwind scheme. Then we run several simulations to validate the schemes, to compare the models, and to show that our models captures many of the features of vole population dynamics as they have been observed in real life, for example, changing the mortality rate will influence the density of the population, which mentioned in the results of [29]. Further, the different landscapes were obtained by changing the mortality as well as the birth rate and changing the distribution matrix to show the high ratio of movement of voles toward their favored landscape, where this matrix can depend on time. This approach is accomplished in a preprint [19], in collaboration with my supervisors Carlotta Donadello and Ulrich Razafison.

From the previous results of the model for the spatial dynamics of the vole population, we are interested in the interaction between the predator-prey system, for example between voles and foxes in the area. Inspired by the existence and uniqueness of the solutions of a system hyperbolic predator and parabolic preys proposed in [13], we introduce a new system, in which the hyperbolic-parabolic model of voles replaces the preys equation and modifies slightly by adding another mortality rate of prey, $\mathfrak{b}(a,u)$, which depends on the density of

predators u and the age of voles, for example, the ratio of juvenile voles will be caught by predators is much higher. Besides, the predator's equation we consider follows

$$\partial_t u + \mathrm{div}_x \left(u v(\phi) \right) = (\mathfrak{b}(\phi) - \beta) u,$$

where $\mathfrak{b}(\phi)$ is the birth rate of predators, depending on the total density of voles, $\beta > 0$ is the mortality rate of predators. The drift here depends nonlocally on the density of preys, introduced in [13], meaning that the predators tend to move towards the regions where preys concentrate highly, as expressed in the velocity map

$$v(\phi) = \kappa \frac{\nabla(\phi * \eta)}{\sqrt{1 + \left\| \nabla(\phi * \eta) \right\|^2}},$$

where η is a positive smooth mollifier, and $\kappa > 0$ is the maximal speed of predators. The fixed point argument used in [13] to prove existence and stability for a predator-prey system does not apply to our system in a straightforward way because it requires extremely fine information on the coefficients appearing in the a priori estimates for both predators' and preys' equations. This is not easy to achieve in our case, because the equation we use for the prey come from a specific population model and its analytical study is rather technical. In this system, we use the vanishing viscosity method to establish suitable estimates to obtain the strong-compactness of those entropy solutions. Since the estimates on u and ρ are related closely, we use the convolution properties to shift the difficulty of estimates on ϕ to η, then we choose the appropriate assumptions on η to obtain estimates on u and ρ, and finally we can apply the results from the first model. This work is achieved in a preprint [11] in collaboration with my supervisors Carlotta Donadello and Giuseppe M. Coclite.

Concerning the numerical simulation of the first model in one-dimensional space, that is an ongoing work in collaboration with my supervisor Ulrich Razafison and Frédéric Lagoutière. We obtain a finite volume discretization by using the upwind scheme. We validate the numerical scheme by comparison with an exact solution of the model using special initial conditions for which the dispersal does not occur, and then comparing once again with a reference solution corresponding to a generic initial condition and computed with a very fine mesh.

In summary, we introduced a PDE model of spatial dynamics of a vole population and then studied the existence, uniqueness and stability of the solution. This model is suitable to describe the vole population in Eastern France, as monitored and presented by empirical observations in [21],[29],[4]. We provided the wellposedness of a nonlocal mixed hyperbolic-parabolic system related to the previous model of the vole population. We implemented and validated the proposed scheme in one-dimensional space. Moreover, the numerical simulations of the model of vole populations spatial dynamics via transport equations on graphs shows that our model captures many of the features of vole populations dynamics in real life. The parameters in the reproduction and mortality rates allow to reproduce the evolution in different landscapes. Furthermore, the simulations that we presented show the ability of the models to reproduce cycles of dispersals in the populations of voles, as well as persistence or

extinction of a colony.

In addition, I have participated to a 6-weeks summer school (CEMRACS) where I collaborated to a project entitled "A multi-scale epidemic model of Salmonella infection with heterogeneous shedding". It does not relate to the main topic of my thesis but about the population dynamics of a bacterial infection. It was led by Simon Labarthe, Béatrice Laroche, Bastien Polizzi and Magali Ribot, it led to a publication, [27], in collaboration with the other members of the working group. Salmonella infection is the most common vector of collective food poisoning in the developed world. As such, deciphering the mechanisms of infection in humans and animals is a fundamental step towards the design of efficient epidemiological policies, in order to reduce the burden on agrifood industry and healthcare systems resulting from Salmonella zoonoses. Salmonella is a bacterial genus composed of various pathogenic strains, that colonize and infect the digestive tract of farm livestock, such as chickens or pigs, representing a threat for human health ranging from food poisoning to typhoid fever.

In the project, we propose a generic multiscale modeling framework of heterogeneous pathogen transmission in a livestock, accounting for the interaction dynamic between the commensal microbiota, the pathogen and the inflammatory response at the intra-host level and transmission at the between-host scale in a single animal population. This model is further extended at the metapopulation level, to model transmission between several populations. I contributed to the theoretical part, to study the existence and stability of the solution, and then run a simulation task, named "cleaning strategy". The cleaning treatment removes a constant fraction of the pathogen reservoir per time unit. Moreover, cleaning might start after a given time and/or might be periodic. The aim of the task is to study various control strategies to limit the spreading of pathogens within the population.

The content of this thesis articulates into five chapters. The first 4 chapters relate to the model spatial dynamics of the vole population and chapter 5 concerns the project on Salmonella. They are summarized as follows

- In Chapter 1, we introduce and explain the above PDE model in more detail. In section 1.1, we give the suitable assumptions on the parameters to be used in the next proofs, the definition of the entropy weak solutions, and the main results. In Section 1.2, we introduce a sequence of parabolic approximations of problem (1.1.7), then we establish estimates on the regularity of the solutions and their derivatives with respect to the age and space variables. We can not achieve the BV on x and on t of the sequence, especially, estimates on the time derivatives are not available, which motivates the application of a compensated compactness lemma due to Panov, see [35], to get the strong-compactness of the sequence. One additional difficulty comes from the fact that our flux is not genuinely nonlinear and depends explicitly on all the variables. We overcome this obstacle by using the same idea as in [12, 7], see the proof of Lemma 1.9. From that, we gain the existence of the entropy solution of the system. Moreover, the uniqueness and stability of entropy weak solutions are proved in Sec-

tion 1.3 using a doubling of variables type argument. The application of this technique is not too difficult even if the flux depends explicitly from all of the variables thanks to the high regularity of $\{\rho_\varepsilon\}_\varepsilon$ with respect of the space variables.

- In Chapter 2, we propose two models to describe the spatial dynamic of vole populations and motivate our assumptions on the basis of observed population characteristics. The models are based on age-structured transport equations set on a graph. The chapter is organized as follows. In Section 2.1 we describe the models and motivate our assumptions on the basis of observed population characteristics. In Section 2.2 we present the corresponding finite volumes numerical schemes and validate them by comparison to explicitely computed exact solutions, and present the first comparison of the two models. Section 2.3 collects some numerical simulations on simple graphs, which show that the models reproduce the qualitative features of the population dynamics.

- In Chapter 3, we introduce a prey-predator system in Section 3.1, where we replace the prey's equation by the model of the vole population structured in age, and then we present all of the necessary assumptions on the parameters in the system, the definition of the weak entropy solutions, and the main results. In Section 3.2, we introduce a sequence of parabolic approximations of the pair of solutions, then perform a priori estimates of these sequences, before we apply the compensated compactness lemma by Panov to show the strong compactness of the sequence for voles. Besides, since we prove L^∞ and BV estimates on the approximate solutions of predator, u_ε, we can apply Helly's theorem to obtain the strong compactness of predators. Lemma 3.12 establishes the existence of an entropy solution in the sense of Definition 3.2. The uniqueness and stability of the solutions are proved in Section 3.3 using a doubling of variables type argument. In Section 3.4, we prove the lemma related to the estimates on η mollifier.

- In Chapter 4, we present the numerical scheme of the model spatial dynamics of the vole population structured in age in one-dimensional space. We validate the implementation of the scheme, which is adapted by the upwind scheme and using the implicit treatment to avoid possible difficulties of the CFL condition for the diffusion, where we add the Neumann boundary condition on space variable. In Section 4.1, we introduce the scheme of model in one-dimensional space, and establish the linear system for the scheme. In Section 4.2, we find an exact solution for the scheme under a suitable assumption forbidding dispersal, then compare it with the numerical solution. Next, we validate the complete model by comparing it with a reference solution, which is computed by choosing a fine mesh.

- In Chapter 5, the single population model is described in Section 5.1. The different scales and their interconnection are detailed. We start from an ODE equation modeling the intra-host evolution of the pathogen load with respect to time, including the

host response. We next introduce a stochastic perturbation to this dynamics to account for biological variability. This SDE is used to derive a drift-diffusion PDE describing the evolution of a population density with respect to time and to pathogen load. The well-posedness of the model and asymptotic convergence towards a steady state is analyzed and an extension to the case with transmission of salmonella within the population through a reservoir is also proposed, leading to the coupling between a drift-diffusion PDE for the population and an ODE for the reservoir variable. Section 5.2 is devoted to some simulations of the two previous models, with or without a reservoir, and we observe that in both cases, the solution always converges towards a steady state. In Section 5.3, some simulations of epidemic control strategies based on cleaning or drug treatment, are performed and compared. Cleaning is modeled through the addition of a term in the ODE for the reservoir variable, whereas drug treatment is described by the addition of a drift term in the population PDE equation. Then, in Section 5.4, a compartment model taking into account some exchanges between populations is introduced and studied numerically. The model becomes in this section a large system that couples through transfer flux terms the models of the compartment dynamics composed of the previous drift-diffusion PDEs for the populations coupled to the ODE for the reservoir variables.

From the results obtained and the ongoing projects in this thesis, we have the following perspective directions

— The results that we obtained in Chapter 2 allow us to pursue the work with the construction of a hybrid model combining the instantaneous dispersal (ID) model to describe the vole populations dynamics at the nodes and the agent-based model developed in [29] to reproduce the spatial dynamics on large graphs. This work could be accomplished in collaboration with an expert research engineer in LMB, in collaboration with Lang and Marilleau. Another direction of further research could be the enhancement of both models, GD and ID, by considering a distribution matrix that depends on the current state of the system. For example, one could imagine that dispersers would avoid an already overcrowded node.

— We introduce a discretization of the model in Chapter 1 in two-dimensional space, by finite volume scheme. This work is more challenging: since there are four variables (time t, age a, and space (x_1, x_2)), the implementation of the numerical scheme is more complicated but still feasible. Indeed, similarly to building on the 1-D finite volume scheme presented in Chapter 4, its 2-D version can be accomplished. After that we could validate the scheme and run simulations in a large domain, that may use parallel computing and the biological and topographic data coming from observations. Particular care should be put in the processes of data storage and transmission among computers.

— In [3], the authors studied the cycle of the parasite *Echinococcus multilocularis*, a dis-

ease very present in central Europe (north of the Alps), on the plateaus in the north of the Himalayas. The parasite's eggs laid in the environment are then ingested by intermediate hosts which potentially include small rodent mammals, like voles. After that, the intermediate host is consumed by a definitive canine host (fox, dog, wolf, coyote). The lifespan of the worms in the definitive host is 3 to 4 months, during which the oncospheres produced are discharged via the feces into the environment. Humans accidentally can become infected through the ingestion of eggs, either through contact with definitive hosts or through food and possibly water. This parasite's egg causes the disease called human alveolar echinococcosis, which is rare but can exceed 1 case over 1000 in the cantons of Haut-Doubs (France). The course of the disease is often fatal without early treatment. In this paper, they analyse the general ecoepidemiological model describing the dynamics of clinical states population of the parasite's intermediate and definitive hosts by ordinary differential equations. For this epidemic, there were around ten mechanistic dynamic models written with ordinary differential equations. From the modeling point of view, it could be interesting to study a PDE system for cycle of the parasite from the perspective of a predator-prey PDE model, as we did in Chapter 3.

Chapter 1

A model for the spatial dynamics of a vole population structured in age

1.1 Mathematical formulation of the model

In this section we introduce the essential mathematical features of our model. The precise assumptions are postponed to the next section.

Motivated by the ecological observations above, we consider the density of voles' population as a function of fours variables

$$\begin{array}{rccc} \rho: & \mathbb{R}^+ \times \mathbb{R}^+ \times \mathbb{R}^2 & \to & \mathbb{R} \\ & (t, a, x = (x_1, x_2)) & \mapsto & \rho(t, a, x), \end{array} \tag{1.1.1}$$

where t is the time, a the age and x the space variables. We are only interested in the dynamics over a finite interval of time $[0, T]$ and we introduce constants $0 < A_1 < A_2 < T$ so that a vole is young if its age a is in $(0, A_1)$, juvenile if its age a is in (A_1, A_2) and adult otherwise. The call total density of voles at (t, x) the integral

$$\phi(t, x) := \int_0^T \rho(t, a, x) \mathrm{d}a. \tag{1.1.2}$$

As ϕ approaches the threshold value R, juvenile disperses leave the colony with velocity $\mathbf{v} = \mathbf{v}(x)$. It depends on the topography, namely $\mathbf{v}(x) \approx \mathbf{V}(\nabla z(x))$ where $z(x)$ is the height of the elevation at x, and it is assumed to be strictly positive. Instead of considering separate equations for the three age groups (or to see them as branches of a graph, as in [14]) we decided to write a single equation with age-dependent parameters. In particular, to single out the dispersers, who are a fraction of juveniles, we consider $\rho\chi_1(a)$, where χ_1 is a smooth approximation of (a multiple of) the indicator function of the interval (A_1, A_2).

Then, the equation describing the evolution of our population writes as

$$\partial_t \rho + \partial_a \rho + \mathrm{div}_x \left(\rho \chi_1(a) \mathbf{v}(x) Y_\theta(\phi - R)\right) = \mu \Delta_x \rho - \mathfrak{d}(t, a, x)\rho, \qquad (t, a, x) \in (0, T) \times (0, T) \times \mathbb{R}^2, \tag{1.1.3}$$

where Y_θ is an approximation of the Heaviside function, $\mathfrak{d} = \mathfrak{d}(t,a,x)$ is the mortality rate and the second order term $\mu\Delta_x\rho$ can be seen as the limit of a Brownian motion and represent the foraging activities performed by all individuals. Everywhere in the paper the coefficient $\mu > 0$ is fixed and we are not consider the limit as $\mu \to 0$.

The boundary condition at $a = 0$ takes the form

$$\rho(t,0,x) = \mathscr{A}(\phi)\left(\int_0^T \rho(t,a,x)\, Y_\theta(a - A_1)\mathrm{d}a\right)\omega(t,x), \qquad (t,x) \in (0,T)\times\mathbb{R}^2, \tag{1.1.4}$$

where ω is the reproduction rate and the coefficient $\mathscr{A}(\phi)$ reproduces Allee's effect, see [32]. This means that if the total population of a colony falls below a certain threshold, reproduction rate also diminishes and might become too small to compensate for mortality. All of our results remain valid if $\mathscr{A}$ is a constant function taking value in $(0,1]$. Examples of non constant $\mathscr{A}$ are functions of the form

$$\mathscr{A}(\phi) = \frac{\alpha\phi^\gamma}{(\beta+\phi)^\gamma},$$

for different choices of α, β and γ.

Finally, we fix an initial condition at $t = 0$ to complete our problem

$$\rho(0,a,x) = \rho_0(a,x), \qquad (a,x) \in (0,T)\times\mathbb{R}^2. \tag{1.1.5}$$

1.1.1 Assumptions

The functions Y_θ are defined as follows. Consider a function $Y \in C^\infty(\mathbb{R})$ such that

$$Y(\xi) = \begin{cases} 1, & \text{if } \xi \geq 0, \\ 0, & \text{if } \xi \leq -1, \end{cases} \qquad Y'(\xi) \geq 0,$$

then

$$Y_\theta(\xi) = Y\left(\frac{\xi}{\theta}\right).$$

Starting from Y_θ one can pick a suitable $k \in (0,1)$ and define

$$\chi_1(a) = k\, Y_\theta(a - A_1)\, Y_\theta(A_2 - a).$$

To limit the number of constants appearing in the equations we set $k = 1$, but this has no effect on the analysis.

Our wellposedness analysis is performed on a problem which differs from the model presented in the previous section for two reasons:

— to avoid additional difficulties coming from the presence of a boundary at $T > 0$ we write our equation for $t \in \mathbb{R}^+$, but we introduce cut-off functions to neglect the presence of individuals of age larger than T ;

— when computing the total population of the colony we neglect newborn individuals. More precisely we fix $0 < \sigma << 1$ and replace the definition of ϕ in (1.1.2) by

$$\phi(t,x) := \int_0^\infty \rho(t,a,x)\chi_2(a)\mathrm{d}a, \tag{1.1.6}$$

where

$$\chi_2(a) = Y_\sigma(a-\sigma)\,Y_\theta(T-a).$$

Finally, our problem writes as

$$\begin{cases} \partial_t\rho + \partial_a\rho + \mathrm{div}_x\left(\rho\chi_1(a)\mathbf{v}(x)\,Y_\theta(\phi - R)\right) = \mu\Delta_x\rho - \mathfrak{d}(t,a,x)\rho, & (t,a,x)\in(0,\infty)\times(0,\infty)\times\mathbb{R}^2,\\ \rho(t,0,x) = \mathscr{A}\left(\phi\right)\left(\int_0^\infty \rho(t,a,x)\chi_3(a)\mathrm{d}a\right)\omega(t,x), & (t,x)\in(0,\infty)\times\mathbb{R}^2,\\ \rho(0,a,x) = \rho_0(a,x), & (a,x)\in(0,\infty)\times\mathbb{R}^2, \end{cases} \tag{1.1.7}$$

where

$$\chi_3(a) = Y_\theta(a-A_1)\,Y_\theta(T-a).$$

We choose $\theta > 0$ so small that

$$\chi_1(0) = \chi_3(0) = Y_\theta(-A_1) = 0, \tag{1.1.8}$$

and we observe that

$$\chi_1 \le \chi_3 \le \chi_2, \qquad \chi_2(0) = Y_\sigma(-\sigma) = Y(-1) = 0. \tag{1.1.9}$$

On $\mathbf{v}, \mathfrak{d}, \mathscr{A}, \omega, \rho_0$ we shall assume that

$$\mathbf{v}\in C^\infty(\mathbb{R}^2)\cap L^2(\mathbb{R}^2)\cap L^\infty(\mathbb{R}^2), \qquad \mathrm{div}_x(\mathbf{v})\in L^1(\mathbb{R}^2)\cap W^{2,\infty}(\mathbb{R}^2), \tag{1.1.10}$$

$$\mathfrak{d}\in C^\infty([0,\infty)\times[0,\infty)\times\mathbb{R}^2)\cap W^{1,\infty}((0,\infty)\times(0,\infty)\times\mathbb{R}^2), \qquad 0 < d_* \le \mathfrak{d}(\cdot,\cdot,\cdot) \le d^*, \tag{1.1.11}$$

$$\mathscr{A}\in C^\infty(\mathbb{R})\cap L^\infty(\mathbb{R}), \qquad \mathscr{A}(\cdot)\ge 0, \quad \mathscr{A}(0) = 0, \qquad |\mathscr{A}'(\xi)\xi|, |\mathscr{A}''(\xi)\xi| \le C_0, \tag{1.1.12}$$

$$\omega\in C^\infty([0,\infty)\times\mathbb{R}^2)\cap W^{1,\infty}((0,\infty)\times\mathbb{R}^2), \qquad \omega(\cdot,\cdot)\ge 0, \tag{1.1.13}$$

$$\rho_0\in L^1((0,\infty)\times\mathbb{R}^2)\cap L^\infty((0,\infty)\times\mathbb{R}^2), \quad \rho_0\ge 0, \tag{1.1.14}$$

$$\sup_{x\in\mathbb{R}^2}\left\|\rho_0(\cdot,x)\right\|_{L^1(\mathbb{R})}, \sup_{a\ge 0}\left\|\rho_0(a,\cdot)\right\|_{L^1(\mathbb{R}^2)}, \int_{\mathbb{R}^2} TV(\rho_0(\cdot,x))\mathrm{d}x \le C_0, \tag{1.1.15}$$

for some positive constants d_*, d^* and C_0.

1.1.2 Main result

We use the following definitions of solution.

Definition 1.1. *We say that a function $\rho : [0,\infty)\times[0,\infty)\times\mathbb{R}^2 \to \mathbb{R}$ is a weak solution of (1.1.7) if the following holds for every $T > 0$*

(***D.1***) $\rho \geq 0$, $\rho \in L^\infty(0,T;L^1((0,\infty)\times\mathbb{R}^2)) \cap L^\infty((0,T)\times(0,\infty)\times\mathbb{R}^2) \cap L^2((0,T)\times(0,\infty);H^2(\mathbb{R}^2))$;

(***D.2***) *the integral function* ϕ *defined in* (1.1.6) *satisfies* $\phi \geq 0$, $\phi \in L^\infty(0,T;H^3(\mathbb{R}^2)) \cap L^2(0,T;H^4(\mathbb{R}^2)) \cap H^1((0,T)\times\mathbb{R}^2)$;

(***D.3***) *for almost every* $(t,x) \in (0,T)\times\mathbb{R}^2$, $\rho(t,\cdot,x) \in BV(0,\infty)$ *and*

$$\rho(t,0^+,x) = \mathscr{A}(\phi)\left(\int_0^\infty \rho(t,a,x)\chi_3(a)da\right)\omega(t,x),$$

where $\rho(t,0^+,x)$ *is the trace of* $\rho(t,\cdot,x)$ *at* $a=0$;

(***D.4***) *for every test function* $\xi \in C_c^\infty(\mathbb{R}^4)$

$$\begin{aligned}
&\int_0^\infty\int_0^\infty\int_{\mathbb{R}^2} \left(\rho\partial_t\xi + \rho\partial_a\xi + \rho\chi_1(a)\mathbf{v}\cdot\nabla_x\xi Y_\theta(\phi-R) + \mu\rho\Delta_x\xi - \mathfrak{d}\rho\xi\right)dx\,da\,dt\\
&\quad + \int_0^\infty\int_0^\infty\int_{\mathbb{R}^2} \mathscr{A}(\phi)\,\rho(t,a,x)\chi_3(a)\omega(t,x)\xi(t,0,x)dx\,da\,dt\\
&\quad + \int_0^\infty\int_{\mathbb{R}^2} \rho_0(a,x)\xi(0,a,x)dx\,da = 0.
\end{aligned}$$

Definition 1.2. *We say that a weak solution* ρ *is an entropy weak solution of* (1.1.7) *if for any nonnegative test function* $\xi \in C^\infty(\mathbb{R}^4)$ *with compact support and for any constant* $k \in \mathbb{R}$ *there holds*

$$\begin{aligned}
&\int_0^\infty\int_0^\infty\int_{\mathbb{R}^2} \left(|\rho-k|\left(\partial_t\xi+\partial_a\xi\right) - \mathrm{div}_x\left(|\rho-k|\chi_1\mathbf{v}Y_\theta(\phi-R)\right)\xi\right.\\
&\qquad\qquad \left. +\mu\Delta_x|\rho-k|\xi - \mathrm{sign}\left(\rho-k\right)\mathfrak{d}\rho\xi\right)dx\,da\,dt\\
&+\int_0^\infty\int_{\mathbb{R}^2} |\rho(t,0^+,x)-k|\xi(t,0,x)dx\,dt\\
&+\int_0^\infty\int_{\mathbb{R}^2} |\rho_0(a,x)-k|\xi(0,a,x)\,dx\,da\\
&\quad\geq \int_0^\infty\int_0^\infty\int_{\mathbb{R}^2} \mathrm{sign}\left(\rho-k\right)k\chi_1(a)\mathrm{div}_x\left(\mathbf{v}(x)Y_\theta(\phi-R)\right)\xi\,dx\,da\,dt.
\end{aligned} \tag{1.1.16}$$

Remark 1.1. *Obviously we can rewrite our equation as*

$$\partial_t\rho + \mathrm{div}_{a,x}(F(\rho)) = \mu\Delta_x\rho - \mathfrak{d}\rho,$$

with

$$F(\rho) = (\rho, \rho\chi_1(a)v_1(x)Y_\theta(\phi-R), \rho\chi_1(a)v_2(x)Y_\theta(\phi-R))$$

and $\mathbf{v} = (v_1, v_2)$.

In Definition 1.2 *we exploit the fact that the first component of the flux is linear, hence no boundary layer appears at* $a=0$, *see [2]. Then the second term in the entropy inequality* (1.1.16) *is equivalent to*

$$\int_0^\infty\int_{\mathbb{R}^2} \mathrm{sign}\left(\mathscr{A}(\phi)\left(\int_0^\infty \rho(t,a,x)\chi_3(a)\,da\right)\omega(t,x) - k\right)\left(\rho(t,0^+,x)-k\right)\xi(t,0,x)dx\,dt.$$

The main result of this chapter is the following.

Theorem 1.1. *Assume* (1.1.10), (1.1.11), (1.1.12), (1.1.13), (1.1.14), *and,* (1.1.15). *Then, the initial boundary value problem* (1.1.7) *admits a unique entropy weak solution* ρ *in the sense of Definition* 1.1. *Moreover, if* ρ *and* r *are the two entropy weak solutions of* (1.1.7) *obtained in correspondence of the initial data* ρ_0 *and* r_0*, then the following stability estimate holds*

$$\left\|\rho(t,\cdot,\cdot)-r(t,\cdot,\cdot)\right\|_{L^1((0,\infty)\times\mathbb{R}^2)} \leq Ce^{Ce^{Ct}}\left\|\rho_0-r_0\right\|_{L^1((0,\infty)\times\mathbb{R}^2)} \tag{1.1.17}$$

for a positive constant $C>0$ *and almost every* $t\geq 0$.

1.2 Existence

In order to prove the existence of a solution to problem (1.1.7) we consider a sequence of its parabolic approximations and we establish suitable a priori estimates on their solutions, see Section 1.2.1. Then, thanks to the multidimensional compensated compactness introduced by Panov in [35, 36], we show the existence of a vanishing viscosity limit satisfying the properties of Definitions 1.1 and 1.2, see Section 1.2.2.

Let $\{\rho_{0,\varepsilon}\}_\varepsilon$ be a $C^\infty((0,\infty)\times\mathbb{R}^2)$ family of approximations of the initial condition ρ_0 such that

$$\begin{aligned}
&\rho_{0,\varepsilon}\to\rho_0, \quad \text{a.e. and in } L^p((0,\infty)\times\mathbb{R}^2), 1\leq p<\infty \text{ as } \varepsilon\to 0,\\
&\rho_{0,\varepsilon}\geq 0,\ \left\|\rho_{0,\varepsilon}\right\|_{L^1((0,\infty)\times\mathbb{R}^2)}\leq C,\\
&\sup_{x\in\mathbb{R}^2}\left\|\rho_{0,\varepsilon}(\cdot,x)\right\|_{L^1(\mathbb{R})}, \sup_{a\geq 0}\left\|\rho_{0,\varepsilon}(a,\cdot)\right\|_{L^1(\mathbb{R}^2)}, \left\|\partial_a\rho_{0,\varepsilon}\right\|_{L^1((0,\infty)\times\mathbb{R}^2)}\leq C,
\end{aligned} \tag{1.2.18}$$

where, here and in the following, C denotes some positive constant independent on ε.

For any given $\varepsilon>0$, we call $\rho_\varepsilon=\rho_\varepsilon(t,a,x)$ the unique classical solution of the following problem

$$\begin{cases}
\partial_t\rho_\varepsilon+\partial_a\rho_\varepsilon+\operatorname{div}_x\left(\rho_\varepsilon\chi_1(a)\mathbf{v}Y_\theta(\phi_\varepsilon-R)\right)=\mu\Delta_x\rho_\varepsilon+\varepsilon\partial^2_{aa}\rho_\varepsilon-\mathfrak{d}\rho_\varepsilon, & (t,a,x)\in(0,\infty)\times(0,\infty)\times\mathbb{R}^2,\\
\rho_\varepsilon(t,0,x)=\mathscr{A}\left(|\phi_\varepsilon|\right)\left(\int_0^\infty|\rho_\varepsilon(t,a,x)|\chi_3(a)\mathrm{d}a\right)\omega(t,x), & (t,x)\in(0,\infty)\times\mathbb{R}^2,\\
\rho_\varepsilon(0,a,x)=\rho_{0,\varepsilon}(a,x), & (a,x)\in(0,\infty)\times\mathbb{R}^2,
\end{cases} \tag{1.2.19}$$

where

$$\phi_\varepsilon(t,x):=\int_0^\infty\rho_\varepsilon(t,a,x)\chi_2(a)\mathrm{d}a. \tag{1.2.20}$$

The well-posedness of (1.2.19) can be proved following the same arguments of [7, 8, 10]. Namely, one applies the Duhamel principle to get preliminary estimates on solutions, then establishes the local existence of a unique solution by a fixed point argument. Further energy estimates permit to extend the existence result globally in time.

1.2.1 A priori estimates

Lemma 1.1 (**Nonnegativity**). *We have that*

$$\rho_\varepsilon \geq 0, \qquad \phi_\varepsilon \geq 0. \tag{1.2.21}$$

Proof. Consider the function

$$\xi \mapsto \eta(\xi) = -\rho \mathbb{1}_{(-\infty,0)}(\xi).$$

and observe that

$$\eta'(\xi) = -\mathbb{1}_{(-\infty,0)}(\xi), \qquad \eta(\xi) = \xi\eta'(\xi).$$

From (1.2.19) we obtain

$$\begin{aligned}
&\frac{d}{dt}\int_0^\infty\int_{\mathbb{R}^2}\eta(\rho_\varepsilon)\mathrm{d}x\,\mathrm{d}a = \int_0^\infty\int_{\mathbb{R}^2}\eta'(\rho_\varepsilon)\partial_t\rho_\varepsilon\mathrm{d}x\,\mathrm{d}a\\
&= -\int_0^\infty\int_{\mathbb{R}^2}\eta'(\rho_\varepsilon)\partial_a\rho_\varepsilon\mathrm{d}x\,\mathrm{d}a - \int_0^\infty\int_{\mathbb{R}^2}\mathrm{div}_x\left(\rho_\varepsilon\chi_1\mathbf{v}Y_\theta\right)\eta'(\rho_\varepsilon)\mathrm{d}x\,\mathrm{d}a\\
&\quad + \mu\int_0^\infty\int_{\mathbb{R}^2}\eta'(\rho_\varepsilon)\Delta_x\rho_\varepsilon\mathrm{d}x\,\mathrm{d}a - \int_0^\infty\int_{\mathbb{R}^2}\eta'(\rho_\varepsilon)\mathfrak{d}\rho_\varepsilon\mathrm{d}x\,\mathrm{d}a + \varepsilon\int_0^\infty\int_{\mathbb{R}^2}\eta'(\rho_\varepsilon)\partial_{aa}^2\rho_\varepsilon\mathrm{d}x\,\mathrm{d}a\\
&= \int_{\mathbb{R}^2}\underbrace{\eta(\rho_\varepsilon(t,0,x))}_{=0}\mathrm{d}x + \underbrace{\int_0^\infty\int_{\mathbb{R}^2}\rho_\varepsilon\chi_1(\mathbf{v}\cdot\nabla_x\rho_\varepsilon)Y_\theta\eta''(\rho_\varepsilon)\mathrm{d}x\,\mathrm{d}a}_{=0}\\
&\quad \underbrace{-\mu\int_0^\infty\int_{\mathbb{R}^2}\eta''(\rho_\varepsilon)\left(\nabla_x\rho_\varepsilon\right)^2\mathrm{d}x\,\mathrm{d}a}_{\leq 0}\underbrace{-\int_0^\infty\int_{\mathbb{R}^2}\mathfrak{d}\eta(\rho_\varepsilon)\mathrm{d}x\,\mathrm{d}a}_{\leq 0}\\
&\quad + \varepsilon\int_0^\infty\int_{\mathbb{R}^2}\partial_a\left(\eta'(\rho_\varepsilon)\partial_a\rho_\varepsilon\right)\mathrm{d}x\,\mathrm{d}a\underbrace{-\varepsilon\int_0^\infty\int_{\mathbb{R}^2}\eta''(\rho_\varepsilon)(\partial_a\rho_\varepsilon)^2\mathrm{d}x\,\mathrm{d}a}_{\leq 0}\\
&\leq -\varepsilon\int_{\mathbb{R}^2}\underbrace{\eta'(\rho_\varepsilon(t,0,x))}_{=0}\partial_a\rho_\varepsilon(t,0,x)\mathrm{d}x = 0.
\end{aligned}$$

Thus, integrating on $(0,t)$ we get

$$0 \leq \int_0^\infty\int_{\mathbb{R}^2}\eta(\rho_\varepsilon(t,a,x))\mathrm{d}x\,\mathrm{d}a \leq \int_0^\infty\int_{\mathbb{R}^2}\eta(\rho_{0,\varepsilon}(a,x))\mathrm{d}x\,\mathrm{d}a = 0,$$

and then

$$\eta(\rho_\varepsilon(t,a,x)) = 0.$$

As a consequence we have that $\rho_\varepsilon \geq 0$. The nonnegativity of ϕ_ε follows from the one of ρ_ε and the definition of ϕ_ε. □

Remark 1.2. *Thanks to Lemma 1.1, we can improve the boundary condition in (1.2.19) removing the absolute values, i.e.*

$$\rho_\varepsilon(t,0,x) = \mathscr{A}(\phi)\left(\int_0^\infty \rho_\varepsilon(t,a,x)\chi_3(a)da\right)\omega(t,x).$$

In our proofs we exploit the fact that the functions χ_i, $i=1,2,3$ have similar shapes and in particular $\chi_i(0)=0$, as this means that the estimates in the next lemma apply to all the integral functions of the form

$$\int_0^\infty \rho_\varepsilon(t,a,x)\chi_i(a)\mathrm{d}a, \qquad i=1,2,3.$$

Lemma 1.2. *Let $\xi \in C^\infty([0,\infty))$ be any of the functions χ_i, $i=1,2,3$, and consider*

$$\psi_\varepsilon(t,x) = \int_0^\infty \rho_\varepsilon(t,a,x)\xi(a)da.$$

The following estimates hold

$$\|\psi_\varepsilon(t,\cdot)\|_{L^1(\mathbb{R}^2)} \le e^{Ct}C, \tag{1.2.22}$$

$$\|\psi_\varepsilon(t,\cdot)\|_{L^2(\mathbb{R}^2)}, \|\nabla_x\psi_\varepsilon\|_{L^2((0,t)\times\mathbb{R}^2)} \le e^{Ct}C, \tag{1.2.23}$$

$$\|\nabla_x\psi_\varepsilon(t,\cdot)\|_{L^2(\mathbb{R}^2)}, \|D_x^2\psi_\varepsilon\|_{L^2((0,t)\times\mathbb{R}^2)} \le e^{Ct}C, \tag{1.2.24}$$

$$\|D_x^2\psi_\varepsilon(t,\cdot)\|_{L^2(\mathbb{R}^2)}, \|D_x^3\psi_\varepsilon\|_{L^2((0,t)\times\mathbb{R}^2)} \le e^{Ct}C, \tag{1.2.25}$$

$$\|D_x^3\psi_\varepsilon(t,\cdot)\|_{L^2(\mathbb{R}^2)}, \|D_x^4\psi_\varepsilon\|_{L^2((0,t)\times\mathbb{R}^2)} \le e^{Ct}C, \tag{1.2.26}$$

for every $t\ge 0$ and for a suitable constant $C>0$ independent on ε. In particular

$$\|\partial_t\psi_\varepsilon(t,\cdot)\|_{L^1(\mathbb{R}^2)}, \|\partial_t\psi_\varepsilon(t,\cdot)\|_{L^2(\mathbb{R}^2)}, \|\psi_\varepsilon(t,\cdot)\|_{L^\infty(\mathbb{R}^2)}, \|\nabla_x\psi_\varepsilon(t,\cdot)\|_{L^\infty(\mathbb{R}^2)} \le e^{Ct}C, \tag{1.2.27}$$

for every $t\ge 0$.

Proof. Everywhere in the proof we denote generically by c the constants not depending on ε.

We multiply (1.2.19) by $\xi(a)$ and integrate with respect to a

$$\partial_t\psi_\varepsilon - \mu\Delta_x\psi_\varepsilon + \mathrm{div}_x\left(\left(\int_0^\infty \rho_\varepsilon\chi_1\xi\mathrm{d}a\right)\mathbf{v}Y_\theta\right) = \int_0^\infty \rho_\varepsilon\left(\varepsilon\xi'' + \xi' - \mathfrak{d}\xi\right)\mathrm{d}a. \tag{1.2.28}$$

Using the nonnegativity of ρ_ε, ψ_ε and the boundedness of ξ'/ξ, ξ''/ξ, $\mathfrak{d}$

$$\frac{d}{dt}\int_{\mathbb{R}^2}|\psi_\varepsilon|\mathrm{d}x = \frac{d}{dt}\int_{\mathbb{R}^2}\psi_\varepsilon\mathrm{d}x = \underbrace{\mu\int_{\mathbb{R}^2}\Delta_x\psi_\varepsilon\mathrm{d}x - \int_{\mathbb{R}^2}\mathrm{div}_x\left(\left(\int_0^\infty\rho_\varepsilon\chi_1\xi\mathrm{d}a\right)\mathbf{v}Y_\theta\right)\mathrm{d}x}_{=0}$$
$$+\int_{\mathbb{R}^2}\int_0^\infty \rho_\varepsilon\underbrace{\left(\varepsilon\xi'' + \xi' - \mathfrak{d}\xi\right)}_{\le c\xi}\mathrm{d}a\,\mathrm{d}x \le c\int_{\mathbb{R}^2}\psi_\varepsilon\mathrm{d}x.$$

Therefore, (1.2.22) follows from the Gronwall Lemma and (1.2.18).

We continue by proving (1.2.23). We multiply (1.2.28) by ψ_ε

$$\begin{aligned}
&\frac{d}{dt}\int_{\mathbb{R}^2}\frac{\psi_\varepsilon^2}{2}\mathrm{d}x=\int_{\mathbb{R}^2}\psi_\varepsilon\partial_t\psi_\varepsilon\mathrm{d}x\\
&=\mu\int_{\mathbb{R}^2}\psi_\varepsilon\Delta_x\psi_\varepsilon\mathrm{d}x-\int_{\mathbb{R}^2}\psi_\varepsilon\mathrm{div}_x\left(\left(\int_0^\infty\rho_\varepsilon\chi_1\xi\mathrm{d}a\right)\mathbf{v}Y_\theta\right)\mathrm{d}x+\int_{\mathbb{R}^2}\int_0^\infty\rho_\varepsilon\underbrace{\left(\varepsilon\xi''+\xi'-\mathfrak{d}\xi\right)}_{\leq c\xi}\psi_\varepsilon\mathrm{d}a\mathrm{d}x\\
&\leq-\mu\int_{\mathbb{R}^2}|\nabla_x\psi_\varepsilon|^2\mathrm{d}x+\int_{\mathbb{R}^2}\nabla_x\psi_\varepsilon\cdot\mathbf{v}\left(\int_0^\infty\rho_\varepsilon\chi_1\xi\mathrm{d}a\right)Y_\theta\mathrm{d}x+c\int_{\mathbb{R}^2}\psi_\varepsilon^2\mathrm{d}x\\
&\leq-\frac{\mu}{2}\int_{\mathbb{R}^2}|\nabla_x\psi_\varepsilon|^2\mathrm{d}x+\frac{1}{2\mu}\int_{\mathbb{R}^2}\underbrace{|\mathbf{v}|^2\left(\int_0^\infty\rho_\varepsilon\chi_1\xi\mathrm{d}a\right)^2Y_\theta}_{\leq c\psi_\varepsilon^2}\mathrm{d}x+c\int_{\mathbb{R}^2}\psi_\varepsilon^2\mathrm{d}x\\
&\leq-\frac{\mu}{2}\int_{\mathbb{R}^2}|\nabla_x\psi_\varepsilon|^2\mathrm{d}x+c\int_{\mathbb{R}^2}\psi_\varepsilon^2\mathrm{d}x.
\end{aligned}$$

Using again the Gronwall Lemma we get (1.2.23).

We continue by proving (1.2.24). We multiply (1.2.28) by $-\Delta_x\psi_\varepsilon$

$$\begin{aligned}
&\frac{d}{dt}\int_{\mathbb{R}^2}\frac{|\nabla_x\psi_\varepsilon|^2}{2}\mathrm{d}x=\int_{\mathbb{R}^2}\nabla_x\psi_\varepsilon\cdot\partial_t\nabla_x\psi_\varepsilon\mathrm{d}x=-\int_{\mathbb{R}^2}\Delta_x\psi_\varepsilon\partial_t\psi_\varepsilon\mathrm{d}x\\
&=-\mu\int_{\mathbb{R}^2}|D_x^2\psi_\varepsilon|^2\mathrm{d}x+\int_{\mathbb{R}^2}\Delta_x\psi_\varepsilon\mathrm{div}_x\left(\left(\int_0^\infty\rho_\varepsilon\chi_1\xi\mathrm{d}a\right)\mathbf{v}Y_\theta\right)\mathrm{d}x-\int_{\mathbb{R}^2}\int_0^\infty\rho_\varepsilon\underbrace{\left(\varepsilon\xi''+\xi'-\mathfrak{d}\xi\right)}_{\leq c\xi}\Delta_x\psi_\varepsilon\mathrm{d}a\mathrm{d}x\\
&\leq-\frac{\mu}{2}\int_{\mathbb{R}^2}|D_x^2\psi_\varepsilon|^2\mathrm{d}x+c\int_{\mathbb{R}^2}\left(\mathrm{div}_x\left(\left(\int_0^\infty\rho_\varepsilon\chi_1\xi\mathrm{d}a\right)\mathbf{v}Y_\theta\right)\right)^2\mathrm{d}x+c\int_{\mathbb{R}^2}\psi_\varepsilon^2\mathrm{d}x\\
&\leq-\frac{\mu}{2}\int_{\mathbb{R}^2}|D_x^2\psi_\varepsilon|^2\mathrm{d}x+c\int_{\mathbb{R}^2}\left|\nabla_x\int_0^\infty\rho_\varepsilon\chi_1\xi\mathrm{d}a\right|^2\underbrace{|\mathbf{v}|^2Y_\theta^2}_{\leq c}\mathrm{d}x\\
&\quad+c\int_{\mathbb{R}^2}\left(\int_0^\infty\rho_\varepsilon\chi_1\xi\mathrm{d}a\right)^2\underbrace{|\mathrm{div}_x(\mathbf{v})|^2Y_\theta^2}_{\leq c}\mathrm{d}x+c\int_{\mathbb{R}^2}\underbrace{\left(\int_0^\infty\rho_\varepsilon\chi_1\xi\mathrm{d}a\right)^2(Y_\theta')^2|\mathbf{v}|^2}_{\leq c\,(\text{as supp}(\xi)\subset(0,T))}|\nabla_x\phi_\varepsilon|^2\mathrm{d}x+c\int_{\mathbb{R}^2}\psi_\varepsilon^2\mathrm{d}x.
\end{aligned}$$

Using the Gronwall Lemma we get

$$\begin{aligned}
&\left\|\nabla_x\psi_\varepsilon(t,\cdot)\right\|_{L^2(\mathbb{R}^2)}^2+\mu e^{ct}\int_0^t e^{-cs}\left\|D_x^2\psi_\varepsilon(s,\cdot)\right\|_{L^2(\mathbb{R}^2)}^2\mathrm{d}s\\
&\quad\leq e^{ct}\left\|\nabla_x\psi_\varepsilon(0,\cdot)\right\|_{L^2(\mathbb{R}^2)}^2+ce^{ct}\int_0^t\int_{\mathbb{R}^2}e^{-cs}\left(\int_0^\infty\rho_\varepsilon\chi_1\xi\mathrm{d}a\right)^2\mathrm{d}x\mathrm{d}s\\
&\qquad+ce^{ct}\int_0^t\int_{\mathbb{R}^2}e^{-cs}\left|\nabla_x\int_0^\infty\rho_\varepsilon\chi_1\xi\mathrm{d}a\right|^2\mathrm{d}x\mathrm{d}s+ce^{ct}\int_0^t\int_{\mathbb{R}^2}e^{-cs}|\nabla_x\phi_\varepsilon|^2\mathrm{d}x\mathrm{d}s.
\end{aligned}$$

Since the functions

$$\phi_\varepsilon,\qquad(t,x)\mapsto\int_0^\infty\rho_\varepsilon\chi_1\xi\mathrm{d}a$$

have the same structure as ψ_ε we can use (1.2.23) and get (1.2.24).

We continue by proving (1.2.25). We multiply (1.2.28) by $D_x^4\psi_\varepsilon$.

$$
\begin{aligned}
&\frac{d}{dt}\int_{\mathbb{R}^2}\frac{|\Delta_x\psi_\varepsilon|^2}{2}\mathrm{d}x=\int_{\mathbb{R}^2}\Delta_x\psi_\varepsilon\cdot\partial_t\Delta_x\psi_\varepsilon\mathrm{d}x=\int_{\mathbb{R}^2}D_x^4\psi_\varepsilon\partial_t\psi_\varepsilon\mathrm{d}x\\
&=\mu\int_{\mathbb{R}^2}\Delta_x\psi_\varepsilon D_x^4\psi_\varepsilon\mathrm{d}x-\int_{\mathbb{R}^2}D_x^4\psi_\varepsilon\mathrm{div}_x\left(\left(\int_0^\infty\rho_\varepsilon\chi_1\xi\mathrm{d}a\right)\mathbf{v}Y_\theta\right)\mathrm{d}x\\
&\quad+\int_{\mathbb{R}^2}\int_0^\infty\rho_\varepsilon\left(\varepsilon\xi''+\xi'-\mathfrak{d}\xi\right)D_x^4\psi_\varepsilon\mathrm{d}a\,\mathrm{d}x\\
&=-\mu\int_{\mathbb{R}^2}|D_x^3\psi_\varepsilon|^2\mathrm{d}x+\int_{\mathbb{R}^2}D_x^3\psi_\varepsilon\cdot\nabla_x\mathrm{div}_x\left(\left(\int_0^\infty\rho_\varepsilon\chi_1\xi\mathrm{d}a\right)\mathbf{v}Y_\theta\right)\mathrm{d}x\\
&\quad-\int_{\mathbb{R}^2}\nabla_x\left(\int_0^\infty\rho_\varepsilon\left(\varepsilon\xi''+\xi'-\mathfrak{d}\xi\right)\mathrm{d}a\right)\cdot D_x^3\psi_\varepsilon\mathrm{d}x\\
&\le-\frac{\mu}{2}\int_{\mathbb{R}^2}|D_x^3\psi_\varepsilon|^2\mathrm{d}x+c\int_{\mathbb{R}^2}\left(\nabla_x\mathrm{div}_x\left(\left(\int_0^\infty\rho_\varepsilon\chi_1\xi\mathrm{d}a\right)\mathbf{v}Y_\theta\right)\right)^2\mathrm{d}x\\
&\quad+c\int_{\mathbb{R}^2}\left|\nabla_x\int_0^\infty\rho_\varepsilon\left(\varepsilon\xi''+\xi'-\mathfrak{d}\xi\right)\mathrm{d}a\right|^2\mathrm{d}x\\
&\le-\frac{\mu}{2}\int_{\mathbb{R}^2}|D_x^3\psi_\varepsilon|^2\mathrm{d}x+c\int_{\mathbb{R}^2}\left|D_x^2\int_0^\infty\rho_\varepsilon\chi_1\xi\mathrm{d}a\right|^2\underbrace{|\mathbf{v}|^2Y_\theta^2}_{\le c}\mathrm{d}x+c\int_{\mathbb{R}^2}\left|\int_0^\infty\rho_\varepsilon\chi_1\xi\mathrm{d}a\right|^2\underbrace{|D_x^2\mathbf{v}|^2Y_\theta^2}_{\le c}\mathrm{d}x\\
&\quad+c\int_{\mathbb{R}^2}\underbrace{\left|\int_0^\infty\rho_\varepsilon\chi_1\xi\mathrm{d}a\right|^2|\mathbf{v}|^2(Y_\theta'')^2}_{\le c\,(\text{as supp}(\xi)\subset(0,T))}|\nabla_x\phi_\varepsilon|^4\mathrm{d}x+c\int_{\mathbb{R}^2}\underbrace{\left|\int_0^\infty\rho_\varepsilon\chi_1\xi\mathrm{d}a\right|^2|\mathbf{v}|^2(Y_\theta')^2}_{\le c\,(\text{as supp}(\xi)\subset(0,T))}|D_x^2\phi_\varepsilon|^2\mathrm{d}x\\
&\quad+c\int_{\mathbb{R}^2}\left|\nabla_x\int_0^\infty\rho_\varepsilon\chi_1\xi\mathrm{d}a\right|^2\underbrace{|\nabla_x\mathbf{v}|^2Y_\theta^2}_{\le c}\mathrm{d}x+c\int_{\mathbb{R}^2}\underbrace{\left|\int_0^\infty\rho_\varepsilon\chi_1\xi\mathrm{d}a\right|^2|\nabla_x\mathbf{v}|^2(Y_\theta')^2}_{\le c\,(\text{as supp}(\xi)\subset(0,T))}|\nabla_x\phi_\varepsilon|^2\mathrm{d}x\\
&\quad+c\int_{\mathbb{R}^2}\left|\nabla_x\int_0^\infty\rho_\varepsilon\chi_1\xi\mathrm{d}a\right|^2\underbrace{|\mathbf{v}|^2(Y_\theta')^2}_{\le c}|\nabla_x\phi_\varepsilon|^2\mathrm{d}x+c\int_{\mathbb{R}^2}\left|\nabla_x\int_0^\infty\rho_\varepsilon\left(\varepsilon\xi''+\xi'-\mathfrak{d}\xi\right)\mathrm{d}a\right|^2\mathrm{d}x\\
&\le-\frac{\mu}{2}\int_{\mathbb{R}^2}|D_x^3\psi_\varepsilon|^2\mathrm{d}x+c\int_{\mathbb{R}^2}\left|D_x^2\int_0^\infty\rho_\varepsilon\chi_1\xi\mathrm{d}a\right|^2\mathrm{d}x+c\int_{\mathbb{R}^2}\left|\int_0^\infty\rho_\varepsilon\chi_1\xi\mathrm{d}a\right|^2\mathrm{d}x\\
&\quad+c\int_{\mathbb{R}^2}\left|\nabla_x\int_0^\infty\rho_\varepsilon\chi_1\xi\mathrm{d}a\right|^2\mathrm{d}x+c\int_{\mathbb{R}^2}|\nabla_x\phi_\varepsilon|^2\mathrm{d}x+c\int_{\mathbb{R}^2}|\nabla_x\phi_\varepsilon|^4\mathrm{d}x\\
&\quad+c\int_{\mathbb{R}^2}|D_x^2\phi_\varepsilon|^2\mathrm{d}x+c\int_{\mathbb{R}^2}\left|\nabla_x\int_0^\infty\rho_\varepsilon\chi_1\xi\mathrm{d}a\right|^4\mathrm{d}x\\
&\quad+c\int_{\mathbb{R}^2}\left|\nabla_x\int_0^\infty\rho_\varepsilon\left(\varepsilon\xi''+\xi'-\mathfrak{d}\xi\right)_+\mathrm{d}a\right|^2\mathrm{d}x+c\int_{\mathbb{R}^2}\left|\nabla_x\int_0^\infty\rho_\varepsilon\left(\varepsilon\xi''+\xi'-\mathfrak{d}\xi\right)_-\mathrm{d}a\right|^2\mathrm{d}x,
\end{aligned}
$$

where

$$
\begin{aligned}
\left(\varepsilon\xi''+\xi'-\mathfrak{d}\xi\right)_+&=\max\{\left(\varepsilon\xi''+\xi'-\mathfrak{d}\xi\right),0\},\\
\left(\varepsilon\xi''+\xi'-\mathfrak{d}\xi\right)_-&=\max\{-\left(\varepsilon\xi''+\xi'-\mathfrak{d}\xi\right),0\}.
\end{aligned}
$$

We remind that

$$\begin{aligned}&\left(\varepsilon\xi''+\xi'-\mathfrak{d}\xi\right)_+\geq 0,\qquad \left(\varepsilon\xi''+\xi'-\mathfrak{d}\xi\right)_-\geq 0,\\&\left(\varepsilon\xi''+\xi'-\mathfrak{d}\xi\right)=\left(\varepsilon\xi''+\xi'-\mathfrak{d}\xi\right)_+-\left(\varepsilon\xi''+\xi'-\mathfrak{d}\xi\right)_-.\end{aligned}$$

Integrating over $(0,t)$ we get

$$\begin{aligned}&\left\|D_x^2\psi_\varepsilon(t,\cdot)\right\|^2_{L^2(\mathbb{R}^2)}+\mu\left\|D_x^3\psi_\varepsilon\right\|^2_{L^2((0,t)\times\mathbb{R}^2)}\\&\quad\leq\left\|D_x^2\psi_\varepsilon(0,\cdot)\right\|^2_{L^2(\mathbb{R}^2)}+\int_0^t\left\|\left(\int_0^\infty\rho_\varepsilon\chi_1\xi\,da\right)(s)\right\|^2_{H^2(\mathbb{R}^2)}ds+\int_0^t\left\|\phi_\varepsilon(s,\cdot)\right\|^2_{H^2(\mathbb{R}^2)}ds\\&\qquad+\int_0^t\left\|\left(\nabla_x\int_0^\infty\rho_\varepsilon\chi_1\xi da\right)(s)\right\|^4_{L^4(\mathbb{R}^2)}ds+\int_0^t\left\|\nabla_x\phi_\varepsilon(s,\cdot)\right\|^4_{L^4(\mathbb{R}^2)}ds\\&\qquad+\int_0^t\left\|\left(\nabla_x\int_0^\infty\rho_\varepsilon\left(\varepsilon\xi''+\xi'-\mathfrak{d}\xi\right)_+da\right)(s)\right\|^2_{L^2(\mathbb{R}^2)}ds\\&\qquad+\int_0^t\left\|\left(\nabla_x\int_0^\infty\rho_\varepsilon\left(\varepsilon\xi''+\xi'-\mathfrak{d}\xi\right)_-da\right)(s)\right\|^2_{L^2(\mathbb{R}^2)}ds.\end{aligned}$$

To achieve the proof of (1.2.25) we use the embedding $H^1(\mathbb{R}^2)\subset L^4(\mathbb{R}^2)$ and we remark that the estimates (1.2.23), (1.2.24) apply to the functions

$$\phi_\varepsilon,\qquad (t,x)\mapsto\int_0^\infty\rho_\varepsilon\chi_1\xi da,\qquad \int_0^\infty\rho_\varepsilon\left(\varepsilon\xi''+\xi'-\mathfrak{d}\xi\right)_\pm da.$$

Indeed a classical regularization argument applied to the continuous cut-off functions in the last expression allows to prove estimates (1.2.23), (1.2.24).

We continue by proving (1.2.26). We multiply (1.2.28) by $-D_x^6\psi_\varepsilon$

$$\begin{aligned}&\frac{d}{dt}\int_{\mathbb{R}^2}\frac{|D_x^3\psi_\varepsilon|^2}{2}dx=\int_{\mathbb{R}^2}D_x^3\psi_\varepsilon\cdot\partial_tD_x^3\psi_\varepsilon dx=-\int_{\mathbb{R}^2}D_x^6\psi_\varepsilon\partial_t\psi_\varepsilon dx\\&=-\mu\int_{\mathbb{R}^2}\Delta_x\psi_\varepsilon D_x^6\psi_\varepsilon dx+\int_{\mathbb{R}^2}D_x^6\psi_\varepsilon\mathrm{div}_x\left(\left(\int_0^\infty\rho_\varepsilon\chi_1\xi da\right)\mathbf{v}Y_\theta\right)dx\\&\quad-\int_{\mathbb{R}^2}\int_0^\infty\rho_\varepsilon\left(\varepsilon\xi''+\xi'-\mathfrak{d}\xi\right)D_x^6\psi_\varepsilon da\,dx\\&=-\mu\int_{\mathbb{R}^2}|D_x^4\psi_\varepsilon|^2dx+\int_{\mathbb{R}^2}D_x^4\psi_\varepsilon\Delta_x\mathrm{div}_x\left(\left(\int_0^\infty\rho_\varepsilon\chi_1\xi da\right)\mathbf{v}Y_\theta\right)dx\\&\quad-\int_{\mathbb{R}^2}\Delta_x\left(\int_0^\infty\rho_\varepsilon\left(\varepsilon\xi''+\xi'-\mathfrak{d}\xi\right)da\right)D_x^4\psi_\varepsilon dx\\&\leq-\frac{\mu}{2}\int_{\mathbb{R}^2}|D_x^4\psi_\varepsilon|^2dx+c\int_{\mathbb{R}^2}\left(\Delta_x\mathrm{div}_x\left(\left(\int_0^\infty\rho_\varepsilon\chi_1\xi da\right)\mathbf{v}Y_\theta\right)\right)^2dx\\&\quad+c\int_{\mathbb{R}^2}\left|D_x^2\int_0^\infty\rho_\varepsilon\left(\varepsilon\xi''+\xi'-\mathfrak{d}\xi\right)_+da\right|^2dx+c\int_{\mathbb{R}^2}\left|D_x^2\int_0^\infty\rho_\varepsilon\left(\varepsilon\xi''+\xi'-\mathfrak{d}\xi\right)_-da\right|^2dx\\&\leq-\frac{\mu}{2}\int_{\mathbb{R}^2}|D_x^4\psi_\varepsilon|^2dx+c\int_{\mathbb{R}^2}\left|D_x^3\int_0^\infty\rho_\varepsilon\chi_1\xi da\right|^2\underbrace{|\mathbf{v}|^2Y_\theta^2}_{\leq c}dx\end{aligned}$$

$$
\begin{aligned}
&+c\int_{\mathbb{R}^2}\left|D_x^2\int_0^\infty \rho_\varepsilon\chi_1\xi\,\mathrm{d}a\right|^2\underbrace{|\nabla_x\mathbf{v}|^2Y_\theta^2}_{\le c}\,\mathrm{d}x+c\int_{\mathbb{R}^2}\left|\nabla_x\int_0^\infty \rho_\varepsilon\chi_1\xi\,\mathrm{d}a\right|^2\underbrace{|D_x^2\mathbf{v}|^2Y_\theta^2}_{\le c}\,\mathrm{d}x\\
&+c\int_{\mathbb{R}^2}\left|\int_0^\infty \rho_\varepsilon\chi_1\xi\,\mathrm{d}a\right|^2\underbrace{|D_x^3\mathbf{v}|^2Y_\theta^2}_{\le c}\,\mathrm{d}x+c\int_{\mathbb{R}^2}\left|D_x^2\int_0^\infty \rho_\varepsilon\chi_1\xi\,\mathrm{d}a\right|^2\underbrace{|\mathbf{v}|^2(Y_\theta')^2}_{\le c}|\nabla_x\phi_\varepsilon|^2\,\mathrm{d}x\\
&+c\int_{\mathbb{R}^2}\underbrace{\left|\int_0^\infty \rho_\varepsilon\chi_1\xi\,\mathrm{d}a\right|^2|D_x^2\mathbf{v}|^2(Y_\theta')^2}_{\le c}|\nabla_x\phi_\varepsilon|^2\,\mathrm{d}x+c\int_{\mathbb{R}^2}\left|\nabla_x\int_0^\infty \rho_\varepsilon\chi_1\xi\,\mathrm{d}a\right|^2\underbrace{|\nabla_x\mathbf{v}|^2(Y_\theta')^2}_{\le c}|\nabla_x\phi_\varepsilon|^2\,\mathrm{d}x\\
&+c\int_{\mathbb{R}^2}\left|\nabla_x\int_0^\infty \rho_\varepsilon\chi_1\xi\,\mathrm{d}a\right|^2\underbrace{|\mathbf{v}|^2(Y_\theta'')^2}_{\le c}|\nabla_x\phi_\varepsilon|^4\,\mathrm{d}x+c\int_{\mathbb{R}^2}\left|\nabla_x\int_0^\infty \rho_\varepsilon\chi_1\xi\,\mathrm{d}a\right|^2\underbrace{|\mathbf{v}|^2(Y_\theta')^2}_{\le c}|D_x^2\phi_\varepsilon|^2\,\mathrm{d}x\\
&+c\int_{\mathbb{R}^2}\underbrace{\left|\int_0^\infty \rho_\varepsilon\chi_1\xi\,\mathrm{d}a\right|^2|\nabla_x\mathbf{v}|^2(Y_\theta'')^2}_{\le c}|\nabla_x\phi_\varepsilon|^4\,\mathrm{d}x+c\int_{\mathbb{R}^2}\underbrace{\left|\int_0^\infty \rho_\varepsilon\chi_1\xi\,\mathrm{d}a\right|^2|\nabla_x\mathbf{v}|^2(Y_\theta')^2}_{\le c}|D_x^2\phi_\varepsilon|^2\,\mathrm{d}x\\
&+c\int_{\mathbb{R}^2}\underbrace{\left|\int_0^\infty \rho_\varepsilon\chi_1\xi\,\mathrm{d}a\right|^2|\mathbf{v}|^2(Y_\theta''')^2}_{\le c}|\nabla_x\phi_\varepsilon|^6\,\mathrm{d}x+c\int_{\mathbb{R}^2}\underbrace{\left|\int_0^\infty \rho_\varepsilon\chi_1\xi\,\mathrm{d}a\right|^2|\mathbf{v}|^2(Y_\theta'')^2}_{\le c}|D_x^2\phi_\varepsilon|^2|\nabla_x\phi_\varepsilon|^2\,\mathrm{d}x\\
&+c\int_{\mathbb{R}^2}\underbrace{\left|\int_0^\infty \rho_\varepsilon\chi_1\xi\,\mathrm{d}a\right|^2|\mathbf{v}|^2(Y_\theta')^2}_{\le c}|D_x^3\phi_\varepsilon|^2\,\mathrm{d}x\\
&+c\int_{\mathbb{R}^2}\left|D_x^2\int_0^\infty \rho_\varepsilon\left(\varepsilon\xi''+\xi'-\mathfrak{d}\xi\right)_+\mathrm{d}a\right|^2\mathrm{d}x+c\int_{\mathbb{R}^2}\left|D_x^2\int_0^\infty \rho_\varepsilon\left(\varepsilon\xi''+\xi'-\mathfrak{d}\xi\right)_-\mathrm{d}a\right|^2\mathrm{d}x\\
\le&-\frac{\mu}{2}\int_{\mathbb{R}^2}|D_x^4\psi_\varepsilon|^2\mathrm{d}x+c\int_{\mathbb{R}^2}\left|D_x^3\int_0^\infty \rho_\varepsilon\chi_1\xi\,\mathrm{d}a\right|^2\mathrm{d}x+c\int_{\mathbb{R}^2}\left|D_x^2\int_0^\infty \rho_\varepsilon\chi_1\xi\,\mathrm{d}a\right|^2\mathrm{d}x\\
&+c\int_{\mathbb{R}^2}\left|\nabla_x\int_0^\infty \rho_\varepsilon\chi_1\xi\,\mathrm{d}a\right|^2\mathrm{d}x+c\int_{\mathbb{R}^2}\left|\int_0^\infty \rho_\varepsilon\chi_1\xi\,\mathrm{d}a\right|^2\mathrm{d}x+c\int_{\mathbb{R}^2}\left|D_x^2\int_0^\infty \rho_\varepsilon\chi_1\xi\,\mathrm{d}a\right|^4\mathrm{d}x\\
&+c\int_{\mathbb{R}^2}\left|\nabla_x\int_0^\infty \rho_\varepsilon\chi_1\xi\,\mathrm{d}a\right|^4\mathrm{d}x+c\int_{\mathbb{R}^2}|D_x^3\phi_\varepsilon|^2\mathrm{d}x+c\int_{\mathbb{R}^2}|D_x^2\phi_\varepsilon|^2\mathrm{d}x+c\int_{\mathbb{R}^2}|D_x^2\phi_\varepsilon|^4\mathrm{d}x\\
&+c\int_{\mathbb{R}^2}|\nabla_x\phi_\varepsilon|^2\mathrm{d}x+c\int_{\mathbb{R}^2}|\nabla_x\phi_\varepsilon|^4\mathrm{d}x+c\int_{\mathbb{R}^2}|\nabla_x\phi_\varepsilon|^6\mathrm{d}x+c\int_{\mathbb{R}^2}|\nabla_x\phi_\varepsilon|^8\mathrm{d}x\\
&+c\int_{\mathbb{R}^2}\left|D_x^2\int_0^\infty \rho_\varepsilon\left(\varepsilon\xi''+\xi'-\mathfrak{d}\xi\right)_+\mathrm{d}a\right|^2\mathrm{d}x+c\int_{\mathbb{R}^2}\left|D_x^2\int_0^\infty \rho_\varepsilon\left(\varepsilon\xi''+\xi'-\mathfrak{d}\xi\right)_-\mathrm{d}a\right|^2\mathrm{d}x.
\end{aligned}
$$

Integrating over $(0,t)$ we get

$$
\begin{aligned}
&\left\|D_x^3\psi_\varepsilon(t,\cdot)\right\|^2_{L^2(\mathbb{R}^2)}+\mu\left\|D_x^4\psi_\varepsilon\right\|^2_{L^2((0,t)\times\mathbb{R}^2)}\\
&\quad\le\left\|D_x^3\psi_\varepsilon(0,\cdot)\right\|^2_{L^2(\mathbb{R}^2)}+\int_0^t\left\|\left(\int_0^\infty \rho_\varepsilon\chi_1\xi\,\mathrm{d}a\right)(s)\right\|^2_{H^3(\mathbb{R}^2)}\mathrm{d}s+\int_0^t\left\|\phi_\varepsilon(s,\cdot)\right\|^2_{H^3(\mathbb{R}^2)}\mathrm{d}s\\
&\qquad+\int_0^t\left\|\left(D_x^2\int_0^\infty \rho_\varepsilon\chi_1\xi\,\mathrm{d}a\right)(s)\right\|^4_{L^4(\mathbb{R}^2)}\mathrm{d}s+\int_0^t\left\|\left(\nabla_x\int_0^\infty \rho_\varepsilon\chi_1\xi\,\mathrm{d}a\right)(s)\right\|^4_{L^4(\mathbb{R}^2)}\mathrm{d}s
\end{aligned}
$$

$$
\begin{aligned}
&+\int_0^t \left\|D_x^2\phi_\varepsilon(s,\cdot)\right\|^4_{L^4(\mathbb{R}^2)}\,\mathrm{d}s+\int_0^t \left\|\nabla_x\phi_\varepsilon(s,\cdot)\right\|^4_{L^4(\mathbb{R}^2)}\,\mathrm{d}s\\
&+\int_0^t \left\|\nabla_x\phi_\varepsilon(s,\cdot)\right\|^6_{L^6(\mathbb{R}^2)}\,\mathrm{d}s+\int_0^t \left\|\nabla_x\phi_\varepsilon(s,\cdot)\right\|^8_{L^8(\mathbb{R}^2)}\,\mathrm{d}s\\
&+\int_0^t \left\|\left(D_x^2\int_0^\infty \rho_\varepsilon\left(\varepsilon\xi''+\xi'-\mathfrak{d}\xi\right)_+\mathrm{d}a\right)(s)\right\|^2_{L^2(\mathbb{R}^2)}\,\mathrm{d}s\\
&+\int_0^t \left\|\left(D_x^2\int_0^\infty \rho_\varepsilon\left(\varepsilon\xi''+\xi'-\mathfrak{d}\xi\right)_-\mathrm{d}a\right)(s)\right\|^2_{L^2(\mathbb{R}^2)}\,\mathrm{d}s.
\end{aligned}
$$

Since $H^1(\mathbb{R}^2)\subset L^p(\mathbb{R}^2)$, for very $1\le p<\infty$ and the functions

$$
\phi_\varepsilon,\qquad (t,x)\mapsto\int_0^\infty \rho_\varepsilon\chi_1\xi\mathrm{d}a,\qquad (t,x)\mapsto\int_0^\infty \rho_\varepsilon\left(\varepsilon\xi''+\xi'-\mathfrak{d}\xi\right)_\pm\mathrm{d}a,
$$

have the structure we assume for ψ_ε, we can use (1.2.23), (1.2.24) and (1.2.25) to obtain (1.2.26).

Finally, (1.2.27) follows from (1.2.23), (1.2.24), (1.2.25), (1.2.26), (1.2.28) and the embedding $H^2(\mathbb{R}^2)\subset L^\infty(\mathbb{R}^2)$. □

Corollary 1.1. *Define*

$$
\rho^0_\varepsilon(t,x)=\rho_\varepsilon(t,0,x).
$$

The following estimates hold

$$
\left\|\rho^0_\varepsilon(t,\cdot)\right\|_{L^1(\mathbb{R}^2)},\left\|D_x^2\rho^0_\varepsilon\right\|_{L^1((0,t)\times\mathbb{R}^2)},\left\|\partial_t\rho^0_\varepsilon\right\|_{L^1((0,t)\times\mathbb{R}^2)}\le e^{Ct}C, \tag{1.2.29}
$$

$$
\left\|\rho^0_\varepsilon(t,\cdot)\right\|_{L^2(\mathbb{R}^2)},\left\|\nabla_x\rho^0_\varepsilon(t,\cdot)\right\|_{L^2(\mathbb{R}^2)}\le e^{Ct}C, \tag{1.2.30}
$$

$$
\left\|\nabla_x\rho^0_\varepsilon\right\|_{L^2((0,t)\times\mathbb{R}^2)},\left\|D_x^2\rho^0_\varepsilon\right\|_{L^2((0,t)\times\mathbb{R}^2)},\left\|\partial_t\rho^0_\varepsilon\right\|_{L^2((0,t)\times\mathbb{R}^2)}\le e^{Ct}C, \tag{1.2.31}
$$

$$
\left\|\rho^0_\varepsilon(t,\cdot)\right\|_{L^\infty(\mathbb{R}^2)}\le e^{Ct}C, \tag{1.2.32}
$$

for every $t\ge 0$ and a constant $C>0$ independent on ε.

Proof. Thanks to (1.1.12), (1.1.13), (1.2.21), we have

$$
\begin{aligned}
0\le\rho^0_\varepsilon&=\underbrace{\mathscr{A}(\phi_\varepsilon)\omega}_{\le c}\int_0^\infty\rho_\varepsilon\chi_3\mathrm{d}a,\\
|\nabla_x\rho^0_\varepsilon|&\le\underbrace{|\mathscr{A}'(\phi_\varepsilon)||\omega|\int_0^\infty\rho_\varepsilon\chi_3\mathrm{d}a}_{\le c}\left|\nabla_x\phi_\varepsilon\right|+\underbrace{\mathscr{A}(\phi_\varepsilon)|\omega|}_{\le c}\left|\nabla_x\int_0^\infty\rho_\varepsilon\chi_3\mathrm{d}a\right|+\underbrace{\mathscr{A}(\phi_\varepsilon)|\nabla_x\omega|}_{\le c}\int_0^\infty\rho_\varepsilon\chi_3\mathrm{d}a,\\
|D_x^2\rho^0_\varepsilon|&\le\underbrace{|\mathscr{A}'(\phi_\varepsilon)||\omega|\int_0^\infty\rho_\varepsilon\chi_3\mathrm{d}a}_{\le c}\left|D_x^2\phi_\varepsilon\right|+\underbrace{|\mathscr{A}''(\phi_\varepsilon)||\omega|\int_0^\infty\rho_\varepsilon\chi_3\mathrm{d}a}_{\le c}\left|\nabla_x\phi_\varepsilon\right|^2\\
&\quad+\underbrace{\mathscr{A}(\phi_\varepsilon)|\omega|}_{\le c}\left|D_x^2\int_0^\infty\rho_\varepsilon\chi_3\mathrm{d}a\right|+\underbrace{\mathscr{A}(\phi_\varepsilon)|D_x^2\omega|}_{\le c}\int_0^\infty\rho_\varepsilon\chi_3\mathrm{d}a+\underbrace{2|\mathscr{A}'(\phi_\varepsilon)||\nabla_x\omega|\int_0^\infty\rho_\varepsilon\chi_3\mathrm{d}a}_{\le c}\left|\nabla_x\phi_\varepsilon\right|
\end{aligned}
$$

$$+\underbrace{2|\mathscr{A}'(\phi_\varepsilon)||\omega|}_{\le c}\left|\nabla_x\int_0^\infty \rho_\varepsilon\chi_3\mathrm{d}a\right|\left|\nabla_x\phi_\varepsilon\right|+\underbrace{2|\mathscr{A}(\phi_\varepsilon)||\nabla_x\omega|}_{\le c}\left|\nabla_x\int_0^\infty \rho_\varepsilon\chi_3\mathrm{d}a\right|,$$

$$|\partial_t\rho_\varepsilon^0|\le\underbrace{|\mathscr{A}'(\phi_\varepsilon)||\omega|\int_0^\infty \rho_\varepsilon\chi_3\mathrm{d}a}_{\le c}\left|\partial_t\phi_\varepsilon\right|+\underbrace{\mathscr{A}(\phi_\varepsilon)|\omega|}_{\le c}\left|\partial_t\int_0^\infty \rho_\varepsilon\chi_3\mathrm{d}a\right|+\underbrace{\mathscr{A}(\phi_\varepsilon)|\partial_t\omega|}_{\le c}\int_0^\infty \rho_\varepsilon\chi_3\mathrm{d}a.$$

Therefore, (1.2.29), (1.2.30), (1.2.31), and (1.2.32) follow from (1.2.22), (1.2.23), (1.2.24), (1.2.25), (1.2.26), and (1.2.27). □

Lemma 1.3 (L^∞ **estimate on** ρ_ε)**.** *We have that*

$$\left\|\rho_\varepsilon(t,\cdot,\cdot)\right\|_{L^\infty((0,\infty)\times\mathbb{R}^2)}\le Ce^{Ct}, \tag{1.2.33}$$

for every $t\ge 0$.

Proof. Let c be a positive constant that will be fixed later. Define

$$\overline{\rho}_\varepsilon(t,a,x)=e^{-ct}\rho_\varepsilon(t,a,x).$$

$\overline{\rho}_\varepsilon$ satisfies the problem

$$\begin{cases}\partial_t\overline{\rho}_\varepsilon+c\overline{\rho}_\varepsilon+\partial_a\overline{\rho}_\varepsilon+\mathrm{div}_x\left(\overline{\rho}_\varepsilon\chi_1(a)\mathbf{v}Y_\theta(\phi_\varepsilon-R)\right)=\mu\Delta_x\overline{\rho}_\varepsilon+\varepsilon\partial_{aa}^2\overline{\rho}_\varepsilon-\mathfrak{d}\overline{\rho}_\varepsilon, & (t,a,x)\in(0,\infty)\times(0,\infty)\times\mathbb{R}^2,\\ \overline{\rho}_\varepsilon(t,0,x)=\mathscr{A}\left(\phi_\varepsilon\right)\left(\int_0^\infty\overline{\rho}_\varepsilon(t,a,x)\chi_3(a)\mathrm{d}a\right)\omega(t,x), & (t,x)\in(0,\infty)\times\mathbb{R}^2,\\ \overline{\rho}_\varepsilon(0,a,x)=\rho_{0,\varepsilon}(a,x), & (a,x)\in(0,\infty)\times\mathbb{R}^2.\end{cases} \tag{1.2.34}$$

Moreover, for any given $T>0$ there exists a sufficiently large constant $k>0$ such that for any $t\le T$ and $x\in\mathbb{R}^2$ (1.2.18), (1.2.21), and (1.2.32) imply

$$0\le\overline{\rho}_\varepsilon(t,0,x),\ \rho_{0,\varepsilon}(a,x)\le k. \tag{1.2.35}$$

Consider the function

$$\xi\mapsto\eta(\xi)=(\xi-k)\mathbb{1}_{(k,\infty)}(\xi),$$

and observe that

$$\eta'(\xi)=\mathbb{1}_{(k,\infty)}(\xi),\qquad \xi\eta'(\xi)=\eta(\xi)+k\eta'(\xi).$$

From the equation in problem (1.2.34) we obtain

$$
\begin{aligned}
&\frac{d}{dt}\int_0^\infty\int_{\mathbb{R}^2}\eta(\overline{\rho}_\varepsilon)\mathrm{d}x\,\mathrm{d}a=\int_0^\infty\int_{\mathbb{R}^2}\eta'(\overline{\rho}_\varepsilon)\partial_t\overline{\rho}_\varepsilon\mathrm{d}x\,\mathrm{d}a\\
&=-c\int_0^\infty\int_{\mathbb{R}^2}\eta'(\overline{\rho}_\varepsilon)\overline{\rho}_\varepsilon\mathrm{d}x\,\mathrm{d}a-\int_0^\infty\int_{\mathbb{R}^2}\eta'(\overline{\rho}_\varepsilon)\partial_a\overline{\rho}_\varepsilon\mathrm{d}x\,\mathrm{d}a-\int_0^\infty\int_{\mathbb{R}^2}\mathrm{div}_x\left(\overline{\rho}_\varepsilon\chi_1\mathbf{v}Y_\theta\right)\eta'(\overline{\rho}_\varepsilon)\mathrm{d}x\,\mathrm{d}a\\
&\quad+\mu\int_0^\infty\int_{\mathbb{R}^2}\eta'(\overline{\rho}_\varepsilon)\Delta_x\overline{\rho}_\varepsilon\mathrm{d}x\,\mathrm{d}a\underbrace{-\int_0^\infty\int_{\mathbb{R}^2}\eta'(\overline{\rho}_\varepsilon)\mathfrak{d}\overline{\rho}_\varepsilon\mathrm{d}x\,\mathrm{d}a}_{\leq 0}+\varepsilon\int_0^\infty\int_{\mathbb{R}^2}\eta'(\overline{\rho}_\varepsilon)\partial_{aa}^2\overline{\rho}_\varepsilon\mathrm{d}x\,\mathrm{d}a\\
&\leq\underbrace{-c\int_0^\infty\int_{\mathbb{R}^2}\eta(\overline{\rho}_\varepsilon)\mathrm{d}x\,\mathrm{d}a}_{\leq 0}-ck\int_0^\infty\int_{\mathbb{R}^2}\eta'(\overline{\rho}_\varepsilon)\mathrm{d}x\,\mathrm{d}a+\int_{\mathbb{R}^2}\eta(\overline{\rho}_\varepsilon(t,0,x))dx\\
&\quad-\int_0^\infty\int_{\mathbb{R}^2}\mathrm{div}_x\left((\overline{\rho}_\varepsilon-k)\chi_1\mathbf{v}Y_\theta\right)\eta'(\overline{\rho}_\varepsilon)\mathrm{d}x\,\mathrm{d}a\\
&\quad-k\int_0^\infty\int_{\mathbb{R}^2}\mathrm{div}_x\left(\chi_1\mathbf{v}Y_\theta\right)\eta'(\overline{\rho}_\varepsilon)\mathrm{d}x\,\mathrm{d}a\underbrace{-\mu\int_0^\infty\int_{\mathbb{R}^2}\eta''(\overline{\rho}_\varepsilon)\left(\nabla_x\overline{\rho}_\varepsilon\right)^2\mathrm{d}x\,\mathrm{d}a}_{\leq 0}\\
&\quad-\varepsilon\int_{\mathbb{R}^2}\eta'(\overline{\rho}_\varepsilon(t,0,x))\partial_a\overline{\rho}_\varepsilon(t,0,x)dx\underbrace{-\varepsilon\int_0^\infty\int_{\mathbb{R}^2}\eta''(\overline{\rho}_\varepsilon)(\partial_a\overline{\rho}_\varepsilon)^2dadx}_{\leq 0}\\
&\leq\int_{\mathbb{R}^2}\eta(\overline{\rho}_\varepsilon(t,0,x))dx+\underbrace{\int_0^\infty\int_{\mathbb{R}^2}(\overline{\rho}_\varepsilon-k)\chi_1(\mathbf{v}\cdot\nabla_x\overline{\rho}_\varepsilon)Y_\theta\eta''(\overline{\rho}_\varepsilon)\mathrm{d}x\,\mathrm{d}a}_{=0}\\
&\quad-k\int_0^\infty\int_{\mathbb{R}^2}(c+\mathrm{div}_x\left(\chi_1\mathbf{v}Y_\theta\right))\eta'(\overline{\rho}_\varepsilon)\mathrm{d}x\,\mathrm{d}a-\varepsilon\int_{\mathbb{R}^2}\eta'(\overline{\rho}_\varepsilon(t,0,x))\partial_a\overline{\rho}_\varepsilon(t,0,x)dx.
\end{aligned}
$$

Thanks to (1.1.13), (1.2.35), and (1.2.27) we notice that for c large enough

$$
\eta(\overline{\rho}_\varepsilon(t,0,x))=0,\qquad\eta'(\overline{\rho}_\varepsilon(t,0,x))=0,\qquad c+\mathrm{div}_x\left(\chi_1\mathbf{v}Y_\theta\right)\geq 0,
$$

which imply

$$
\frac{d}{dt}\int_0^\infty\int_{\mathbb{R}^2}\eta(\overline{\rho}_\varepsilon)\mathrm{d}x\,\mathrm{d}a\leq 0.
$$

Thus, we integrate over $(0,t)$ and recalling the inequalities (1.2.35) we obtain

$$
0\leq\int_0^\infty\int_{\mathbb{R}^2}\eta(\overline{\rho}_\varepsilon(t,a,x))\mathrm{d}x\,\mathrm{d}a\leq\int_0^\infty\int_{\mathbb{R}^2}\eta(\rho_{0,\varepsilon}(a,x))\mathrm{d}x\,\mathrm{d}a=0,
$$

and

$$
\eta(\overline{\rho}_\varepsilon(t,a,x))=0.
$$

As a consequence we have that $\overline{\rho}_\varepsilon\leq k$. □

Lemma 1.4 (L^1 **estimate on** ρ_ε)**.** *We have that*

$$\left\|\rho_\varepsilon(t,\cdot,\cdot)\right\|_{L^1((0,\infty)\times\mathbb{R}^2)} \leq Ce^{Ct}, \tag{1.2.36}$$

for every $t \geq 0$.

Proof. Let $\lambda \in C^\infty([0,\infty))$ be a nonincreasing nonnegative function with support concentrated in 0 where it takes value 1, more precisely

$$\lambda' \leq 0 \leq \lambda, \quad \lambda(0) = 1, \quad \lambda\chi_1 \equiv 0. \tag{1.2.37}$$

In practice, as we can assume without loss of generality that $\theta < A_1/4$, we could set $\lambda(a) = Y_\theta(A_1/2 - a)$, but this specific expression plays no role in the following.

Consider the function

$$r_\varepsilon(t,a,x) = \rho_\varepsilon(t,a,x) - \lambda(a)\rho_\varepsilon(t,0,x).$$

Clearly r_ε satisfies the boundary condition

$$r_\varepsilon(t,0,x) = 0 \tag{1.2.38}$$

and the equation

$$\begin{aligned} \partial_t r_\varepsilon + \partial_a r_\varepsilon + \operatorname{div}_x\left(r_\varepsilon\chi_1\mathbf{v}Y_\theta\right) - \mu\Delta_x r_\varepsilon - \varepsilon\partial^2_{aa} r_\varepsilon + \mathfrak{d} r_\varepsilon \\ = \lambda\left(\mu\Delta_x\rho^0_\varepsilon - \partial_t\rho^0_\varepsilon - \mathfrak{d}\rho^0_\varepsilon\right) - \lambda'\rho^0_\varepsilon + \varepsilon\lambda''\rho^0_\varepsilon. \end{aligned} \tag{1.2.39}$$

Multiplying both sides of (1.2.39) by $\operatorname{sign}(r_\varepsilon)$ and using [2, Lemma 2]

$$\begin{aligned} &\frac{d}{dt}\int_0^\infty\int_{\mathbb{R}^2}|r_\varepsilon|\mathrm{d}x\,\mathrm{d}a = \int_0^\infty\int_{\mathbb{R}^2}\partial_t r_\varepsilon\operatorname{sign}(r_\varepsilon)\,\mathrm{d}x\,\mathrm{d}a \\ &= \underbrace{-\int_0^\infty\int_{\mathbb{R}^2}\partial_a r_\varepsilon\operatorname{sign}(r_\varepsilon)\,\mathrm{d}x\,\mathrm{d}a - \int_0^\infty\int_{\mathbb{R}^2}\operatorname{div}_x\left(r_\varepsilon\chi_1\mathbf{v}Y_\theta\right)\operatorname{sign}(r_\varepsilon)\,\mathrm{d}x\,\mathrm{d}a}_{=0} \\ &\underbrace{+\mu\int_0^\infty\int_{\mathbb{R}^2}\Delta_x r_\varepsilon\operatorname{sign}(r_\varepsilon)\,\mathrm{d}x\,\mathrm{d}a + \varepsilon\int_0^\infty\int_{\mathbb{R}^2}\partial^2_{aa} r_\varepsilon\operatorname{sign}(r_\varepsilon)\,\mathrm{d}x\,\mathrm{d}a - \int_0^\infty\int_{\mathbb{R}^2}\mathfrak{d}|r_\varepsilon|\mathrm{d}x\,\mathrm{d}a}_{\leq 0} \\ &+\int_0^\infty\int_{\mathbb{R}^2}\lambda\left(\mu\Delta_x\rho^0_\varepsilon - \partial_t\rho^0_\varepsilon - \mathfrak{d}\rho^0_\varepsilon\right)\operatorname{sign}(r_\varepsilon)\,\mathrm{d}x\,\mathrm{d}a \\ &-\int_0^\infty\int_{\mathbb{R}^2}\lambda'\rho^0_\varepsilon\operatorname{sign}(r_\varepsilon)\,\mathrm{d}x\,\mathrm{d}a + \varepsilon\int_0^\infty\int_{\mathbb{R}^2}\lambda''\rho^0_\varepsilon\operatorname{sign}(r_\varepsilon)\,\mathrm{d}x\,\mathrm{d}a \\ &\leq \|\lambda\|_{L^1(0,\infty)}\int_{\mathbb{R}^2}\left|\mu\Delta_x\rho^0_\varepsilon - \partial_t\rho^0_\varepsilon - \mathfrak{d}\rho^0_\varepsilon\right|dx + \left(\|\lambda'\|_{L^1(0,\infty)} + \varepsilon\|\lambda''\|_{L^1(0,\infty)}\right)\int_{\mathbb{R}^2}\rho^0_\varepsilon dx, \end{aligned}$$

Integrating over $(0,t)$ and using (1.2.18), Corollary 1.1

$$\|r_\varepsilon(t,\cdot,\cdot)\|_{L^1((0,\infty)\times\mathbb{R}^2)} \leq Ce^{Ct}.$$

Finally, using again Corollary 1.1,

$$\left\|\rho_\varepsilon(t,\cdot,\cdot)\right\|_{L^1((0,\infty)\times\mathbb{R}^2)} \leq \|r_\varepsilon(t,\cdot,\cdot)\|_{L^1((0,\infty)\times\mathbb{R}^2)} + \|\lambda\|_{L^1(0,\infty)}\left\|\rho^0_\varepsilon(t,\cdot)\right\|_{L^1(\mathbb{R}^2)} \leq Ce^{Ct},$$

that is (1.2.36). □

Lemma 1.5 (L^2 **estimate on** ρ_ε)**.** *We have that*

$$\left\|\rho_\varepsilon(t,\cdot,\cdot)\right\|_{L^2((0,\infty)\times\mathbb{R}^2)}, \left\|\nabla_x\rho_\varepsilon\right\|_{L^2((0,t)\times(0,\infty)\times\mathbb{R}^2)}, \sqrt{\varepsilon}\left\|\partial_a\rho_\varepsilon\right\|_{L^2((0,t)\times(0,\infty)\times\mathbb{R}^2)} \le Ce^{Ct} \tag{1.2.40}$$

for every $t \ge 0$.

Proof. We argue as in the proof of Lemma 1.4 and we prove first an L^2 estimate on r_ε.

We multiply both sides of (1.2.39) by r_ε

$$\begin{aligned}
&\frac{d}{dt}\int_0^\infty\int_{\mathbb{R}^2}\frac{r_\varepsilon^2}{2}\mathrm{d}x\,\mathrm{d}a = \int_0^\infty\int_{\mathbb{R}^2} r_\varepsilon\partial_t r_\varepsilon\mathrm{d}x\,\mathrm{d}a\\
&= \underbrace{-\int_0^\infty\int_{\mathbb{R}^2} r_\varepsilon\partial_a r_\varepsilon\mathrm{d}x\,\mathrm{d}a}_{=0} - \int_0^\infty\int_{\mathbb{R}^2}\mathrm{div}_x\left(r_\varepsilon\chi_1\mathbf{v}Y_\theta\right)r_\varepsilon\mathrm{d}x\,\mathrm{d}a\\
&\quad+\mu\int_0^\infty\int_{\mathbb{R}^2} r_\varepsilon\Delta_x r_\varepsilon\mathrm{d}x\,\mathrm{d}a+\varepsilon\int_0^\infty\int_{\mathbb{R}^2} r_\varepsilon\partial_{aa}^2 r_\varepsilon\mathrm{d}x\,\mathrm{d}a-\int_0^\infty\int_{\mathbb{R}^2}\mathfrak{d}r_\varepsilon^2\mathrm{d}x\,\mathrm{d}a\\
&\quad+\int_0^\infty\int_{\mathbb{R}^2}\lambda\left(\mu\Delta_x\rho_\varepsilon^0-\partial_t\rho_\varepsilon^0-\mathfrak{d}\rho_\varepsilon^0\right)r_\varepsilon\mathrm{d}x\,\mathrm{d}a-\int_0^\infty\int_{\mathbb{R}^2}\lambda'\rho_\varepsilon^0 r_\varepsilon\mathrm{d}x\,\mathrm{d}a+\varepsilon\int_0^\infty\int_{\mathbb{R}^2}\lambda''\rho_\varepsilon^0 r_\varepsilon\mathrm{d}x\,\mathrm{d}a\\
&\le\int_0^\infty\int_{\mathbb{R}^2} r_\varepsilon\chi_1 Y_\theta\mathbf{v}\cdot\nabla_x r_\varepsilon\mathrm{d}x\,\mathrm{d}a-\mu\int_0^\infty\int_{\mathbb{R}^2}|\nabla_x r_\varepsilon|^2\mathrm{d}x\,\mathrm{d}a-\varepsilon\int_0^\infty\int_{\mathbb{R}^2}(\partial_a r_\varepsilon)^2\mathrm{d}x\,\mathrm{d}a\\
&\quad+\int_0^\infty\int_{\mathbb{R}^2}\lambda\left(\mu\Delta_x\rho_\varepsilon^0-\partial_t\rho_\varepsilon^0-\mathfrak{d}\rho_\varepsilon^0\right)r_\varepsilon\mathrm{d}x\,\mathrm{d}a+\int_0^\infty\int_{\mathbb{R}^2}\left(\varepsilon\lambda''-\lambda'\right)\rho_\varepsilon^0 r_\varepsilon\mathrm{d}x\,\mathrm{d}a\\
&=-\int_0^\infty\int_{\mathbb{R}^2}\frac{r_\varepsilon^2}{2}\underbrace{\mathrm{div}_x\left(\chi_1 Y_\theta\mathbf{v}\right)}_{\le c}\mathrm{d}x\,\mathrm{d}a-\mu\int_0^\infty\int_{\mathbb{R}^2}|\nabla_x r_\varepsilon|^2\mathrm{d}x\,\mathrm{d}a-\varepsilon\int_0^\infty\int_{\mathbb{R}^2}(\partial_a r_\varepsilon)^2\mathrm{d}x\,\mathrm{d}a\\
&\quad+\int_0^\infty\int_{\mathbb{R}^2}\lambda\left(\mu\Delta_x\rho_\varepsilon^0-\partial_t\rho_\varepsilon^0-\mathfrak{d}\rho_\varepsilon^0\right)r_\varepsilon\mathrm{d}x\,\mathrm{d}a+\int_0^\infty\int_{\mathbb{R}^2}\left(\varepsilon\lambda''-\lambda'\right)\rho_\varepsilon^0 r_\varepsilon\mathrm{d}x\,\mathrm{d}a\\
&\le c\int_0^\infty\int_{\mathbb{R}^2} r_\varepsilon^2\mathrm{d}x\,\mathrm{d}a-\mu\int_0^\infty\int_{\mathbb{R}^2}|\nabla_x r_\varepsilon|^2\mathrm{d}x\,\mathrm{d}a-\varepsilon\int_0^\infty\int_{\mathbb{R}^2}(\partial_a r_\varepsilon)^2\mathrm{d}x\,\mathrm{d}a\\
&\quad+c\left\|\lambda\right\|_{L^2(0,\infty)}^2\int_{\mathbb{R}^2}\left(\mu^2(\Delta_x\rho_\varepsilon^0)^2+(\partial_t\rho_\varepsilon^0)^2+\mathfrak{d}^2(\rho_\varepsilon^0)^2\right)\mathrm{d}x\\
&\quad+c\left(\varepsilon^2\left\|\lambda''\right\|_{L^2(0,\infty)}^2+\left\|\lambda'\right\|_{L^2(0,\infty)}^2\right)\int_{\mathbb{R}^2}(\rho_\varepsilon^0)^2\mathrm{d}x.
\end{aligned}$$

We integrate the inequality above over $(0,t)$ and the claim follows from (1.2.18), Gronwall Lemma and Corollary 1.1. □

Lemma 1.6 (H^2 **estimate on** ρ_ε)**.** *We have that*

$$\left\|\nabla_x\rho_\varepsilon(t,\cdot,\cdot)\right\|_{L^2((0,\infty)\times\mathbb{R}^2)}, \left\|D_x^2\rho_\varepsilon\right\|_{L^2((0,t)\times(0,\infty)\times\mathbb{R}^2)}, \sqrt{\varepsilon}\left\|\partial_a\nabla_x\rho_\varepsilon\right\|_{L^2((0,t)\times(0,\infty)\times\mathbb{R}^2)} \le Ce^{Ct} \tag{1.2.41}$$

for every $t \ge 0$.

Proof. We argue as in the proof of Lemma 1.4 and we prove first an H^2 estimate on r_ε.

We multiply both sides of (1.2.39) by $-\Delta_x r_\varepsilon$

$$\begin{aligned}
&\frac{d}{dt}\int_0^\infty\int_{\mathbb{R}^2}\frac{|\nabla_x r_\varepsilon|^2}{2}\mathrm{d}x\,\mathrm{d}a=\int_0^\infty\int_{\mathbb{R}^2}\nabla_x r_\varepsilon\cdot\partial_t\nabla_x r_\varepsilon\mathrm{d}x\,\mathrm{d}a=-\int_0^\infty\int_{\mathbb{R}^2}\Delta_x r_\varepsilon\partial_t r_\varepsilon\mathrm{d}x\,\mathrm{d}a\\
&=\int_0^\infty\int_{\mathbb{R}^2}\Delta_x r_\varepsilon\partial_a r_\varepsilon\mathrm{d}x\,\mathrm{d}a+\int_0^\infty\int_{\mathbb{R}^2}\mathrm{div}_x\left(r_\varepsilon\chi_1\mathbf{v}Y_\theta\right)\Delta_x r_\varepsilon\mathrm{d}x\,\mathrm{d}a\\
&\quad-\mu\int_0^\infty\int_{\mathbb{R}^2}(\Delta_x r_\varepsilon)^2\mathrm{d}x\,\mathrm{d}a-\varepsilon\int_0^\infty\int_{\mathbb{R}^2}\Delta_x r_\varepsilon\partial_{aa}^2 r_\varepsilon\mathrm{d}x\,\mathrm{d}a+\int_0^\infty\int_{\mathbb{R}^2}\mathfrak{d}r_\varepsilon\Delta_x r_\varepsilon\mathrm{d}x\,\mathrm{d}a\\
&\quad-\int_0^\infty\int_{\mathbb{R}^2}\lambda\left(\mu\Delta_x\rho_\varepsilon^0-\partial_t\rho_\varepsilon^0-\mathfrak{d}\rho_\varepsilon^0\right)\Delta_x r_\varepsilon\mathrm{d}x\,\mathrm{d}a+\int_0^\infty\int_{\mathbb{R}^2}\lambda'\rho_\varepsilon^0\Delta_x r_\varepsilon\mathrm{d}x\,\mathrm{d}a-\varepsilon\int_0^\infty\int_{\mathbb{R}^2}\lambda''\rho_\varepsilon^0\Delta_x r_\varepsilon\mathrm{d}x\,\mathrm{d}a\\
&=\underbrace{-\int_0^\infty\int_{\mathbb{R}^2}\partial_a\left(\frac{|\nabla_x r_\varepsilon|^2}{2}\right)\mathrm{d}x\,\mathrm{d}a}_{=0}+\int_0^\infty\int_{\mathbb{R}^2}\nabla_x r_\varepsilon\cdot\mathbf{v}\chi_1 Y_\theta\Delta_x r_\varepsilon\mathrm{d}x\,\mathrm{d}a+\int_0^\infty\int_{\mathbb{R}^2}r_\varepsilon\mathrm{div}_x\left(\chi_1\mathbf{v}Y_\theta\right)\Delta_x r_\varepsilon\mathrm{d}x\,\mathrm{d}a\\
&\quad-\mu\int_0^\infty\int_{\mathbb{R}^2}(\Delta_x r_\varepsilon)^2\mathrm{d}x\,\mathrm{d}a-\varepsilon\int_0^\infty\int_{\mathbb{R}^2}|\nabla_x\partial_a r_\varepsilon|^2\mathrm{d}x\,\mathrm{d}a+\int_0^\infty\int_{\mathbb{R}^2}\mathfrak{d}r_\varepsilon\Delta_x r_\varepsilon\mathrm{d}x\,\mathrm{d}a\\
&\quad-\int_0^\infty\int_{\mathbb{R}^2}\lambda\left(\mu\Delta_x\rho_\varepsilon^0-\partial_t\rho_\varepsilon^0-\mathfrak{d}\rho_\varepsilon^0\right)\Delta_x r_\varepsilon\mathrm{d}x\,\mathrm{d}a+\int_0^\infty\int_{\mathbb{R}^2}\lambda'\rho_\varepsilon^0\Delta_x r_\varepsilon\mathrm{d}x\,\mathrm{d}a-\varepsilon\int_0^\infty\int_{\mathbb{R}^2}\lambda''\rho_\varepsilon^0\Delta_x r_\varepsilon\mathrm{d}x\,\mathrm{d}a\\
&\le-\frac{\mu}{2}\int_0^\infty\int_{\mathbb{R}^2}(\Delta_x r_\varepsilon)^2\mathrm{d}x\,\mathrm{d}a-\varepsilon\int_0^\infty\int_{\mathbb{R}^2}|\nabla_x\partial_a r_\varepsilon|^2\mathrm{d}x\,\mathrm{d}a\\
&\quad+c\int_0^\infty\int_{\mathbb{R}^2}((r_\varepsilon)^2+|\nabla_x r_\varepsilon|^2+\lambda^2\left(\Delta_x\rho_\varepsilon^0\right)^2+\lambda^2(\partial_t\rho_\varepsilon^0)^2+(\lambda^2+(\lambda')^2+(\lambda'')^2)(\rho_\varepsilon^0)^2))\mathrm{d}x\,\mathrm{d}a.
\end{aligned}$$

Therefore, the claim follows from (1.2.18), the Gronwall Lemma, Corollary 1.1, and Lemma 1.5. □

Lemma 1.7 (L^1 **estimate on** $\partial_a\rho_\varepsilon$)**.** *We have that*

$$\left\|\partial_a\rho_\varepsilon(t,\cdot,\cdot)\right\|_{L^1((0,\infty)\times\mathbb{R}^2)}\le Ce^{Ct},$$

for every $t\ge 0$ *and a suitable constant* C *independent on* ε.

Proof. Observe that differentiating the equation in (1.2.19) with respect to a we get

$$\begin{aligned}
&\partial_{ta}^2\rho_\varepsilon+\partial_{aa}^2\rho_\varepsilon+\mathrm{div}_x\left(\partial_a\rho_\varepsilon\chi_1\mathbf{v}Y_\theta\right)+\mathrm{div}_x\left(\rho_\varepsilon\chi_1'\mathbf{v}Y_\theta\right)\\
&\qquad=\mu\Delta_x\partial_a\rho_\varepsilon+\varepsilon\partial_{aaa}^3\rho_\varepsilon-\partial_a\mathfrak{d}\rho_\varepsilon-\mathfrak{d}\partial_a\rho_\varepsilon.
\end{aligned}\tag{1.2.42}$$

Using [2, Lemma 2] we get

$$\begin{aligned}
&\frac{d}{dt}\int_0^\infty\int_{\mathbb{R}^2}|\partial_a\rho_\varepsilon|\mathrm{d}x\,\mathrm{d}a=\int_0^\infty\int_{\mathbb{R}^2}\partial_{ta}^2\rho_\varepsilon\mathrm{sign}\left(\partial_a\rho_\varepsilon\right)\mathrm{d}x\,\mathrm{d}a\\
&=\int_0^\infty\int_{\mathbb{R}^2}(\varepsilon\partial_{aaa}^3\rho_\varepsilon-\partial_{aa}^2\rho_\varepsilon)\mathrm{sign}\left(\partial_a\rho_\varepsilon\right)\mathrm{d}x\,\mathrm{d}a\underbrace{+\mu\int_0^\infty\int_{\mathbb{R}^2}\Delta_x\partial_a\rho_\varepsilon\mathrm{sign}\left(\partial_a\rho_\varepsilon\right)\mathrm{d}x\,\mathrm{d}a}_{\le 0}\\
&\underbrace{-\int_0^\infty\int_{\mathbb{R}^2}\mathrm{div}_x\left(\partial_a\rho_\varepsilon\chi_1\mathbf{v}Y_\theta\right)\mathrm{sign}\left(\partial_a\rho_\varepsilon\right)\mathrm{d}x\,\mathrm{d}a}_{=0}-\int_0^\infty\int_{\mathbb{R}^2}\nabla_x\rho_\varepsilon\cdot\mathbf{v}\chi_1' Y_\theta\mathrm{sign}\left(\partial_a\rho_\varepsilon\right)\mathrm{d}x\,\mathrm{d}a
\end{aligned}$$

$$
\begin{aligned}
&-\int_0^\infty\int_{\mathbb{R}^2}\rho_\varepsilon\chi_1'\mathrm{div}_x(\mathbf{v})\,Y_\theta\mathrm{sign}\left(\partial_a\rho_\varepsilon\right)\mathrm{d}x\,\mathrm{d}a-\int_0^\infty\int_{\mathbb{R}^2}\rho_\varepsilon\chi_1'\mathbf{v}\cdot\nabla_x\phi_\varepsilon\,Y_\theta'\mathrm{sign}\left(\partial_a\rho_\varepsilon\right)\mathrm{d}x\,\mathrm{d}a\\
&-\int_0^\infty\int_{\mathbb{R}^2}\partial_a\mathfrak{d}\rho_\varepsilon\mathrm{sign}\left(\partial_a\rho_\varepsilon\right)\mathrm{d}x\,\mathrm{d}a\underbrace{-\int_0^\infty\int_{\mathbb{R}^2}\mathfrak{d}|\partial_a\rho_\varepsilon|\mathrm{d}x\,\mathrm{d}a}_{\leq 0}\\
\leq&\int_{\mathbb{R}^2}|(\varepsilon\partial_{aa}^2\rho_\varepsilon-\partial_a\rho_\varepsilon)(t,0,x)|dx+c\left\|\nabla_x\rho_\varepsilon(t,\cdot,\cdot)\right\|_{L^2((0,\infty)\times\mathbb{R}^2)}\|\mathbf{v}\|_{L^2(\mathbb{R}^2)}\\
&+c\left\|\rho_\varepsilon(t,\cdot,\cdot)\right\|_{L^2((0,\infty)\times\mathbb{R}^2)}\|\mathrm{div}_x(\mathbf{v})\|_{L^2(\mathbb{R}^2)}+c\left\|\rho_\varepsilon(t,\cdot,\cdot)\right\|_{L^2((0,\infty)\times\mathbb{R}^2)}\left\|\nabla_x\phi_\varepsilon(t,\cdot)\right\|_{L^2(\mathbb{R}^2)}\\
&+c\left\|\rho_\varepsilon(t,\cdot,\cdot)\right\|_{L^1((0,\infty)\times\mathbb{R}^2)}.
\end{aligned}
$$

Since

$$
(\varepsilon\partial_{aa}^2\rho_\varepsilon-\partial_a\rho_\varepsilon)(t,0,x)=\partial_t\rho_\varepsilon^0-\mu\Delta_x\rho_\varepsilon^0+\mathfrak{d}\rho_\varepsilon^0,
$$

the claim follows from (1.2.18), (1.2.24), the Gronwall Lemma, Corollary 1.1, Lemma 1.4 and Lemma 1.5. □

1.2.2 Convergence to an entropy weak solution

We are now ready to prove the existence of a converging subsequence of $\{\rho_\varepsilon\}_\varepsilon$. To this end we apply the multidimensional compensated compactness result introduced by Panov in [35, 36], which does not require estimates on $\{\partial_t\rho_\varepsilon\}_\varepsilon$. For the reader's convenience we recall the exact statement by Panov in Lemma 1.8. It should be noticed, however, that the application of this technique to our setting is not straightforward, as the flux of our equation does not satisfy the hypothesis of the lemma. We can overcome this difficulty, as it has been done in [12, 7], because we have estimates on $\{\nabla_{(a,x)}\rho_\varepsilon\}_\varepsilon$. Namely, we rewrite (1.2.19) as follows

$$
\begin{aligned}
\partial_t\rho_\varepsilon+\mathrm{div}_{(a,x)}\begin{pmatrix}\rho_\varepsilon^2/2\\ \rho_\varepsilon^2/2\end{pmatrix}&=(\rho_\varepsilon-1)\partial_a\rho_\varepsilon+\rho_\varepsilon\mathrm{div}_x\left(\rho_\varepsilon\right)\\
&\quad-\mathrm{div}_x\left(\rho_\varepsilon\chi_1(a)\mathbf{v}Y_\theta(\phi_\varepsilon-R)\right)+\mu\Delta_x\rho_\varepsilon+\varepsilon\partial_{aa}^2\rho_\varepsilon-\mathfrak{d}\rho_\varepsilon,
\end{aligned}
\tag{1.2.43}
$$

and we consider the original flux of the equation as a part of the source term.

Lemma 1.8 (Theorem 5, in [14]). *Let $\{u_\nu\}_{\nu\in\mathbb{N}}$ be a sequence of functions defined in $[0,\infty)\times\mathbb{R}^d$ with values in $\mathbb{R}$. Assume that*

- *$\{u_\nu\}_{\nu\in\mathbb{N}}$ is bounded in $L^\infty_{loc}((0,\infty)\times\mathbb{R}^d)$;*
- *$F\in C^2(\mathbb{R}^d;\mathbb{R}^d)$ is a genuinely nonlinear vector field, in the sense that for any unit vector $n\in\mathbb{R}^d$ the map $u\in\mathbb{R}^d\mapsto F(u)\cdot n$ is not affine on any non-trivial interval ;*
- *for every convex entropy $\eta\in C^2(\mathbb{R})$ with flux $Q\in C^2(\mathbb{R};\mathbb{R}^d)$ such that $Q'=F'\eta'$ the sequence*

$$
\{\partial_t\eta(u_\nu)+div(Q(u_\nu))\}_{\nu\in\mathbb{N}}
$$

is compact in $H^{-1}_{loc}((0,\infty)\times\mathbb{R}^d)$.

Then there exist a function $u\in L^\infty_{loc}((0,\infty)\times\mathbb{R}^d)$ and a sequence $\{\nu_k\}_{k\in\mathbb{N}}$, $\nu_k\to 0$, such that

$$
u_{\nu_k}\to u,\quad a.e.\ in\ (0,\infty)\times\mathbb{R}^d\quad and\ in\ L^p_{loc}((0,\infty)\times\mathbb{R}^d),\ 1\leq p<\infty.
$$

Lemma 1.9 (**Strong compactness of** $\{\rho_\varepsilon\}_\varepsilon$)**.** *There exist a function* $\rho : [0,\infty)\times[0,\infty)\times\mathbb{R}^2 \to \mathbb{R}$ *and a sequence* $\{\varepsilon_k\}_{k\in\mathbb{N}} \subset (0,\infty)$, $\varepsilon_k \to 0$, *such that for every* $T>0$

$$\begin{aligned}
&\rho_{\varepsilon_k} \to \rho, \quad \text{a.e. in } (0,T)\times(0,\infty)\times\mathbb{R}^2 \quad \text{and in } L^p_{loc}((0,\infty)\times(0,\infty)\times\mathbb{R}^2),\ 1\le p<\infty,\\
&\rho(\cdot,\cdot,\cdot)\ge 0,\\
&\rho \in L^\infty(0,T;L^1((0,\infty)\times\mathbb{R}^2))\cap L^\infty((0,T)\times(0,\infty)\times\mathbb{R}^2)\cap L^2((0,T)\times(0,\infty);H^2(\mathbb{R}^2)),\\
&\rho(t,\cdot,x)\in BV(0,\infty), \quad \text{for a.e. } (t,x)\in(0,\infty)\times\mathbb{R}^2.
\end{aligned} \tag{1.2.44}$$

Proof. We rewrite (1.2.19) as follows

$$\begin{aligned}
\partial_t\rho_\varepsilon + \operatorname{div}_{(a,x)}\begin{pmatrix}\rho_\varepsilon^2/2\\ \rho_\varepsilon^2/2\end{pmatrix} &= (\rho_\varepsilon-1)\partial_a\rho_\varepsilon + \rho_\varepsilon \operatorname{div}_x\left(\rho_\varepsilon\right)\\
&\quad - \operatorname{div}_x\left(\rho_\varepsilon\chi_1(a)\mathbf{v}Y_\theta(\phi_\varepsilon - R)\right) + \mu\Delta_x\rho_\varepsilon + \varepsilon\partial^2_{aa}\rho_\varepsilon - \mathfrak{d}\rho_\varepsilon.
\end{aligned} \tag{1.2.45}$$

Let $\eta\in C^2(\mathbb{R}^2)$ be a convex entropy with flux $Q\in C^2(\mathbb{R};\mathbb{R}^2)$ such that

$$Q'(\rho) = \begin{pmatrix}\rho\eta'(\rho)\\ \rho\eta'(\rho)\end{pmatrix}.$$

Multiplying both sides of (1.2.45) by $\eta'(\rho_\varepsilon)$ we get

$$\begin{aligned}
&\partial_t\eta(\rho_\varepsilon) + \operatorname{div}_{(a,x)}\left(Q(\rho_\varepsilon)\right)\\
&\quad = \underbrace{\eta'(\rho_\varepsilon)\left[(\rho_\varepsilon-1)\partial_a\rho_\varepsilon + \rho_\varepsilon\operatorname{div}_x\left(\rho_\varepsilon\right) - \operatorname{div}_x\left(\rho_\varepsilon\chi_1(a)\mathbf{v}Y_\theta(\phi_\varepsilon-R)\right) + \mu\Delta_x\rho_\varepsilon - \mathfrak{d}\rho_\varepsilon\right]}_{\mathscr{L}_{1,\varepsilon}}\\
&\quad + \underbrace{\varepsilon\partial^2_{aa}\eta(\rho_\varepsilon)}_{\mathscr{L}_{2,\varepsilon}} - \underbrace{\varepsilon\eta''(\rho_\varepsilon)(\partial_a\rho_\varepsilon)^2}_{\mathscr{L}_{3,\varepsilon}}.
\end{aligned} \tag{1.2.46}$$

We claim that

$$\{\mathscr{L}_{1,\varepsilon}\}_\varepsilon \text{ is bounded in } L^1_{loc}((0,\infty)\times(0,\infty)\times\mathbb{R}^2), \tag{1.2.47}$$

$$\{\mathscr{L}_{2,\varepsilon}\}_\varepsilon \text{ is compact in } H^{-1}_{loc}((0,\infty)\times(0,\infty)\times\mathbb{R}^2), \tag{1.2.48}$$

$$\{\mathscr{L}_{3,\varepsilon}\}_\varepsilon \text{ is bounded in } L^1_{loc}((0,\infty)\times(0,\infty)\times\mathbb{R}^2). \tag{1.2.49}$$

Indeed for every $K\subset\subset(0,\infty)\times(0,\infty)\times\mathbb{R}^2$, thanks to Lemmas 1.2, 1.3, 1.4, 1.5, 1.6, 1.7,

$$\begin{aligned}
\left\|\mathscr{L}_{1,\varepsilon}\right\|_{L^1(K)} \le{}& \left\|\eta'(\rho_\varepsilon)\right\|_{L^\infty(K)}\Big[\left(\left\|\rho_\varepsilon\right\|_{L^\infty(K)}+1\right)\left\|\partial_a\rho_\varepsilon\right\|_{L^1(K)} + \left\|\rho_\varepsilon\right\|_{L^2(K)}\left\|\nabla_x\rho_\varepsilon\right\|_{L^2(K)}\\
&+ c\left\|\rho_\varepsilon\right\|_{L^2(K)}\left\|\nabla_x\phi_\varepsilon\right\|_{L^2(K)} + c\left\|\phi_\varepsilon\right\|_{L^2(K)}\left\|\rho_\varepsilon\right\|_{L^2(K)} + c\left\|\phi_\varepsilon\right\|_{L^2(K)}\left\|\nabla_x\rho_\varepsilon\right\|_{L^2(K)}\\
&+ c\left\|\Delta_x\rho_\varepsilon\right\|_{L^2(K)} + \|\mathfrak{d}\|_{L^\infty(K)}\left\|\rho_\varepsilon\right\|_{L^1(K)}\Big] \le c,\\
\mathscr{L}_{2,\varepsilon} ={}& \partial_a(\varepsilon\eta'(\rho_\varepsilon)\partial_a\rho_\varepsilon),\\
\left\|\varepsilon\eta'(\rho_\varepsilon)\partial_a\rho_\varepsilon\right\|_{L^2(K)} \le{}& \varepsilon\left\|\eta'(\rho_\varepsilon)\right\|_{L^\infty(K)}\left\|\partial_a\rho_\varepsilon\right\|_{L^2(K)} \le c\sqrt{\varepsilon}\to 0,\\
\left\|\mathscr{L}_{3,\varepsilon}\right\|_{L^1(K)} \le{}& \varepsilon\left\|\eta''(\rho_\varepsilon)\right\|_{L^\infty(K)}\left\|\partial_a\rho_\varepsilon\right\|^2_{L^2(K)} \le c.
\end{aligned}$$

The Murat Lemma [31] implies that

$$\{\partial_t \eta(\rho_\varepsilon) + \mathrm{div}_{(a,x)}\left(Q(\rho_\varepsilon)\right)\}_\varepsilon \text{ is compact in } H^{-1}_{loc}((0,\infty)\times(0,\infty)\times\mathbb{R}^2).$$

□

Lemma 1.10 (**Existence**). *The function ρ introduced in Lemma 1.9 is an entropy weak solution of (1.1.7) in the sense of Defintion 1.2.*

Proof. Thanks to Lemma 1.9 we have only to verify that (1.1.16) holds. We follow the argument of [2].

Let $\xi \in C^\infty(\mathbb{R}^4)$ be a nonnegative test function with compact support and $k \in \mathbb{R}$ be a constant. Multiplying (1.2.19) by $\mathrm{sign}\left(\rho_\varepsilon - k\right)$ we gain

$$\begin{aligned}\partial_t|\rho_\varepsilon - k| + \partial_a|\rho_\varepsilon - k| + \mathrm{div}_x\left(|\rho_\varepsilon - k|\chi_1 \mathbf{v} Y_\theta(\phi_\varepsilon - R)\right)\\ + k\,\mathrm{sign}\left(\rho_\varepsilon - k\right)\chi_1 \mathrm{div}_x\left(\mathbf{v}Y_\theta(\phi_\varepsilon - R)\right)\\ \leq \mu\Delta_x|\rho_\varepsilon - k| + \varepsilon\partial^2_{aa}|\rho_\varepsilon - k| - \mathrm{sign}\left(\rho_\varepsilon - k\right)\mathfrak{d}\rho_\varepsilon.\end{aligned}$$

testing with ξ

$$\begin{aligned}&\int_0^\infty\int_0^\infty\int_{\mathbb{R}^2}\Big(|\rho_\varepsilon - k|(\partial_t\xi + \partial_a\xi) + |\rho_\varepsilon - k|\chi_1 Y_\theta(\phi_\varepsilon - R)\mathbf{v}\cdot\nabla_x\xi\\ &\qquad - k\,\mathrm{sign}\left(\rho_\varepsilon - k\right)\chi_1\mathrm{div}_x\left(\mathbf{v}Y_\theta(\phi_\varepsilon - R)\right)\xi\\ &\qquad + \mu|\rho_\varepsilon - k|\Delta_x\xi - \varepsilon\partial_a|\rho_\varepsilon - k|\partial_a\xi - \mathrm{sign}\left(\rho_\varepsilon - k\right)\mathfrak{d}\rho_\varepsilon\xi\Big)\mathrm{d}x\,\mathrm{d}a\,\mathrm{d}t\\ &+\int_0^\infty\int_{\mathbb{R}^2}\left(\left|\mathscr{A}\left(\phi_\varepsilon\right)\left(\int_0^\infty \rho_\varepsilon(t,a,x)\chi_3(a)\mathrm{d}a\right)\omega(t,x) - k\right| - \varepsilon\partial_a|\rho_\varepsilon - k|(t,0,x)\right)\xi(t,0,x)\mathrm{d}x\,\mathrm{d}t\\ &+\int_0^\infty\int_{\mathbb{R}^2}|\rho_{0,\varepsilon}(a,x) - k|\xi(0,a,x)\,\mathrm{d}x\,\mathrm{d}a \geq 0.\end{aligned}$$

As $\varepsilon \to 0$, thanks to Lemmas 1.5 and 1.9 and the Dominate Convergence Theorem we gain

$$\begin{aligned}&\int_0^\infty\int_0^\infty\int_{\mathbb{R}^2}\Big(|\rho - k|(\partial_t\xi + \partial_a\xi) + |\rho - k|\chi_1(a)\,Y_\theta(\phi - R)\mathbf{v}\cdot\nabla_x\xi\\ &\qquad - k\,\mathrm{sign}\left(\rho - k\right)\chi_1\mathrm{div}_x\left(\mathbf{v}Y_\theta(\phi - R)\right)\xi + \mu|\rho - k|\Delta_x\xi - \mathrm{sign}\left(\rho - k\right)\mathfrak{d}\rho\xi\Big)\mathrm{d}x\,\mathrm{d}a\,\mathrm{d}t\\ &+\int_0^\infty\int_{\mathbb{R}^2}\left|\mathscr{A}\left(\phi\right)\left(\int_0^\infty \rho(t,a,x)\chi_3(a)\mathrm{d}a\right)\omega(t,x) - k\right|\xi(t,0,x)\mathrm{d}x\,\mathrm{d}t\\ &-\lim_{\varepsilon\to 0}\varepsilon\int_0^\infty\int_{\mathbb{R}^2}\partial_a|\rho_\varepsilon - k|(t,0,x)\xi(t,0,x)\mathrm{d}x\,\mathrm{d}t\\ &+\int_0^\infty\int_{\mathbb{R}^2}|\rho_0(a,x) - k|\xi(0,a,x)\,\mathrm{d}x\,\mathrm{d}a \geq 0.\end{aligned}$$

Thanks to Remark 1.1 we have to prove that

$$\begin{aligned}
&\lim_{\varepsilon\to 0}\varepsilon\int_0^\infty\int_{\mathbb{R}^2}\partial_a|\rho_\varepsilon-k|(t,0,x)\xi(t,0,x)\mathrm{d}x\,\mathrm{d}t\\
&\quad=\int_0^\infty\int_{\mathbb{R}^2}\operatorname{sign}\left(\mathscr{A}(\phi)\left(\int_0^\infty\rho(t,a,x)\chi_3(a)\,\mathrm{d}a\right)\omega(t,x)-k\right)\\
&\qquad\qquad\times\left(\mathscr{A}(\phi)\left(\int_0^\infty\rho(t,a,x)\chi_3(a)\,\mathrm{d}a\right)\omega(t,x)-\rho(t,0^+,x)\right)\xi(t,0,x)\mathrm{d}x\,\mathrm{d}t.
\end{aligned}\tag{1.2.50}$$

Observe that

$$\begin{aligned}
&\varepsilon\int_0^\infty\int_{\mathbb{R}^2}\partial_a|\rho_\varepsilon-k|(t,0,x)\xi(t,0,x)\mathrm{d}x\,\mathrm{d}t\\
&\quad=\varepsilon\int_0^\infty\int_{\mathbb{R}^2}\operatorname{sign}\left(\mathscr{A}(\phi_\varepsilon)\left(\int_0^\infty\rho_\varepsilon(t,a,x)\chi_3(a)\mathrm{d}a\right)\omega(t,x)-k\right)\partial_a\rho_\varepsilon(t,0,x)\xi(t,0,x)\mathrm{d}x\,\mathrm{d}t.
\end{aligned}$$

Therefore, due to Lemma 1.9, in order to prove (1.2.50) it is enough to prove that

$$\begin{aligned}
&\lim_{\varepsilon\to 0}\varepsilon\int_0^\infty\int_{\mathbb{R}^2}\partial_a\rho_\varepsilon(t,0,x)\xi(t,0,x)\mathrm{d}x\,\mathrm{d}t\\
&\quad=\int_0^\infty\int_{\mathbb{R}^2}\left(\mathscr{A}(\phi)\left(\int_0^\infty\rho(t,a,x)\chi_3(a)\,\mathrm{d}a\right)\omega(t,x)-\rho(t,0^+,x)\right)\xi(t,0,x)\mathrm{d}x\,\mathrm{d}t.
\end{aligned}\tag{1.2.51}$$

Consider the cut-off functions $\{\lambda_n\}_n$ such that

$$0\le\lambda_n\le 1,\qquad \lambda_n(0)=1,\qquad \lambda_n\left(\frac{1}{n}\right)=0,\qquad -n\le\lambda_n'\le 0.\tag{1.2.52}$$

Testing (1.2.19) with $\lambda_n(a)\xi(t,a,x)$

$$\begin{aligned}
&\int_0^\infty\int_0^\infty\int_{\mathbb{R}^2}\left(\rho_\varepsilon(\partial_t\xi+\partial_a\xi)+\rho_\varepsilon\chi_1(a)\mathbf{v}\cdot\nabla_x\xi Y_\theta(\phi_\varepsilon-R)+\mu\rho_\varepsilon\Delta_x\xi-\varepsilon\partial_a\rho_\varepsilon\partial_a\xi-\mathfrak{d}\rho_\varepsilon\xi\right)\lambda_n\mathrm{d}x\,\mathrm{d}a\,\mathrm{d}t\\
&\quad+\int_0^\infty\int_0^\infty\int_{\mathbb{R}^2}(\rho_\varepsilon-\varepsilon\partial_a\rho_\varepsilon)\lambda_n'\xi\mathrm{d}x\,\mathrm{d}a\,\mathrm{d}t\\
&\quad+\int_0^\infty\int_0^\infty\int_{\mathbb{R}^2}\mathscr{A}(\phi_\varepsilon)\rho_\varepsilon(t,a,x)\chi_3(a)\omega(t,x)\xi(t,0,x)\mathrm{d}x\,\mathrm{d}a\,\mathrm{d}t\\
&\quad-\varepsilon\int_0^\infty\int_{\mathbb{R}^2}\partial_a\rho_\varepsilon(t,0,x)\xi(t,0,x)\mathrm{d}x\,\mathrm{d}t\\
&\quad+\int_0^\infty\int_{\mathbb{R}^2}\rho_{0,\varepsilon}(a,x)\lambda_n\xi(0,a,x)\mathrm{d}x\,\mathrm{d}a=0.
\end{aligned}$$

Thanks to Lemmas 1.5 and 1.9, as $\varepsilon\to 0$ we get

$$\begin{aligned}
&\lim_{\varepsilon\to 0}\varepsilon\int_0^\infty\int_{\mathbb{R}^2}\partial_a\rho_\varepsilon(t,0,x)\xi(t,0,x)\mathrm{d}x\,\mathrm{d}t\\
&\quad=\int_0^\infty\int_0^\infty\int_{\mathbb{R}^2}\left(\rho(\partial_t\xi+\partial_a\xi)+\rho\chi_1(a)\mathbf{v}\cdot\nabla_x\xi Y_\theta(\phi-R)+\mu\rho\Delta_x\xi-\mathfrak{d}\rho\xi\right)\lambda_n\mathrm{d}x\,\mathrm{d}a\,\mathrm{d}t\\
&\qquad+\int_0^\infty\int_0^\infty\int_{\mathbb{R}^2}\rho\lambda_n'\xi\mathrm{d}x\,\mathrm{d}a\,\mathrm{d}t+\int_0^\infty\int_0^\infty\int_{\mathbb{R}^2}\mathscr{A}(\phi)\rho(t,a,x)\chi_3(a)\omega(t,x)\xi(t,0,x)\mathrm{d}x\,\mathrm{d}a\,\mathrm{d}t\\
&\qquad+\int_0^\infty\int_{\mathbb{R}^2}\rho_0(a,x)\lambda_n\xi(0,a,x)\mathrm{d}x\,\mathrm{d}a.
\end{aligned}$$

Finally, sending $n \to \infty$ we get (1.2.51) and the proof is concluded. □

1.3 Uniqueness and stability

In this section we conclude the proof of Theorem 1.1 proving (1.1.17).
We follow [2] and prove the following preliminary lemma.

Lemma 1.11. *Let ρ and r be two entropy weak solutions of (1.1.7) obtained in correspondence of the initial data ρ_0 and r_0. For every nonnegative test function $\xi \in C^\infty(\mathbb{R}^4)$ with compact support the following inequality holds*

$$\begin{aligned}
&\int_0^\infty \int_0^\infty \int_{\mathbb{R}^2} \Big(|\rho - r| \left(\partial_t \xi + \partial_a \xi\right) - \operatorname{div}_x \left(|\rho - r| \chi_1 \mathbf{v} (Y_\theta(\phi - R) + Y_\theta(f - R)) \right) \xi \\
&\qquad + \mu \Delta_x |\rho - r| \xi - |\rho - r| \mathfrak{d} \xi \Big) \, dx \, da \, dt \\
&+ \int_0^\infty \int_{\mathbb{R}^2} |\rho(t, 0^+, x) - r(t, 0^+, x)| \xi(t, 0, x) dx \, dt + \int_0^\infty \int_{\mathbb{R}^2} |\rho_0(a, x) - r_0(a, x)| \xi(0, a, x) \, dx \, da \\
&\geq \int_0^\infty \int_0^\infty \int_{\mathbb{R}^2} \operatorname{sign}\left(\rho - r\right) \chi_1 \left(r \operatorname{div}_x \left(\mathbf{v} Y_\theta(\phi - R) \right) - \rho \operatorname{div}_x \left(\mathbf{v}(x) Y_\theta(f - R) \right) \right) \xi \, dx \, da \, dt,
\end{aligned} \tag{1.3.53}$$

where

$$f(t, x) := \int_0^\infty r(t, a, x) \chi_2(a) da.$$

Proof. We double the variables and write

$$\rho = \rho(t, a, x), \qquad r = r(s, b, y), \qquad \phi = \phi(t, x), \qquad f = f(s, y),$$

where $x = (x_1, x_2)$ and $y = (y_1, y_2)$.

Consider the following test function

$$\Xi_n(t, s, a, b, x, y) = \xi\left(\frac{t+s}{2}, \frac{a+b}{2}, \frac{x+y}{2} \right) \lambda_n\left(\frac{s-t}{2} \right) \lambda_n\left(\frac{b-a}{2} \right) \lambda_n\left(\frac{y_1 - x_1}{2} \right) \lambda_n\left(\frac{y_2 - x_2}{2} \right),$$

where

$$\lambda_n(u) = n\lambda(nu), \qquad \lambda \in C^\infty(\mathbb{R}), \qquad \lambda \geq 0, \qquad \|\lambda\|_{L^1(\mathbb{R})} = 1, \qquad \operatorname{supp}(\lambda) \subset [-1, 1].$$

We write (1.1.16) for $\rho(t, a, x)$ using $r(s, b, y)$ as a constant and integrate over (s, b, y)

$$\begin{aligned}
&\iiiiint \Big(|\rho - r| \left(\partial_t \Xi_n + \partial_a \Xi_n\right) - \operatorname{div}_x \left(|\rho - r| \chi_1(a) \mathbf{v}(x) Y_\theta(\phi - R) \right) \Xi_n \\
&\qquad + \mu \Delta_x |\rho - r| \Xi_n - \operatorname{sign}\left(\rho - r\right) \mathfrak{d} \rho \Xi_n \Big) \, \mathrm{d}x \, \mathrm{d}y \, \mathrm{d}a \, \mathrm{d}b \, \mathrm{d}t \, \mathrm{d}s \\
&+ \iiiiint |\rho(t, 0^+, x) - r| \Xi_n(t, s, 0, b, x, y) \mathrm{d}x \, \mathrm{d}y \, \mathrm{d}b \, \mathrm{d}t \, \mathrm{d}s \\
&+ \iiiiint |\rho_0(a, x) - r| \Xi_n(0, s, a, b, x, y) \, \mathrm{d}x \, \mathrm{d}y \, \mathrm{d}a \, \mathrm{d}b \, \mathrm{d}s \\
&\qquad \geq \iiiiint \operatorname{sign}\left(\rho - r\right) r \chi_1(a) \operatorname{div}_x \left(\mathbf{v}(x) Y_\theta(\phi - R) \right) \Xi_n \, \mathrm{d}x \, \mathrm{d}y \, \mathrm{d}a \, \mathrm{d}b \, \mathrm{d}t \, \mathrm{d}s,
\end{aligned} \tag{1.3.54}$$

and we write (1.1.16) for $r(s,b,y)$ using $\rho(t,a,x)$ as a constant and integrate over (t,a,x)

$$\begin{aligned}
&\iiiiii \big(|\rho-r|\,(\partial_s\Xi_n+\partial_b\Xi_n)-\operatorname{div}_y\big(|\rho-r|\chi_1(b)\mathbf{v}(y)\,Y_\theta(f-R)\big)\Xi_n\\
&\qquad\qquad +\mu\Delta_y|\rho-r|\Xi_n+\operatorname{sign}\big(\rho-r\big)\mathfrak{d}\rho\Xi_n\big)\,\mathrm{d}x\,\mathrm{d}y\,\mathrm{d}a\,\mathrm{d}b\,\mathrm{d}t\,\mathrm{d}s\\
&+\iiiiii |\rho-r(s,0^+,y)|\Xi_n(t,s,a,0,x,y)\mathrm{d}x\,\mathrm{d}y\,\mathrm{d}a\,\mathrm{d}t\,\mathrm{d}s\\
&+\iiiiii |\rho-r_0(b,y)|\Xi_n(t,0,a,b,x,y)\,\mathrm{d}x\,\mathrm{d}y\,\mathrm{d}a\,\mathrm{d}b\,\mathrm{d}t\\
&\quad\geq-\iiiiii \operatorname{sign}\big(\rho-r\big)\rho\chi_1(b)\operatorname{div}_y\big(\mathbf{v}(y)\,Y_\theta(f-R)\big)\Xi_n\,\mathrm{d}x\,\mathrm{d}y\,\mathrm{d}a\,\mathrm{d}b\,\mathrm{d}t\,\mathrm{d}s.
\end{aligned}\tag{1.3.55}$$

Adding (1.3.54) and (1.3.55)

$$\begin{aligned}
&\iiiiii \Big(|\rho-r|\,(\partial_t\Xi_n+\partial_s\Xi_n+\partial_a\Xi_n+\partial_b\Xi_n)\\
&\qquad-\operatorname{div}_x\big(|\rho-r|\chi_1(a)\mathbf{v}(x)\,Y_\theta(\phi-R)\big)\Xi_n-\operatorname{div}_y\big(|\rho-r|\chi_1(b)\mathbf{v}(y)\,Y_\theta(f-R)\big)\Xi_n\\
&\qquad+\mu\Delta_x|\rho-r|\Xi_n+\mu\Delta_y|\rho-r|\Xi_n\\
&\qquad-\operatorname{sign}\big(\rho-r\big)\,(\mathfrak{d}(t,a,x)\rho-\mathfrak{d}(s,b,y)r)\Xi_n\Big)\,\mathrm{d}x\,\mathrm{d}y\,\mathrm{d}a\,\mathrm{d}b\,\mathrm{d}t\,\mathrm{d}s\\
&+\iiiiii |\rho(t,0^+,x)-r|\Xi_n(t,s,0,b,x,y)\mathrm{d}x\,\mathrm{d}y\,\mathrm{d}b\,\mathrm{d}t\,\mathrm{d}s\\
&+\iiiiii |\rho-r(s,0^+,y)|\Xi_n(t,s,a,0,x,y)\mathrm{d}x\,\mathrm{d}y\,\mathrm{d}a\,\mathrm{d}t\,\mathrm{d}s\\
&+\iiiiii |\rho_0(a,x)-r|\Xi_n(0,s,a,b,x,y)\,\mathrm{d}x\,\mathrm{d}y\,\mathrm{d}a\,\mathrm{d}b\,\mathrm{d}s\\
&+\iiiiii |\rho-r_0(b,y)|\Xi_n(t,0,a,b,x,y)\,\mathrm{d}x\,\mathrm{d}y\,\mathrm{d}a\,\mathrm{d}b\,\mathrm{d}t\\
&\geq\iiiiii \operatorname{sign}\big(\rho-r\big)\,r\chi_1(a)\operatorname{div}_x\big(\mathbf{v}(x)\,Y_\theta(\phi-R)\big)\Xi_n\,\mathrm{d}x\,\mathrm{d}y\,\mathrm{d}a\,\mathrm{d}b\,\mathrm{d}t\,\mathrm{d}s\\
&\quad-\iiiiii \operatorname{sign}\big(\rho-r\big)\rho\chi_1(b)\operatorname{div}_y\big(\mathbf{v}(y)\,Y_\theta(f-R)\big)\Xi_n\,\mathrm{d}x\,\mathrm{d}y\,\mathrm{d}a\,\mathrm{d}b\,\mathrm{d}t\,\mathrm{d}s.
\end{aligned}$$

Since

$$\begin{aligned}
\partial_t\Xi_n+\partial_s\Xi_n=&\partial_{\frac{t+s}{2}}\xi\left(\frac{t+s}{2},\frac{a+b}{2},\frac{x+y}{2}\right)\lambda_n\left(\frac{s-t}{2}\right)\lambda_n\left(\frac{b-a}{2}\right)\lambda_n\left(\frac{y_1-x_1}{2}\right)\lambda_n\left(\frac{y_2-x_2}{2}\right),\\
\partial_a\Xi_n+\partial_b\Xi_n=&\partial_{\frac{a+b}{2}}\xi\left(\frac{t+s}{2},\frac{a+b}{2},\frac{x+y}{2}\right)\lambda_n\left(\frac{s-t}{2}\right)\lambda_n\left(\frac{b-a}{2}\right)\lambda_n\left(\frac{y_1-x_1}{2}\right)\lambda_n\left(\frac{y_2-x_2}{2}\right),
\end{aligned}$$

As $n\to\infty$ due to the regularity in x of ρ and r we get (1.3.53). □

Lemma 1.12. *The following inequality holds*

$$\begin{aligned}
&\big\|\phi(t,\cdot)-f(t,\cdot)\big\|^2_{L^2(\mathbb{R}^2)}+\mu e^{ct}\int_0^t\int_{\mathbb{R}^2}e^{-cs}|\nabla_x(\phi-f)|^2\,dx\,ds\\
&\qquad\leq ce^{ct}\big\|\rho_0-r_0\big\|^2_{L^1((0,\infty)\times\mathbb{R}^2)}+ce^{ct}\int_0^t\int_0^\infty\int_{\mathbb{R}^2}e^{-cs}(\rho-r)^2\,dx\,da\,ds.
\end{aligned}\tag{1.3.56}$$

for every $t \geq 0$. In particular, we have that

$$\begin{aligned}\left(\int_0^t \int_{\mathbb{R}^2} e^{-cs} |\nabla_x(\phi - f)|^2 \, dx \, ds\right)^{1/2} \\ \leq c e^{ct} \left\|\rho_0 - r_0\right\|_{L^1((0,\infty)\times\mathbb{R}^2)} + c e^{ct} \left(\int_0^t \left\|\rho(s,\cdot,\cdot) - r(s,\cdot,\cdot)\right\|^2_{L^1((0,\infty)\times\mathbb{R}^2)} \, ds\right)^{1/2},\end{aligned} \tag{1.3.57}$$

for every $t \geq 0$.

Proof. Since $\phi_{\varepsilon_k} e$ satisfies

$$\partial_t \phi_{\varepsilon_k} - \mu \Delta_x \phi_{\varepsilon_k} + \operatorname{div}_x \left(\left(\int_0^\infty \rho_{\varepsilon_k} \chi_1 \, \mathrm{d}a\right) \mathbf{v} Y_\theta(\phi_{\varepsilon_k} - R)\right) = \int_0^\infty \rho_{\varepsilon_k} \left(\varepsilon_k \chi_2'' + \chi_2' - \mathfrak{d}\chi_2\right) \mathrm{d}a.$$

as $k \to \infty$ we get the equation for ϕ

$$\partial_t \phi - \mu \Delta_x \phi + \operatorname{div}_x \left(\left(\int_0^\infty \rho \chi_1 \, \mathrm{d}a\right) \mathbf{v} Y_\theta(\phi - R)\right) = \int_0^\infty \rho \left(\chi_2' - \mathfrak{d}\chi_2\right) \mathrm{d}a. \tag{1.3.58}$$

Analogously, f satisfies

$$\partial_t f - \mu \Delta_x f + \operatorname{div}_x \left(\left(\int_0^\infty r \chi_1 \, \mathrm{d}a\right) \mathbf{v} Y_\theta(f - R)\right) = \int_0^\infty r \left(\chi_2' - \mathfrak{d}\chi_2\right) \mathrm{d}a. \tag{1.3.59}$$

Subtracting (1.3.58) and (1.3.59)

$$\begin{aligned}\partial_t(\phi - f) - \mu \Delta_x(\phi - f) + \operatorname{div}_x \left(\left(\int_0^\infty (\rho - r)\chi_1 \, \mathrm{d}a\right) \mathbf{v} Y_\theta(\phi - R)\right) \\ + \operatorname{div}_x \left(\left(\int_0^\infty r \chi_1 \, \mathrm{d}a\right) \mathbf{v}(Y_\theta(\phi - R) - Y_\theta(f - R))\right) \\ = \int_0^\infty (\rho - r) \left(\chi_2' - \mathfrak{d}\chi_2\right) \mathrm{d}a.\end{aligned} \tag{1.3.60}$$

Then

$$\begin{aligned}&\frac{d}{dt} \int_{\mathbb{R}^2} \frac{(\phi - f)^2}{2} \, \mathrm{d}x + \mu \int_{\mathbb{R}^2} \left|\nabla_x(\phi - f)\right|^2 \, \mathrm{d}x \\ &= \int_{\mathbb{R}^2} (\phi - f) \left(\int_0^\infty (\rho - r) \left(\chi_2' - \mathfrak{d}\chi_2\right) \mathrm{d}a\right) \mathrm{d}x \\ &\quad - \int_{\mathbb{R}^2} (\phi - f) \operatorname{div}_x \left(\left(\int_0^\infty (\rho - r)\chi_1 \, \mathrm{d}a\right) \mathbf{v} Y_\theta(\phi - R)\right) \mathrm{d}x \\ &\quad - \int_{\mathbb{R}^2} (\phi - f) \operatorname{div}_x \left(\left(\int_0^\infty r \chi_1 \, \mathrm{d}a\right) \mathbf{v}(Y_\theta(\phi - R) - Y_\theta(f - R))\right) \mathrm{d}x \\ &= \int_{\mathbb{R}^2} (\phi - f) \left(\int_0^\infty (\rho - r) \left(\chi_2' - \mathfrak{d}\chi_2\right) \mathrm{d}a\right) \mathrm{d}x \\ &\quad + \int_{\mathbb{R}^2} \nabla_x(\phi - f) \cdot \mathbf{v} \left(\int_0^\infty (\rho - r)\chi_1 \, \mathrm{d}a\right) Y_\theta(\phi - R) \, \mathrm{d}x\end{aligned}$$

$$
\begin{aligned}
&+\int_{\mathbb{R}^2}\nabla_x(\phi-f)\cdot\mathbf{v}\left(\int_0^\infty r\chi_1\mathrm{d}a\right)(Y_\theta(\phi-R)-Y_\theta(f-R))\,\mathrm{d}x\\
\le&\frac{1}{2}\int_{\mathbb{R}^2}(\phi-f)^2\,\mathrm{d}x+\frac{1}{2}\int_{\mathbb{R}^2}\left(\int_0^\infty(\rho-r)\left(\chi_2'-\mathfrak{d}\chi_2\right)\mathrm{d}a\right)^2\mathrm{d}x\\
&+\frac{\mu}{2}\int_{\mathbb{R}^2}\left|\nabla_x(\phi-f)\right|^2\mathrm{d}x+\frac{1}{\mu}\int_{\mathbb{R}^2}|\mathbf{v}|^2\left(\int_0^\infty(\rho-r)\chi_1\mathrm{d}a\right)^2Y_\theta(\phi-R)^2\,\mathrm{d}x\\
&+\frac{1}{\mu}\int_{\mathbb{R}^2}|\mathbf{v}|^2\left(\int_0^\infty r\chi_1\mathrm{d}a\right)^2(Y_\theta(\phi-R)-Y_\theta(f-R))^2\,\mathrm{d}x\\
\le&c\int_{\mathbb{R}^2}(\phi-f)^2\,\mathrm{d}x+ce^{ct}\int_0^\infty\int_{\mathbb{R}^2}(\rho-r)^2\,\mathrm{d}x\,\mathrm{d}a+\frac{\mu}{2}\int_{\mathbb{R}^2}\left|\nabla_x(\phi-f)\right|^2\mathrm{d}x.
\end{aligned}
$$

Using the Gronwall Lemma and we get

$$
\begin{aligned}
&\left\|\phi(t,\cdot)-f(t,\cdot)\right\|^2_{L^2(\mathbb{R}^2)}+\mu e^{ct}\int_0^t\int_{\mathbb{R}^2}e^{-cs}|\nabla_x(\phi-f)|^2\,\mathrm{d}x\,\mathrm{d}s\\
&\qquad\le e^{ct}\left\|\phi_0-f_0\right\|^2_{L^2(\mathbb{R}^2)}+ce^{ct}\int_0^t\int_0^\infty\int_{\mathbb{R}^2}e^{-cs}(\rho-r)^2\,\mathrm{d}x\,\mathrm{d}a\,\mathrm{d}s.
\end{aligned}
$$

The definition of ϕ and f gives (1.3.56).

Finally, we prove (1.3.57). Using (1.2.33) and (1.3.56) we gain

$$
\begin{aligned}
&\left(\int_0^t\int_{\mathbb{R}^2}|\nabla_x(\phi-f)|^2\,\mathrm{d}x\,\mathrm{d}s\right)^{1/2}\\
&\qquad\le c\left(\mu e^{ct}\int_0^t\int_{\mathbb{R}^2}e^{-cs}|\nabla_x(\phi-f)|^2\,\mathrm{d}x\,\mathrm{d}s\right)^{1/2}\\
&\qquad\le c\left(e^{ct}\left\|\rho_0-r_0\right\|^2_{L^1((0,\infty)\times\mathbb{R}^2)}+ce^{ct}\int_0^t\int_0^\infty\int_{\mathbb{R}^2}e^{-cs}(\rho-r)^2\,\mathrm{d}x\,\mathrm{d}a\,\mathrm{d}s\right)^{1/2}\\
&\qquad\le ce^{ct}\left\|\rho_0-r_0\right\|_{L^1((0,\infty)\times\mathbb{R}^2)}+ce^{ct}\left(\int_0^t\left\|\rho(s,\cdot,\cdot)-r(s,\cdot,\cdot)\right\|^2_{L^2((0,\infty)\times\mathbb{R}^2)}\,\mathrm{d}s\right)^{1/2}\\
&\qquad\le ce^{ct}\left\|\rho_0-r_0\right\|_{L^1((0,\infty)\times\mathbb{R}^2)}+ce^{ct}\left(\int_0^t\left\|\rho(s,\cdot,\cdot)-r(s,\cdot,\cdot)\right\|^2_{L^1((0,\infty)\times\mathbb{R}^2)}\,\mathrm{d}s\right)^{1/2}.
\end{aligned}
$$

□

Proof of Theorem 1.1. Thanks to Lemma 1.10, we need only to prove (1.1.17). We rewrite (1.3.53) in the following form

$$
\begin{aligned}
&\int_0^\infty\int_0^\infty\int_{\mathbb{R}^2}\left(|\rho-r|\left(\partial_t\xi_n+\partial_a\xi_n\right)+|\rho-r|\chi_1(Y_\theta(\phi-R)+Y_\theta(f-R))\mathbf{v}\cdot\nabla_x\xi_n\right.\\
&\qquad\left.+\mu|\rho-r|\Delta_x\xi_n-|\rho-r|\mathfrak{d}\xi_n\right)\mathrm{d}x\,\mathrm{d}a\,\mathrm{d}t\\
&+\int_0^\infty\int_{\mathbb{R}^2}|\rho(t,0^+,x)-r(t,0^+,x)|\xi_n(t,0,x)\mathrm{d}x\,\mathrm{d}t+\int_0^\infty\int_{\mathbb{R}^2}|\rho_0(a,x)-r_0(a,x)|\xi_n(0,a,x)\,\mathrm{d}x\,\mathrm{d}a\\
&\quad\ge\int_0^\infty\int_0^\infty\int_{\mathbb{R}^2}\operatorname{sign}\left(\rho-r\right)\chi_1(a)\left(r\operatorname{div}_x\left(\mathbf{v}(x)Y_\theta(\phi-R)\right)-\rho\operatorname{div}_x\left(\mathbf{v}(x)Y_\theta(f-R)\right)\right)\xi_n\,\mathrm{d}x\,\mathrm{d}a\,\mathrm{d}t,
\end{aligned}
$$

for a sequence $\{\xi_n\}_n$ of nonnegative test functions approximating the characteristic function of the strip $(-\infty, t)\times\mathbb{R}\times\mathbb{R}^2$. Sending $n\to\infty$

$$\begin{aligned}
&\left\|\rho(t,\cdot,\cdot)-r(t,\cdot,\cdot)\right\|_{L^1((0,\infty)\times\mathbb{R}^2)}\\
&\qquad\le \left\|\rho_0-r_0\right\|_{L^1((0,\infty)\times\mathbb{R}^2)}+\int_0^t\int_{\mathbb{R}^2}|\rho(s,0^+,x)-r(s,0^+,x)|\mathrm{d}x\,\mathrm{d}s\\
&\qquad\quad-\int_0^t\int_0^\infty\int_{\mathbb{R}^2}\operatorname{sign}\left(\rho-r\right)\chi_1(a)\left(r\operatorname{div}_x\left(\mathbf{v}Y_\theta(\phi-R)\right)-\rho\operatorname{div}_x\left(\mathbf{v}Y_\theta(f-R)\right)\right)\mathrm{d}x\,\mathrm{d}a\,\mathrm{d}s
\end{aligned}$$

Thanks to Remark 1.1

$$\begin{aligned}
&\left\|\rho(t,\cdot,\cdot)-r(t,\cdot,\cdot)\right\|_{L^1((0,\infty)\times\mathbb{R}^2)}\\
&\qquad\le \left\|\rho_0-r_0\right\|_{L^1((0,\infty)\times\mathbb{R}^2)}+\int_0^t\int_0^\infty\int_{\mathbb{R}^2}\left|\mathscr{A}\left(\phi\right)\rho-\mathscr{A}\left(f\right)r\right|\chi_3\omega\mathrm{d}x\,\mathrm{d}a\,\mathrm{d}s\\
&\qquad\quad-\int_0^t\int_0^\infty\int_{\mathbb{R}^2}\operatorname{sign}\left(\rho-r\right)\chi_1(a)\left(r\operatorname{div}_x\left(\mathbf{v}Y_\theta(\phi-R)\right)-\rho\operatorname{div}_x\left(\mathbf{v}Y_\theta(f-R)\right)\right)\mathrm{d}x\,\mathrm{d}a\,\mathrm{d}s\\
&\qquad\le \left\|\rho_0-r_0\right\|_{L^1((0,\infty)\times\mathbb{R}^2)}+\int_0^t\int_0^\infty\int_{\mathbb{R}^2}\mathscr{A}\left(\phi\right)\left|\rho-r\right|\chi_3\omega\mathrm{d}x\,\mathrm{d}a\,\mathrm{d}s\\
&\qquad\quad+\int_0^t\int_0^\infty\int_{\mathbb{R}^2}\left|\mathscr{A}\left(\phi\right)-\mathscr{A}\left(f\right)\right|r\chi_3\omega\mathrm{d}x\,\mathrm{d}a\,\mathrm{d}s\\
&\qquad\quad+\int_0^t\int_0^\infty\int_{\mathbb{R}^2}|\rho-r|\chi_1(a)\operatorname{div}_x\left(\mathbf{v}Y_\theta(\phi-R)\right)\mathrm{d}x\,\mathrm{d}a\,\mathrm{d}s\\
&\qquad\quad+\int_0^t\int_0^\infty\int_{\mathbb{R}^2}\operatorname{sign}\left(\rho-r\right)\chi_1(a)\rho\operatorname{div}_x\left(\mathbf{v}\right)\left(Y_\theta(\phi-R)-Y_\theta(f-R)\right)\mathrm{d}x\,\mathrm{d}a\,\mathrm{d}s\\
&\qquad\quad+\int_0^t\int_0^\infty\int_{\mathbb{R}^2}\operatorname{sign}\left(\rho-r\right)\chi_1(a)\rho\mathbf{v}\cdot\nabla_x(Y_\theta(\phi-R)-Y_\theta(f-R))\mathrm{d}x\,\mathrm{d}a\,\mathrm{d}s\\
&\qquad\le \left\|\rho_0-r_0\right\|_{L^1((0,\infty)\times\mathbb{R}^2)}+c\int_0^t\left\|\rho(s,\cdot,\cdot)-r(s,\cdot,\cdot)\right\|_{L^1((0,\infty)\times\mathbb{R}^2)}\mathrm{d}s\\
&\qquad\quad+ce^{ct}\int_0^t\int_{\mathbb{R}^2}\left|\mathscr{A}\left(\phi\right)-\mathscr{A}\left(f\right)\right|\mathrm{d}x\,\mathrm{d}s\\
&\qquad\quad+ce^{ct}\int_0^t\int_{\mathbb{R}^2}\left|Y_\theta(\phi-R)-Y_\theta(f-R)\right|\mathrm{d}x\,\mathrm{d}s\\
&\qquad\quad+ce^{ct}\left(\int_0^t\int_{\mathbb{R}^2}\left|\nabla_x(Y_\theta(\phi-R)-Y_\theta(f-R))\right|^2\mathrm{d}x\,\mathrm{d}s\right)^{1/2}.
\end{aligned}$$

Thanks to the regularity of the functions $\mathscr{A}$ and Y_θ we can conclude

$$\begin{aligned}
&\left\|\rho(t,\cdot,\cdot)-r(t,\cdot,\cdot)\right\|_{L^1((0,\infty)\times\mathbb{R}^2)}\\
&\qquad\le \left\|\rho_0-r_0\right\|_{L^1((0,\infty)\times\mathbb{R}^2)}+c(1+e^{ct})\int_0^t\left\|\rho(s,\cdot,\cdot)-r(s,\cdot,\cdot)\right\|_{L^1((0,\infty)\times\mathbb{R}^2)}\mathrm{d}s\\
&\qquad\quad+ce^{ct}\left(\int_0^t\int_{\mathbb{R}^2}\left|\nabla_x(\phi-f)\right|^2\mathrm{d}x\,\mathrm{d}s\right)^{1/2}.
\end{aligned}\tag{1.3.61}$$

Using (1.3.56) in (1.3.61)

$$\begin{aligned}
&\left\|\rho(t,\cdot,\cdot)-r(t,\cdot,\cdot)\right\|_{L^1((0,\infty)\times\mathbb{R}^2)}\\
&\quad\le \left\|\rho_0-r_0\right\|_{L^1((0,\infty)\times\mathbb{R}^2)}+ce^{ct}\left\|\rho_0-r_0\right\|_{L^1((0,\infty)\times\mathbb{R}^2)}\\
&\qquad+c(1+e^{ct})\int_0^t\left\|\rho(s,\cdot,\cdot)-r(s,\cdot,\cdot)\right\|_{L^1((0,\infty)\times\mathbb{R}^2)}\,\mathrm{d}s\\
&\qquad+ce^{ct}\left(\int_0^t\left\|\rho(s,\cdot,\cdot)-r(s,\cdot,\cdot)\right\|^2_{L^1((0,\infty)\times\mathbb{R}^2)}\,\mathrm{d}s\right)^{1/2}.
\end{aligned}\tag{1.3.62}$$

Squaring both sides and using the Hölder Inequality we get

$$\begin{aligned}
&\left\|\rho(t,\cdot,\cdot)-r(t,\cdot,\cdot)\right\|^2_{L^1((0,\infty)\times\mathbb{R}^2)}\\
&\quad\le \left\|\rho_0-r_0\right\|^2_{L^1((0,\infty)\times\mathbb{R}^2)}+ce^{ct}\left\|\rho_0-r_0\right\|^2_{L^1((0,\infty)\times\mathbb{R}^2)}\\
&\qquad+c(1+e^{ct})\left(\int_0^t\left\|\rho(s,\cdot,\cdot)-r(s,\cdot,\cdot)\right\|_{L^1((0,\infty)\times\mathbb{R}^2)}\,\mathrm{d}s\right)^2\\
&\qquad+ce^{ct}\int_0^t\left\|\rho(s,\cdot,\cdot)-r(s,\cdot,\cdot)\right\|^2_{L^1((0,\infty)\times\mathbb{R}^2)}\,\mathrm{d}s\\
&\quad\le \left\|\rho_0-r_0\right\|^2_{L^1((0,\infty)\times\mathbb{R}^2)}+ce^{ct}\left\|\rho_0-r_0\right\|^2_{L^1((0,\infty)\times\mathbb{R}^2)}\\
&\qquad+c(1+e^{ct})\int_0^t\left\|\rho(s,\cdot,\cdot)-r(s,\cdot,\cdot)\right\|^2_{L^1((0,\infty)\times\mathbb{R}^2)}\,\mathrm{d}s.
\end{aligned}\tag{1.3.63}$$

Using the Gronwall Lemma we gain (1.1.17) and the proof is concluded. □

Chapter 2

On the mathematical modeling of vole populations spatial dynamics via transport equations on a graph

2.1 Description of our models

We propose two models to describe the spatial dynamics of a voles population structured in age. Both models write as transport equations on graph.

Voles' sex ratio at birth is 1-1, [6, 37], so that it is enough to model the female population, which is structured into three age classes: young voles, whose age a varies between 0 and A_1, juveniles, $a \in [A_1, A_2]$, and adults, $a > A_2$. The same observations suggest that $A_1 \approx 18$ days and $A_2 \approx 56$ days, but for simplicity we assume the normalization $A_2 = 3A_1$. Since most voles die out of predation, disease or starvation, at a first approximation we could neglect aging when describing the adult population: in particular it is not necessary to consider a decline of fertility over age. Nevertheless, to avoid non realistic results when performing simulations on a large time horizon (e.g. 4 years), we define A_3 as the maximal age that a vole individual can attain (different values will be taken into account) and we set our model so that individuals of age larger than A_3, if any, do not participate any more in the evolution of the system. As numerical values for age transitions, we fix $A_1 = 1$, $A_2 = 3$ and $A_3 = 20$.

We partition the natural space into squared cells of side length 100 m, V_i, $i = 1, \dots, n_v$. We measure the distances between cells centers and, based on observations, we estimate the average time needed by a vole to cover such distances. Then we define a finite weighted graph $\Gamma = (\mathscr{E}, \mathscr{V})$, whose set of nodes $\mathscr{V} = \{V_1, \dots, V_{n_v}\}$ represents the cells, while the set of its edges $\mathscr{E}$ consists of the triples (V_i, V_j, ℓ_{ij}) where $V_i \neq V_j$ belong to $\mathscr{V}$ (no loops are allowed) and $\ell_{ij} > 0$ is the travel time between the two vertices. For simplicity we will always assume that Γ is not directed, therefore $\ell_{ij} = \ell_{ji}$. In general it is possible to assume that the graph is complete, i.e. that there exists an edge joining any given pair of nodes. From the modeling point of view this is compatible with the fact that some individuals (long range dispersers) can be recaptured at

observation sites more than 5 Km apart from each other.

Each node V_i is endowed with an initial boundary value problem representing the evolution of the density of voles in V_i, ρ_i, with respect to the time and age variables t and a,

$$\begin{array}{rccc} \rho_i : & \mathbb{R}^+ \times \mathbb{R}^+ & \to & \mathbb{R}^+ \\ & (t,a) & \mapsto & \rho_i(t,a). \end{array} \tag{2.1.1}$$

The total number of voles in V_i at time t is given by the integral

$$\Phi_i(t) = \int_0^{A_3} \rho_i(t,a)\,\mathrm{d}a. \tag{2.1.2}$$

The spatial dynamics of the population is represented by transmissions of density from one node to the others. The local spatial dynamics, related to foraging activities is neglected. We recall that while most individuals spend almost all of their lives in burrows, where they also breed, some of the juveniles have a significant spatial dynamics during dispersals. The mechanism triggering dispersal is still not completely understood and it is most probably related to the interaction of several factors (see for instance [1, 4, 6, 16, 21, 24, 25, 41, 42] and references therein). However, for modeling purposes, it is reasonable to link stress conditions to overcrowding, and say that dispersal begins when the total number of individuals in a colony reaches a threshold value, fixed as a fraction of the carrying capacity of the environment, R. New colonies most often appear in a radius of a few hundreds meters around the original one, but individuals might disperse over more than 5 Km. Topography, in particular relief, drives the dispersal direction, and during this phase voles' mortality is very high.

We define a stochastic matrix $\mathbf{K}$ of size $n_v \times n_v$. Its coefficients k_{ij} fix which fraction of voles leaving the node V_i would head toward V_j. Since no loops are allowed, we set $k_{ii} = 0$ for any $i \in \{1,\dots,n_v\}$. At a modeling level we can imagine that k_{ij} depends, for example, on the height or the landscapes in V_i and V_j, therefore in general $k_{ij} \neq k_{ji}$. From the modeling point of view it makes sense to consider a time dependent matrix $\mathbf{K}$. An example in this direction is given in Section 2.3.2, but for the simplicity of the presentation, we keep $\mathbf{K}$ constant for the moment.

Assume that at time $\bar{t}$ some of the voles initially at V_i disperse. Since voles age and die during dispersal but cannot reproduce, the evolution of voles leaving V_i at time $\bar{t}$ and age a and heading toward V_j, is described by the ODE problem

$$\begin{cases} \partial_s u(s) = -\mathfrak{d}_{dis} u(s), \\ u(0) = k_{ij}\rho_i(\bar{t},a) \end{cases} \tag{2.1.3}$$

where $\mathfrak{d}_{dis}$ represents mortality during dispersal. The estimated travel time from V_i to V_j is the weight ℓ_{ij}, therefore the density of voles of age $a+\ell_{ij}$ reaching V_j at time $\bar{t}+\ell_{ij}$ is

$$k_{ij}\rho_i(\bar{t},a)\exp(-\ell_{ij}\mathfrak{d}_{dis}) = K_{ij}\rho_i(\bar{t},a).$$

Remark that the matrix $\mathscr{K} = (K_{ij}) \in \mathbb{R}^{n_v \times n_v}$ is not stochastic, not symmetric and depends on time if and only if $\mathbf{K}$ does.

2.1.1 A model with gradual dispersal (GD model)

We always assume that a dispersal begins from the node V_i whenever its total population Φ_i reaches the threshold R_i. In the first model, the dispersal lasts for a time $\eta > 0$ after the moment at which Φ_i passes again below R_i and the departure rate of juveniles during dispersal is c/η, where $c > 0$ is a parameter to be chosen. Notice that R_i is not the capacity of the node V_i but a fraction of it, which means that voles are uncomfortable for $\Phi_i = R_i$ but they are not missing resources.

To introduce the initial boundary value problem at the node V_i we consider the balance law

$$\partial_t \rho_i + \partial_a \rho_i = -\mathfrak{d}_i(t,a)\rho_i + P_i(t,a), \tag{2.1.4}$$

where t and a are respectively the time and age variables, $\mathfrak{d}_i$ is the mortality rate at V_i, depending on time and age, and $P_i(t,a)$ is a source term which accounts for the possible departure/arrival of voles due to dispersal. The exact form of P_i is given below.

Together with (2.1.4) we consider the initial condition

$$\rho_i(0,a) = \rho_{0,i}(a), \tag{2.1.5}$$

and the boundary condition

$$\rho_i(t,0) = \mathscr{A}_i(\Phi_i(t)) \int_0^{A_3} b_i(t,a)\rho_i(t,a)\,\mathrm{d}a, \tag{2.1.6}$$

where b_i is the reproduction rate of the node V_i and the coefficient $\mathscr{A}_i(\Phi_i)$ reproduces Allee's effect, see [33]. This means that if the total population of a colony falls below a certain threshold, reproduction rate also diminishes and might become too small to compensate for mortality. The experimental observations suggest that this situation rarely occurs for voles, so that $\mathscr{A}_i \equiv 1$ is a reasonable choice in our simulations. However from the numerical point of view no additional difficulty comes from considering non constant $\mathscr{A}_i$, see also the Section 2.4 for a short additional discussion.

For $t > 0$ given and $i \in \{1,\dots,n_v\}$, we call $\mathscr{T}_i(t) = \left\{\tau_1^i,\dots,\tau_{m_i(t)}^i\right\}$ the (possibly empty) set of times $\tau_r^i < t$ at which a dispersal outbreak took place from V_i. Then the term $P_i(t,a)$ in equation (2.1.4) takes the form

$$\begin{aligned} P_i(t,a) = &-\frac{c}{\eta}\chi_{[R_i,+\infty)}\Big(\sup_{z\in[(t-\eta)^+,t]}\Phi_i(z)\Big)\chi_{[A_1,A_2)}(a)\rho_i(t,a) \\ &+\frac{c}{\eta}\sum_{\substack{j=1,\dots,n_v\\ j\neq i}}\sum_{r=1}^{m_j(t)}\delta_{\tau_r^j}(t-\ell_{ji})\chi_{[A_1,A_2)}(a-\ell_{ji})K_{ji}\rho_j(t-\ell_{ji},a-\ell_{ji}), \end{aligned} \tag{2.1.7}$$

where $\chi_{[R_i,+\infty)}$ and $\chi_{[A_1,A_2)}$ are the characteristic functions of the intervals $[R_i,+\infty)$ and $[A_1,A_2)$ respectively, $t \mapsto \delta_\tau(t)$ is the Kronecker delta centered at τ and we use the notation $x^+ = \max(x,0)$.

2.1.2 A model with instantaneous dispersal (ID model)

The model with gradual dispersal introduced above is very solid as it is based on classical PDE's for which a complete well-posedness theory is available. Moreover, the examples in the next section show that it reproduces the main features of the voles' population dynamics. Nevertheless, in order to bring the model to full size, on a graph counting several hundreds of nodes, one should overcome a number of technical difficulties in parallelization and data storage. For this reason and in view of the possible construction of an hybrid PDE-Multi Agent model similar to the MLG, we propose here a second model which leads to a slightly less precise description of the dynamics, but should be easier to implement on large graphs.

Roughly speaking, we modify the previous model so that whenever the total population at a node V_i reaches the threshold value R_i, the departure of dispersers takes place instantaneously. As a consequence, all the voles who left V_i heading for V_j will reach the node V_j at the same time. These "instantaneous" departures/arrivals are easier to implement in a finite volume scheme and are not too demanding in term of data storage.

In order to write the model for the node V_i, we introduce $\mathscr{F}_i = \{\sigma_0^i, \sigma_1^i, \dots, \sigma_{m_i}^i\}$, where $\sigma_0^i = 0$ and $\sigma_{m_i}^i = T$, be the (possibly reduced to $\{0, T\}$) set of all the times between 0 and the final time T at which, either a dispersal outbreak, or an arrival of voles, took place for the node V_i.

Then between two times σ_K^i and σ_{K+1}^i, where $K = 0, \dots, m_i - 1$, the model can be written as follows

$$
\begin{cases}
\partial_t \rho_i + \partial_a \rho_i = -\mathfrak{d}(t,a)\rho_i, \\
\rho_i(t,0) = \mathscr{A}\left(\Phi_i(t)\right) \displaystyle\int_0^{A_3} b_i(t,a)\rho_i(t,a)\,\mathrm{d}a, \\
\rho_i(\sigma_K^i+,a) = \chi_{[0,A_1)\cup[A_2,A_3]}(a)\rho_i(\sigma_K^i-,a) + \left(1 - \chi_{[R_i,+\infty)}(\Phi_i(\sigma_K^i-))\right)\chi_{[A_1,A_2)}(a)\rho_i(\sigma_K^i-,a) \\
\quad + \displaystyle\sum_{\substack{j\neq i \\ j=1,\dots,n_v}} \sum_{r=1}^{m_j-1} \delta_{\sigma_r^j}(\sigma_K^i - \ell_{ji})\chi_{[R_j,+\infty)}(\Phi_j(\sigma_K^i - \ell_{ji}))\chi_{[A_1,A_2)}(a-\ell_{ji})K_{ji}\rho_j(\sigma_K^i - \ell_{ji}, a - \ell_{ji}).
\end{cases}
\tag{2.1.8}
$$

2.1.3 Reproduction and mortality rates

Voles' reproduction season lasts typically from April to October, but variations are possible due to weather conditions and, of course, depending on the landscape characteristics. The ideal environment for fossorial voles is grassland where both food and shelter are easily available, but they can also settle in woodlands and farmlands. Mortality also depends on landscape characteristics as it is strongly related to the density and the kind of predators, but is everywhere higher during the winter season as food becomes scarce.

Based on [40, 26], the basic reproduction number $\mathscr{R}_0$ of a voles' population is 0.0165 females per female and per day during the reproduction season and only juvenile and adult individuals reproduce. In the time scale of our models this correspond to 0.3 per juvenile/adult

vole per unit time. In Section 2.2.1, to validate our numerical schemes, we use as reproduction rate the piecewise constant function $b(a) = 0.3\chi_{[A_1,A_3](a)}$. Everywhere else in the paper we consider a smooth approximation of b, namely

$$b_1(a) = \alpha \cdot \begin{cases} 0.15\exp(K(a-A_1-\varepsilon)) & \text{if} \quad 0 \le a \le A_1+\varepsilon, \\ 0.3-0.15\exp(-K(a-A_1-\varepsilon)) & \text{if} \quad a > A_1+\varepsilon, \end{cases} \tag{2.1.9}$$

where we set $K = 10$ and $\varepsilon = 0.2$. The parameter $\alpha \in (0,1]$ allows to adapt the average rate to specific situations, as we do in Sections 2.3.1 and 2.3.2.

Observations reported in [26] suggest that the average mortality rate during the reproduction season varies between 0.04 and 0.6 per 2 weeks, but the mortality rate for juvenile and newborn individuals is 1 to 3 times larger than for adults. Translated to our setting the value of mortality rate is between 0.05 and 0.77 per unit time. These informations lead us to define a mortality rate function of the following form

$$\mathfrak{d}_1(a) = \delta \cdot \begin{cases} 0.1-0.025\exp(K(a-A_2-\varepsilon)) & \text{if} \quad 0 \le a \le A_2+\varepsilon, \\ 0.05+0.025\exp(-K(a-A_2-\varepsilon)) & \text{if} \quad a > A_2+\varepsilon, \end{cases} \tag{2.1.10}$$

where $\delta > 1$ is a parameter to be tuned. The graphs of b_1 and $\mathfrak{d}_1$ for $\alpha = \delta = 1$ appear in Figure 2.1.

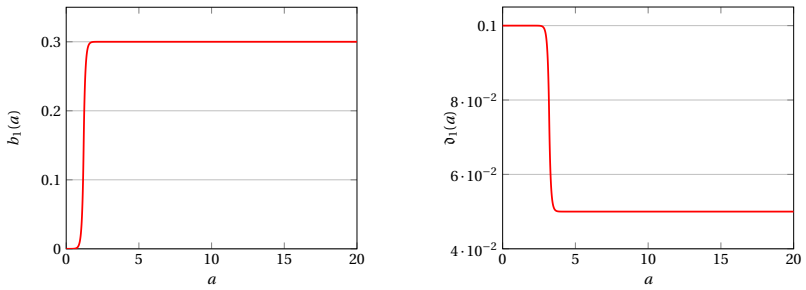

(a) The reproduction rate b_1 for $\alpha = 1$.

(b) The mortality rate $\mathfrak{d}_1$ for $\delta = 1$.

Figure 2.1 – The reproduction and mortality rates as functions of age.

To validate our schemes it is enough to run simulations over a short interval of time, $t \in [0, 1.3]$, which corresponds to less than one month in real time. In general however we wish to simulate the population dynamics over one or more years, so that we have to take into account the difference between the reproduction season, lasting from april to october, and the cold season where the reproduction stops and the mortality rate is more important, see for instance [22]. In our context, one year starting from April 1st corresponds to the period $[0,T]$, where $T = 20$, and the reproduction season is $[0,T^*]$, where $T^* = 12$. Given $\kappa > 1$ we take

$$K_b(t) = \begin{cases} 1 & \text{if} \quad 0 \le t \le T^*, \\ 0 & \text{if} \quad T^* < t \le T, \end{cases} \qquad \text{and} \qquad K_{\mathfrak{d}}(t) = \begin{cases} 1 & \text{if} \quad 0 \le t \le T^*, \\ \kappa & \text{if} \quad T^* < t \le T, \end{cases} \tag{2.1.11}$$

and we compute the reproduction and mortality rates as functions of two variables defined on $[0,T]\times[0,A_3]$ as

$$b_K(t,a)=K_b(t)b_1(a) \qquad \text{and} \qquad \mathfrak{d}_K(t,a)=K_{\mathfrak{d}}(t)\mathfrak{d}_1(a). \tag{2.1.12}$$

The values of α, δ and κ will be specified for each of our examples.

To give a first, basic example of the evolution induced from the parameter functions above we consider the evolution internal to one single node over one year computed by the two models. The initial condition at $t=0$ consists of 70 adults equidistributed over their age class. We set $\alpha=1$, $\kappa=1.5$ and observe that if we choose $\delta=1$ several dispersals take place in both models starting at time $t\simeq 8.1$. After $T^*=12$, the total populations decreases and the only voles remaining at $t=T$ are the adult ones. Their total number is larger than the initial condition ($\simeq 90$ for the GD model and $\simeq 80$ for the ID model), so we say that the colony persists. On the other hand, if the mortality rate is higher, with $\delta=5.5$, the population declines, no dispersal occurs and the colony disappears before the end of the simulation.

The models coincide in this latter case, while in the first one we can observe several differences. Essentially, some of the juvenile voles do not leave the node during dispersal in the GD model, therefore the total population remains higher and we see more dispersals for the GD model than for the ID one.

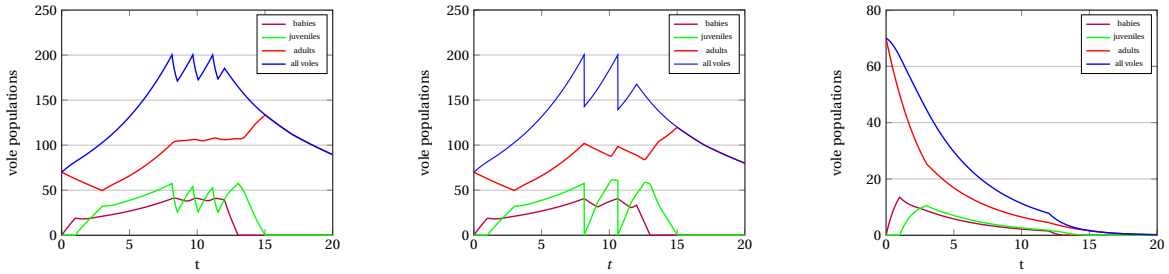

(a) GD model, persistence. (b) ID model, persistence. (c) Both models, extinction.

Figure 2.2 – With reference to Section 2.1.3: the evolution of the voles population at one node. Left and center: low mortality in the GD and ID models respectively. Right : high mortality.

2.2 Finite volumes approximations of the models

In this section, we propose finite volumes numerical schemes for the models described above and we validate them by comparison with exact solutions, for which analytical expressions exist and can be computed via the classical method of characteristics, [20, 38]. As the models rely on transport equations, the schemes are based on upwind schemes, [28].

Given a finite time horizon $T>0$ and a suitable maximal age A_3, we consider the computational domain $[0,T]\times[0,A_3]$ and let Δt and Δa be respectively the constant time and age steps. We set $N_T=\lfloor T/\Delta t\rfloor$, $N_1=\lfloor A_1/\Delta a\rfloor$, $N_2=\lfloor A_2/\Delta a\rfloor$ and $N_A=\lfloor A_3/\Delta a\rfloor$. Then for any

$1 \le h \le N_A$, we introduce the cells $K_h = [a_{h-1/2}, a_{h+1/2})$, the cells centers $a_h = (h-1/2)\Delta a$ and, for $0 \le n \le N_T$, we define the times $t^n = n\Delta t$. For any given $i, j \in \{1,\dots,n_v\}$, $i \neq j$, we approximate the edge (V_i, V_j, ℓ_{ij}) by $(V_i, V_j, L_{ij}\Delta t)$, where $L_{ij} = \lfloor \ell_{ij}/\Delta t \rfloor$. Analogously, we approximate the age increase during dispersal by $L^*_{ij}\Delta a$ where $L^*_{ij} = \lfloor \ell_{ij}/\Delta a \rfloor$.

Given a node V_i, $1 \le i \le n_v$, we denote by $b^n_{i,h}$, $\mathfrak{d}^n_{i,h}$ and $\rho^n_{i,h}$, for $1 \le h \le N_A$ and $0 \le n \le N_T$, the approximation of the averages of $b_i(t^n,\cdot)$, $\mathfrak{d}_i(t^n,\cdot)$ and $\rho_i(t^n,\cdot)$ on the cell K_h, namely

$$\begin{aligned} b^n_{i,h} &= \frac{1}{\Delta a}\int_{K_h} b_i(t^n,a)\,\mathrm{d}a \quad , \qquad \mathfrak{d}^n_{i,h} = \frac{1}{\Delta a}\int_{K_h} \mathfrak{d}_i(t^n,a)\,\mathrm{d}a, \\ \rho^0_{i,h} &= \frac{1}{\Delta a}\int_{K_h} \rho_{i,0}(a)\,\mathrm{d}a \qquad \text{and} \qquad \rho^n_{i,h} \simeq \frac{1}{\Delta a}\int_{K_h} \rho(t^n,a)\,\mathrm{d}a \quad \text{if} \quad n>0. \end{aligned} \tag{2.2.13}$$

For each $i \in \{1,\dots,n_v\}$ and $n \in \{0,\dots,N_T\}$ the total population of voles in V_i at time t^n is

$$\Phi^n_i = \Delta a \sum_{h=1}^{N_A} \rho^n_{i,h}.$$

The numerical scheme for the GD model For any given value of the parameter $\eta > 0$, minimal time span of any dispersal in our model, we introduce the number of time steps $N_\eta = \lfloor \eta/\Delta t \rfloor$ and we fix to $N_\eta \Delta t$ the minimal duration of a dispersal in the numerical scheme. For $n \in \mathbb{N}$ fixed and τ^i_K in $\mathcal{T}_i(t^n) = \left\{\tau^i_1,\dots,\tau^i_{m_i(t^n)}\right\}$, the set of outbreak times taking place from V_i before t^n, we introduce $N_{\tau^i_K} = \lfloor \tau^i_K/\Delta t \rfloor$. We next define

$$\widetilde{\Phi}^n_i = \sup_{(n-N_\eta)^+ \le m \le n} \Phi^m_i \quad , \quad N^{ij}_K = N_{\tau^i_K} + L_{ij} \quad \text{and} \quad \delta^n_{N^{ij}_K} = \begin{cases} 1 & \text{if } n = N^{ij}_K, \\ 0 & \text{otherwise.} \end{cases}$$

We finally set

$$d^{n+1}_{i,h} = 1 + \Delta t\left(\mathfrak{d}^{n+1}_{i,h} + \frac{c}{\eta}\chi_{[R_i,+\infty)}\left(\widetilde{\Phi}^n_i\right)\chi_{[N_1,N_1+N_2)}(h)\right),$$

which comes from the implicit treatment of the mortality term in (2.1.4) and the semi-implicit treatment of the dispersal term in (2.1.7). Then, writing a standard upwind scheme for the transport part of (2.1.4) and using an explicit treatment of the last term of (2.1.7) we obtain the following scheme

$$\begin{cases} \rho^{n+1}_{i,h} = \\ \quad \dfrac{1}{d^{n+1}_{i,h}}\left[\left(1-\dfrac{\Delta t}{\Delta a}\right)\rho^n_{i,h} + \dfrac{\Delta t}{\Delta a}\rho^n_{i,h-1} + c\dfrac{\Delta t}{\eta}\sum_{\substack{j\neq i \\ j=1,\dots,n_v}}\sum_{K=1}^{m_j(t^n)} \delta^n_{N^{ji}_K}\chi_{[N_1,N_1+N_2]}(h-L^*_{ji})K_{ji}\rho^{n-L_{ji}}_{j,h-L^*_{ji}}\right], \\ \qquad \text{for } 1 \le i \le n_v,\ 1 \le h \le N_A,\ 0 \le n \le N_T-1, \\ \\ \rho^n_{i,0} = \mathscr{A}_i(\Phi^n_i)\Delta a \sum_{h=1}^{N_A} b^n_{i,h}\rho^n_{i,h}, \quad 1 \le i \le n_v,\ 0 \le n \le N_T-1. \end{cases} \tag{2.2.14}$$

The numerical scheme for the ID model For $n \in \mathbb{N}$, let σ_K^i be in the set

$$\mathscr{F}_i(t^n) = \left\{\sigma_1^i, \dots, \sigma_{m_i(t^n)}^i\right\}$$

of times at which either a dispersal or an arrival took place in the node V_i before t^n. We introduce $N_{\sigma_K^i} = \lfloor \sigma_K^i / \Delta t \rfloor$.

Writing again a standard upwind scheme for (2.1.8), we get for each $i \in \{1, \dots, n_v\}$,

$$\begin{cases} \rho_{i,h}^{n+1} = \dfrac{1}{1+\Delta t \mathfrak{d}_{i,h}^{n+1}} \left(\left(1 - \dfrac{\Delta t}{\Delta a}\right) \rho_{i,h}^n + \dfrac{\Delta t}{\Delta a} \rho_{i,h-1}^n \right), \quad 1 \le h \le N_A, \quad N_{\sigma_K^i} \le n < N_{\sigma_{K+1}^i}, \\ \rho_{i,0}^n = \mathscr{A}_i(\Phi_i^n) \Delta a \displaystyle\sum_{h=1}^{N_A} b_{i,h}^n \rho_{i,h}^n, \quad N_{\sigma_K^i} \le n < N_{\sigma_{K+1}^i} \\ \rho_{i,h}^{N_{\sigma_K^i}} = \rho_{i,h}^{N_{\sigma_K^i}-} - \chi_{[R_i,+\infty)}(\Phi_i^{N_{\sigma_K^i}-}) \chi_{[N_1, N_1+N_2)}(h) \rho_{i,h}^{N_{\sigma_K^i}-} \\ + \displaystyle\sum_{\substack{j \neq i \\ j=1,\dots,n_v}} \sum_{r=1}^{m_j - 1} \delta_{N_{\sigma_K^i} - L_{ji}}^{N_{\sigma_r^j}} \chi_{[R_j,+\infty)}(\Phi_j^{N_{\sigma_K^i}-L_{ji}}) \chi_{[N_1,N_1+N_2)}(h - L_{ji}^*) K_{ji} \rho_{j,h-L_{ji}^*}^{N_{\sigma_K^i}-L_{ji}}, \quad 1 \le h \le N_A. \end{cases} \tag{2.2.15}$$

2.2.1 Validation

In this part, we validate the implementation of the numerical schemes described above by comparison to exact solutions for which an analytical expression exists.

We consider a simple graph consisting of two nodes V_1 and V_2 and, denoting by $\mathscr{L}$ the matrix of the travel times and $\mathbf{K}$ the distribution matrix, we set

$$\mathscr{L} = \begin{pmatrix} 0 & 0.5 \\ 0.5 & 0 \end{pmatrix}, \qquad \text{and} \qquad \mathbf{K} = \begin{pmatrix} 0 & 1 \\ 1 & 0 \end{pmatrix}, \tag{2.2.16}$$

which means that, during a dispersal in the node V_1, all the juvenile voles will move to the node V_2 and vice versa. The initial conditions at the nodes are the following

— At V_1, we consider 50 juveniles and 170 adults. Individuals are equidistributed over their age class.

$$\rho_1(0,a) = \frac{50}{A_2 - A_1} \chi_{[A_1,A_2)}(a) + \frac{170}{A_3 - A_2} \chi_{[A_2,A_3]}(a). \tag{2.2.17}$$

— At V_2, we consider 120 adults. Individuals are equidistributed over this age class.

$$\rho_2(0,a) = \frac{120}{A_3 - A_2} \chi_{[A_2,A_3]}(a). \tag{2.2.18}$$

For simplicity we assume all the other parameters of our models to be piecewise constant and identical on the two nodes

— Reproduction rate: $b(a) = 0.3\chi_{[A_1,A_3]}(a)$;

— Mortality rate: $\mathfrak{d}(a) = \mathfrak{d}_{bj}\chi_{[0,A_2)}(a) + \mathfrak{d}_{ad}\chi_{[A_2,A_3]}(a) = 0.2\chi_{[0,A_2)}(a) + 0.1\chi_{[A_2,A_3]}(a)$;
— Dispersal threshold: $R = 200$;
— Mortality rate during dispersal: $\mathfrak{d}_{dis}(a) = 0.5$.

For the GD model we set $c = 1$ and we also have to fix the value of the minimal time span of dispersal and we set $\eta = 0.25$.

The exact solution for the GD model

In this section we provide a detailed description of the explicit solution in the time interval $[0, 1.3]$ for the GD model with the settings and initial conditions introduced in Section 2.2.1. The travel time between the two nodes is $\ell = 0.5$.

Solution at V_1 during the first dispersal, $t \in [0, t_1]$ The given initial condition makes the total population in V_1 at $t = 0$ larger than the dispersal threshold R and triggers a first dispersal. The density of voles in V_1 is a function of time and age, defined piecewise with respect to age

$$\rho_1(t,a) = \begin{cases} \text{babies}_1(t,a) = be^{-\mathfrak{d}_{bj}a}\int_{A_1}^{A_3}\rho_1(t-a,c)\,dc, & a \in [0,t), \\ 0, & a \in [t, A_1+t), \\ \text{juv}_1(t,a) = \frac{50}{A_2-A_1}e^{-(\mathfrak{d}_{bj}+1/\eta)t} = 25e^{-4.2t}, & a \in [A_1+t, A_2), \\ \text{newad}_1(t,a) = \frac{50}{A_2-A_1}e^{-(\mathfrak{d}_{bj}+1/\eta)(t-(a-A_2))-\mathfrak{d}_{ad}(a-A_2)} & \\ \qquad = 25e^{-4.2(t-(a-A_2))-0.1(a-A_2)}, & a \in [A_2, A_2+t), \\ \text{adults}_1(t,a) = \frac{170}{A_3-A_2}e^{-\mathfrak{d}_{ad}t} = 10e^{-0.1t}, & a \in [A_2+t, A_3]. \end{cases} \tag{2.2.19}$$

We observe that the total density of juvenile voles of age a who have left V_1 at time t is given by

$$\frac{50}{A_2-A_1}e^{-\mathfrak{d}_{bj}t} - \text{juv}_1(t,a),$$

so that the density of voles of age a leaving V_1 at time t is

$$\text{disp}(t,a) = \frac{50}{A_2-A_1}e^{-\mathfrak{d}_{bj}t}\left(-\mathfrak{d}_{bj} - \left(\mathfrak{d}_{bj} + \frac{1}{\eta}\right)e^{-t/\eta}\right). \tag{2.2.20}$$

The value of the total population in V_1, Φ_1, equals the threshold R at $t_0 \simeq 0.18755$. From this moment the dispersal continues for a time η more, and we denote by $t_1 = t_0 + \eta \simeq 0.43755$ the instant at which it ends.

Solution at V_1 between two dispersals, $t \in [t_1, t_2]$. The function ρ_1 is still piecewise defined with respect to the age variable, but its components are different. The evolution of the component juv_1 is juv_{12}. The new components correspond to the babies born at $t > t_1$, babies_2,

and to the voles passing from juveniles to adults at $t > t_1$, newad_2.

$$\rho_1(t,a) = \begin{cases} \text{babies}_2(t,a) = be^{-\mathfrak{d}_{bj}a}\int_{A_1}^{A_3}\rho_1(t-a,c)\,dc, & a\in[0,t-t_1),\\ \text{juv}_{12}(t,a) = \text{juv}_1(t_1,a-(t-t_1))e^{-\mathfrak{d}_{bj}(t-t_1)}, & a\in[A_1+t,A_2),\\ \text{newad}_2(t,a) = & \\ \qquad \text{juv}_1(t_1,a-(t-t_1))e^{-\mathfrak{d}_{bj}(t-t_1-(a-A_2))-\mathfrak{d}_{ad}(a-A_2)}, & a\in[A_2,A_2+(t-t_1)),\\ \rho_1(t_1,a-(t-t_1))e^{-\mathfrak{d}(a)(t-t_1)}, & \text{otherwise.}\end{cases} \tag{2.2.21}$$

The total population at V_1, Φ_1, increases up to reach again the value R at $t = t_2 \simeq 0.84818$. This triggers a second dispersal.

Solution at V_1 for $t \in [t_2, A_1]$. The second dispersal modifies the dynamics of the juveniles, so that the functions giving the density of newborns and the density of new adults also need to be updated. The evolution of the component juv_{12} is juv_{123}.

$$\rho_1(t,a) = \begin{cases} \text{babies}_3(t,a) = be^{-\mathfrak{d}_{bj}a}\int_{A_1}^{A_3}\rho_1(t-a,c)\,dc, & a\in[0,t-t_2),\\ \text{juv}_{123}(t,a) = \text{juv}_{12}(t_2,a-(t-t_2))e^{-(\mathfrak{d}_{bj}+1/\eta)(t-t_2)}, & a\in[A_1+t,A_2),\\ \text{newad}_3(t,a) = & \\ \qquad \text{juv}_{12}(t_2,a-(t-t_2))e^{-\mathfrak{d}_{bj}(t-t_2-(a-A_2))-\mathfrak{d}_{ad}(a-A_2)}, & a\in[A_2,A_2+(t-t_2)),\\ \rho_1(t_2,a-(t-t_2))e^{-\mathfrak{d}(a)(t-t_1)}, & \text{otherwise.}\end{cases} \tag{2.2.22}$$

It should be noticed that the total population in V_1 reaches again the value R at time $t_3 \simeq 0.94675$. This does not produce an immediate change in the dynamics because the difference $t_3 - t_2$ is less that η, but tells us that the second dispersal will last up to time $t_4 = t_3 + \eta \simeq 1.44675$.

Solution at V_1 for $t \in [A_1, 1.3]$. For $t > A_1$ we have to consider two additional age classes : some of the babies becomes juvenile and start to reproduce, we denote them by newjuv_4, and babies born after time $t = A_1$, babies_4.

$$\rho_1(t,a) = \begin{cases} \text{babies}_4(t,a) = be^{-\mathfrak{d}(a)a}\int_{A_1}^{A_3}\rho_1(t-a,c)\,dc, & a\in[0,t-A_1),\\ \text{babies}_1(t,a), & a\in[t-t_1,A_1),\\ \text{newjuv}_4(t,a) = \text{babies}_1(A_1,a-(t-A_1))e^{-\mathfrak{d}_{bj}(t-a)-(\mathfrak{d}_{bj}+1/\eta)(a-A_1)} & a\in[A_1,t),\\ \rho_1(A_1,a-(t-A_1))e^{-\mathfrak{d}(a)(t-A_1)}, & \text{otherwise.}\end{cases} \tag{2.2.23}$$

Solution at V_2 before the arrival of voles from V_1, $t \in [0, \ell]$. At time $t = 0$ the total population at V_2 is 120. We will see that no dispersal takes place from this node for $t = [0, 1.3]$. We use a different font to distinguish the age groups appearing in the solution at node V_2, while the

indices are given in the same way.

$$\rho_2(t,a)=\begin{cases}\texttt{babies}_1(t,a)=be^{-\mathfrak{d}_{bj}a}\int_{A_1}^{A_3}\rho_2(t-a,c)\,dc, & a\in[0,t),\\ 0 & a\in[t,A_2+t),\\ \texttt{adults}_1(t,a)=\frac{120}{A_3-A_2}e^{-\mathfrak{d}_{ad}t}=\frac{12}{17}e^{-0.1t}, & a\in[A_2+t,A_3].\end{cases}\tag{2.2.24}$$

Solution at V_2 during the arrival of the first group of dispersers, $t\in[\ell,\ell+t_1]$. We have to take into account several new groups of individuals. The new components correspond to the babies born at $t>\ell$, $\texttt{babies}_2$, and to the voles arriving from the node V_1. Some of them arrive as juveniles, $\texttt{juv}_2$, some as adults, $\texttt{adults}_2$. Some of the juveniles become adults after their arrival, we call them $\texttt{newad}_2$. The voles whose age is in $(A_2+\ell,A_2+t)$ originated from V_1, but when they arrived they were jounger than $A_2+\ell$, we call this group $\texttt{adultsevol}_2$. We compute their density using (2.2.20) and the fact that while travelling from V_1 to V_2 the dispersers solve the ODE $y'=-\mathfrak{d}_{dis}y$.

$$\rho_2(t,a)=\begin{cases}\texttt{babies}_2(t,a), & a\in[0,t-\ell),\\ \texttt{juv}_2(t,a), & a\in[A_1+t,A_2),\\ \texttt{newad}_2(t,a)+\texttt{adults}_2(t,a), & a\in[A_2,A_2+(t-\ell)),\\ \texttt{adults}_2(t,a), & a\in[A_2+(t-\ell),A_2+\ell),\\ \texttt{adultsevol}_2(t,a), & a\in[A_2+\ell,A_2+t),\\ \rho_2(\ell,a-(t-\ell))e^{-\mathfrak{d}(a)(t-\ell)}, & \text{otherwise,}\end{cases}\tag{2.2.25}$$

that is

$$\rho_2(t,a)=\begin{cases}be^{-\mathfrak{d}_{bj}a}\int_{A_1}^{A_3}\rho_2(t-a,c)\,dc, & a\in[0,t-\ell),\\ \int_\ell^t e^{-\mathfrak{d}_{bj}(t-s)}e^{-\mathfrak{d}_{dis}\ell}\mathrm{disp}(s-\ell,a-(t-s+\ell))\,ds, & a\in[A_1+t,A_2),\\ \texttt{juv}_2(t-(a-A_2),A_2)e^{-\mathfrak{d}_{ad}(a-A_2)}+ & \\ \quad\int_{t-(a-A_2)}^t e^{-\mathfrak{d}_{ad}(t-s)}e^{-\mathfrak{d}_{dis}\ell}\mathrm{disp}(s-\ell,a-(t-s+\ell))\,ds, & a\in[A_2,A_2+(t-\ell)),\\ \int_\ell^t e^{-\mathfrak{d}_{ad}(t-s)}e^{-\mathfrak{d}_{dis}\ell}\mathrm{disp}(s-\ell,a-(t-s+\ell))\,ds, & a\in[A_2+(t-\ell),A_2+\ell),\\ \texttt{adults}_2(t-(a-(A_2+\ell)),A_2+\ell)e^{-\mathfrak{d}_{ad}(a-(A_2+\ell))}, & a\in[A_2+\ell,A_2+t),\\ \rho_2(\ell,a-(t-\ell))e^{-\mathfrak{d}(a)(t-\ell)}, & \text{otherwise.}\end{cases}\tag{2.2.26}$$

Solution at V_2 for $t\in[\ell+t_1,1.3]$. In the interval of time $[\ell+t_1,\ell+t_2]$ no more voles arrive from V_1 and the total population of V_2 does not attain the threschold value R. For our validation we only compute the solution up to time $t=1.3<\ell+t_2$. The age groups already present in the dynamics just evolve following the prescribed mortality rates, until time $t=A_1$ when some on the individuals in $\texttt{babies}_1$ become juvenile. Therefore for $t\in[\ell+t_1,A_1]$ the function

ρ_2 takes the form

$$\rho_2(t,a) = \begin{cases} \texttt{babies}_3(t,a) = be^{-\mathfrak{d}_{bj}a}\int_{A_1}^{A_3}\rho_2(t-a,c)\,dc, & a\in[0,t-(\ell+t_1)),\\ \texttt{newad}_3(t,a) = & \\ \texttt{juv}_2(\ell+t_1,a-(t-\ell-t_1))e^{-\mathfrak{d}_{bj}(t-(\ell+t_1)-(a-A_2))-\mathfrak{d}_{ad}(a-A_2)}, & a\in[A_2,A_2+t-(\ell+t_1)),\\ \rho_2(\ell+t_1,a-(t-\ell-t_1))e^{-\mathfrak{d}(a)(t-(\ell+t_1))}, & \text{otherwise.}\end{cases} \tag{2.2.27}$$

While for $t\in[A_1,1.3]$ ρ_2 becomes

$$\rho_2(t,a) = \begin{cases} \texttt{babies}_4(t,a) = be^{-\mathfrak{d}_{bj}a}\int_{A_1}^{A_3}\rho_2(t-a,c)\,dc, & a\in[0,t-A_1),\\ \texttt{babies}_1(t,a), & a\in[t-A_1,A_1),\\ \texttt{newjuv}_4(t,a) = \texttt{babies}_1(A_1,a-(t-A_1))e^{-\mathfrak{d}_{bj}(t-A_1)}, & a\in[A_1,t),\\ \texttt{newad}_4(t,a) = & \\ \qquad \texttt{juv}_2(A_1,a-(t-A_1))e^{-\mathfrak{d}_{bj}(t-A_1-(a-A_2))-\mathfrak{d}_{ad}(a-A_2)}, & a\in[A_2,A_2+t-A_1),\\ \rho_2(A_1,a-(t-A_1))e^{-\mathfrak{d}(a)(t-A_1)}, & \text{otherwise.}\end{cases} \tag{2.2.28}$$

Figure 2.3 shows the comparison between the exact and the numerical solutions at the two nodes for the GD model at the final time $T=1.3$. We observe a perfect matching between the two solutions where the numerical one was computed with $\Delta a=\Delta t=0.00625$.

The exact solution for the ID model

In this section we provide a detailed description of the explicit solution in the time interval $[0,1.3]$ for the ID model with the settings and initial conditions introduced in Section 2.2.1. The travel time between the two nodes is $\ell=0.5$.

Solution at V_1 for $t\in[0,A_1]$. The given initial condition makes the total population in V_1 at $t=0$ higher than the dispersal threshold R, therefore the juvenile individuals immediately leave the node. The density of voles in V_1 is a function of time and age, defined piecewise with respect to age

$$\rho_1(t,a) = \begin{cases} \text{babies}_1(t,a) = be^{-\mathfrak{d}_{bj}a}\int_{A_1}^{A_3}\rho_1(t-a,c)\,dc, & a\in[0,t),\\ 0, & a\in[t,A_2+t),\\ \text{adults}_1(t,a) = \frac{170}{A_3-A_2}e^{-\mathfrak{d}_{ad}t} = 10e^{-0.1t}, & a\in[A_2+t,A_3].\end{cases} \tag{2.2.29}$$

Solution at V_1 for $t\in[A_1,1.3]$. Starting from time $t=A_1$ a fraction of the babies will become juveniles and their reproductive process has to be taken into account. This leads to the formation of two more age groups : the babies born after time $t=A_1$, babies$_2$, and the individuals

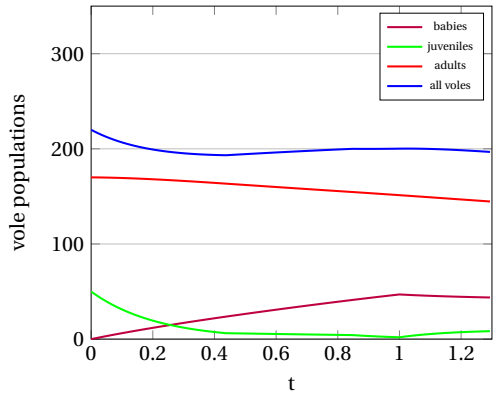

(a) Exact solution for GD model for node V_1

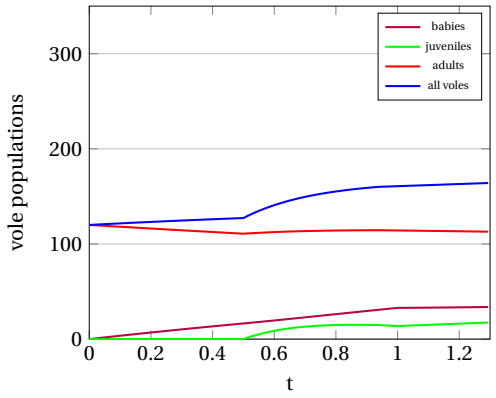

(b) Exact solution for GD model for node V_2

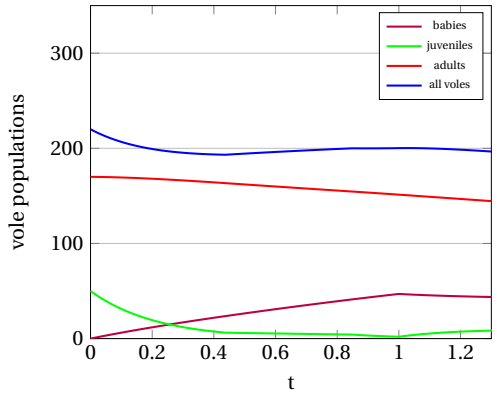

(c) Computed solution for GD model for node V_1

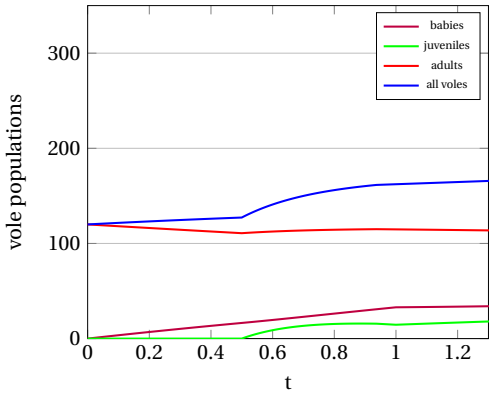

(d) Computed solution for GD model for node V_2

Figure 2.3 – With reference to Section 2.2.1: the comparison between the population of voles in the exact solution and the GD model for $\eta = 0.25$.

passing from the babies to juveniles, newjuv_2.

$$\rho_1(t,a) = \begin{cases} \text{babies}_2(t,a) = be^{-\mathfrak{d}_{bj}a}\int_{A_1}^{A_3}\rho_1(t-a,c)\,dc, & a\in[0,t-A_1), \\ \text{babies}_1(t,a), & a\in[t-A_1,A_1), \\ \text{newjuv}_2(t,a) = \text{babies}_1(A_1,a-(t-A_1))e^{-\mathfrak{d}_{bj}(t-A_1)}, & a\in[A_1,t), \\ 0, & a\in[t,A_2+t), \\ \text{adults}_1(t,a) = \text{adults}_1(A_1,a-(t-A_1))e^{-\mathfrak{d}_{ad}(t-A_1)}, & a\in[A_2+t,A_3]. \end{cases} \tag{2.2.30}$$

Solution at V_2 before the arrival of voles from V_1, $t\in[0,\ell]$. The dynamics is the same in the two models. The explicit form of the solution is given in (2.2.24).

Solution at V_2 for $t \in [\ell, A_1]$. The density of voles reaching V_2 at $t = \ell = 0.5$ are

$$\frac{50}{A_2 - A_1} \chi_{[A_1+\ell, A_2+\ell]}(a) e^{-\ell \mathfrak{d}_{dis}},$$

then some of them are juveniles, $\texttt{juv}_2$, some are adults, $\texttt{adults}_2$. Some of the juveniles become adults after their arrival, we call them $\texttt{newad}_2$. We call $\texttt{babies}_2$ the babies born for $t > \ell$.

$$\rho_2(t,a) = \begin{cases} \texttt{babies}_2(t,a) = b e^{-\mathfrak{d}_{bj} a} \int_{A_1}^{A_3} \rho_2(t-a,c)\, dc, & a \in [0, t-\ell), \\ \texttt{juv}_2(t,a) = \frac{50}{A_2 - A_1} e^{-\ell \mathfrak{d}_{dis} - \mathfrak{d}_{bj}(t-\ell)}, & a \in [A_1 + t, A_2), \\ \texttt{newad}_2(t,a) = \texttt{juv}_2(t-(a-A_2), A_2) e^{-\mathfrak{d}_{ad}(a-A_2)}, & a \in [A_2, A_2 + (t-\ell)), \\ \texttt{adults}_2(t,a) = \frac{50}{A_2 - A_1} e^{-\ell \mathfrak{d}_{dis} - \mathfrak{d}_{ad}(t-\ell)}, & a \in [A_2 + (t-\ell), A_2 + t), \\ \rho_2(\ell, a-(t-\ell)) e^{-\mathfrak{d}(a)(t-\ell)}, & \text{otherwise.} \end{cases} \tag{2.2.31}$$

Solution at V_2 for $t \in [A_1, 1.3]$. Starting from time $t = A_1$ a fraction of the babies will become juveniles and their reproductive process has to be taken into account. This leads to the formation of two more age groups : the babies born after time $t = A_1$, $\texttt{babies}_3$, and the individuals passing from the babies to juveniles, newjuv_3.

$$\rho_2(t,a) = \begin{cases} \texttt{babies}_3(t,a) = b e^{-\mathfrak{d}_{bj} a} \int_{A_1}^{A_3} \rho_2(t-a,c)\, dc, & a \in [0, t-A_1), \\ \texttt{babies}_1(t,a), & a \in [t-\ell, A_1), \\ \texttt{newjuv}_3(t,a) = \text{babies}_1(A_1, a-(t-A_1)) e^{-\mathfrak{d}_{bj}(t-A_1)}, & a \in [A_1, t), \\ \rho_2(A_1, a-(t-A_1)) e^{-\mathfrak{d}(a)(t-A_1)}, & \text{otherwise.} \end{cases} \tag{2.2.32}$$

Figure 2.4 illustrates the comparison between the explicit solution and its numerical solution at the two nodes for the ID model at the final time $T = 1.3$. We again observe a perfect agreement between the two solutions. The numerical solutions was computed with $\Delta a = \Delta t = 0.00625$.

2.2.2 Numerical convergence

We introduce here the following relative L^1-discrete error for the density in the node V_i, $i = 1, 2$, at a given time t^n

$$e_i^n = \frac{\sum_{1 \le h \le N_a} |\rho_i(t^n, a_h) - \rho_{i,h}^n|}{\sum_{1 \le h \le N_a} |\rho_i(t^n, a_h)|},$$

where $\rho(t^n, a_h)$ is an exact solution evaluated at the point a_h and at time t^n.

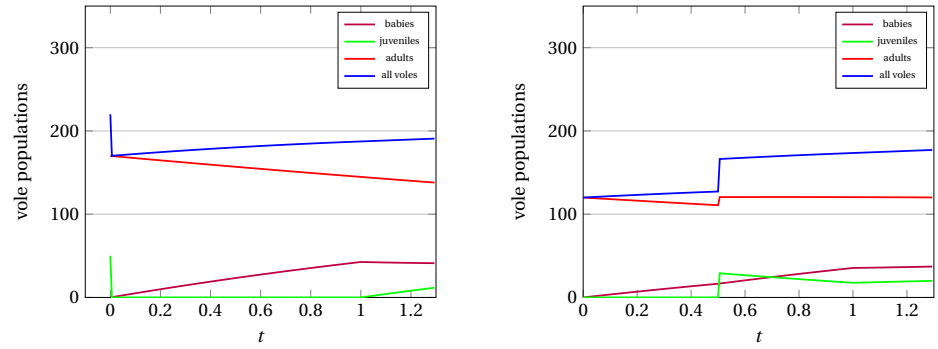

(a) Node V_1 (b) Node V_2

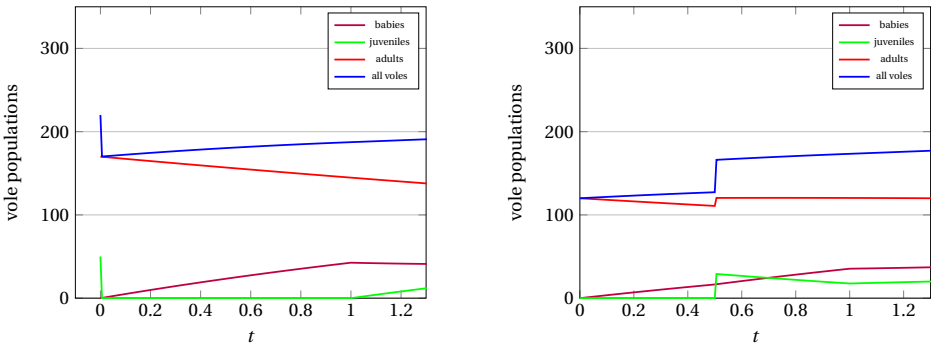

(c) Node V_1 (d) Node V_2

Figure 2.4 – With reference to Section 2.2.1: the comparison between the population of voles in the exact solution and in the ID model.

In tables 2.1 and 2.2, we have reported the relative L^1-discrete errors for both models in the two nodes V_1 and V_2, computed for different values of age and times steps at two final times $T = 0.6$ and $T = 1.2$. The results suggest the convergence of the numerical schemes. Moreover, figures 2.5 and 2.6 suggest that order of convergence of the scheme for the GD model is approximately between 0.71 and 1, and the one for the ID model is 1. We can also observe that the loss of accuracy of the scheme for the GD model is mainly due to the approximation of the arrival term in (2.1.7).

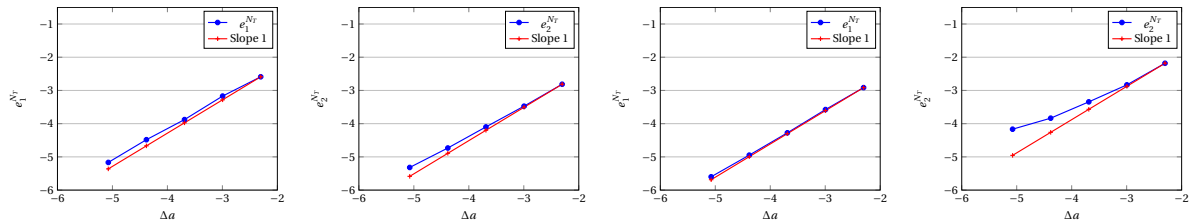

(a) V_1 at $T = 0.6$ (b) V_2 at $T = 0.6$ (c) V_1 at $T = 1.2$ (d) V_2 at $T = 1.2$

Figure 2.5 – L^1-discrete relative errors for the GD Model in log/log scale at $T = 0.6$ and $T = 1.2$

Δt	Δa	$e_1^{N_T}$, $T=0.6$	$e_2^{N_T}$, $T=0.6$	$e_1^{N_T}$, $T=1.2$	$e_2^{N_T}$, $T=1.2$
0.1	0.1	7.51×10^{-2}	$6.\times10^{-2}$	5.42×10^{-2}	1.128×10^{-2}
0.05	0.05	4.2×10^{-2}	3.1×10^{-2}	2.8×10^{-2}	5.89×10^{-2}
0.025	0.025	2.07×10^{-2}	1.66×10^{-2}	1.39×10^{-2}	3.53×10^{-2}
0.0125	0.0125	1.13×10^{-2}	8.8×10^{-3}	7.1×10^{-3}	2.16×10^{-2}
0.00625	0.00625	5.7×10^{-3}	4.9×10^{-3}	3.7×10^{-3}	1.55×10^{-2}

Table 2.1 – L^1-discrete relative errors for the GD model

Δt	Δa	$e_1^{N_T}$, $T=0.6$	$e_2^{N_T}$, $T=0.6$	$e_1^{N_T}$, $T=1.2$	$e_2^{N_T}$, $T=1.2$
0.1	0.1	4.33×10^{-4}	1.22×10^{-2}	1.2×10^{-3}	1.38×10^{-2}
0.05	0.05	2.19×10^{-4}	6.13×10^{-3}	6.05×10^{-4}	6.93×10^{-3}
0.025	0.025	1.1×10^{-4}	3.07×10^{-3}	3.03×10^{-4}	3.47×10^{-3}
0.0125	0.0125	5.56×10^{-5}	1.53×10^{-3}	1.52×10^{-4}	1.73×10^{-3}
0.00625	0.00625	2.75×10^{-5}	7.66×10^{-4}	7.63×10^{-5}	8.67×10^{-4}

Table 2.2 – L^1-discrete relative errors for the ID model

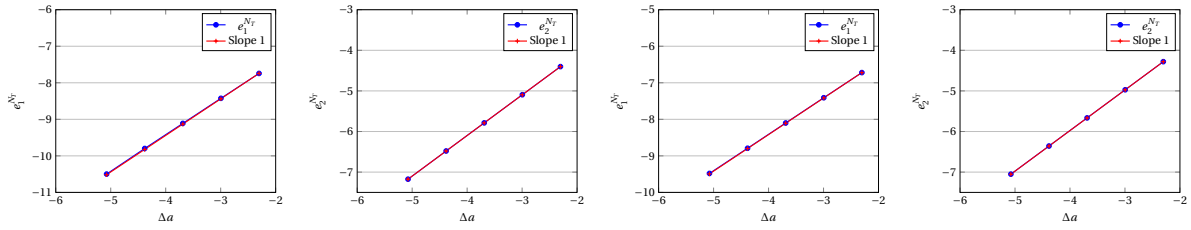

(a) V_1 at $T=0.6$ (b) V_2 at $T=0.6$ (c) V_1 at $T=1.2$ (d) V_2 at $T=1.2$

Figure 2.6 – L^1-discrete relative errors for the ID model in log/log scale at $T=0.6$ and $T=1.2$

2.2.3 A first comparison between the two models

In this section we consider once again the initial conditions (2.2.17), (2.2.18) and we compute the evolution of the vole populations in the two nodes by the GD model when the parameter of minimal time span for a dispersal is reduced to $\eta=3\times10^{-3}$, $c=1$ and the final time is $T=1.3$. The result obtained for $\Delta a=\Delta t=3\times10^{-4}$ is in Figures 2.7.

We can observe that the profile of the solution is, at a first approximation, similar to the solution obtained from the same initial condition by the ID model, see Figure 2.4. In particular we observe that the two dispersals occuring in the fist cell for $t>1$ concerne a so small number of juveniles that none of them reaches the second cell, so that the dynamics of the second cell is almost identical in the two simulations.

This means that, even if the ID model is necessarily less precise, it suffices to capture the dynamics we would observe in the GD model for small values of η.

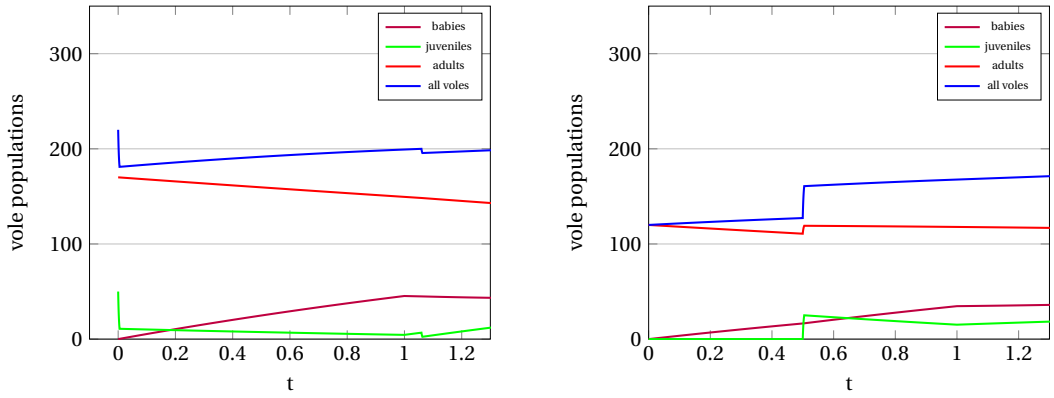

(a) Node V_1 (b) Node V_2

Figure 2.7 – The voles populations of the two nodes computed with GD model for $\eta = 3 \times 10^{-3}$

2.3 Numerical simulations

In this section, we perform numerical simulations on the two models, in order to show their ability to reproduce the qualitative behavior of vole populations and in particular their spatial dynamics. In this chapter we limit our attention to simple toy models as the implementation of the schemes on graph representing large regions would require a large effort in optimization and in parallelization of the codes, which we defer to future investigation.

Everywhere in the following we assume that the minimal duration of a dispersal in the GD model is $\eta = 7/18$ that corresponds to one week in real time.

2.3.1 Two-nodes dynamics

In this section, we investigate the evolution of a population of voles on a graph consisting of two nodes assumed to represent two different types of landscapes and the edge linking them. The landscapes we consider are described below:

— The first node represents a crop field, which is a source of abundant food and shelter for voles during summer and spring. This traduces into high reproduction rate and low mortality rate in the warm season. On the contrary mortality becomes high at harvesting time and remains so up to the end of one year cycle.
To reproduce such properties, we consider the reproduction and mortality rate functions defined by (2.1.9), (2.1.10) and (2.1.12) where we assume $\alpha = 1$, $\delta = 1$ and $\kappa = 2.6$.

— The second node represents a forest, where the population of voles is almost stable over several years. The reproduction rate is lower than in the crop field, but the mortality varies less dramatically from warm to cold season.
To reproduce such properties, we consider the reproduction and mortality rate functions defined by (2.1.9), (2.1.10) and (2.1.12) where we assume $\alpha = 0.656$, $\delta = 1$ and $\kappa = 1.5$.

We assume that the travel time from one node to the other is $\ell = 0.5$. Then we consider

the travel time matrix and the distribution matrix as

$$\mathscr{L} = \begin{pmatrix} 0 & 0.5 \\ 0.5 & 0 \end{pmatrix} \quad \text{and} \quad \mathbf{K} = \begin{pmatrix} 0 & 1 \\ 1 & 0 \end{pmatrix}$$

respectively. The initial conditions are of 70 adult individuals in each node, equidistributed over their age class. The simulations, performed with $\Delta a = \Delta t = 0.00625$, are depicted in Figures 2.8.

Both models reproduce the cyclic behavior of the population. A characteristic feature of the ID model is the appearance of sharp peaks, as in Figure 2.8(d). This is due to the fact that voles coming from the node representing the crop field reach their destination at moments where the total population in the node representing forest is close to the dispersal threshold. This sudden population increase, sufficient to trigger dispersal, lasts only one time step. On the contrary, no peaks arise in Figure 2.8(c) as in the GD model, dispersals and arrivals happen progressively. Moreover, since not all of the juveniles leave, the variation in the total population is lower, see Figures 2.8(a) and 2.8(c).

2.3.2 Three-nodes dynamics

In this section we run our models on a complete graph with three nodes, V_i, $i = 1,2,3$. This allows us to use a more interesting distribution matrix to reproduce, for example, the fact that voles prefer to move downhill rather than uphill, and that they are more likely to stop at places where resources are more abundant. Since the availability of food may change in time, we consider a time dependent distribution matrix in our second example.

The simulations of this section are performed with $\Delta a = \Delta t = 0.0125$.

Scenario 1: Three nodes located at different heights

We assume here that the node V_1 is located at the highest spot and V_3 at the lowest one. For all the nodes, we use the mortality and the reproduction rates defined by (2.1.9), (2.1.10) and (2.1.12) with $\alpha = \delta = 1$ and $\kappa = 1.5$. As initial conditions we take $\phi_1(0) = 100$, $\phi_2(0) = 50$ and $\phi_3(0) = 0$, that means that the third node is initially empty. It has been observed that when dispersal occur, voles move more frequently downhill (2 times out of 3), see for instance [16, 29]. In other to take into account this characteristic, we consider the following distribution matrix

$$\mathbf{K} = \begin{pmatrix} 0 & 1 & 0 \\ 1/3 & 0 & 2/3 \\ 0 & 1 & 0 \end{pmatrix}.$$

In particular, this means that all the dispersals taking place from V_1 or V_3 head toward V_2, while 2 out of 3 voles leaving V_2 would go to V_3. We fix the that the travel times matrix as

$$\mathscr{L} = \begin{pmatrix} 0 & 1 & 1.5 \\ 1 & 0 & 0.5 \\ 1.5 & 0.5 & 0 \end{pmatrix}. \tag{2.3.33}$$

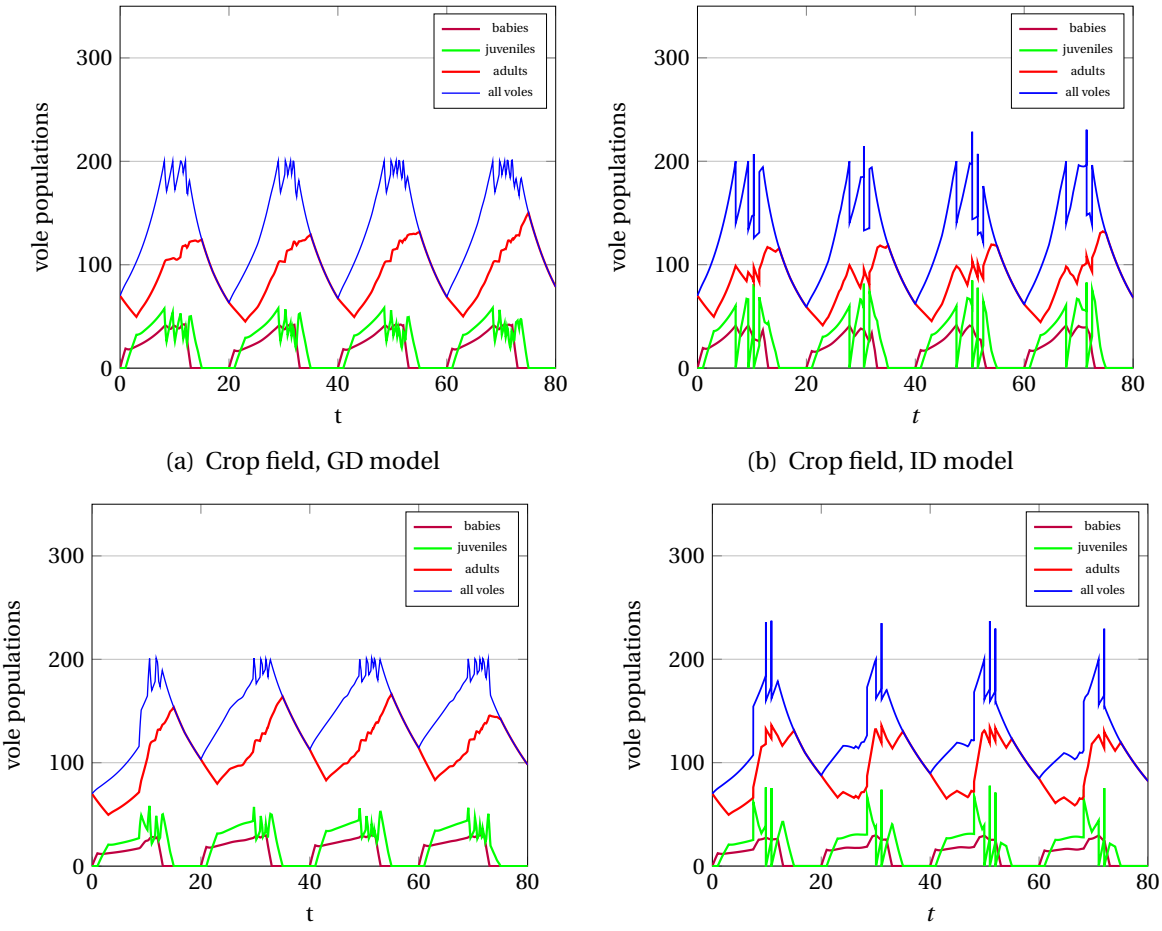

(a) Crop field, GD model

(b) Crop field, ID model

(c) Forest, GD model

(d) Forest, ID model

Figure 2.8 – With reference to subsection 2.3.1: the evolution of the population over 4 years for the two models.

Figures 2.9 show the evolution of the population for both models over three years. We can observe numerous outbreaks from V_2, which are due to the fact that all the voles that disperse from V_1 and V_3 arrive in this node. Moreover from Figure 2.9(c), we can see that, due to the relatively long duration of dispersal, the total population in V_2 largely exceeds the threshold 200 in the second and third year.

We can also notice that a persistent colony appears in V_3 thanks to the individuals arriving from the other nodes.

Scenario 2: Time dependent distribution matrix

We consider a domain partitioned into three cells. The first one, V_1, is located at a higher elevation than the two others, which are on the same level. We make the following choice of parameters :

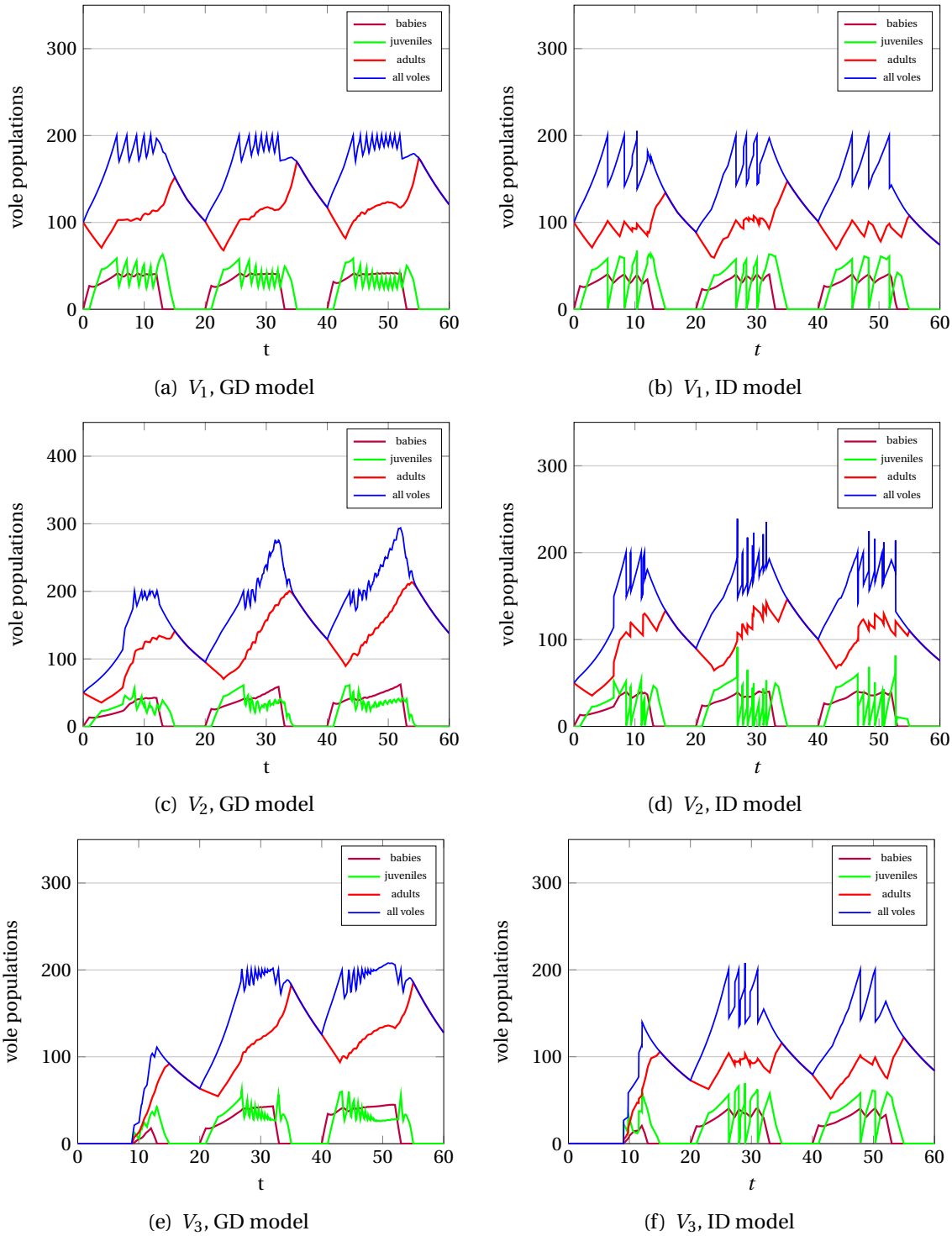

(a) V_1, GD model

(b) V_1, ID model

(c) V_2, GD model

(d) V_2, ID model

(e) V_3, GD model

(f) V_3, ID model

Figure 2.9 – With reference to Section 2.3.2: The population of voles over 3 years in V_1, V_2 and V_3 for both models.

— In V_1 $\alpha = \delta = 1$, $\kappa = 1.5$ and the initial condition consists of 100 adults individuals equidistributed over their age class.
— In V_2 we imagine to have a crop field. as in Section 2.3.1. Then we set $\alpha = \delta = 1$, $\kappa = 2.6$ and the initial condition consists of 70 adults individuals equidistributed over their age class.
— In V_3 we have a forest as in Section 2.3.1. Then we set $\alpha = 0.656$, $\delta = 1$, $\kappa = 1.5$ and take the same initial condition as in V_2.

We assume now that during spring and summer, i.e. for $t \in [0,10]$, eventual dispersers tend to move to the second colony because of the abundance of food source in a crop landscape. While in autumn and winter, i.e. for $t \in [10,20]$, they rather move downhill to the third cell, as we mentioned in Section 2.3.1. Therefore we consider the dispersal ratio matrix $\mathbf{K}_1$ for $t \in [0,10]$ and $\mathbf{K}_2$ for $t \in [10,20]$,

$$\mathbf{K}_1 = \begin{pmatrix} 0 & 0.7 & 0.3 \\ 0.3 & 0 & 0.7 \\ 0.2 & 0.8 & 0 \end{pmatrix}, \qquad \mathbf{K}_2 = \begin{pmatrix} 0 & 0.3 & 0.7 \\ 0.3 & 0 & 0.7 \\ 0.3 & 0.7 & 0 \end{pmatrix}. \tag{2.3.34}$$

We assume that the travel time between any two nodes is 0.5, so that

$$\mathscr{L} = \begin{pmatrix} 0 & 0.5 & 0.5 \\ 0.5 & 0 & 0.5 \\ 0.5 & 0.5 & 0 \end{pmatrix}. \tag{2.3.35}$$

In Figures 2.10 we present the evolution of the populations of voles in the three nodes for both models during three years. We can observe several dispersals occuring every year from each node. As we already noticed in previous simulations, the arrivals of voles increase the frequency of outbreaks. Moreover, we can see that in V_2, that is the crop field landscape, the population of voles increases over the reproduction season with the appearance of peaks for the second model in Figure 2.10(d). However, due to the high mortality rate after harvesting the increase of the total population each year is slow and contained, in particular its minimal value in a one year period is amost constant. On the contrary, in V_3, the minimal value of the total population increases over one year, which means that there are more and more adults. At the end of the third year, we have approximatively 110 and 96 adult individuals in Figure 2.10(e) and Figure 2.10(f) respectively. As a consequence of the increment of the adult population, we can see in the two figures that there are more and more dispersal outbreaks. Figure 2.10(f) also shows more peaks than in Figure 2.10(d).

2.4 Allee's effect : survival number of a colony

We investigate in this part the minimal number of juvenile or adult individuals needed to maintain the existence of a colony when we consider the reproduction and the mortality rates defined by (2.1.9), (2.1.10) and (2.1.12) with $\alpha = \delta = 1$ and $\kappa = 1.5$. To that end, in the boundary condition at $a = 0$, (2.1.6), we consider a non constant function $\mathscr{A}$ of the form

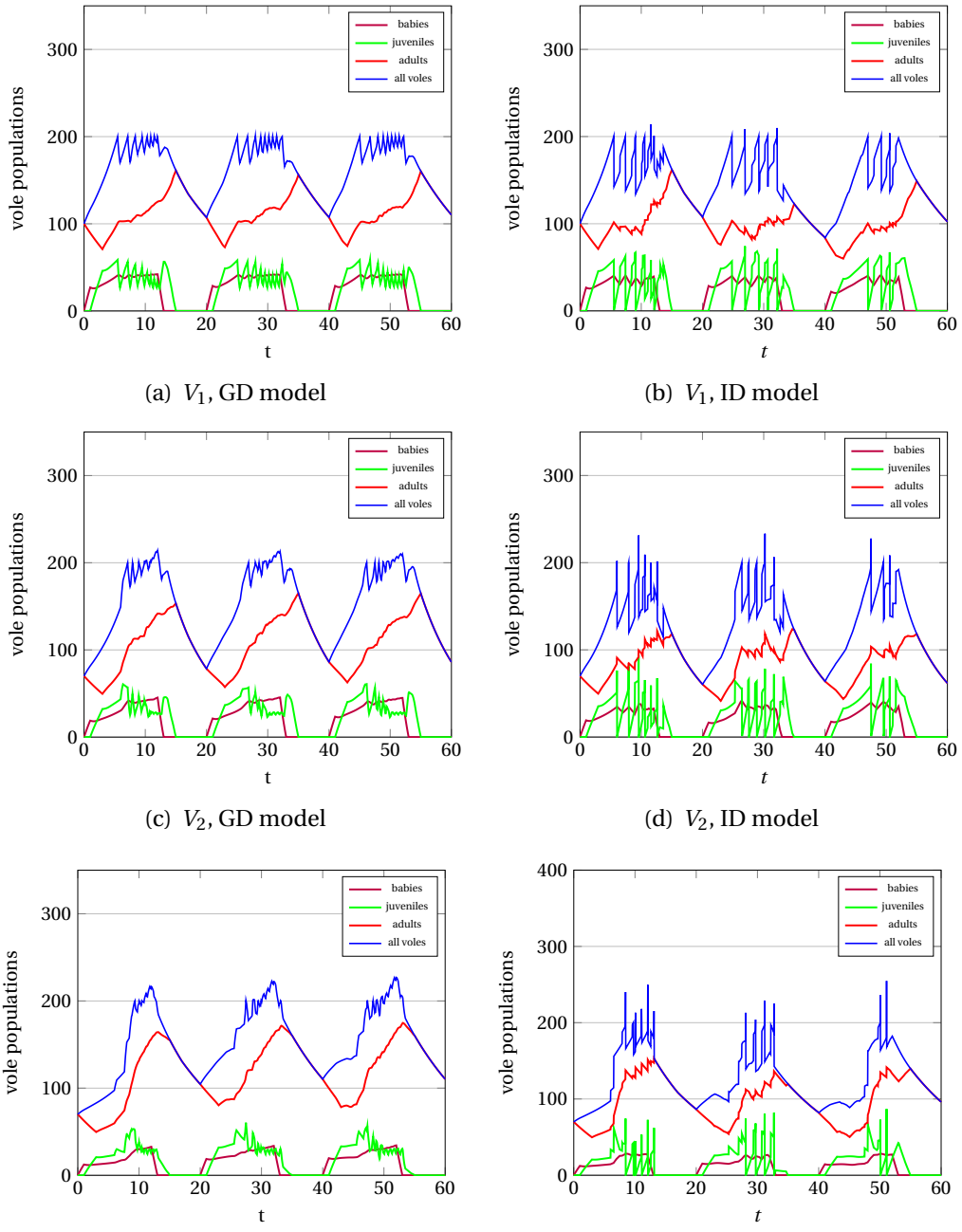

(a) V_1, GD model

(b) V_1, ID model

(c) V_2, GD model

(d) V_2, ID model

(e) V_3, GD model

(f) V_3, ID model

Figure 2.10 – With reference to Section 2.3.2: the population of voles over 3 years on three nodes representing different landscapes.

$$\mathscr{A}(\phi) = \frac{\beta\phi^{\gamma}}{(B+\phi)^{\gamma}}.$$

so that the model can reproduce the Allee's effect. For simplicity, we just consider case in

which $\beta = 1$, $\gamma \in \mathbb{N}$, and

$$B = \left(\frac{\gamma+1}{\gamma-1}\right)\phi_*^{\gamma}, \tag{2.4.36}$$

where ϕ_* is a given value. As an example, if we take $\gamma = 8$ and $\phi_* = 20$ we obtain

$$\mathscr{A}(\phi) = \frac{\phi^8}{\left(\frac{9.20^8}{7} + \phi^8\right)}, \quad \phi \geq 0. \tag{2.4.37}$$

This function has an inflection point at $\phi = 20$ whose value is $\mathscr{A}(20) = 7/16 = 0.4375$, see Figure 2.11. This factor makes the reproduction rate almost insignificant when the total pop-

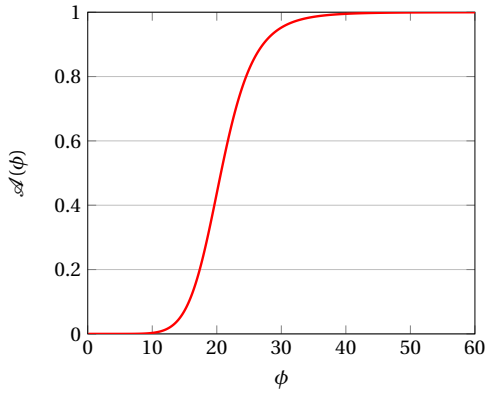

Figure 2.11 – The function defined in (2.4.37).

ulation is less than 20. Considering one node and using the mortality and the reproduction rates defined by (2.1.9), (2.1.10) and (2.1.12) with $\alpha = \delta = 1$ and $\kappa = 1.5$, that is the same parameters as in Figures 2.2(a) and 2.2(b), we can see in Figures 2.12, that we need at least 19 juvenile individuals or 20 adult individuals in the initial condition for the colony to persist over several years without any external support. Figures 2.13 show the evolution of the populations of voles inside a colony during two years when we start from 18 juvenile and 19 adult individuals respectively. As we can see, the colony disappears in less than two years. We can calibrate the model to obtain a realistic survival number by changing the inflection point of the function $\mathscr{A}$.

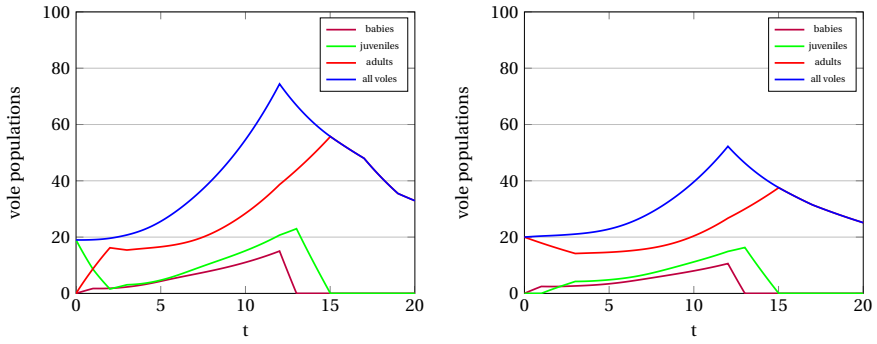

Figure 2.12 – Populations of voles in a colony starting with 19 juvenile (left) or 20 adult (right) individuals.

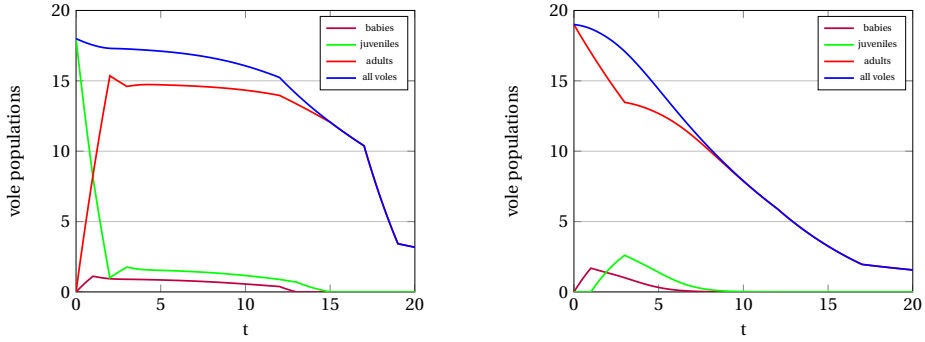

Figure 2.13 – Populations of voles in a colony starting with 18 juvenile (left) or 19 adult (right) individuals.

Chapter 3

An hyperbolic-parabolic predator-prey model involving a vole population structured in age

3.1 The model and the assumptions

Our goal in this chapter is to investigate the wellposedness of a predator-prey model extending the model for a vole population structured in age we introduced in [9]. To this end we couple the latter equation to the hyperbolic equation for predators proposed in [13] in which the drift depends nonlocally on the density of preys, so that the predators tend to move toward the regions in which preys are more abundant. The system we consider writes as follows

$$\begin{cases} \partial_t u + \operatorname{div}_x\big(uv(\phi)\big) = (\mathfrak{b}(\phi) - \beta)u, & (t,x) \in (0,T)\times\mathbb{R}^2, \\ \partial_t \rho + \partial_a \rho + \operatorname{div}_x\big(\rho\chi_1(a)\mathbf{v}(x)Y_\theta(\phi - R)\big) = \mu\Delta_x\rho - \mathfrak{d}(t,a,x)\rho - \mathfrak{p}(a,u)\rho, & (t,a,x) \in (0,T)^2\times\mathbb{R}^2, \\ \rho(t,0,x) = \mathscr{A}(\phi)\left(\displaystyle\int_0^\infty \rho(t,a,x)\chi_3(a)\,\mathrm{d}a\right)\omega(t,x), & (t,x) \in (0,T)\times\mathbb{R}^2, \\ \rho(0,a,x) = \rho_0(a,x), & (a,x) \in (0,T)\times\mathbb{R}^2, \\ u(0,x) = u_0(x), & x \in \mathbb{R}^2, \end{cases} \tag{3.1.1}$$

where $u = u(t,x)$ and $\phi = \phi(t,x)$ represent the respective density of predators and preys at (t,x). Since the prey population is also structured on age its dynamics is better described by $\rho = \rho(t,a,x)$, which is the density of preys of age a at (t,x). More precisely, the relation between ϕ and ρ is given by

$$\phi(t,x) = \int_0^\infty \rho(t,a,x)\chi_2(a)\,\mathrm{d}a, \tag{3.1.2}$$

where $\chi_2(a)$ is an approximation of the indicator function of the interval (σ,T), where T is the target time of our observation and $0 < \sigma \ll 1$. The parameter σ does not play a role in the

modeling, but allows to avoid technical difficulties in our analysis. In the first equation, the function $\mathfrak{b}(\phi)$ represents the reproduction rate of predators depending on preys' availability, while $\beta > 0$, the predators' mortality rate, is assumed to be constant. As in [13] the flux of u is driven to the direction of higher preys' concentration by a nonlinear, nonlocal velocity v of the form

$$v(\phi) = \kappa \frac{\nabla(\phi * \eta)}{\sqrt{1 + \left\|\nabla(\phi * \eta)\right\|^2}}, \tag{3.1.3}$$

where $\kappa > 0$ is the maximal speed of predators and η is a positive smooth mollifier with $\int_{\mathbb{R}^2} \eta \, \mathrm{d}x = 1$ so that the convolution $(\phi(t) * \eta)(x)$ represents an average of the density of preys in a neighborhood of x at time t.

The equation for the preys, introduced in [9], is related to classical models for the dynamics of a population structured in age, see [14, 32], but the choice of the coefficients and boundary conditions at $a = 0$ takes into account the data collections and ecological considerations in [4, 17, 21, 23, 41]. We recall here the essential assumptions on the form of the coefficients.

We introduce constants $0 < A_1 < A_2$ so that a vole is young (baby) if its age a is in $(0, A_1)$, juvenile if its age is in (A_1, A_2) and adult otherwise. The three age classes differ as babies do not reproduce, adults' mortality rate is lower and juveniles exibit a significantspatial dynamic during dispersals. Dispersal is a characteristic phenomenum of vole populations, correlated to overcrowding. Whenever the density of voles ϕ rises above a threshold value $R > 0$, representing a fraction of the capacity of the environment, the juvenile individuals leave their original colony and disperse over relatively large distances (0.5 to 5 km) with velocity $\mathbf{v}(x)$. We fix $\theta > 0$ and we consider an approximation of the Heaviside function, Y_θ, defined as

$$Y(\xi) = \begin{cases} 1, & \text{if } \xi \geq 0, \\ 0, & \text{if } \xi \leq -1, \end{cases} \qquad Y'(\xi) \geq 0, \qquad Y_\theta(\xi) = Y\left(\frac{\xi}{\theta}\right).$$

From Y_θ we costruct the approximations of the indicator functions of the intervals (σ, T), (A_1, A_2), and (A_1, T)

$$\chi_1(a) = Y_\theta(a - A_1)\, Y_\theta(A_2 - a), \quad \chi_2(a) = Y_\theta(a - \sigma)\, Y_\theta(T - a), \quad \chi_3(a) = Y_\theta(a - A_1)\, Y_\theta(T - a).$$

The mortality rate of voles splits into two terms: $\mathfrak{p} = \mathfrak{p}(a, u)$ represents the mortality due to the presence of the specific predator whose density is u, while $\mathfrak{d} = \mathfrak{d}(t, a, x)$ stands for all other casualties (sickness, starvation, generic predation, etc).

The second-order term $\mu \Delta_x \rho$ represents short range spatial dynamics related to foraging activities. Everywhere in the following θ and $\mu > 0$ are fixed.

In the boundary condition at $a = 0$, the function $\omega = \omega(t, x)$ is the reproduction rate of voles depending on time and position. The function $\mathscr{A}(\phi)$ describes the influence of the total density of voles on natality.

The fourth and fifth equations are the respective initial conditions at $t = 0$ for voles and predators.

3.1.1 Assumptions

The coefficients $\mathfrak{b}, \mathbf{v}, \mathfrak{d}, \mathfrak{p}, \mathscr{A}, \omega$ and the initial data ρ_0, u_0 of system (3.1.1) satisfy the following conditions:

$$\mathfrak{b} \in C^\infty(\mathbb{R}) \cap W^{1,\infty}(\mathbb{R}), \quad \mathfrak{b}(\cdot) \geq 0, \tag{3.1.4}$$

$$\mathbf{v} \in C^\infty(\mathbb{R}^2) \cap L^2(\mathbb{R}^2) \cap L^\infty(\mathbb{R}^2), \quad \mathrm{div}_x(\mathbf{v}) \in L^1(\mathbb{R}^2) \cap W^{2,\infty}(\mathbb{R}^2), \quad \mathbf{v} > 0, \tag{3.1.5}$$

$$\mathfrak{d} \in C^\infty([0,\infty) \times [0,\infty) \times \mathbb{R}^2) \cap W^{1,\infty}((0,\infty) \times (0,\infty) \times \mathbb{R}^2), \qquad 0 < d_* \leq \mathfrak{d}(\cdot,\cdot,\cdot) \leq d^*, \tag{3.1.6}$$

$$\mathfrak{p} \in C^\infty([0,\infty) \times \mathbb{R}) \cap W^{2,\infty}((0,\infty) \times \mathbb{R}), \quad 0 < p_* \leq \mathfrak{p}(\cdot,\cdot) \leq p^*, \tag{3.1.7}$$

$$\mathscr{A} \in C^\infty(\mathbb{R}) \cap L^\infty(\mathbb{R}), \qquad \mathscr{A}(\cdot) \geq 0, \quad \mathscr{A}(0) = 0, \qquad |\mathscr{A}'(\xi)\xi|, |\mathscr{A}''(\xi)\xi| \leq C_0, \tag{3.1.8}$$

$$\omega \in C^\infty([0,\infty) \times \mathbb{R}^2) \cap W^{1,\infty}((0,\infty) \times \mathbb{R}^2), \qquad \omega(\cdot,\cdot) \geq 0, \tag{3.1.9}$$

$$\rho_0 \in L^1((0,\infty) \times \mathbb{R}^2) \cap L^\infty((0,\infty) \times \mathbb{R}^2), \quad \rho_0 \geq 0, \tag{3.1.10}$$

$$\sup_{x \in \mathbb{R}^2} \left\| \rho_0(\cdot, x) \right\|_{L^1(0,\infty)}, \sup_{a>0} \left\| \rho_0(a,\cdot) \right\|_{L^1(\mathbb{R}^2)}, \int_{\mathbb{R}^2} TV(\rho_0(\cdot, x))\mathrm{d}x \leq C_0, \tag{3.1.11}$$

$$u_0 \in L^1(\mathbb{R}^2) \cap BV(\mathbb{R}^2) \cap L^\infty(\mathbb{R}^2), \qquad u_0 \geq 0. \tag{3.1.12}$$

for some positive constants d_*, d^*, p_*, p^*, C_0.

For what the velocity of predators, v, is concerned, we fix the mollifier η so to ensure the estimates in the following Lemma, whose proof is postposed to Section 3.4 (see also [13, Lemma 4.1])

Lemma 3.1. *Let η be such that*

$$\nabla_x \eta \in (C^2 \cap W^{2,2} \cap W^{1,\infty})(\mathbb{R}^2, \mathbb{R}^2). \tag{3.1.13}$$

Then the map $v : L^1(\mathbb{R}^2;\mathbb{R}) \mapsto C^\infty(\mathbb{R}) \cap W^{1,\infty}(\mathbb{R}^2;\mathbb{R}^2)$ satisfies

$$\left\| v(\phi) \right\|_{L^\infty(\mathbb{R}^2;\mathbb{R}^2)} \leq K \left\| \phi \right\|_{L^1(\mathbb{R}^2,\mathbb{R})}, \tag{3.1.14}$$

$$\left\| \mathrm{div}_x\left(v(\phi)\right) \right\|_{L^2(\mathbb{R}^2,\mathbb{R})} \leq K \left\| \phi \right\|_{L^1(\mathbb{R}^2;\mathbb{R})}, \tag{3.1.15}$$

$$\left\| \nabla_x v(\phi) \right\|_{L^\infty(\mathbb{R}^2,\mathbb{R}^{2\times 2})} \leq K \left\| \phi \right\|_{L^1(\mathbb{R}^2;\mathbb{R})}, \tag{3.1.16}$$

$$\left\| v(\phi_1) - v(\phi_2) \right\|_{L^\infty(\mathbb{R}^2,\mathbb{R}^2)} \leq K \left\| \phi_1 - \phi_2 \right\|_{L^1(\mathbb{R}^2,\mathbb{R})}, \tag{3.1.17}$$

$$\left\| \nabla_x(\mathrm{div}_x\left(v(\phi)\right)) \right\|_{L^2(\mathbb{R}^2,\mathbb{R}^2)} \leq K\left(1 + K \left\| \phi \right\|_{L^1(\mathbb{R}^2,\mathbb{R})}\right) \left\| \phi \right\|_{L^1(\mathbb{R}^2,\mathbb{R})}, \tag{3.1.18}$$

$$\left\| \mathrm{div}_x\left(v(\phi_1) - v(\phi_2)\right) \right\|_{L^2(\mathbb{R}^2,\mathbb{R})} \leq K\left(1 + K \left\| \phi_2 \right\|_{L^1(\mathbb{R}^2,\mathbb{R})}\right) \left\| \phi_1 - \phi_2 \right\|_{L^1(\mathbb{R}^2,\mathbb{R})}, \tag{3.1.19}$$

where K is a positive constant.

3.1.2 Main result.

Our main result is the wellposedness of entropy weak solutions for system (3.1.1), stated in Theorem 3.1. We adopt the following definitions of weak solution and entropy solution

Definition 3.1. *We say that the pair (u,ρ) is a weak solution of (3.1.1) if the following holds for every $T>0$*

(D.1) $\rho \geq 0$, $\rho \in L^\infty(0,T;L^1((0,\infty)\times\mathbb{R}^2)) \cap L^\infty((0,T)\times(0,\infty)\times\mathbb{R}^2) \cap L^2((0,T)\times(0,\infty);H^2(\mathbb{R}^2))$.

(D.2) $u \in L^1((0,T)\times\mathbb{R}^2) \cap BV((0,T)\times\mathbb{R}^2)$.

(D.3) *For almost every $(t,x)\in(0,T)\times\mathbb{R}^2$, $\rho(t,\cdot,x)\in BV(0,\infty)$ and*

$$\rho(t,0^+,x) = \mathscr{A}(\phi)\left(\int_0^\infty \rho(t,a,x)\chi_3(a)da\right)\omega(t,x),$$

where $\rho(t,0^+,x)$ is the trace of $\rho(t,\cdot,x)$ at $a=0$.

(D.4) *For every test function $\xi \in C_c^\infty(\mathbb{R}^4)$*

$$\begin{aligned}
&\int_0^\infty\int_0^\infty\int_{\mathbb{R}^2} \left(\rho\partial_t\xi + \rho\partial_a\xi + \rho\chi_1(a)\mathbf{v}\cdot\nabla_x\xi Y_\theta(\phi-R) + \mu\rho\Delta_x\xi - \mathfrak{d}\rho\xi - \mathfrak{p}\rho\xi\right)dx\,da\,dt\\
&\quad+\int_0^\infty\int_0^\infty\int_{\mathbb{R}^2} \mathscr{A}(\phi)\rho(t,a,x)\chi_3(a)\omega(t,x)\xi(t,0,x)dx\,da\,dt\\
&\quad+\int_0^\infty\int_{\mathbb{R}^2}\rho_0(a,x)\xi(0,a,x)dx\,da = 0,
\end{aligned}$$

$$\int_0^\infty\int_0^\infty\int_{\mathbb{R}^2}(u\partial_t\xi + uv(\phi)\cdot\nabla_x\xi + (\mathfrak{b}(\phi)-\beta)u\xi)\,dx\,da\,dt + \int_0^\infty\int_{\mathbb{R}^2} u_0(x)\xi(0,a,x)dx\,da = 0.$$

Definition 3.2. *We say that a weak solution (u,ρ) is an entropy solution of (3.1.1) if for any non-negative test function $\xi\in C^\infty(\mathbb{R}^4)$ with compact support and for any constant $\mathfrak{c}\in\mathbb{R}$ there hold*

$$\begin{aligned}
&\int_0^\infty\int_0^\infty\int_{\mathbb{R}^2}\Big(|\rho-\mathfrak{c}|(\partial_t\xi+\partial_a\xi) - \mathrm{div}_x\left(|\rho-\mathfrak{c}|\chi_1\mathbf{v}Y_\theta(\phi-R)\right)\xi\\
&\qquad\qquad+\mu\Delta_x|\rho-\mathfrak{c}|\xi - \mathrm{sign}\left(\rho-\mathfrak{c}\right)(\mathfrak{d}+\mathfrak{p})\rho\xi\Big)\,dx\,da\,dt\\
&\quad+\int_0^\infty\int_{\mathbb{R}^2}|\rho(t,0^+,x)-\mathfrak{c}|\xi(t,0,x)dx\,dt\\
&\quad+\int_0^\infty\int_{\mathbb{R}^2}|\rho_0(a,x)-\mathfrak{c}|\xi(0,a,x)\,dx\,da\\
&\quad\geq\int_0^\infty\int_0^\infty\int_{\mathbb{R}^2}\mathfrak{c}\,\mathrm{sign}\left(\rho-\mathfrak{c}\right)\chi_1(a)\mathrm{div}_x\left(\mathbf{v}(x)Y_\theta(\phi-R)\right)\xi\,dx\,da\,dt
\end{aligned}\tag{3.1.20}$$

and

$$\begin{aligned}
&\int_0^\infty\int_0^\infty\int_{\mathbb{R}^2}\left(|u-\mathfrak{c}|\partial_t\xi + |u-\mathfrak{c}|v(\phi)\cdot\nabla_x\xi + \mathrm{sign}\,(u-\mathfrak{c})\,(\mathfrak{b}(\phi)-\beta)u\xi\right)dx\,da\,dt\\
&\quad+\int_0^\infty\int_{\mathbb{R}^2}|u_0(x)-\mathfrak{c}|\xi(0,a,x)\,dx\,da \geq \int_0^\infty\int_0^\infty\int_{\mathbb{R}^2}\mathfrak{c}\,\mathrm{sign}\,(u-\mathfrak{c})\,\mathrm{div}_x\left(v(\phi)\right)\xi\,dx\,da\,dt.
\end{aligned}\tag{3.1.21}$$

Theorem 3.1. *Assume* (3.1.4)-(3.1.13)*, then the initial boundary value problem* (3.1.1) *admits a unique entropy solution* (u,ρ) *in the sense of Definition* 3.2*. Moreover, if* (u_1,ρ_1) *and* (u_2,ρ_2) *are the two entropy solutions of* (3.1.1) *having initial data* $(u_{1,0},\rho_{1,0})$ *and* $(u_{2,0},\rho_{2,0})$*, then there exists a positive constant* C *such that the following estimate holds for almost every* $t\geq 0$

$$\begin{aligned}\|u_1(t,\cdot)-u_2(t,\cdot)\|_{L^1(\mathbb{R}^2)}+\left\|\rho_1(t,\cdot,\cdot)-\rho_2(t,\cdot,\cdot)\right\|_{L^1((0,\infty)\times\mathbb{R}^2)}\\ \leq Ce^{Ce^{Ct}}\left\|\rho_{1,0}-\rho_{2,0}\right\|_{L^1((0,\infty)\times\mathbb{R}^2)}+Ce^{Ce^{Ct}}\left\|u_{1,0}-u_{2,0}\right\|_{L^1((\mathbb{R}^2)}.\end{aligned} \tag{3.1.22}$$

3.2 Existence

The existence argument is based on the compactness analysis of a sequence of solutions to approximating problems defined as follows. For any given $\varepsilon>0$, we let $(\rho_\varepsilon=\rho_\varepsilon(t,a,x),u_\varepsilon=u_\varepsilon(t,x))$ be a solution of the problem

$$\begin{cases}\partial_t u_\varepsilon+\operatorname{div}_x\left(u_\varepsilon v(\phi_\varepsilon)\right)=(\mathfrak{b}(\phi_\varepsilon)-\beta)u_\varepsilon+\varepsilon\Delta_x u_\varepsilon, & (t,x)\in(0,T)\times\mathbb{R}^2,\\ \partial_t\rho_\varepsilon+\partial_a\rho_\varepsilon+\operatorname{div}_x\left(\rho_\varepsilon\chi_1(a)\mathbf{v}(x)Y_\theta(\phi_\varepsilon-R)\right)\\ \qquad=\mu\Delta_x\rho_\varepsilon-\mathfrak{d}(t,a,x)\rho_\varepsilon-\mathfrak{p}(a,u_\varepsilon)\rho_\varepsilon+\varepsilon\partial^2_{aa}\rho_\varepsilon, & (t,a,x)\in(0,T)^2\times\mathbb{R}^2,\\ \rho_\varepsilon(t,0,x)=\mathscr{A}\left(|\phi_\varepsilon|\right)\left(\displaystyle\int_0^\infty|\rho_\varepsilon(t,a,x)|\chi_3(a)\mathrm{d}a\right)\omega(t,x), & (t,x)\in(0,T)\times\mathbb{R}^2,\\ \rho_\varepsilon(0,a,x)=\rho_{0,\varepsilon}(a,x), & (a,x)\in(0,T)^2\times\mathbb{R}^2,\\ u_\varepsilon(0,x)=u_{0,\varepsilon}(x), & x\in\mathbb{R}^2,\end{cases} \tag{3.2.23}$$

where

$$\phi_\varepsilon(t,x)=\int_0^\infty\rho_\varepsilon(t,a,x)\chi_2(a)\mathrm{d}a,$$

and $\{(\rho_{0,\varepsilon},u_{0,\varepsilon})\}_\varepsilon$ is a family of approximations of the initial condition (ρ_0,u_0) such that

$$\begin{aligned}&\rho_{0,\varepsilon}\in C^\infty((0,\infty)\times\mathbb{R}^2),\ u_{0,\varepsilon}\in C^\infty(\mathbb{R}^2), && \varepsilon>0,\\ &\rho_{0,\varepsilon}\to\rho_0,\quad\text{a.e. and in } L^p((0,\infty)\times\mathbb{R}^2),1\leq p<\infty,\text{ as }\varepsilon\to 0,\\ &u_{0,\varepsilon}\to u_0,\quad\text{a.e. and in } L^p(\mathbb{R}^2),1\leq p<\infty,\text{ as }\varepsilon\to 0,\\ &\rho_{0,\varepsilon}\geq 0,\ \left\|\rho_{0,\varepsilon}\right\|_{L^1((0,\infty)\times\mathbb{R}^2)}\leq C, && \varepsilon\geq 0,\\ &\sup_{x\in\mathbb{R}^2}\left\|\rho_{0,\varepsilon}(\cdot,x)\right\|_{L^1(\mathbb{R})},\sup_{a\geq 0}\left\|\rho_{0,\varepsilon}(a,\cdot)\right\|_{L^1(\mathbb{R}^2)},\left\|\partial_a\rho_{0,\varepsilon}\right\|_{L^1((0,\infty)\times\mathbb{R}^2)}\leq C, && \varepsilon\geq 0,\\ &\left\|u_{0,\varepsilon}\right\|_{L^1(\mathbb{R}^2)},\left\|\nabla_x u_{0,\varepsilon}\right\|_{L^1(\mathbb{R}^2)},\varepsilon\left\|\Delta_x u_{0,\varepsilon}\right\|_{L^1(\mathbb{R}^2)}\leq C,\ u_{0,\varepsilon}\geq 0, && \varepsilon>0.\end{aligned} \tag{3.2.24}$$

3.2.1 A priori estimates.

In this section we establish the a priori estimates on $(u_\varepsilon,\rho_\varepsilon)$ which are necessary to pass to the limit as $\varepsilon\to 0$ in (3.2.23).

From now on we use the notation C for all the positive constants independent on ε appearing in the text or in the statements of our results, while in proofs we write c to indicate any positive constant non depending on ε, and c_T for quantities of the form ce^{ct}, $t\in(0,T)$.

Lemma 3.2 (**Nonnegativity of $\rho_\varepsilon, \phi_\varepsilon$, u_ε**). *We have that*

$$\rho_\varepsilon \geq 0, \quad \phi_\varepsilon \geq 0, \quad u_\varepsilon \geq 0. \tag{3.2.25}$$

Proof. Consider the function

$$x \mapsto \eta(x) = -\rho \mathbb{1}_{(-\infty,0)}(x).$$

and observe that

$$\eta'(x) = -\mathbb{1}_{(-\infty,0)}(x), \qquad \eta(x) = x\eta'(x).$$

From (3.2.23) we obtain

$$\begin{aligned}
&\frac{d}{dt}\int_0^\infty\int_{\mathbb{R}^2}\eta(\rho_\varepsilon)\mathrm{d}x\,\mathrm{d}a = \int_0^\infty\int_{\mathbb{R}^2}\eta'(\rho_\varepsilon)\partial_t\rho_\varepsilon\mathrm{d}x\,\mathrm{d}a\\
&= -\int_0^\infty\int_{\mathbb{R}^2}\eta'(\rho_\varepsilon)\partial_a\rho_\varepsilon\mathrm{d}x\,\mathrm{d}a - \int_0^\infty\int_{\mathbb{R}^2}\mathrm{div}_x\left(\rho_\varepsilon\chi_1\mathbf{v}Y_\theta\right)\eta'(\rho_\varepsilon)\mathrm{d}x\,\mathrm{d}a\\
&\quad + \mu\int_0^\infty\int_{\mathbb{R}^2}\eta'(\rho_\varepsilon)\Delta_x\rho_\varepsilon\mathrm{d}x\,\mathrm{d}a - \int_0^\infty\int_{\mathbb{R}^2}\eta'(\rho_\varepsilon)(\mathfrak{d}+\mathfrak{p})\rho_\varepsilon\mathrm{d}x\,\mathrm{d}a + \varepsilon\int_0^\infty\int_{\mathbb{R}^2}\eta'(\rho_\varepsilon)\partial_{aa}^2\rho_\varepsilon\mathrm{d}x\,\mathrm{d}a\\
&= \int_{\mathbb{R}^2}\underbrace{\eta(\rho_\varepsilon(t,0,x))}_{=0}\mathrm{d}x + \underbrace{\int_0^\infty\int_{\mathbb{R}^2}\rho_\varepsilon\chi_1(\mathbf{v}\cdot\nabla_x\rho_\varepsilon)Y_\theta\eta''(\rho_\varepsilon)\mathrm{d}x\,\mathrm{d}a}_{=0}\\
&\quad \underbrace{-\mu\int_0^\infty\int_{\mathbb{R}^2}\eta''(\rho_\varepsilon)\left(\nabla_x\rho_\varepsilon\right)^2\mathrm{d}x\,\mathrm{d}a}_{\leq 0} \underbrace{-\int_0^\infty\int_{\mathbb{R}^2}(\mathfrak{d}+\mathfrak{p})\eta(\rho_\varepsilon)\mathrm{d}x\,\mathrm{d}a}_{\leq 0}\\
&\quad + \varepsilon\int_0^\infty\int_{\mathbb{R}^2}\partial_a\left(\eta'(\rho_\varepsilon)\partial_a\rho_\varepsilon\right)\mathrm{d}x\,\mathrm{d}a \underbrace{-\varepsilon\int_0^\infty\int_{\mathbb{R}^2}\eta''(\rho_\varepsilon)(\partial_a\rho_\varepsilon)^2\mathrm{d}x\,\mathrm{d}a}_{\leq 0}\\
&\leq -\varepsilon\int_{\mathbb{R}^2}\underbrace{\eta'(\rho_\varepsilon(t,0,x))}_{=0}\partial_a\rho_\varepsilon(t,0,x)\mathrm{d}x = 0.
\end{aligned}$$

Thus, integrating on $(0,t)$ we obtain $\eta(\rho_\varepsilon(t,a,x)) = 0$ which implies that $\rho_\varepsilon \geq 0$, and then $\phi_\varepsilon \geq 0$.

From (3.2.23) we obtain

$$\begin{aligned}
&\frac{d}{dt}\int_{\mathbb{R}^2}\eta(u_\varepsilon)\mathrm{d}x = \int_{\mathbb{R}^2}\eta'(u_\varepsilon)\partial_t u_\varepsilon\mathrm{d}x\\
&\quad = -\underbrace{\int_{\mathbb{R}^2}\eta'(u_\varepsilon)\mathrm{div}_x\left(u_\varepsilon\nu(\phi_\varepsilon)\right)\mathrm{d}x}_{=0} + \int_{\mathbb{R}^2}\eta'(u_\varepsilon)\underbrace{(\mathfrak{b}(\phi)-\beta)}_{\leq c}u_\varepsilon\mathrm{d}x + \underbrace{\varepsilon\int_{\mathbb{R}^2}\eta'(u_\varepsilon)\Delta_x u_\varepsilon\mathrm{d}x}_{\leq 0}\\
&\quad \leq c\int_{\mathbb{R}^2}\eta(u_\varepsilon)\mathrm{d}x.
\end{aligned}$$

Integrating on $(0,t)$ and applying Gronwall Lemma we obtain $\eta(u_\varepsilon(t,x)) = 0$, so that $u_\varepsilon \geq 0$. □

Remark 3.1. *Without loss of information, we can remove the absolute value in the boundary condition for ρ_ε in (3.2.23).*

We consider the class of functions

$$\psi_\varepsilon(t,x)=\int_0^\infty \rho_\varepsilon(t,a,x)\xi(a)\mathrm{d}a,$$

for $\xi\in C^\infty([0,\infty])$ such that

$$\operatorname{supp}(\xi)\subset(0,T). \tag{3.2.26}$$

In particular any of the functions χ_i, $i=1,2,3$, can play the role of ξ, so that the estimates obtained for ψ_ε apply to ϕ_ε.

Lemma 3.3 (L^1 **estimate on** ψ_ε)**.** *For all $t\geq 0$, we have that*

$$\left\|\psi_\varepsilon(t,\cdot)\right\|_{L^1(\mathbb{R}^2)}\leq e^{Ct}C. \tag{3.2.27}$$

Proof. We multiply by $\xi(a)$ the equation for ρ_ε in system (3.2.23) then, integrating with respect to a, we get

$$\partial_t\psi_\varepsilon-\mu\Delta_x\psi_\varepsilon+\operatorname{div}_x\left(\left(\int_0^\infty \rho_\varepsilon\chi_1\xi\mathrm{d}a\right)\mathbf{v}Y_\theta\right)=\int_0^\infty \rho_\varepsilon\left(\varepsilon\xi''+\xi'-\mathfrak{d}\xi-\mathfrak{p}(a,u_\varepsilon)\xi\right)\mathrm{d}a. \tag{3.2.28}$$

Due to the nonnegativity of ρ_ε, ψ_ε and the boundedness of ξ'/ξ, ξ''/ξ, $\mathfrak{d},\mathfrak{p}$ we have

$$\begin{aligned}\frac{d}{dt}\int_{\mathbb{R}^2}|\psi_\varepsilon|\mathrm{d}x=\frac{d}{dt}\int_{\mathbb{R}^2}\psi_\varepsilon\mathrm{d}x=&\underbrace{\mu\int_{\mathbb{R}^2}\Delta_x\psi_\varepsilon\mathrm{d}x-\int_{\mathbb{R}^2}\operatorname{div}_x\left(\left(\int_0^\infty\rho_\varepsilon\chi_1\xi\mathrm{d}a\right)\mathbf{v}Y_\theta\right)\mathrm{d}x}_{=0}\\&+\int_{\mathbb{R}^2}\int_0^\infty\rho_\varepsilon\underbrace{\left(\varepsilon\xi''+\xi'-\mathfrak{d}\xi-\mathfrak{p}\xi\right)}_{\leq c\xi}\mathrm{d}a\,\mathrm{d}x\leq c\int_{\mathbb{R}^2}\psi_\varepsilon\mathrm{d}x.\end{aligned}$$

The result comes from the Gronwall Lemma and the assumptions in (3.2.24). □

Lemma 3.4 (L^2 **estimate on** ψ_ε)**.** *For any $t\geq 0$, we have*

$$\left\|\psi_\varepsilon(t,\cdot)\right\|_{L^2(\mathbb{R}^2)},\left\|\nabla_x\psi_\varepsilon\right\|_{L^2((0,t)\times\mathbb{R}^2)}\leq e^{Ct}C. \tag{3.2.29}$$

Proof. We multiply (3.2.28) by ψ_ε and have

$$\begin{aligned}
\frac{d}{dt}\int_{\mathbb{R}^2}\frac{\psi_\varepsilon^2}{2}\mathrm{d}x &= \int_{\mathbb{R}^2}\psi_\varepsilon\partial_t\psi_\varepsilon\mathrm{d}x\\
&= \mu\int_{\mathbb{R}^2}\psi_\varepsilon\Delta_x\psi_\varepsilon\mathrm{d}x - \int_{\mathbb{R}^2}\psi_\varepsilon\mathrm{div}_x\left(\left(\int_0^\infty\rho_\varepsilon\chi_1\xi\mathrm{d}a\right)\mathbf{v}Y_\theta\right)\mathrm{d}x\\
&\qquad + \int_{\mathbb{R}^2}\int_0^\infty\rho_\varepsilon\underbrace{\left(\varepsilon\xi'' + \xi' - \mathfrak{d}\xi - \mathfrak{p}\xi\right)}_{\le c\xi}\psi_\varepsilon\mathrm{d}a\,\mathrm{d}x\\
&\le -\mu\int_{\mathbb{R}^2}|\nabla_x\psi_\varepsilon|^2\mathrm{d}x + \int_{\mathbb{R}^2}\nabla_x\psi_\varepsilon\cdot\mathbf{v}\left(\int_0^\infty\rho_\varepsilon\chi_1\xi\mathrm{d}a\right)Y_\theta\mathrm{d}x + c\int_{\mathbb{R}^2}\psi_\varepsilon^2\mathrm{d}x\\
&\le -\frac{\mu}{2}\int_{\mathbb{R}^2}|\nabla_x\psi_\varepsilon|^2\mathrm{d}x + \frac{1}{2\mu}\int_{\mathbb{R}^2}\underbrace{|\mathbf{v}|^2\left(\int_0^\infty\rho_\varepsilon\chi_1\xi\mathrm{d}a\right)^2}_{\le c\psi_\varepsilon^2}Y_\theta\,\mathrm{d}x + c\int_{\mathbb{R}^2}\psi_\varepsilon^2\mathrm{d}x\\
&\le -\frac{\mu}{2}\int_{\mathbb{R}^2}|\nabla_x\psi_\varepsilon|^2\mathrm{d}x + c\int_{\mathbb{R}^2}\psi_\varepsilon^2\mathrm{d}x.
\end{aligned}$$

Integrating over $(0,t)$ and using the Gronwall Lemma we get (3.2.29). □

Lemma 3.5 (L^∞ **estimate on** u_ε)**.** *For every $t\ge 0$, we have*

$$\|u_\varepsilon(t,\cdot)\|_{L^\infty(\mathbb{R}^2)} \le Ce^{Ct}. \tag{3.2.30}$$

Proof. Let $\mathscr{C}$ be a positive constant that will be fixed later. We define

$$\overline{u}_\varepsilon(t,x) = e^{-\mathscr{C}t}u_\varepsilon(t,x),$$

and we consider the associated problem

$$\begin{cases}\partial_t\overline{u}_\varepsilon + \mathrm{div}_x\left(\overline{u}_\varepsilon v(\phi_\varepsilon)\right) = (\mathfrak{b}(\phi_\varepsilon) - \beta - \mathscr{C})\overline{u}_\varepsilon + \varepsilon\Delta_x\overline{u}_\varepsilon,\\ \overline{u}_\varepsilon(0,x) = u_{0,\varepsilon}(x).\end{cases}$$

We claim that for any given $T>0$ there exist a sufficiently large constant $k>0$ and a suitable $\mathscr{C}$ such that $u_\varepsilon(t,x)\le k$ for any $t\le T$ and $x\in\mathbb{R}^2$, provided $u_{0,\varepsilon}(x)\le k$ for all $x\in\mathbb{R}^2$.

Consider the function

$$x\mapsto\eta(x) = (x-k)\mathbb{1}_{(k,+\infty)}(x),$$

and observe that

$$\eta'(x) = \mathbb{1}_{(k,+\infty)}(x), \qquad x\eta'(x) = \eta(x) + k\eta'(x).$$

We have

$$\begin{aligned}
\frac{d}{dt}\int_{\mathbb{R}^2}\eta(\overline{u}_\varepsilon)\mathrm{d}x &= \int_{\mathbb{R}^2}\eta'(\overline{u}_\varepsilon)\partial_t\overline{u}_\varepsilon\,\mathrm{d}x\\
&= -\int_{\mathbb{R}^2}\eta'(\overline{u}_\varepsilon)\mathrm{div}_x\left(\overline{u}_\varepsilon v(\phi_\varepsilon)\right)\mathrm{d}x + \int_{\mathbb{R}^2}\eta'(\overline{u}_\varepsilon)(\mathfrak{b}(\phi_\varepsilon)-\beta-\mathscr{C})\overline{u}_\varepsilon\,\mathrm{d}x + \underbrace{\varepsilon\int_{\mathbb{R}^2}\eta'(\overline{u}_\varepsilon)\Delta_x\overline{u}_\varepsilon\,\mathrm{d}x}_{\leq 0}\\
&\leq -\underbrace{\int_{\mathbb{R}^2}\eta'(\overline{u}_\varepsilon)\mathrm{div}_x\left((\overline{u}_\varepsilon-k)v(\phi_\varepsilon)\right)\mathrm{d}x}_{=0} - k\int_{\mathbb{R}^2}\eta'(\overline{u}_\varepsilon)\mathrm{div}_x\left(v(\phi_\varepsilon)\right)\mathrm{d}x\\
&\quad + \int_{\mathbb{R}^2}(\eta(\overline{u}_\varepsilon)+k\eta'(\overline{u}_\varepsilon))(\mathfrak{b}(\phi_\varepsilon)-\beta-\mathscr{C})\,\mathrm{d}x\\
&\leq \int_{\mathbb{R}^2}\eta(\overline{u}_\varepsilon)(\mathfrak{b}(\phi_\varepsilon)-\beta-\mathscr{C})\,\mathrm{d}x - k\int_{\mathbb{R}^2}\eta'(\overline{u}_\varepsilon)(\mathscr{C}+\beta+\mathrm{div}_x\left(v(\phi_\varepsilon)\right)-\mathfrak{b}(\phi_\varepsilon))\,\mathrm{d}x.
\end{aligned}$$

From the inequality $\left\|\mathrm{div}_x\left(v(\phi_\varepsilon)\right)\right\|_{L^\infty}\leq 2\left\|\nabla v(\phi_\varepsilon)\right\|_{L^\infty}$ and the estimates in (3.1.16) and (3.2.27), it follows that for $\mathscr{C}$ large enough

$$\mathscr{C}+\beta-\mathfrak{b}(\phi_\varepsilon)\geq 0,\quad \mathscr{C}+\beta+\mathrm{div}_x\left(v(\phi_\varepsilon)\right)-\mathfrak{b}(\phi_\varepsilon)\geq 0,$$

thus,

$$\frac{d}{dt}\int_{\mathbb{R}^2}\eta(\overline{u}_\varepsilon)\mathrm{d}x\leq 0.$$

Integrating over $(0,t)$ we obtain

$$0\leq\int_{\mathbb{R}^2}\eta(\overline{u}_\varepsilon(t,x))\,\mathrm{d}x\leq\int_{\mathbb{R}^2}\eta(u_{0,\varepsilon}(x))\,\mathrm{d}x=0,$$

which means $\overline{u}_\varepsilon\leq k$. The inequality (3.2.30) follows. □

Lemma 3.6. *For all $t\geq 0$, the following estimates on u_ε hold*

$$\|u_\varepsilon(t,\cdot)\|_{L^1(\mathbb{R}^2)}\leq e^{Ct}C, \tag{3.2.31}$$

$$\|u_\varepsilon(t,\cdot)\|_{L^2(\mathbb{R}^2)},\|\nabla_x u_\varepsilon\|_{L^2((0,t)\times\mathbb{R}^2)}\leq e^{Ct}C, \tag{3.2.32}$$

$$\|\nabla_x u_\varepsilon(t,\cdot)\|_{L^2(\mathbb{R}^2)},\|\Delta_x u_\varepsilon\|_{L^2((0,t)\times\mathbb{R}^2)}\leq e^{Ct}C. \tag{3.2.33}$$

Proof. We recall the equation of u_ε

$$\partial_t u_\varepsilon+\mathrm{div}_x\left(u_\varepsilon v(\phi_\varepsilon)\right)=(\mathfrak{b}(\phi_\varepsilon)-\beta)u_\varepsilon+\varepsilon\Delta_x u_\varepsilon. \tag{3.2.34}$$

(3.2.31). Using the nonnegativity of u_ε we have

$$\begin{aligned}
\frac{d}{dt}\int_{\mathbb{R}^2}|u_\varepsilon|\mathrm{d}x=\frac{d}{dt}\int_{\mathbb{R}^2}u_\varepsilon\mathrm{d}x &= \underbrace{\varepsilon\int_{\mathbb{R}^2}\Delta_x u_\varepsilon\,\mathrm{d}x-\int_{\mathbb{R}^2}\mathrm{div}_x\left(u_\varepsilon v(\phi_\varepsilon)\right)\mathrm{d}x}_{=0}\\
&\quad+\int_{\mathbb{R}^2}\underbrace{(\mathfrak{b}(\phi_\varepsilon)-\beta)}_{\leq c}u_\varepsilon\mathrm{d}x\leq c\int_{\mathbb{R}^2}u_\varepsilon\mathrm{d}x.
\end{aligned}$$

Then, applying the Gronwall Lemma we gain

$$\|u_\varepsilon(t,\cdot)\|_{L^1(\mathbb{R}^2)} \le \left\|u_{0,\varepsilon}(\cdot)\right\|_{L^1(\mathbb{R}^2)} e^{ct}.$$

(3.2.32). We multiply (3.2.34) by u_ε to obtain

$$\begin{aligned}
&\frac{d}{dt}\int_{\mathbb{R}^2}\frac{u_\varepsilon^2}{2}\mathrm{d}x = \int_{\mathbb{R}^2} u_\varepsilon \partial_t u_\varepsilon \mathrm{d}x \\
&= -\int_{\mathbb{R}^2} \mathrm{div}_x\left(u_\varepsilon \nu(\phi_\varepsilon)\right) u_\varepsilon \mathrm{d}x + \int_{\mathbb{R}^2} (\mathfrak{b}(\phi_\varepsilon)-\beta) u_\varepsilon^2 \mathrm{d}x + \varepsilon\int_{\mathbb{R}^2} \Delta_x u_\varepsilon u_\varepsilon \mathrm{d}x \\
&\le \int_{\mathbb{R}^2} u_\varepsilon \nu(\phi_\varepsilon).\nabla u_\varepsilon \mathrm{d}x + c\int_{\mathbb{R}^2} u_\varepsilon^2 \mathrm{d}x - \varepsilon\int_{\mathbb{R}^2} |\nabla_x u_\varepsilon|^2 \mathrm{d}x \\
&\le \int_{\mathbb{R}^2} \nabla_x\left(\frac{u_\varepsilon^2}{2}\right).\nu(\phi_\varepsilon)\mathrm{d}x + c\int_{\mathbb{R}^2} u_\varepsilon^2 \mathrm{d}x - \varepsilon\int_{\mathbb{R}^2} |\nabla_x u_\varepsilon|^2 \mathrm{d}x \\
&\le \int_{\mathbb{R}^2} \frac{u_\varepsilon^2}{2}\mathrm{div}_x\left(\nu(\phi_\varepsilon)\right)\mathrm{d}x + c\int_{\mathbb{R}^2} u_\varepsilon^2 \mathrm{d}x - \varepsilon\int_{\mathbb{R}^2} |\nabla_x u_\varepsilon|^2 \mathrm{d}x \\
&\le c_T\int_{\mathbb{R}^2} |u_\varepsilon|\mathrm{d}x + c\int_{\mathbb{R}^2} u_\varepsilon^2 \mathrm{d}x - \varepsilon\int_{\mathbb{R}^2} |\nabla_x u_\varepsilon|^2 \mathrm{d}x.
\end{aligned}$$

Integrating over $(0,t)$ and then using the Gronwall Lemma we get

$$\|u_\varepsilon(t,\cdot)\|^2_{L^2(\mathbb{R}^2)} + 2\varepsilon e^{ct}\int_0^t e^{-cs}\|\nabla_x u_\varepsilon(s,\cdot)\|^2_{L^2(\mathbb{R}^2)}\mathrm{d}s \le e^{ct}\|u_\varepsilon(0,\cdot)\|^2_{L^2(\mathbb{R}^2)} + ce^{ct}.$$

(3.2.33). We multiply (3.2.34) by $-\Delta_x u_\varepsilon$ to obtain

$$\begin{aligned}
&\frac{d}{dt}\int_{\mathbb{R}^2}\frac{|\nabla_x u_\varepsilon|^2}{2}\mathrm{d}x = \int_{\mathbb{R}^2}\nabla_x u_\varepsilon\cdot\partial_t\nabla_x u_\varepsilon \mathrm{d}x = -\int_{\mathbb{R}^2}\Delta_x u_\varepsilon \partial_t u_\varepsilon \mathrm{d}x \\
&= \int_{\mathbb{R}^2}\Delta_x u_\varepsilon \mathrm{div}_x\left(u_\varepsilon\nu(\phi_\varepsilon)\right)\mathrm{d}x - \int_{\mathbb{R}^2}\Delta_x u_\varepsilon(\mathfrak{b}(\phi_\varepsilon)-\beta)u_\varepsilon\mathrm{d}x - \varepsilon\int_{\mathbb{R}^2}|\Delta_x u_\varepsilon|^2\mathrm{d}x \\
&= -\int_{\mathbb{R}^2}\nabla_x u_\varepsilon\nabla_x\left(\nabla_x u_\varepsilon.\nu(\phi) + u_\varepsilon\mathrm{div}_x\left(\nu(\phi)\right)\right)\mathrm{d}x + \int_{\mathbb{R}^2}(\mathfrak{b}(\phi)-\beta)|\nabla_x u_\varepsilon|^2\mathrm{d}x \\
&\quad + \int_{\mathbb{R}^2}\mathfrak{b}'(\phi)\nabla_x\phi.\nabla_x u_\varepsilon\, u_\varepsilon\mathrm{d}x - \varepsilon\int_{\mathbb{R}^2}|\Delta_x u_\varepsilon|^2\mathrm{d}x \\
&\le -\varepsilon\int_{\mathbb{R}^2}|\Delta_x u_\varepsilon|^2\mathrm{d}x + c\int_{\mathbb{R}^2}|\nabla_x u_\varepsilon|^2\,dx + c_T\int_{\mathbb{R}^2}|\nabla_x\psi_\varepsilon|^2\,dx \\
&\quad + \int_{\mathbb{R}^2}\nabla_x\left(\frac{|\nabla_x u_\varepsilon|^2}{2}\right).\nu(\phi)\mathrm{d}x + \int_{\mathbb{R}^2}|\nabla_x u|^2\underbrace{|\nabla_x\nu(\phi)|}_{\le c_T}\mathrm{d}x + \int_{\mathbb{R}^2}|\nabla_x u|^2\underbrace{|\mathrm{div}_x\left(\nu(\phi)\right)|}_{\le c_T}\mathrm{d}x \\
&\quad + \int_{\mathbb{R}^2}|\nabla_x u_\varepsilon||u_\varepsilon|\nabla_x\mathrm{div}_x\left(\nu(\phi)\right)|\mathrm{d}x \\
&\le -\varepsilon\int_{\mathbb{R}^2}|\Delta_x u_\varepsilon|^2\mathrm{d}x + c_T\int_{\mathbb{R}^2}|\nabla_x u_\varepsilon|^2\mathrm{d}x + c_T\int_{\mathbb{R}^2}|\nabla_x\psi_\varepsilon|^2\mathrm{d}x + c_T\int_{\mathbb{R}^2}|\nabla_x\mathrm{div}_x\left(\nu(\phi)\right)|^2\mathrm{d}x.
\end{aligned}$$

Integrating over $(0,t)$ and using the estimates in (3.1.18) and (3.2.29) we gain

$$\|\nabla_x u_\varepsilon(t,\cdot)\|_{L^2(\mathbb{R}^2)} + \varepsilon\|\Delta_x u_\varepsilon(\cdot,\cdot)\|_{L^2((0,t)\times\mathbb{R}^2)} \le ce^{ct}.$$

□

Lemma 3.7. *For every $t \geq 0$, the following estimates on ψ_ε hold*

$$\left\|\nabla_x \psi_\varepsilon(t,\cdot)\right\|_{L^2(\mathbb{R}^2)}, \left\|D_x^2 \psi_\varepsilon\right\|_{L^2((0,t)\times\mathbb{R}^2)} \leq e^{Ct} C, \tag{3.2.35}$$

$$\left\|D_x^2 \psi_\varepsilon(t,\cdot)\right\|_{L^2(\mathbb{R}^2)}, \left\|D_x^3 \psi_\varepsilon\right\|_{L^2((0,t)\times\mathbb{R}^2)} \leq e^{Ct} C, \tag{3.2.36}$$

$$\left\|\psi_\varepsilon(t,\cdot)\right\|_{L^\infty(\mathbb{R}^2)} \leq e^{Ct} C, \tag{3.2.37}$$

$$\left\|D_x^3 \psi_\varepsilon(t,\cdot)\right\|_{L^2(\mathbb{R}^2)}, \left\|D_x^4 \psi_\varepsilon\right\|_{L^2((0,t)\times\mathbb{R}^2)} \leq e^{Ct} C, \tag{3.2.38}$$

$$\left\|\partial_t \psi_\varepsilon(t,\cdot)\right\|_{L^1(\mathbb{R}^2)}, \left\|\partial_t \psi_\varepsilon(t,\cdot)\right\|_{L^2(\mathbb{R}^2)}, \left\|\nabla_x \psi_\varepsilon(t,\cdot)\right\|_{L^\infty(\mathbb{R}^2)} \leq e^{Ct} C. \tag{3.2.39}$$

Proof. **(3.2.35).** The proof is identical to the proof of [9, Lemma 2.2, Eq. (2.8)], due to the boundedness of the mortality rate related to predation $\mathfrak{p}(\cdot, u)$.
(3.2.36). At first, we consider the following estimate

$$\begin{aligned}
&\frac{d}{dt}\int_{\mathbb{R}^2} \frac{(\psi_\varepsilon u_\varepsilon)^2}{2} \mathrm{d}x = \int_{\mathbb{R}^2} (u_\varepsilon^2 \psi_\varepsilon \partial_t \psi_\varepsilon + \psi_\varepsilon^2 u_\varepsilon \partial_t u_\varepsilon) \mathrm{d}x \\
&= \mu \int_{\mathbb{R}^2} u_\varepsilon^2 \psi_\varepsilon \Delta_x \psi_\varepsilon \mathrm{d}x - \int_{\mathbb{R}^2} u_\varepsilon^2 \psi_\varepsilon \mathrm{div}_x \left(\left(\int_0^\infty \rho_\varepsilon \chi_1 \xi \mathrm{d}a \right) \mathbf{v} Y_\theta \right) \mathrm{d}x \\
&\quad + \int_{\mathbb{R}^2} u_\varepsilon^2 \int_0^\infty \rho_\varepsilon \underbrace{\left(\varepsilon \xi'' + \xi' - \mathfrak{d}\xi - \mathfrak{p}\xi \right)}_{\leq c, \text{ see (3.2.26)}} \psi_\varepsilon \mathrm{d}a \, \mathrm{d}x - \int_{\mathbb{R}^2} u_\varepsilon \psi_\varepsilon^2 \mathrm{div}_x \left(u_\varepsilon \nu(\phi_\varepsilon) \right) \mathrm{d}x \\
&\quad + \int_{\mathbb{R}^2} \psi_\varepsilon^2 (\mathfrak{b}(\phi_\varepsilon) - \beta) u_\varepsilon^2 \mathrm{d}x + \varepsilon \int_{\mathbb{R}^2} \psi_\varepsilon^2 \Delta_x u_\varepsilon u_\varepsilon \mathrm{d}x \\
&\leq -\mu \int_{\mathbb{R}^2} \nabla_x (u_\varepsilon^2 \psi_\varepsilon) \nabla_x \psi_\varepsilon \mathrm{d}x - \varepsilon \int_{\mathbb{R}^2} \nabla_x (\psi_\varepsilon^2 u_\varepsilon) \nabla_x u_\varepsilon \mathrm{d}x + c \int_{\mathbb{R}^2} (\psi_\varepsilon u_\varepsilon)^2 \mathrm{d}x \\
&\quad + c_T \int_{\mathbb{R}^2} \psi_\varepsilon^2 \mathrm{d}x + c_T \int_{\mathbb{R}^2} \left(\mathrm{div}_x \left(\left(\int_0^\infty \rho_\varepsilon \chi_1 \xi \mathrm{d}a \right) \mathbf{v} Y_\theta \right) \right)^2 \mathrm{d}x \\
&\quad + \int_{\mathbb{R}^2} \nabla_x (\psi_\varepsilon^2 u_\varepsilon) \cdot \nu(\phi_\varepsilon) u_\varepsilon \mathrm{d}x \\
&\leq -\mu \int_{\mathbb{R}^2} u_\varepsilon^2 |\nabla_x \psi_\varepsilon|^2 \mathrm{d}x - \varepsilon \int_{\mathbb{R}^2} \psi_\varepsilon^2 |\nabla_x u_\varepsilon|^2 \mathrm{d}x - 2(\mu + \varepsilon) \int_{\mathbb{R}^2} \nabla_x \left(\frac{u_\varepsilon^2}{2} \right) \nabla_x \left(\frac{\psi_\varepsilon^2}{2} \right) \mathrm{d}x \\
&\quad + c \int_{\mathbb{R}^2} (\psi_\varepsilon u_\varepsilon)^2 \mathrm{d}x + c_T \int_{\mathbb{R}^2} \psi_\varepsilon^2 \mathrm{d}x + c_T \int_{\mathbb{R}^2} \left| \nabla_x \int_0^\infty \rho_\varepsilon \chi_1 \xi \mathrm{d}a \right|^2 \underbrace{|\mathbf{v}|^2 Y_\theta^2}_{\leq c} \mathrm{d}x \\
&\quad + c_T \int_{\mathbb{R}^2} \left(\int_0^\infty \rho_\varepsilon \chi_1 \xi \mathrm{d}a \right)^2 \underbrace{|\mathrm{div}_x(\mathbf{v})|^2 Y_\theta^2}_{\leq c} \mathrm{d}x + c_T \int_{\mathbb{R}^2} \underbrace{\left(\int_0^\infty \rho_\varepsilon \chi_1 \xi \mathrm{d}a \right)^2 (Y_\theta')^2 |\mathbf{v}|^2}_{\leq c, \text{ see (3.2.26)}} |\nabla_x \phi_\varepsilon|^2 \mathrm{d}x \\
&\quad + 2 \int_{\mathbb{R}^2} \nabla_x \psi_\varepsilon \psi_\varepsilon \underbrace{u_\varepsilon^2 \nu(\phi_\varepsilon)}_{\leq c_T} \mathrm{d}x + \int_{\mathbb{R}^2} \psi_\varepsilon^2 \nabla_x \left(\frac{u_\varepsilon^2}{2} \right) \cdot \nu(\phi_\varepsilon) \mathrm{d}x \\
&\leq -\mu \int_{\mathbb{R}^2} u_\varepsilon^2 |\nabla_x \psi_\varepsilon|^2 \mathrm{d}x - \varepsilon \int_{\mathbb{R}^2} \psi_\varepsilon^2 |\nabla_x u_\varepsilon|^2 \mathrm{d}x + (\mu + \varepsilon) \int_{\mathbb{R}^2} \underbrace{u_\varepsilon^2}_{\leq c_T} \left(|\nabla_x \psi_\varepsilon|^2 + \psi_\varepsilon \Delta_x \psi_\varepsilon \right) \mathrm{d}x \\
&\quad + c \int_{\mathbb{R}^2} (\psi_\varepsilon u_\varepsilon)^2 \mathrm{d}x + c_T \int_{\mathbb{R}^2} \psi_\varepsilon^2 \mathrm{d}x + c_T \int_{\mathbb{R}^2} \left| \nabla_x \int_0^\infty \rho_\varepsilon \chi_1 \xi \mathrm{d}a \right|^2 \mathrm{d}x
\end{aligned}$$

$$
\begin{aligned}
&+c_T\int_{\mathbb{R}^2}\left(\int_0^\infty \rho_\varepsilon\chi_1\xi\,\mathrm{d}a\right)^2\mathrm{d}x+c_T\int_{\mathbb{R}^2}|\nabla_x\phi_\varepsilon|^2\mathrm{d}x+c_T\int_{\mathbb{R}^2}\nabla_x\psi_\varepsilon\psi_\varepsilon\mathrm{d}x+\int_{\mathbb{R}^2}\underbrace{\frac{u_\varepsilon^2}{2}\mathrm{div}_x\left(\nu(\phi_\varepsilon)\right)}_{\le c_T}\psi_\varepsilon^2\mathrm{d}x\\
\le&-\mu\int_{\mathbb{R}^2}u_\varepsilon^2|\nabla_x\psi_\varepsilon|^2\mathrm{d}x-\varepsilon\int_{\mathbb{R}^2}\psi_\varepsilon^2|\nabla_x u_\varepsilon|^2\mathrm{d}x+c_T\int_{\mathbb{R}^2}|\nabla_x\psi_\varepsilon|^2\mathrm{d}x+c_T\int_{\mathbb{R}^2}|\Delta_x\psi_\varepsilon|^2\mathrm{d}x\\
&+c\int_{\mathbb{R}^2}(\psi_\varepsilon u_\varepsilon)^2\mathrm{d}x+c_T\int_{\mathbb{R}^2}\psi_\varepsilon^2\mathrm{d}x+c_T\int_{\mathbb{R}^2}\left|\nabla_x\int_0^\infty\rho_\varepsilon\chi_1\xi\,\mathrm{d}a\right|^2\mathrm{d}x\\
&+c_T\int_{\mathbb{R}^2}\left(\int_0^\infty\rho_\varepsilon\chi_1\xi\,\mathrm{d}a\right)^2\mathrm{d}x+c_T\int_{\mathbb{R}^2}|\nabla_x\phi_\varepsilon|^2\mathrm{d}x.
\end{aligned}
$$

Using the Gronwall Lemma and the estimates in (3.2.29), (3.2.35) we gain

$$
\begin{aligned}
&\left\|\psi_\varepsilon(t,\cdot)u_\varepsilon(t,\cdot)\right\|^2_{L^2(\mathbb{R}^2)}+2\mu e^{ct}\int_0^t e^{-cs}\int_{\mathbb{R}^2}u_\varepsilon^2(s,x)|\nabla_x\psi_\varepsilon(s,x)|^2\mathrm{d}x\mathrm{d}s\\
&\qquad+2\varepsilon e^{ct}\int_0^t e^{-cs}\int_{\mathbb{R}^2}\psi_\varepsilon^2(s,x)|\nabla_x u_\varepsilon(s,x)|^2\mathrm{d}x\mathrm{d}s\le ce^{ct}.
\end{aligned}
\tag{3.2.40}
$$

Then, we multiply (3.2.28) by $D_x^4\psi_\varepsilon$ to have

$$
\begin{aligned}
&\frac{d}{dt}\int_{\mathbb{R}^2}\frac{|\Delta_x\psi_\varepsilon|^2}{2}\mathrm{d}x=\int_{\mathbb{R}^2}\Delta_x\psi_\varepsilon\cdot\partial_t\Delta_x\psi_\varepsilon\mathrm{d}x=\int_{\mathbb{R}^2}D_x^4\psi_\varepsilon\partial_t\psi_\varepsilon\mathrm{d}x\\
=&\mu\int_{\mathbb{R}^2}\Delta_x\psi_\varepsilon D_x^4\psi_\varepsilon\mathrm{d}x-\int_{\mathbb{R}^2}D_x^4\psi_\varepsilon\mathrm{div}_x\left(\left(\int_0^\infty\rho_\varepsilon\chi_1\xi\,\mathrm{d}a\right)\mathbf{v}Y_\theta\right)\mathrm{d}x\\
&+\int_{\mathbb{R}^2}\int_0^\infty\rho_\varepsilon\left(\varepsilon\xi''+\xi'-\mathfrak{d}\xi-\mathfrak{p}(a,u_\varepsilon)\xi\right)D_x^4\psi_\varepsilon\mathrm{d}a\mathrm{d}x\\
=&-\mu\int_{\mathbb{R}^2}|D_x^3\psi_\varepsilon|^2\mathrm{d}x+\int_{\mathbb{R}^2}D_x^3\psi_\varepsilon\cdot\nabla_x\mathrm{div}_x\left(\left(\int_0^\infty\rho_\varepsilon\chi_1\xi\,\mathrm{d}a\right)\mathbf{v}Y_\theta\right)\mathrm{d}x\\
&-\int_{\mathbb{R}^2}\nabla_x\left(\int_0^\infty\rho_\varepsilon\left(\varepsilon\xi''+\xi'-\mathfrak{d}\xi-\mathfrak{p}(a,u_\varepsilon)\xi\right)\mathrm{d}a\right)\cdot D_x^3\psi_\varepsilon\mathrm{d}x\\
\le&-\frac{\mu}{2}\int_{\mathbb{R}^2}|D_x^3\psi_\varepsilon|^2\mathrm{d}x+c\int_{\mathbb{R}^2}\left(\nabla_x\mathrm{div}_x\left(\left(\int_0^\infty\rho_\varepsilon\chi_1\xi\,\mathrm{d}a\right)\mathbf{v}Y_\theta\right)\right)^2\mathrm{d}x\\
&+c\int_{\mathbb{R}^2}\left|\nabla_x\int_0^\infty\rho_\varepsilon\left(\varepsilon\xi''+\xi'-\mathfrak{d}\xi-\mathfrak{p}(a,u_\varepsilon)\xi\right)\mathrm{d}a\right|^2\mathrm{d}x\\
\le&-\frac{\mu}{2}\int_{\mathbb{R}^2}|D_x^3\psi_\varepsilon|^2\mathrm{d}x+c\int_{\mathbb{R}^2}\left|D_x^2\int_0^\infty\rho_\varepsilon\chi_1\xi\,\mathrm{d}a\right|^2\underbrace{|\mathbf{v}|^2Y_\theta^2}_{\le c}\mathrm{d}x+c\int_{\mathbb{R}^2}\left|\int_0^\infty\rho_\varepsilon\chi_1\xi\,\mathrm{d}a\right|^2\underbrace{|D_x^2\mathbf{v}|^2Y_\theta^2}_{\le c}\mathrm{d}x\\
&+c\int_{\mathbb{R}^2}\underbrace{\left|\int_0^\infty\rho_\varepsilon\chi_1\xi\,\mathrm{d}a\right|^2}_{\le c,\text{ see (3.2.26)}}|\mathbf{v}|^2(Y_\theta'')^2|\nabla_x\phi_\varepsilon|^4\mathrm{d}x+c\int_{\mathbb{R}^2}\underbrace{\left|\int_0^\infty\rho_\varepsilon\chi_1\xi\,\mathrm{d}a\right|^2}_{\le c,\text{ see (3.2.26)}}|\mathbf{v}|^2(Y_\theta')^2|D_x^2\phi_\varepsilon|^2\mathrm{d}x\\
&+c\int_{\mathbb{R}^2}\left|\nabla_x\int_0^\infty\rho_\varepsilon\chi_1\xi\,\mathrm{d}a\right|^2\underbrace{|\nabla_x\mathbf{v}|^2Y_\theta^2}_{\le c}\mathrm{d}x+c\int_{\mathbb{R}^2}\underbrace{\left|\int_0^\infty\rho_\varepsilon\chi_1\xi\,\mathrm{d}a\right|^2}_{\le c,\text{ see (3.2.26)}}|\nabla_x\mathbf{v}|^2(Y_\theta')^2|\nabla_x\phi_\varepsilon|^2\mathrm{d}x
\end{aligned}
$$

$$
\begin{aligned}
&+c\int_{\mathbb{R}^2}\left|\nabla_x\int_0^\infty \rho_\varepsilon\chi_1\xi\,\mathrm{d}a\right|^2\underbrace{|\mathbf{v}|^2(Y_\theta')^2}_{\le c}|\nabla_x\phi_\varepsilon|^2\mathrm{d}x+c\int_{\mathbb{R}^2}\left|\nabla_x\int_0^\infty \rho_\varepsilon\left(\varepsilon\xi''+\xi'-\mathfrak{d}\xi\right)\mathrm{d}a\right|^2\mathrm{d}x\\
&+c\int_{\mathbb{R}^2}\left|\int_0^\infty \nabla_x\rho_\varepsilon\mathfrak{p}(a,u_\varepsilon)\xi\,\mathrm{d}a\right|^2\mathrm{d}x+c\int_{\mathbb{R}^2}\left|\int_0^\infty \rho_\varepsilon\underbrace{\partial_u\mathfrak{p}(a,u_\varepsilon)}_{\le c}\nabla_x u_\varepsilon\xi\,\mathrm{d}a\right|^2\mathrm{d}x\\
\le&-\frac{\mu}{2}\int_{\mathbb{R}^2}|D_x^3\psi_\varepsilon|^2\mathrm{d}x+c\int_{\mathbb{R}^2}\left|D_x^2\int_0^\infty \rho_\varepsilon\chi_1\xi\,\mathrm{d}a\right|^2\mathrm{d}x+c\int_{\mathbb{R}^2}\left|\int_0^\infty \rho_\varepsilon\chi_1\xi\,\mathrm{d}a\right|^2\mathrm{d}x\\
&+c\int_{\mathbb{R}^2}\left|\nabla_x\int_0^\infty \rho_\varepsilon\chi_1\xi\,\mathrm{d}a\right|^2\mathrm{d}x+c\int_{\mathbb{R}^2}|\nabla_x\phi_\varepsilon|^2\mathrm{d}x+c\int_{\mathbb{R}^2}|\nabla_x\phi_\varepsilon|^4\mathrm{d}x\\
&+c\int_{\mathbb{R}^2}|D_x^2\phi_\varepsilon|^2\mathrm{d}x+c\int_{\mathbb{R}^2}\left|\nabla_x\int_0^\infty \rho_\varepsilon\chi_1\xi\,\mathrm{d}a\right|^4\mathrm{d}x\\
&+c\int_{\mathbb{R}^2}\left|\nabla_x\int_0^\infty \rho_\varepsilon\left(\varepsilon\xi''+\xi'-\mathfrak{d}\xi\right)_+\mathrm{d}a\right|^2\mathrm{d}x+c\int_{\mathbb{R}^2}\left|\nabla_x\int_0^\infty \rho_\varepsilon\left(\varepsilon\xi''+\xi'-\mathfrak{d}\xi\right)_-\mathrm{d}a\right|^2\mathrm{d}x\\
&+c\int_{\mathbb{R}^2}|\nabla_x\psi_\varepsilon|^2\mathrm{d}x+c\int_{\mathbb{R}^2}\psi_\varepsilon^2|\nabla_x u_\varepsilon|^2\mathrm{d}x,
\end{aligned}
$$

where

$$
\begin{aligned}
\left(\varepsilon\xi''+\xi'-\mathfrak{d}\xi\right)_+&=\max\{\left(\varepsilon\xi''+\xi'-\mathfrak{d}\xi\right),0\},\\
\left(\varepsilon\xi''+\xi'-\mathfrak{d}\xi\right)_-&=\max\{-\left(\varepsilon\xi''+\xi'-\mathfrak{d}\xi\right),0\}.
\end{aligned}
$$

Integrating over $(0,t)$ we get

$$
\begin{aligned}
&\left\|D_x^2\psi_\varepsilon(t,\cdot)\right\|^2_{L^2(\mathbb{R}^2)}+\mu\left\|D_x^3\psi_\varepsilon\right\|^2_{L^2((0,t)\times\mathbb{R}^2)}\\
&\quad\le\left\|D_x^2\psi_\varepsilon(0,\cdot)\right\|^2_{L^2(\mathbb{R}^2)}+\int_0^t\left\|\left(\int_0^\infty\rho_\varepsilon\chi_1\xi\,da\right)(s)\right\|^2_{H^2(\mathbb{R}^2)}\mathrm{d}s+\int_0^t\left\|\phi_\varepsilon(s,\cdot)\right\|^2_{H^2(\mathbb{R}^2)}\mathrm{d}s\\
&\qquad+\int_0^t\left\|\left(\nabla_x\int_0^\infty\rho_\varepsilon\chi_1\xi\,\mathrm{d}a\right)(s)\right\|^4_{L^4(\mathbb{R}^2)}\mathrm{d}s+\int_0^t\left\|\nabla_x\phi_\varepsilon(s,\cdot)\right\|^4_{L^4(\mathbb{R}^2)}\mathrm{d}s\\
&\qquad+\int_0^t\left\|\left(\nabla_x\int_0^\infty\rho_\varepsilon\left(\varepsilon\xi''+\xi'-\mathfrak{d}\xi\right)_+\mathrm{d}a\right)(s)\right\|^2_{L^2(\mathbb{R}^2)}\mathrm{d}s\\
&\qquad+\int_0^t\left\|\left(\nabla_x\int_0^\infty\rho_\varepsilon\left(\varepsilon\xi''+\xi'-\mathfrak{d}\xi\right)_-\mathrm{d}a\right)(s)\right\|^2_{L^2(\mathbb{R}^2)}\mathrm{d}s\\
&\qquad+\int_0^t\left\|\nabla_x\psi_\varepsilon(s,\cdot)\right\|^2_{L^2(\mathbb{R}^2)}\mathrm{d}s+\int_0^t\int_{\mathbb{R}^2}\psi_\varepsilon^2(s,x)|\nabla_x u_\varepsilon(s,x)|^2\mathrm{d}x\mathrm{d}s.
\end{aligned}
$$

We remark that a classical regularization argument applied to the continuous cut-off functions in

$$
I_\pm=\int_0^\infty\rho_\varepsilon\left(\varepsilon\xi''+\xi'-\mathfrak{d}\xi\right)_\pm\mathrm{d}a,
$$

shows that estimates (3.2.29), (3.2.35), apply to $I_\pm$.

Then (3.2.29), (3.2.35), (3.2.40) and the embedding $H^1(\mathbb{R}^2)\subset L^4(\mathbb{R}^2)$ give us (3.2.36).

(3.2.37). Directly follows from (3.2.29), (3.2.35), (3.2.36) and the embedding $H^2(\mathbb{R}^2) \subset L^\infty(\mathbb{R}^2)$.
(3.2.38). We prove first the following estimate using the L^∞ bounds on u_ε and ψ_ε

$$
\begin{aligned}
&\frac{d}{dt}\int_{\mathbb{R}^2}\frac{|\nabla_x\psi_\varepsilon|^2u_\varepsilon^2}{2}\mathrm{d}x=\int_{\mathbb{R}^2}u_\varepsilon^2\nabla_x\psi_\varepsilon\partial_t\nabla_x\psi_\varepsilon\mathrm{d}x+\int_{\mathbb{R}^2}|\nabla_x\psi_\varepsilon|^2u_\varepsilon\partial_t u_\varepsilon\mathrm{d}x\\
&=-\int_{\mathbb{R}^2}u_\varepsilon^2\Delta_x\psi\partial_t\psi_\varepsilon\mathrm{d}x-\int_{\mathbb{R}^2}\nabla_x(u_\varepsilon^2)\cdot\nabla_x\psi_\varepsilon\partial_t\psi_\varepsilon\mathrm{d}x+\int_{\mathbb{R}^2}|\nabla_x\psi_\varepsilon|^2u_\varepsilon\partial_t u_\varepsilon\mathrm{d}x\\
&=-\mu\int_{\mathbb{R}^2}u_\varepsilon^2|D_x^2\psi_\varepsilon|^2\mathrm{d}x+\int_{\mathbb{R}^2}u_\varepsilon^2\Delta_x\psi_\varepsilon\mathrm{div}_x\left(\left(\int_0^\infty\rho_\varepsilon\chi_1\xi\mathrm{d}a\right)\mathbf{v}Y_\theta\right)\mathrm{d}x\\
&\quad-\int_{\mathbb{R}^2}u_\varepsilon^2\int_0^\infty\rho_\varepsilon\underbrace{\left(\varepsilon\xi''+\xi'-\mathfrak{d}\xi-\mathfrak{p}\xi\right)}_{\leq c\xi}\Delta_x\psi_\varepsilon\mathrm{d}a\mathrm{d}x\\
&\quad-\mu\int_{\mathbb{R}^2}\nabla_x(u_\varepsilon^2)\cdot\nabla_x\psi_\varepsilon\Delta_x\psi_\varepsilon\mathrm{d}x+\int_{\mathbb{R}^2}\nabla_x(u_\varepsilon^2)\cdot\nabla_x\psi_\varepsilon\mathrm{div}_x\left(\left(\int_0^\infty\rho_\varepsilon\chi_1\xi\mathrm{d}a\right)\mathbf{v}Y_\theta\right)\mathrm{d}x\\
&\quad-\int_{\mathbb{R}^2}\nabla_x(u_\varepsilon^2)\cdot\nabla_x\psi_\varepsilon\int_0^\infty\rho_\varepsilon\underbrace{\left(\varepsilon\xi''+\xi'-\mathfrak{d}\xi-\mathfrak{p}\xi\right)}_{\leq c\xi}\Delta_x\psi_\varepsilon\mathrm{d}a\mathrm{d}x\\
&\quad-\int_{\mathbb{R}^2}|\nabla_x\psi_\varepsilon|^2u_\varepsilon\mathrm{div}_x\left(u_\varepsilon\nu(\phi_\varepsilon)\right)\mathrm{d}x+\int_{\mathbb{R}^2}|\nabla_x\psi_\varepsilon|^2(\mathfrak{b}(\phi_\varepsilon)-\beta)u_\varepsilon^2\mathrm{d}x+\varepsilon\int_{\mathbb{R}^2}|\nabla_x\psi_\varepsilon|^2\Delta_xu_\varepsilon u_\varepsilon\mathrm{d}x\\
&\leq-\frac{\mu}{2}\int_{\mathbb{R}^2}u_\varepsilon^2|D_x^2\psi_\varepsilon|^2\mathrm{d}x+c_T\int_{\mathbb{R}^2}\left(\mathrm{div}_x\left(\left(\int_0^\infty\rho_\varepsilon\chi_1\xi\mathrm{d}a\right)\mathbf{v}Y_\theta\right)\right)^2\mathrm{d}x+c_T\int_{\mathbb{R}^2}\psi_\varepsilon^2u_\varepsilon^2\mathrm{d}x\\
&\quad+c_T\int_{\mathbb{R}^2}|D_x^2\psi_\varepsilon|^2\mathrm{d}x+c_T\int_{\mathbb{R}^2}|\nabla_x\psi_\varepsilon|^2\mathrm{d}x+c_T\int_{\mathbb{R}^2}|D_x^3\psi_\varepsilon|^2\mathrm{d}x\\
&\quad+c_T\int_{\mathbb{R}^2}\left(\nabla_x\mathrm{div}_x\left(\left(\int_0^\infty\rho_\varepsilon\chi_1\xi\mathrm{d}a\right)\mathbf{v}Y_\theta\right)\right)^2\mathrm{d}x+c_T\int_{\mathbb{R}^2}|\nabla_x\psi_\varepsilon|^4\mathrm{d}x\\
&\quad+3\int_{\mathbb{R}^2}|\nabla_x\psi_\varepsilon||D_x^2\psi_\varepsilon|\underbrace{u_\varepsilon^2\nu(\phi_\varepsilon)}_{\leq c_T}\mathrm{d}x+\int_{\mathbb{R}^2}\underbrace{\frac{u_\varepsilon^2}{2}|\mathrm{div}_x\left(\nu(\phi_\varepsilon)\right)}_{\leq c_T}|\nabla_x\psi_\varepsilon|^2\mathrm{d}x+c\int_{\mathbb{R}^2}|\nabla_x\psi_\varepsilon|^2u_\varepsilon^2\mathrm{d}x\\
&\quad-2\varepsilon\int_{\mathbb{R}^2}\nabla_x\psi_\varepsilon D_x^2\psi_\varepsilon\nabla_x\left(\frac{u_\varepsilon^2}{2}\right)\mathrm{d}x-\varepsilon\int_{\mathbb{R}^2}|\nabla_x\psi_\varepsilon|^2|\nabla_xu_\varepsilon|^2\mathrm{d}x\\
&\leq-\frac{\mu}{2}\int_{\mathbb{R}^2}u_\varepsilon^2|D_x^2\psi_\varepsilon|^2\mathrm{d}x-\varepsilon\int_{\mathbb{R}^2}|\nabla_x\psi_\varepsilon|^2|\nabla_xu_\varepsilon|^2\mathrm{d}x+c_T\int_{\mathbb{R}^2}\left|D_x^2\int_0^\infty\rho_\varepsilon\chi_1\xi\mathrm{d}a\right|^2\mathrm{d}x\\
&\quad+c_T\int_{\mathbb{R}^2}\left|\nabla_x\int_0^\infty\rho_\varepsilon\chi_1\xi\mathrm{d}a\right|^2\mathrm{d}x+c_T\int_{\mathbb{R}^2}\left|\int_0^\infty\rho_\varepsilon\chi_1\xi\mathrm{d}a\right|^2\mathrm{d}x+c_T\int_{\mathbb{R}^2}|\nabla_x\phi_\varepsilon|^2\mathrm{d}x\\
&\quad+c_T\int_{\mathbb{R}^2}|\nabla_x\phi_\varepsilon|^4\mathrm{d}x+c\int_{\mathbb{R}^2}|D_x^2\phi_\varepsilon|^2\mathrm{d}x+c_T\int_{\mathbb{R}^2}\psi_\varepsilon^2u_\varepsilon^2\mathrm{d}x+c_T\int_{\mathbb{R}^2}|D_x^2\psi_\varepsilon|^2\mathrm{d}x+c_T\int_{\mathbb{R}^2}|\nabla_x\psi_\varepsilon|^2\mathrm{d}x\\
&\quad+c_T\int_{\mathbb{R}^2}|D_x^3\psi_\varepsilon|^2\mathrm{d}x+c_T\int_{\mathbb{R}^2}|\nabla_x\psi_\varepsilon|^4\mathrm{d}x+c\int_{\mathbb{R}^2}|\nabla_x\psi_\varepsilon|^2u_\varepsilon^2\mathrm{d}x.
\end{aligned}
$$

Using the Gronwall Lemma and the estimates in (3.2.29), (3.2.35), (3.2.36), (3.2.40) we gain

$$\int_{\mathbb{R}^2}|\nabla_x\psi_\varepsilon(t,x)|^2u_\varepsilon(t,x)^2\mathrm{d}x+\mu e^{ct}\int_0^t e^{-cs}\int_{\mathbb{R}^2}u_\varepsilon(s,x)^2|D_x^2\psi_\varepsilon(s,x)|^2\mathrm{d}x\mathrm{d}s$$

$$+2\varepsilon e^{ct}\int_0^t e^{-cs}\int_{\mathbb{R}^2}|\nabla_x\psi_\varepsilon(s,x)|^2|\nabla_x u_\varepsilon(s,x)|^2\mathrm{d}x\mathrm{d}s\le ce^{ct}. \tag{3.2.41}$$

We continue by proving (3.2.38). We multiply (3.2.28) by $-D_x^6\psi_\varepsilon$

$$\begin{aligned}
&\frac{d}{dt}\int_{\mathbb{R}^2}\frac{|D_x^3\psi_\varepsilon|^2}{2}\mathrm{d}x=\int_{\mathbb{R}^2}D_x^3\psi_\varepsilon\cdot\partial_t D_x^3\psi_\varepsilon\mathrm{d}x=-\int_{\mathbb{R}^2}D_x^6\psi_\varepsilon\partial_t\psi_\varepsilon\mathrm{d}x\\
&=-\mu\int_{\mathbb{R}^2}\Delta_x\psi_\varepsilon D_x^6\psi_\varepsilon\mathrm{d}x+\int_{\mathbb{R}^2}D_x^6\psi_\varepsilon\mathrm{div}_x\left(\left(\int_0^\infty\rho_\varepsilon\chi_1\xi\mathrm{d}a\right)\mathbf{v}Y_\theta\right)\mathrm{d}x\\
&\quad-\int_{\mathbb{R}^2}\int_0^\infty\rho_\varepsilon\left(\varepsilon\xi''+\xi'-\mathfrak{d}\xi-\mathfrak{p}(a,u_\varepsilon)\xi\right)D_x^6\psi_\varepsilon\mathrm{d}a\,\mathrm{d}x\\
&=-\mu\int_{\mathbb{R}^2}|D_x^4\psi_\varepsilon|^2\mathrm{d}x+\int_{\mathbb{R}^2}D_x^4\psi_\varepsilon\Delta_x\mathrm{div}_x\left(\left(\int_0^\infty\rho_\varepsilon\chi_1\xi\mathrm{d}a\right)\mathbf{v}Y_\theta\right)\mathrm{d}x\\
&\quad-\int_{\mathbb{R}^2}\Delta_x\left(\int_0^\infty\rho_\varepsilon\left(\varepsilon\xi''+\xi'-\mathfrak{d}\xi-\mathfrak{p}(a,u_\varepsilon)\xi\right)\mathrm{d}a\right)D_x^4\psi_\varepsilon\mathrm{d}x\\
&\le-\frac{\mu}{2}\int_{\mathbb{R}^2}|D_x^4\psi_\varepsilon|^2\mathrm{d}x+c\int_{\mathbb{R}^2}\left(\Delta_x\mathrm{div}_x\left(\left(\int_0^\infty\rho_\varepsilon\chi_1\xi\mathrm{d}a\right)\mathbf{v}Y_\theta\right)\right)^2\mathrm{d}x\\
&\quad+c\int_{\mathbb{R}^2}\left|D_x^2\int_0^\infty\rho_\varepsilon\left(\varepsilon\xi''+\xi'-\mathfrak{d}\xi\right)_+\mathrm{d}a\right|^2\mathrm{d}x+c\int_{\mathbb{R}^2}\left|D_x^2\int_0^\infty\rho_\varepsilon\left(\varepsilon\xi''+\xi'-\mathfrak{d}\xi\right)_-\mathrm{d}a\right|^2\mathrm{d}x\\
&\quad+c\int_{\mathbb{R}^2}\left|\Delta_x\left(\int_0^\infty\rho_\varepsilon\mathfrak{p}(a,u_\varepsilon)\xi\mathrm{d}a\right)\right|^2\mathrm{d}x\\
&\le-\frac{\mu}{2}\int_{\mathbb{R}^2}|D_x^4\psi_\varepsilon|^2\mathrm{d}x+c\int_{\mathbb{R}^2}\left|D_x^3\int_0^\infty\rho_\varepsilon\chi_1\xi\mathrm{d}a\right|^2\underbrace{|\mathbf{v}|^2Y_\theta^2}_{\le c}\mathrm{d}x\\
&\quad+c\int_{\mathbb{R}^2}\left|D_x^2\int_0^\infty\rho_\varepsilon\chi_1\xi\mathrm{d}a\right|^2\underbrace{|\nabla_x\mathbf{v}|^2Y_\theta^2}_{\le c}\mathrm{d}x+c\int_{\mathbb{R}^2}\left|\nabla_x\int_0^\infty\rho_\varepsilon\chi_1\xi\mathrm{d}a\right|^2\underbrace{|D_x^2\mathbf{v}|^2Y_\theta^2}_{\le c}\mathrm{d}x\\
&\quad+c\int_{\mathbb{R}^2}\left|\int_0^\infty\rho_\varepsilon\chi_1\xi\mathrm{d}a\right|^2\underbrace{|D_x^3\mathbf{v}|^2Y_\theta^2}_{\le c}\mathrm{d}x+c\int_{\mathbb{R}^2}\left|D_x^2\int_0^\infty\rho_\varepsilon\chi_1\xi\mathrm{d}a\right|^2\underbrace{|\mathbf{v}|^2(Y_\theta')^2}_{\le c}|\nabla_x\phi_\varepsilon|^2\mathrm{d}x\\
&\quad+c\int_{\mathbb{R}^2}\underbrace{\left|\int_0^\infty\rho_\varepsilon\chi_1\xi\mathrm{d}a\right|^2}_{\le c}|D_x^2\mathbf{v}|^2(Y_\theta')^2|\nabla_x\phi_\varepsilon|^2\mathrm{d}x\\
&\quad+c\int_{\mathbb{R}^2}\left|\nabla_x\int_0^\infty\rho_\varepsilon\chi_1\xi\mathrm{d}a\right|^2\underbrace{|\nabla_x\mathbf{v}|^2(Y_\theta')^2}_{\le c}|\nabla_x\phi_\varepsilon|^2\mathrm{d}x\\
&\quad+c\int_{\mathbb{R}^2}\left|\nabla_x\int_0^\infty\rho_\varepsilon\chi_1\xi\mathrm{d}a\right|^2\underbrace{|\mathbf{v}|^2(Y_\theta'')^2}_{\le c}|\nabla_x\phi_\varepsilon|^4\mathrm{d}x+c\int_{\mathbb{R}^2}\left|\nabla_x\int_0^\infty\rho_\varepsilon\chi_1\xi\mathrm{d}a\right|^2\underbrace{|\mathbf{v}|^2(Y_\theta')^2}_{\le c}|D_x^2\phi_\varepsilon|^2\mathrm{d}x\\
&\quad+c\int_{\mathbb{R}^2}\underbrace{\left|\int_0^\infty\rho_\varepsilon\chi_1\xi\mathrm{d}a\right|^2}_{\le c}|\nabla_x\mathbf{v}|^2(Y_\theta'')^2|\nabla_x\phi_\varepsilon|^4\mathrm{d}x+c\int_{\mathbb{R}^2}\underbrace{\left|\int_0^\infty\rho_\varepsilon\chi_1\xi\mathrm{d}a\right|^2}_{\le c}|\nabla_x\mathbf{v}|^2(Y_\theta')^2|D_x^2\phi_\varepsilon|^2\mathrm{d}x
\end{aligned}$$

$$
\begin{aligned}
&+c\int_{\mathbb{R}^2}\underbrace{\left|\int_0^\infty \rho_\varepsilon\chi_1\xi\,\mathrm{d}a\right|^2}_{\leq c}|\mathbf{v}|^2(Y_\theta''')^2|\nabla_x\phi_\varepsilon|^6\mathrm{d}x\\
&+c\int_{\mathbb{R}^2}\underbrace{\left|\int_0^\infty \rho_\varepsilon\chi_1\xi\,\mathrm{d}a\right|^2}_{\leq c}|\mathbf{v}|^2(Y_\theta'')^2|D_x^2\phi_\varepsilon|^2|\nabla_x\phi_\varepsilon|^2\mathrm{d}x\\
&+c\int_{\mathbb{R}^2}\underbrace{\left|\int_0^\infty \rho_\varepsilon\chi_1\xi\,\mathrm{d}a\right|^2}_{\leq c}|\mathbf{v}|^2(Y_\theta')^2|D_x^3\phi_\varepsilon|^2\mathrm{d}x+c\int_{\mathbb{R}^2}\left|D_x^2\int_0^\infty \rho_\varepsilon\left(\varepsilon\xi''+\xi'-\mathfrak{d}\xi\right)_+\mathrm{d}a\right|^2\mathrm{d}x\\
&+c\int_{\mathbb{R}^2}\left|D_x^2\int_0^\infty \rho_\varepsilon\left(\varepsilon\xi''+\xi'-\mathfrak{d}\xi\right)_-\mathrm{d}a\right|^2\mathrm{d}x+c\int_{\mathbb{R}^2}\left|\int_0^\infty \nabla_x\rho_\varepsilon\cdot\nabla_x u_\varepsilon\,\xi\,\underbrace{\partial_u\mathfrak{p}(a,u_\varepsilon)}_{\leq c}\mathrm{d}a\right|^2\mathrm{d}x\\
&+c\int_{\mathbb{R}^2}\left|\int_0^\infty \Delta_x\rho_\varepsilon\xi\,\mathfrak{p}(a,u_\varepsilon)\mathrm{d}a\right|^2\mathrm{d}x+c\int_{\mathbb{R}^2}\left|\int_0^\infty \rho_\varepsilon\,\xi\,\underbrace{\partial_{uu}^2\mathfrak{p}(a,u_\varepsilon)}_{\leq c}|\nabla_x u_\varepsilon|^2\mathrm{d}a\right|^2\mathrm{d}x\\
&+c\int_{\mathbb{R}^2}\left|\int_0^\infty \rho_\varepsilon\xi\underbrace{\partial_u\mathfrak{p}(a,u_\varepsilon)}_{\leq c}\Delta_x u_\varepsilon\mathrm{d}a\right|^2\mathrm{d}x\\
\leq&-\frac{\mu}{2}\int_{\mathbb{R}^2}|D_x^4\psi_\varepsilon|^2\mathrm{d}x+c\int_{\mathbb{R}^2}\left|D_x^3\int_0^\infty \rho_\varepsilon\chi_1\xi\mathrm{d}a\right|^2\mathrm{d}x+c\int_{\mathbb{R}^2}\left|D_x^2\int_0^\infty \rho_\varepsilon\chi_1\xi\mathrm{d}a\right|^2\mathrm{d}x\\
&+c\int_{\mathbb{R}^2}\left|\nabla_x\int_0^\infty \rho_\varepsilon\chi_1\xi\mathrm{d}a\right|^2\mathrm{d}x+c\int_{\mathbb{R}^2}\left|\int_0^\infty \rho_\varepsilon\chi_1\xi\mathrm{d}a\right|^2\mathrm{d}x+c\int_{\mathbb{R}^2}\left|D_x^2\int_0^\infty \rho_\varepsilon\chi_1\xi\mathrm{d}a\right|^4\mathrm{d}x\\
&+c\int_{\mathbb{R}^2}\left|\nabla_x\int_0^\infty \rho_\varepsilon\chi_1\xi\mathrm{d}a\right|^4\mathrm{d}x+c\int_{\mathbb{R}^2}|D_x^3\phi_\varepsilon|^2\mathrm{d}x+c\int_{\mathbb{R}^2}|D_x^2\phi_\varepsilon|^2\mathrm{d}x+c\int_{\mathbb{R}^2}|D_x^2\phi_\varepsilon|^4\mathrm{d}x\\
&+c\int_{\mathbb{R}^2}|\nabla_x\phi_\varepsilon|^2\mathrm{d}x+c\int_{\mathbb{R}^2}|\nabla_x\phi_\varepsilon|^4\mathrm{d}x+c\int_{\mathbb{R}^2}|\nabla_x\phi_\varepsilon|^6\mathrm{d}x+c\int_{\mathbb{R}^2}|\nabla_x\phi_\varepsilon|^8\mathrm{d}x\\
&+c\int_{\mathbb{R}^2}\left|D_x^2\int_0^\infty \rho_\varepsilon\left(\varepsilon\xi''+\xi'-\mathfrak{d}\xi\right)_+\mathrm{d}a\right|^2\mathrm{d}x+c\int_{\mathbb{R}^2}\left|D_x^2\int_0^\infty \rho_\varepsilon\left(\varepsilon\xi''+\xi'-\mathfrak{d}\xi\right)_-\mathrm{d}a\right|^2\mathrm{d}x\\
&+c\int_{\mathbb{R}^2}|D_x^2\psi_\varepsilon|^2\mathrm{d}x+c\int_{\mathbb{R}^2}|\nabla_x\psi_\varepsilon|^2|\nabla_x u_\varepsilon|^2\mathrm{d}x+c_T\int_{\mathbb{R}^2}|\nabla_x u_\varepsilon|^4\mathrm{d}x+c_T\int_{\mathbb{R}^2}|\Delta_x u_\varepsilon|^2\mathrm{d}x.
\end{aligned}
$$

We integrate over $(0,t)$, and we remark once again that, up to a regularization argument, the estimates obtained for ψ_ε apply to $I_\pm$ as well. Then (3.2.29), (3.2.35) and (3.2.36), (3.2.41), (3.2.33), together with the embedding $H^1(\mathbb{R}^2)\subset L^p(\mathbb{R}^2)$ for very $1\leq p<\infty$ give us

$$
\left\|D_x^3\psi_\varepsilon(t,\cdot)\right\|_{L^2(\mathbb{R}^2)}^2+\mu\left\|D_x^4\psi_\varepsilon\right\|_{L^2((0,t)\times\mathbb{R}^2)}^2\leq ce^{ct}.
$$

(3.2.39). It follows from (3.2.29), (3.2.35), (3.2.36), (3.2.38), (3.2.28) and the embedding $H^2(\mathbb{R}^2)\subset L^\infty(\mathbb{R}^2)$. □

The following two lemmas provide keys estimates on ρ_ε, its derivatives and its trace at $a=0$. We omit their proofs as they closely follow the argument used in the proofs of [9, Corollary 2.1, Lemma 2.3], using Lemmas 3.3, 3.4, 3.7, 3.2.30, and the boundedness of $\mathfrak{p}$.

Lemma 3.8 (**Estimates on the trace of ρ_ε at $a=0$**). *Define $\rho^0_\varepsilon(t,x)=\rho_\varepsilon(t,0,x)$. For every $t\geq 0$ the following estimates hold*

$$\begin{aligned}
\left\|\rho^0_\varepsilon(t,\cdot)\right\|_{L^1(\mathbb{R}^2)}, \left\|D^2_x\rho^0_\varepsilon\right\|_{L^1((0,t)\times\mathbb{R}^2)}, \left\|\partial_t\rho^0_\varepsilon\right\|_{L^1((0,t)\times\mathbb{R}^2)} &\leq e^{Ct}C,\\
\left\|\rho^0_\varepsilon(t,\cdot)\right\|_{L^2(\mathbb{R}^2)}, \left\|\nabla_x\rho^0_\varepsilon(t,\cdot)\right\|_{L^2(\mathbb{R}^2)} &\leq e^{Ct}C,\\
\left\|\nabla_x\rho^0_\varepsilon\right\|_{L^2((0,t)\times\mathbb{R}^2)}, \left\|D^2_x\rho^0_\varepsilon\right\|_{L^2((0,t)\times\mathbb{R}^2)}, \left\|\partial_t\rho^0_\varepsilon\right\|_{L^2((0,t)\times\mathbb{R}^2)} &\leq e^{Ct}C,\\
\left\|\rho^0_\varepsilon(t,\cdot)\right\|_{L^\infty(\mathbb{R}^2)} &\leq e^{Ct}C.
\end{aligned}$$

Lemma 3.9 (**Estimates on ρ_ε**). *For every $t\geq 0$ the following estimates hold*

$$\left\|\rho_\varepsilon(t,\cdot,\cdot)\right\|_{L^\infty((0,\infty)\times\mathbb{R}^2)} \leq Ce^{Ct}, \tag{3.2.42}$$

$$\left\|\rho_\varepsilon(t,\cdot,\cdot)\right\|_{L^1((0,\infty)\times\mathbb{R}^2)} \leq Ce^{Ct}, \tag{3.2.43}$$

$$\left\|\rho_\varepsilon(t,\cdot,\cdot)\right\|_{L^2((0,\infty)\times\mathbb{R}^2)}, \left\|\nabla_x\rho_\varepsilon\right\|_{L^2((0,t)\times(0,\infty)\times\mathbb{R}^2)}, \sqrt{\varepsilon}\left\|\partial_a\rho_\varepsilon\right\|_{L^2((0,t)\times(0,\infty)\times\mathbb{R}^2)} \leq Ce^{Ct}, \tag{3.2.44}$$

$$\left\|\nabla_x\rho_\varepsilon(t,\cdot,\cdot)\right\|_{L^2((0,\infty)\times\mathbb{R}^2)}, \left\|D^2_x\rho_\varepsilon\right\|_{L^2((0,t)\times(0,\infty)\times\mathbb{R}^2)}, \sqrt{\varepsilon}\left\|\partial_a\nabla_x\rho_\varepsilon\right\|_{L^2((0,t)\times(0,\infty)\times\mathbb{R}^2)} \leq Ce^{Ct}, \tag{3.2.45}$$

$$\left\|\partial_a\rho_\varepsilon(t,\cdot,\cdot)\right\|_{L^1((0,\infty)\times\mathbb{R}^2)} \leq Ce^{Ct}. \tag{3.2.46}$$

Lemma 3.10 (**BV estimate w.r.t. x on u_ε**). *For every $t\geq 0$ the following estimate holds*

$$\|\nabla_x u_\varepsilon(t,\cdot)\|_{L^1(\mathbb{R}^2)} \leq Ce^{Ct}. \tag{3.2.47}$$

Proof. From the equation of u_ε in (3.2.34) we have the equation

$$\partial_t\nabla_x u_\varepsilon + \nabla_x\left(\nabla u_\varepsilon\cdot\nu(\phi_\varepsilon) + u_\varepsilon \mathrm{div}_x\left(\nu(\phi_\varepsilon)\right)\right) = (\mathfrak{b}(\phi_\varepsilon)-\beta)\nabla_x u_\varepsilon + \mathfrak{b}'(\phi_\varepsilon)\nabla_x\phi_\varepsilon\, u_\varepsilon + \varepsilon\nabla_x\Delta_x u_\varepsilon.$$

We define

$$\mathrm{sign}\,(\nabla_x u_\varepsilon) = (\mathrm{sign}\left(\partial_{x_1}(u_\varepsilon)\right), \mathrm{sign}\left(\partial_{x_2}(u_\varepsilon)\right)),$$

where $x=(x_1,x_2)$. Then, using the L^∞ bounds on $\nabla_x\phi_\varepsilon$ and $\nu(\phi_\varepsilon)$ in (3.2.39), (3.1.14), we get

$$\begin{aligned}
&\frac{d}{dt}\int_{\mathbb{R}^2}|\nabla_x u_\varepsilon|\mathrm{d}x = \int_{\mathbb{R}^2}\mathrm{sign}(\nabla_x u_\varepsilon)\partial_t\nabla_x u_\varepsilon\mathrm{d}x\\
&= -\underbrace{\int_{\mathbb{R}^2}\nabla_x(\nabla_x u_\varepsilon\cdot\nu(\phi_\varepsilon))\,\mathrm{sign}(\nabla_x u_\varepsilon)\mathrm{d}x}_{=0} - \int_{\mathbb{R}^2}\nabla_x(u_\varepsilon\mathrm{div}_x\left(\nu(\phi_\varepsilon)\right))\,\mathrm{sign}(\nabla_x u_\varepsilon)\mathrm{d}x\\
&\quad + \underbrace{\varepsilon\int_{\mathbb{R}^2}\nabla_x\Delta_x u_\varepsilon\,\mathrm{sign}(\nabla_x u_\varepsilon)\mathrm{d}x}_{\leq 0} + \int_{\mathbb{R}^2}\underbrace{\mathfrak{b}'(\phi_\varepsilon)\nabla_x\phi_\varepsilon}_{\leq c_T}u_\varepsilon\,\mathrm{sign}(\nabla_x u_\varepsilon)\mathrm{d}x + \int_{\mathbb{R}^2}\underbrace{(\mathfrak{b}(\phi_\varepsilon)-\beta)}_{\leq c}|\nabla_x u_\varepsilon|\mathrm{d}x\\
&\leq \int_{\mathbb{R}^2}|\nabla_x u_\varepsilon||\mathrm{div}_x\left(\nu(\phi_\varepsilon)\right)|\,\mathrm{d}x - \int_{\mathbb{R}^2}u_\varepsilon\nabla_x(\mathrm{div}_x\left(\nu(\phi_\varepsilon)\right))\,\mathrm{sign}\,(\nabla_x u_\varepsilon)\,\mathrm{d}x\\
&\quad + c_T\int_{\mathbb{R}^2}u_\varepsilon\mathrm{d}x + c\int_{\mathbb{R}^2}|\nabla_x u_\varepsilon|\mathrm{d}x\\
&\leq c\int_{\mathbb{R}^2}|\nabla_x u_\varepsilon|\mathrm{d}x + c_T\int_{\mathbb{R}^2}|u_\varepsilon|\mathrm{d}x + c\int_{\mathbb{R}^2}u_\varepsilon^2\mathrm{d}x + c\int_{\mathbb{R}^2}|\nabla_x u_\varepsilon|^2\mathrm{d}x\\
&\quad + \int_{\mathbb{R}^2}|\mathrm{div}_x\left(\nu(\phi_\varepsilon)\right)|^2\mathrm{d}x + \int_{\mathbb{R}^2}|\nabla_x(\mathrm{div}_x\left(\nu(\phi_\varepsilon)\right))|^2\mathrm{d}x.
\end{aligned}$$

We obtain the desired inequality (3.2.47) integrating over $(0,t)$, using the Gronwall Lemma and the estimates in Lemma 3.6, (3.1.15) and (3.1.18). □

Lemma 3.11 (**BV estimate w.r.t. t on u_ε**). *For every $t \geq 0$, the following estimate holds*

$$\|\partial_t u_\varepsilon(t,\cdot)\|_{L^1(\mathbb{R}^2)} \leq Ce^{Ct}. \tag{3.2.48}$$

Proof. From the definition of $\nu(\phi)$ in (3.1.3) we compute

$$\partial_t \nu(\phi_\varepsilon) = \kappa \frac{\partial_t \phi_\varepsilon * \nabla_x \eta}{\left(1 + \left\|\phi_\varepsilon * \nabla_x \eta\right\|^2\right)^{3/2}},$$

then from (3.2.39) we have

$$\left\|\partial_t \nu(\phi_\varepsilon)\right\|_{L^\infty(\mathbb{R}^2;\mathbb{R}^2)} \leq \kappa \left\|\nabla_x \eta\right\|_{L^\infty(\mathbb{R}^2;\mathbb{R}^2)} \left\|\partial_t \phi_\varepsilon\right\|_{L^1(\mathbb{R}^2,\mathbb{R})} \leq Ce^{Ct}.$$

Similarly, explicit computations give us

$$\operatorname{div}_x\left(\nu(\phi_\varepsilon)\right) = \kappa \frac{\phi_\varepsilon * \Delta_x \eta}{\left(1 + \left\|\phi_\varepsilon * \nabla_x \eta\right\|^2\right)^{3/2}}, \tag{3.2.49}$$

and

$$\partial_t \operatorname{div}_x\left(\nu(\phi_\varepsilon)\right) = \kappa \frac{\partial_t \phi_\varepsilon * \Delta_x \eta}{\left(1 + \left\|\phi_\varepsilon * \nabla_x \eta\right\|^2\right)^{3/2}} - 3\kappa (\phi_\varepsilon * \Delta_x \eta) \frac{\phi_\varepsilon * \nabla_x \eta}{\sqrt{1 + \left\|\phi_\varepsilon * \nabla_x \eta\right\|^2}} \frac{\partial_t \phi_\varepsilon * \nabla_x \eta}{\left(1 + \left\|\phi_\varepsilon * \nabla_x \eta\right\|^2\right)^2}.$$

Therefore, from (3.2.27), (3.2.39), we obtain

$$\begin{aligned}
&\left\|\partial_t \operatorname{div}_x\left(\nu(\phi_\varepsilon)\right)\right\|_{L^2(\mathbb{R}^2;\mathbb{R})} \\
&\quad \leq \kappa \left\|\partial_t \phi_\varepsilon * \Delta_x \eta\right\|_{L^2(\mathbb{R}^2;\mathbb{R})} + 3\kappa \left\|\phi_\varepsilon * \Delta_x \eta\right\|_{L^\infty(\mathbb{R}^2;\mathbb{R})} \left\|\partial_t \phi_\varepsilon * \nabla_x \eta\right\|_{L^2(\mathbb{R}^2;\mathbb{R}^2)} \\
&\quad \leq \kappa \left\|\partial_t \phi_\varepsilon\right\|_{L^1(\mathbb{R}^2;\mathbb{R})} \left(\left\|\Delta_x \eta\right\|_{L^2(\mathbb{R}^2;\mathbb{R})} + 3 \left\|\Delta_x \eta\right\|_{L^\infty(\mathbb{R}^2;\mathbb{R})} \left\|\nabla_x \eta\right\|_{L^2(\mathbb{R}^2;\mathbb{R}^2)} \left\|\phi_\varepsilon\right\|_{L^1(\mathbb{R}^2;\mathbb{R})}\right) \\
&\quad \leq Ce^{Ct}.
\end{aligned}$$

The estimates above allow us to prove (3.2.48). From the equation (3.2.34) for u_ε we have

$$\partial_{tt}^2 u_\varepsilon + \operatorname{div}_x\left(\partial_t u_\varepsilon \nu(\phi_\varepsilon)\right) + \operatorname{div}_x\left(u_\varepsilon \partial_t \nu(\phi_\varepsilon)\right) = (\mathfrak{b}(\phi_\varepsilon) - \beta)\partial_t u_\varepsilon + \mathfrak{b}'(\phi_\varepsilon)\partial_t \phi_\varepsilon u_\varepsilon + \varepsilon \Delta_x \partial_t u_\varepsilon,$$

then we consider

$$\begin{aligned}\frac{d}{dt}\int_{\mathbb{R}^2}|\partial_t u_\varepsilon|\,\mathrm{d}x = &\underbrace{-\int_{\mathbb{R}^2}\mathrm{div}_x\left(\partial_t u_\varepsilon \nu(\phi_\varepsilon)\right)\mathrm{sign}\left(\partial_t u_\varepsilon\right)\mathrm{d}x}_{=0}+\underbrace{\varepsilon\int_{\mathbb{R}^2}\Delta_x\partial_t u_\varepsilon\,\mathrm{sign}\left(\partial_t u_\varepsilon\right)\mathrm{d}x}_{\leq 0}\\ &-\int_{\mathbb{R}^2}(\nabla u_\varepsilon\underbrace{\partial_t\nu(\phi_\varepsilon)}_{\leq c_T}+u_\varepsilon\partial_t\mathrm{div}_x\left(\nu(\phi_\varepsilon)\right))\mathrm{sign}\left(\partial_t u_\varepsilon\right)\mathrm{d}x\\ &+\int_{\mathbb{R}^2}\underbrace{(\mathfrak{b}(\phi_\varepsilon)-\beta)}_{\leq c}|\partial_t u_\varepsilon|\mathrm{d}x+\int_{\mathbb{R}^2}\mathfrak{b}'(\phi_\varepsilon)\partial_t\phi_\varepsilon u_\varepsilon\mathrm{sign}\left(\partial_t u_\varepsilon\right)\mathrm{d}x\\ \leq &c_T\int_{\mathbb{R}^2}|\nabla_x u_\varepsilon|\mathrm{d}x+c\int_{\mathbb{R}^2}u_\varepsilon^2\mathrm{d}x+\int_{\mathbb{R}^2}|\partial_t\mathrm{div}_x\left(\nu(\phi_\varepsilon)\right)|^2\,dx\\ &+c_T\int_{\mathbb{R}^2}|\partial_t\phi_\varepsilon|\mathrm{d}x+c\int_{\mathbb{R}^2}|\partial_t u_\varepsilon|\mathrm{d}x.\end{aligned}$$

Integrating on $(0,t)$ we obtain (3.2.48) thanks to (3.2.32), (3.2.39) and (3.2.47) and the Gronwall Lemma. □

We are now ready to prove the compactness of the families $\{\rho_\varepsilon\}_\varepsilon$ and $\{u_\varepsilon\}_\varepsilon$, and the first part of Theorem 3.1, establishing the existence of entropy solutions for the system (3.1.1).

Lemma 3.12 (**Strong compactness of** $\{\rho_\varepsilon\}_\varepsilon$ **and** $\{u_\varepsilon\}_\varepsilon$**).** *There exists a couple of functions* (u,ρ) *and a sequence* $\{\varepsilon_k\}_{k\in\mathbb{N}}\in(0,\infty)$, $\varepsilon_k\to 0$, *such that, for every* $T>0$

$$\begin{aligned}&\rho_{\varepsilon_k}\to\rho,\quad \text{a.e. in } (0,T)\times(0,\infty)\times\mathbb{R}^2\quad \text{and in } L^p_{loc}((0,\infty)\times(0,\infty)\times\mathbb{R}^2),\ 1\leq p<\infty,\\ &\rho(\cdot,\cdot,\cdot)\geq 0,\quad \rho(t,\cdot,x)\in BV(0,\infty),\quad \text{for a.e. } (t,x)\in(0,\infty)\times\mathbb{R}^2,\\ &\rho\in L^\infty(0,T;L^1((0,\infty)\times\mathbb{R}^2))\cap L^\infty((0,T)\times(0,\infty)\times\mathbb{R}^2)\cap L^2((0,T)\times(0,\infty);H^2(\mathbb{R}^2)),\end{aligned}\tag{3.2.50}$$

and

$$\begin{aligned}&u_{\varepsilon_{k_h}}\to u\quad \text{a.e. in } (0,T)\times\mathbb{R}^2\quad \text{and in } L^p_{\mathrm{loc}}((0,\infty)\times\mathbb{R}^2),\ 1\leq p<\infty,\\ &u(\cdot,\cdot)\geq 0,\qquad u\in L^\infty((0,T)\times\mathbb{R}^2)\cap BV((0,T)\times\mathbb{R}^2).\end{aligned}\tag{3.2.51}$$

Proof. The proof of the strong convergence (up to a subsequence) for $\{\rho_\varepsilon\}_\varepsilon$ follows the argument used in [9, Lemma 2.9], which is based on the Murat Lemma, [31], and the compensated compactness result in [35, Th. 5]. Thanks to Lemmas 3.2.30, 3.11, 3.10, $\{u_\varepsilon\}_\varepsilon$ is bounded in $L^\infty((0,T)\times\mathbb{R}^2)\cap BV((0,T)\times\mathbb{R}^2)$ so that Helly's Theorem applies. □

Lemma 3.13. *The couple of functions* (u,ρ) *introduced in Lemma* 3.12 *is an entropy solution of* (3.1.1) *in the sense of Definition* 3.2.

Proof. It is clear that the couple (u,ρ) is a weak solution of (3.1.1) in the sense of Definition 3.1 thanks to the strong convergence results in Lemma 3.12. In particular, the fact that ρ is a weak solution comes directly from [35, Th. 5].

We obtain (3.1.20) as in [9, Lemma 2.10], then we only have to verify that (3.1.21) holds. Let $\xi \in C^\infty(\mathbb{R}^4)$ be a nonnegative text function with compact support and $\mathfrak{c} \in \mathbb{R}$ be a constant. Multiplying the equation of u_ε in (3.2.23) by $\operatorname{sign}(u_\varepsilon - \mathfrak{c})$ we have

$$\partial_t |u_\varepsilon - \mathfrak{c}| + \operatorname{div}_x \left(|u_\varepsilon - \mathfrak{c}| v(\phi_\varepsilon) \right) + \mathfrak{c} \operatorname{sign}(u_\varepsilon - \mathfrak{c}) \operatorname{div}_x \left(v(\phi_\varepsilon) \right) \\ \leq \operatorname{sign}(u_\varepsilon - \mathfrak{c}) (\mathfrak{b}(\phi_\varepsilon) - \beta) u_\varepsilon + \varepsilon \Delta_x |u_\varepsilon - \mathfrak{c}|.$$

Then,

$$\int_0^\infty \int_0^\infty \int_{\mathbb{R}^2} \Big(|u_\varepsilon - \mathfrak{c}| \partial_t \xi + |u_\varepsilon - \mathfrak{c}| v(\phi_\varepsilon) \cdot \nabla_x \xi + \operatorname{sign}(u_\varepsilon - \mathfrak{c}) (\mathfrak{b}(\phi_\varepsilon) - \beta) u_\varepsilon \xi \\ + \varepsilon |u_\varepsilon - \mathfrak{c}| \Delta_x \xi - \mathfrak{c} \operatorname{sign}(u_\varepsilon - \mathfrak{c}) \operatorname{div}_x \left(v(\phi_\varepsilon) \right) \xi \Big) \mathrm{d}x \, \mathrm{d}a \, \mathrm{d}t \\ + \int_0^\infty \int_{\mathbb{R}^2} |u_{\varepsilon,0}(x) - \mathfrak{c}| \xi(0, a, x) \mathrm{d}x \, \mathrm{d}a \geq 0.$$

By taking the limit for $\varepsilon \to 0$, we get (3.1.21). □

3.3 Uniqueness and stability

In this section we establish the inequality (3.1.22), which concludes the proof of Theorem 3.1. To this end we introduce the following preliminary lemma.

Lemma 3.14. *Let (u_1, ρ_1) and (u_2, ρ_2) be two entropy solutions of (3.1.1) obtained from the initial data $(u_{1,0}, \rho_{1,0})$ and $(u_{2,0}, \rho_{2,0})$ respectively. For every nonnegative test function $\xi \in C_c^\infty(\mathbb{R}^4)$ the following inequalities hold*

$$\int_0^\infty \int_0^\infty \int_{\mathbb{R}^2} \Big(|\rho_1 - \rho_2| (\partial_t \xi + \partial_a \xi) - \operatorname{div}_x \left(|\rho_1 - \rho_2| \chi_1 \mathbf{v}(Y_\theta(\phi_1 - R) + Y_\theta(\phi_2 - R)) \right) \xi \\ + \mu \Delta_x |\rho_1 - \rho_2| \xi - |\rho_1 - \rho_2| \mathfrak{d} \xi - |\rho_1 - \rho_2| \mathfrak{p}(a, u_1) \xi \\ - \operatorname{sign}\left(\rho_1 - \rho_2\right) (\mathfrak{p}(a, u_1) - \mathfrak{p}(a, u_2)) \rho_2 \xi \Big) \, dx \, da \, dt \\ + \int_0^\infty \int_{\mathbb{R}^2} |\rho_1(t, 0^+, x) - \rho_2(t, 0^+, x)| \xi(t, 0, x) \, dx \, dt + \int_0^\infty \int_{\mathbb{R}^2} |\rho_{1,0}(a, x) - \rho_{2,0}(a, x)| \xi(0, a, x) \, dx \, da \\ \geq \int_0^\infty \int_0^\infty \int_{\mathbb{R}^2} \operatorname{sign}\left(\rho_1 - \rho_2\right) \chi_1 \left(\rho_2 \operatorname{div}_x \left(\mathbf{v} Y_\theta(\phi_1 - R) \right) - \rho_1 \operatorname{div}_x \left(\mathbf{v}(x) Y_\theta(\phi_2 - R) \right) \right) \xi \, dx \, da \, dt, \tag{3.3.52}$$

where

$$\phi_i(t, x) := \int_0^\infty \rho_i(t, a, x) \chi_2(a) da, \qquad \text{for } i = 1, 2,$$

and

$$\begin{aligned}
&\int_0^\infty\int_0^\infty\int_{\mathbb{R}^2}\Big(|u_1-u_2|\partial_t\xi-\operatorname{div}_x\big(|u_1-u_2|(\nu(\phi_1)+\nu(\phi_2))\big)\xi\\
&\qquad\qquad+|u_1-u_2|(\mathfrak{b}(\phi_1)-\beta)\xi+\operatorname{sign}(u_1-u_2)\,(\mathfrak{b}(\phi_1)-\mathfrak{b}(\phi_2))\,u_2\xi\Big)\,dx\,da\,dt\\
&+\int_0^\infty\int_{\mathbb{R}^2}|u_{1,0}(x)-u_{2,0}(x)|\xi(0,a,x)\,dx\,da\\
&\geq\int_0^\infty\int_0^\infty\int_{\mathbb{R}^2}\operatorname{sign}(u_1-u_2)\big(u_2\operatorname{div}_x\big(\nu(\phi_1)\big)-u_1\operatorname{div}_x\big(\nu(\phi_2)\big)\big)\,\xi\,dx\,da\,dt.
\end{aligned}\tag{3.3.53}$$

Proof. We double the variables and write

$$\rho_1=\rho_1(t,a,x),\quad \rho_2=\rho_2(s,b,y),\quad \phi_1=\phi_1(t,x),\quad \phi_2=\phi_2(s,y)\quad u_1=u_1(t,x)\quad u_2=u_2(s,y),$$

where $x=(x_1,x_2)$ and $y=(y_1,y_2)$.
Consider the test function

$$\Xi_n(t,s,a,b,x,y)=\xi\left(\frac{t+s}{2},\frac{a+b}{2},\frac{x+y}{2}\right)\lambda_n\left(\frac{s-t}{2}\right)\lambda_n\left(\frac{b-a}{2}\right)\lambda_n\left(\frac{y_1-x_1}{2}\right)\lambda_n\left(\frac{y_2-x_2}{2}\right),$$

where

$$\lambda_n(u)=n\lambda(nu),\qquad \lambda\in C^\infty(\mathbb{R}),\qquad \lambda\geq 0,\qquad \|\lambda\|_{L^1(\mathbb{R})}=1,\qquad \operatorname{supp}(\lambda)\subset[-1,1].$$

To prove inequality (3.3.52) we follow the doubling of variables argument appearing in [9, Lemma 3.1], and use the regularity of $\mathfrak{p}$ and the L^∞ bounds on u_1, u_2. Then we have only to verify (3.3.53). We write (3.1.21) for $u_1(t,x)$ using $u_2(s,y)$ as a constant and integrate over (s,y)

$$\begin{aligned}
&\iiiiint\Big(|u_1-u_2|\partial_t\Xi_n-\operatorname{div}_x\big(|u_1-u_2|\nu(\phi_1)\big)\Xi_n\\
&+\qquad\operatorname{sign}(u_1-u_2)\,(\mathfrak{b}(\phi_1)-\beta)\,u_1\Xi_n\Big)\,\mathrm{d}x\,\mathrm{d}y\,\mathrm{d}a\,\mathrm{d}b\,\mathrm{d}t\,\mathrm{d}s\\
&+\iiiiint|u_{1,0}(x)-u_2|\Xi_n(0,s,a,b,x,y)\,\mathrm{d}x\,\mathrm{d}y\,\mathrm{d}a\,\mathrm{d}b\,\mathrm{d}s\\
&\qquad\geq\iiiiint\operatorname{sign}(u_1-u_2)\,u_2\operatorname{div}_x\big(\nu(\phi_1)\big)\,\Xi_n\,\mathrm{d}x\,\mathrm{d}y\,\mathrm{d}a\,\mathrm{d}b\,\mathrm{d}t\,\mathrm{d}s,
\end{aligned}\tag{3.3.54}$$

and we write (3.1.21) for $u_2(s,y)$ using $u_1(t,x)$ as a constant and integrate over (t,x)

$$\begin{aligned}
&\iiiiint\Big(|u_1-u_2|\partial_s\Xi_n-\operatorname{div}_y\big(|u_1-u_2|\nu(\phi_2)\big)\Xi_n\\
&\qquad-\operatorname{sign}(u_1-u_2)\,(\mathfrak{b}(\phi_2)-\beta)\,u_2\Xi_n\Big)\,\mathrm{d}x\,\mathrm{d}y\,\mathrm{d}a\,\mathrm{d}b\,\mathrm{d}t\,\mathrm{d}s\\
&+\iiiiint|u_1-u_{2,0}(y)|\Xi_n(t,0,a,b,x,y)\,\mathrm{d}x\,\mathrm{d}y\,\mathrm{d}a\,\mathrm{d}b\,\mathrm{d}t\\
&\qquad\geq-\iiiiint\operatorname{sign}(u_1-u_2)\,u_1\operatorname{div}_x\big(\nu(\phi_2)\big)\,\Xi_n\,\mathrm{d}x\,\mathrm{d}y\,\mathrm{d}a\,\mathrm{d}b\,\mathrm{d}t\,\mathrm{d}s.
\end{aligned}\tag{3.3.55}$$

Summing (3.3.54) and (3.3.55) we have

$$\begin{aligned}
&\int\int\int\int\int\int \big(|u_1-u_2|(\partial_t\Xi_n+\partial_s\Xi_n)-\mathrm{div}_x\big(|u_1-u_2|\nu(\phi_1)\big)\Xi_n-\mathrm{div}_y\big(|u_1-u_2|\nu(\phi_2)\big)\Xi_n\\
&\qquad +|u_1-u_2|(\mathfrak{b}(\phi_1)-\beta)\Xi_n+\mathrm{sign}\,(u_1-u_2)\,(\mathfrak{b}(\phi_1)-\mathfrak{b}(\phi_2))u_2\Xi_n\big)\,\mathrm{d}x\,\mathrm{d}y\,\mathrm{d}a\,\mathrm{d}b\,\mathrm{d}t\,\mathrm{d}s\\
&+\int\int\int\int\int |u_{1,0}(x)-u_2|\Xi_n(0,s,a,b,x,y)\mathrm{d}x\,\mathrm{d}y\,\mathrm{d}a\,\mathrm{d}b\,\mathrm{d}s\\
&+\int\int\int\int\int |u_1-u_{2,0}(y)|\Xi_n(t,0,a,b,x,y)\mathrm{d}x\,\mathrm{d}y\,\mathrm{d}a\,\mathrm{d}b\,\mathrm{d}t\\
&\quad\geq\int\int\int\int\int\int \mathrm{sign}\,(u_1-u_2)\,u_2\mathrm{div}_x\big(\nu(\phi_1)\big)\Xi_n\mathrm{d}x\,\mathrm{d}y\,\mathrm{d}a\,\mathrm{d}b\,\mathrm{d}t\,\mathrm{d}s\\
&\qquad-\int\int\int\int\int\int \mathrm{sign}\,(u_1-u_2)\,u_1\mathrm{div}_x\big(\nu(\phi_2)\big)\Xi_n\mathrm{d}x\,\mathrm{d}y\,\mathrm{d}a\,\mathrm{d}b\,\mathrm{d}t\,\mathrm{d}s.
\end{aligned}$$

As $n\to\infty$ we get (3.3.53). □

Lemma 3.15. *For every $t\geq 0$, the following inequality holds*

$$\begin{aligned}
\big\|\phi_1(t,\cdot)-\phi_2(t,\cdot)\big\|^2_{L^2(\mathbb{R}^2)}+\mu e^{Ct}\int_0^t\int_{\mathbb{R}^2}e^{-Cs}|\nabla_x(\phi_1-\phi_2)|^2\,dx\,ds\leq Ce^{Ct}\big\|\rho_{1,0}-\rho_{2,0}\big\|^2_{L^1((0,\infty)\times\mathbb{R}^2)}\\
+Ce^{Ct}\int_0^t\int_0^\infty\int_{\mathbb{R}^2}e^{-Cs}(\rho_1-\rho_2)^2\,dx\,da\,ds+Ce^{Ct}\int_0^t\int_{\mathbb{R}^2}e^{-Cs}(u_1-u_2)^2\,dx\,ds.
\end{aligned}\tag{3.3.56}$$

In particular, we have that

$$\begin{aligned}
&\left(\int_0^t\int_{\mathbb{R}^2}e^{-Cs}|\nabla_x(\phi_1-\phi_2)|^2dxds\right)^{1/2}\leq Ce^{Ct}\big\|\rho_{1,0}-\rho_{2,0}\big\|_{L^1((0,\infty)\times\mathbb{R}^2)}\\
&+Ce^{Ct}\left(\int_0^t\big\|\rho_1(s,\cdot,\cdot)-\rho_2(s,\cdot,\cdot)\big\|^2_{L^1((0,\infty)\times\mathbb{R}^2)}\,ds\right)^{1/2}+Ce^{Ct}\left(\int_0^t\|u_1(s,\cdot)-u_2(s,\cdot)\|^2_{L^1(\mathbb{R}^2)}\,ds\right)^{1/2}.
\end{aligned}\tag{3.3.57}$$

Proof. Since ϕ_{ε_k} satisfies

$$\begin{aligned}
\partial_t\phi_{\varepsilon_k}-\mu\Delta_x\phi_{\varepsilon_k}+\mathrm{div}_x\left(\left(\int_0^\infty\rho_{\varepsilon_k}\chi_1\mathrm{d}a\right)\mathbf{v}Y_\theta(\phi_{\varepsilon_k}-R)\right)\\
=\int_0^\infty\rho_{\varepsilon_k}\left(\varepsilon_k\chi_2''+\chi_2'-\mathfrak{d}\chi_2-\mathfrak{p}(a,u_{\varepsilon_k})\chi_2\right)\mathrm{d}a,
\end{aligned}$$

as $k\to\infty$ we get the equation of ϕ. Then, subtracting the equation for ϕ_2 from the equation for ϕ_1 we obtain

$$\begin{aligned}
&\partial_t(\phi_1-\phi_2)-\mu\Delta_x(\phi_1-\phi_2)+\mathrm{div}_x\left(\left(\int_0^\infty(\rho_1-\rho_2)\chi_1\mathrm{d}a\right)\mathbf{v}Y_\theta(\phi_1-R)\right)\\
&\quad+\mathrm{div}_x\left(\left(\int_0^\infty\rho_2\chi_1\mathrm{d}a\right)\mathbf{v}(Y_\theta(\phi_1-R)-Y_\theta(\phi_2-R))\right)\\
&=\int_0^\infty(\rho_1-\rho_2)\left(\chi_2'-\mathfrak{d}\chi_2-\mathfrak{p}(a,u_1)\chi_2\right)\mathrm{d}a-\int_0^\infty\rho_2\left(\mathfrak{p}(a,u_1)-\mathfrak{p}(a,u_2)\right)\chi_2\,\mathrm{d}a.
\end{aligned}\tag{3.3.58}$$

Then

$$
\begin{aligned}
&\frac{d}{dt}\int_{\mathbb{R}^2}\frac{(\phi_1-\phi_2)^2}{2}\,\mathrm{d}x+\mu\int_{\mathbb{R}^2}\left|\nabla_x(\phi_1-\phi_2)\right|^2\,\mathrm{d}x\\
&=\int_{\mathbb{R}^2}(\phi_1-\phi_2)\left(\int_0^\infty(\rho_1-\rho_2)\left(\chi_2'-\mathfrak{d}\chi_2-\mathfrak{p}(a,u_1)\chi_2\right)\mathrm{d}a\right)\mathrm{d}x\\
&\quad-\int_{\mathbb{R}^2}(\phi_1-\phi_2)\Big(\int_0^\infty\rho_2\underbrace{\left(\mathfrak{p}(a,u_1)-\mathfrak{p}(a,u_2)\right)}_{\le c|u_1-u_2|}\chi_2\,\mathrm{d}a\Big)\mathrm{d}x\\
&\quad-\int_{\mathbb{R}^2}(\phi_1-\phi_2)\mathrm{div}_x\left(\left(\int_0^\infty(\rho_1-\rho_2)\chi_1\mathrm{d}a\right)\mathbf{v}Y_\theta(\phi_1-R)\right)\mathrm{d}x\\
&\quad-\int_{\mathbb{R}^2}(\phi_1-\phi_2)\mathrm{div}_x\left(\left(\int_0^\infty\rho_2\chi_1\mathrm{d}a\right)\mathbf{v}(Y_\theta(\phi_1-R)-Y_\theta(\phi_2-R))\right)\mathrm{d}x\\
&\le c\int_{\mathbb{R}^2}(\phi_1-\phi_2)^2\,\mathrm{d}x+ce^{ct}\int_{\mathbb{R}^2}(u_1-u_2)^2\,\mathrm{d}x+ce^{ct}\int_0^\infty\int_{\mathbb{R}^2}(\rho_1-\rho_2)^2\,\mathrm{d}x\,\mathrm{d}a\\
&\quad+\frac{\mu}{2}\int_{\mathbb{R}^2}\left|\nabla_x(\phi_1-\phi_2)\right|^2\,\mathrm{d}x.
\end{aligned}
$$

Using Gronwall Lemma we get

$$
\begin{aligned}
&\left\|\phi_1(t,\cdot)-\phi_2(t,\cdot)\right\|^2_{L^2(\mathbb{R}^2)}+\mu e^{ct}\int_0^t\int_{\mathbb{R}^2}e^{-cs}|\nabla_x(\phi_1-\phi_2)|^2\,\mathrm{d}x\,\mathrm{d}s\\
&\le e^{ct}\left\|\phi_{1,0}-\phi_{2,0}\right\|^2_{L^2(\mathbb{R}^2)}+ce^{ct}\int_0^t\int_0^\infty\int_{\mathbb{R}^2}e^{-cs}(\rho_1-\rho_2)^2\,\mathrm{d}x\,\mathrm{d}a\,\mathrm{d}s+ce^{ct}\int_0^t\int_{\mathbb{R}^2}e^{-cs}(u_1-u_2)^2\,\mathrm{d}x\,\mathrm{d}s.
\end{aligned}
$$

Finally, we obtain (3.3.56) and (3.3.57) from the definition of ϕ_1 and ϕ_2. □

We are now ready to complete the proof of Theorem 3.1.

Proof. Our goal is to prove the inequality (3.1.22). We rewrite (3.3.52) and (3.3.53) as

$$
\begin{aligned}
&\int_0^\infty\int_0^\infty\int_{\mathbb{R}^2}\Big(|\rho_1-\rho_2|\left(\partial_t\xi_n+\partial_a\xi_n\right)-|\rho_1-\rho_2|\chi_1(Y_\theta(\phi_1-R)+Y_\theta(\phi_2-R))\mathbf{v}\cdot\nabla_x\xi_n\\
&\qquad+\mu|\rho_1-\rho_2|\Delta_x\xi_n-|\rho_1-\rho_2|\mathfrak{d}\xi_n-|\rho_1-\rho_2|\mathfrak{p}(a,u_1)\xi_n\\
&\qquad-\mathrm{sign}\left(\rho_1-\rho_2\right)\left(\mathfrak{p}(a,u_1)-\mathfrak{p}(a,u_2)\right)\rho_2\xi_n\Big)\mathrm{d}x\,\mathrm{d}a\,\mathrm{d}t\\
&+\int_0^\infty\int_{\mathbb{R}^2}|\rho_1(t,0^+,x)-\rho_2(t,0^+,x)|\xi_n(t,0,x)\mathrm{d}x\,\mathrm{d}t\\
&+\int_0^\infty\int_{\mathbb{R}^2}|\rho_{1,0}(a,x)-\rho_{2,0}(a,x)|\xi_n(0,a,x)\,\mathrm{d}x\,\mathrm{d}a\\
&\ge\int_0^\infty\int_0^\infty\int_{\mathbb{R}^2}\mathrm{sign}\left(\rho_1-\rho_2\right)\chi_1\left(\rho_2\mathrm{div}_x\left(\mathbf{v}Y_\theta(\phi_1-R)\right)-\rho_1\mathrm{div}_x\left(\mathbf{v}(x)Y_\theta(\phi_2-R)\right)\right)\xi_n\,\mathrm{d}x\,\mathrm{d}a\,\mathrm{d}t,
\end{aligned}
\tag{3.3.59}
$$

and

$$\begin{aligned}
&\int_0^\infty\int_0^\infty\int_{\mathbb{R}^2}\big(|u_1-u_2|\partial_t\xi_n+|u_1-u_2|(\nu(\phi_1)+\nu(\phi_2))\cdot\nabla_x\xi_n+|u_1-u_2|(\mathfrak{b}(\phi_1)-\beta)\xi_n\\
&\qquad\qquad+\operatorname{sign}(u_1-u_2)\,(\mathfrak{b}(\phi_1)-\mathfrak{b}(\phi_2))\,u_2\xi_n\big)\,\mathrm{d}x\,\mathrm{d}a\,\mathrm{d}t\\
&+\int_0^\infty\int_{\mathbb{R}^2}|u_{1,0}(x)-u_{2,0}(x)|\xi_n(0,a,x)\,\mathrm{d}x\,\mathrm{d}a\\
&\geq\int_0^\infty\int_0^\infty\int_{\mathbb{R}^2}\operatorname{sign}(u_1-u_2)\left(u_2\operatorname{div}_x\left(\nu(\phi_1)\right)-u_1\operatorname{div}_x\left(\nu(\phi_2)\right)\right)\xi_n\,\mathrm{d}x\,\mathrm{d}a\,\mathrm{d}t,
\end{aligned}\tag{3.3.60}$$

where $\{\xi_n\}_n$ is a sequence of nonnegative test functions approximating the characteristic function of the strip $(-\infty,t)\times\mathbb{R}\times\mathbb{R}^2$. Sending $n\to\infty$, we have that

$$\begin{aligned}
&\|u_1(t,\cdot)-u_2(t,\cdot)\|_{L^1(\mathbb{R}^2)}\\
&\quad\leq\|u_{1,0}-u_{2,0}\|_{L^1(\mathbb{R}^2)}-\int_0^t\int_{\mathbb{R}^2}\operatorname{sign}(u_1-u_2)\left(u_2\operatorname{div}_x\left(\nu(\phi_1)\right)-u_1\operatorname{div}_x\left(\nu(\phi_2)\right)\right)\mathrm{d}x\,\mathrm{d}s\\
&\qquad+\int_0^t\int_{\mathbb{R}^2}|u_1-u_2|\underbrace{\mathfrak{b}(\phi_1)}_{\leq c}+\operatorname{sign}(u_1-u_2)\underbrace{(\mathfrak{b}(\phi_1)-\mathfrak{b}(\phi_2))}_{\leq c|\phi_1-\phi_2|}u_2\,\mathrm{d}x\,\mathrm{d}s\\
&\quad\leq\|u_{1,0}-u_{2,0}\|_{L^1(\mathbb{R}^2)}+\int_0^t\int_{\mathbb{R}^2}|u_1-u_2|\operatorname{div}_x\left(\nu(\phi_1)\right)\mathrm{d}x\,\mathrm{d}s\\
&\qquad-\int_0^t\int_{\mathbb{R}^2}\operatorname{sign}(u_1-u_2)\,u_1\underbrace{\operatorname{div}_x\left(\nu(\phi_1)-\nu(\phi_2)\right)}_{\text{see (3.1.19)}}\mathrm{d}x\,\mathrm{d}s\\
&\qquad+c\int_0^t\int_{\mathbb{R}^2}|u_1-u_2|\,\mathrm{d}x\,\mathrm{d}s+ce^{ct}\int_0^t\int_{\mathbb{R}^2}|\phi_1-\phi_2|\,\mathrm{d}x\,\mathrm{d}s\\
&\quad\leq\|u_{1,0}-u_{2,0}\|_{L^1(\mathbb{R}^2)}+ce^{ct}\int_0^t\int_{\mathbb{R}^2}|u_1-u_2|\,\mathrm{d}x\,\mathrm{d}s\\
&\qquad+ce^{ct}\int_0^t\left(\int_{\mathbb{R}^2}|\operatorname{div}_x\left(\nu(\phi_1)-\nu(\phi_2)\right)|^2\,\mathrm{d}x\right)^{1/2}\mathrm{d}s\\
&\qquad+c\int_0^t\int_{\mathbb{R}^2}|u_1-u_2|\,\mathrm{d}x\,\mathrm{d}s+ce^{ct}\int_0^t\int_{\mathbb{R}^2}|\phi_1-\phi_2|\,\mathrm{d}x\,\mathrm{d}s\\
&\quad\leq\|u_{1,0}-u_{2,0}\|_{L^1(\mathbb{R}^2)}+c(1+e^{ct})\int_0^t\|u_1(s,\cdot)-u_2(s,\cdot)\|_{L^1(\mathbb{R}^2)}\,\mathrm{d}s\\
&\qquad+ce^{ct}\int_0^t\|\rho_1(s,\cdot,\cdot)-\rho_2(s,\cdot,\cdot)\|_{L^1((0,\infty)\times\mathbb{R}^2)}\,\mathrm{d}s,
\end{aligned}$$

and

$$\begin{aligned}
&\|\rho_1(t,\cdot,\cdot)-\rho_2(t,\cdot,\cdot)\|_{L^1((0,\infty)\times\mathbb{R}^2)}\\
&\leq\|\rho_{1,0}-\rho_{2,0}\|_{L^1((0,\infty)\times\mathbb{R}^2)}+\int_0^t\int_{\mathbb{R}^2}|\rho_1(s,0^+,x)-\rho_2(s,0^+,x)|\mathrm{d}x\,\mathrm{d}s
\end{aligned}$$

$$
\begin{aligned}
&\quad - \int_0^t \int_0^\infty \int_{\mathbb{R}^2} \operatorname{sign}\left(\rho_1-\rho_2\right) \chi_1(a) \left(\rho_2 \operatorname{div}_x\left(\mathbf{v} Y_\theta(\phi_1-R)\right) - \rho_1 \operatorname{div}_x\left(\mathbf{v} Y_\theta(\phi_2-R)\right)\right) \mathrm{d}x\,\mathrm{d}a\,\mathrm{d}s \\
&\quad - \int_0^t \int_0^\infty \int_{\mathbb{R}^2} \operatorname{sign}\left(\rho_1-\rho_2\right) (\mathfrak{p}(a,u_1)-\mathfrak{p}(a,u_2))\rho_2 \,\mathrm{d}x\,\mathrm{d}a\,\mathrm{d}s \\
&\le \left\|\rho_{1,0}-\rho_{2,0}\right\|_{L^1((0,\infty)\times\mathbb{R}^2)} + \int_0^t \int_0^\infty \int_{\mathbb{R}^2} |\mathscr{A}(\phi_1)\rho_1 - \mathscr{A}(\phi_2)\rho_2| \chi_3 \omega \,\mathrm{d}x\,\mathrm{d}s \\
&\quad - \int_0^t \int_0^\infty \int_{\mathbb{R}^2} \operatorname{sign}\left(\rho_1-\rho_2\right) \chi_1(a) \left(\rho_2 \operatorname{div}_x\left(\mathbf{v} Y_\theta(\phi_1-R)\right) - \rho_1 \operatorname{div}_x\left(\mathbf{v} Y_\theta(\phi_2-R)\right)\right) \mathrm{d}x\,\mathrm{d}a\,\mathrm{d}s \\
&\quad - \int_0^t \int_0^\infty \int_{\mathbb{R}^2} \operatorname{sign}\left(\rho_1-\rho_2\right) (\mathfrak{p}(a,u_1)-\mathfrak{p}(a,u_2))\rho_2 \,\mathrm{d}x\,\mathrm{d}a\,\mathrm{d}s \\
&\le \left\|\rho_{1,0}-\rho_{2,0}\right\|_{L^1((0,\infty)\times\mathbb{R}^2)} + \int_0^t \int_0^\infty \int_{\mathbb{R}^2} \mathscr{A}\left(\phi_1\right) \left|\rho_1-\rho_2\right| \chi_3 \omega \mathrm{d}x\,\mathrm{d}a\,\mathrm{d}s \\
&\quad + \int_0^t \int_0^\infty \int_{\mathbb{R}^2} \left|\mathscr{A}\left(\phi_1\right) - \mathscr{A}\left(\phi_2\right)\right| \rho_2 \chi_3 \omega \mathrm{d}x\,\mathrm{d}a\,\mathrm{d}s \\
&\quad + \int_0^t \int_0^\infty \int_{\mathbb{R}^2} |\rho_1-\rho_2| \chi_1(a) \operatorname{div}_x\left(\mathbf{v} Y_\theta(\phi_1-R)\right) \mathrm{d}x\,\mathrm{d}a\,\mathrm{d}s \\
&\quad - \int_0^t \int_0^\infty \int_{\mathbb{R}^2} \operatorname{sign}\left(\rho_1-\rho_2\right) \chi_1(a) \rho_1 \operatorname{div}_x(\mathbf{v}) \left(Y_\theta(\phi_1-R) - Y_\theta(\phi_2-R)\right) \mathrm{d}x\,\mathrm{d}a\,\mathrm{d}s \\
&\quad - \int_0^t \int_0^\infty \int_{\mathbb{R}^2} \operatorname{sign}\left(\rho_1-\rho_2\right) \chi_1(a) \rho_1 \mathbf{v}\cdot\nabla_x \left(Y_\theta(\phi_1-R) - Y_\theta(\phi_2-R)\right) \mathrm{d}x\,\mathrm{d}a\,\mathrm{d}s \\
&\quad + c e^{ct} \int_0^t \|u_1(s,\cdot)-u_2(s,\cdot)\|_{L^1(\mathbb{R}^2)} \,\mathrm{d}s \\
&\le \left\|\rho_{1,0}-\rho_{2,0}\right\|_{L^1((0,\infty)\times\mathbb{R}^2)} + c \int_0^t \left\|\rho_1(s,\cdot,\cdot)-\rho_2(s,\cdot,\cdot)\right\|_{L^1((0,\infty)\times\mathbb{R}^2)} \mathrm{d}s \\
&\quad + c e^{ct} \int_0^t \int_{\mathbb{R}^2} \left|\mathscr{A}\left(\phi_1\right) - \mathscr{A}\left(\phi_2\right)\right| \mathrm{d}x\,\mathrm{d}s \\
&\quad + c e^{ct} \int_0^t \int_{\mathbb{R}^2} \left|Y_\theta(\phi_1-R) - Y_\theta(\phi_2-R)\right| \mathrm{d}x\,\mathrm{d}s \\
&\quad + c e^{ct} \left(\int_0^t \int_{\mathbb{R}^2} \left|\nabla_x \left(Y_\theta(\phi_1-R) - Y_\theta(\phi_2-R)\right)\right|^2 \mathrm{d}x\,\mathrm{d}s\right)^{1/2} \\
&\quad + c e^{ct} \int_0^t \|u_1(s,\cdot)-u_2(s,\cdot)\|_{L^1(\mathbb{R}^2)} \,\mathrm{d}s \\
&\le \left\|\rho_{1,0}-\rho_{2,0}\right\|_{L^1((0,\infty)\times\mathbb{R}^2)} + c(1+e^{ct}) \int_0^t \left\|\rho_1(s,\cdot,\cdot)-\rho_2(s,\cdot,\cdot)\right\|_{L^1((0,\infty)\times\mathbb{R}^2)} \mathrm{d}s \\
&\quad + c e^{ct} \left(\int_0^t \int_{\mathbb{R}^2} \left|\nabla_x(\phi_1-\phi_2)\right|^2 \mathrm{d}x\,\mathrm{d}s\right)^{1/2} + c e^{ct} \int_0^t \|u_1(s,\cdot)-u_2(s,\cdot)\|_{L^1(\mathbb{R}^2)} \,\mathrm{d}s.
\end{aligned}
$$

Using (3.3.57), we have

$$
\begin{aligned}
&\|u_1(t,\cdot)-u_2(t,\cdot)\|_{L^1(\mathbb{R}^2)}^2 + \left\|\rho_1(t,\cdot,\cdot)-\rho_2(t,\cdot,\cdot)\right\|_{L^1((0,\infty)\times\mathbb{R}^2)}^2 \\
&\le \left\|u_{1,0}-u_{2,0}\right\|_{L^1(\mathbb{R}^2)}^2 + c(1+e^{ct}) \int_0^t \|u_1(s,\cdot)-u_2(s,\cdot)\|_{L^1(\mathbb{R}^2)}^2 \mathrm{d}s
\end{aligned}
$$

$$+c(1+e^{ct})\left\|\rho_{1,0}-\rho_{2,0}\right\|^2_{L^1((0,\infty)\times\mathbb{R}^2)}+c(1+e^{ct})\int_0^t\left\|\rho_1(s,\cdot,\cdot)-\rho_2(s,\cdot,\cdot)\right\|^2_{L^1((0,\infty)\times\mathbb{R}^2)}\,\mathrm{d}s.$$

Finally, we use the Gronwall Lemma to obtain the result (3.1.22). □

3.4 Proof of Lemma 3.1

Proof. This lemma is similar to [13, Lemma 4.1], in particular, **(3.1.14)** and **(3.1.17)** already appeared there. For completeness we sketch the proof of the other estimates.

(3.1.15). directly comes from the definition of ν in (3.1.3) and the expression of $\mathrm{div}_x\left(\nu(\phi)\right)$ in (3.2.49).

(3.1.16). We compute $\nabla_x\nu(\phi)$ by using the fact that $\nabla_x(f\nu)=f\nabla_x\nu+\nu\otimes\nabla_x f$

$$\begin{aligned}\nabla_x\nu(\phi)&=\kappa\frac{1}{\left(1+\left\|\phi*\nabla_x\eta\right\|^2\right)^{1/2}}\nabla_x(\phi*\nabla_x\eta)+\kappa(\phi*\nabla_x\eta)\otimes\nabla_x\frac{1}{\left(1+\left\|\phi*\nabla_x\eta\right\|^2\right)^{1/2}}\\&=\kappa\frac{\phi*\nabla_x^2\eta}{\left(1+\left\|\phi*\nabla_x\eta\right\|^2\right)^{1/2}}-\kappa(\phi*\nabla_x\eta)\otimes\frac{(\phi*\nabla_x^2\eta)(\phi*\nabla_x\eta)}{\left(1+\left\|\phi*\nabla_x\eta\right\|^2\right)^{3/2}},\end{aligned}$$

then (notice that to shorten the notations we write L^∞ for $L^\infty(\mathbb{R}^2;\mathbb{R}^{2\times2})$)

$$\begin{aligned}&\left\|\nabla_x\nu(\phi)\right\|_{L^\infty}\\&\le\kappa\frac{\left\|\phi*\nabla_x^2\eta\right\|_{L^\infty}}{\left(1+\left\|\phi*\nabla_x\eta\right\|^2\right)^{1/2}}+\kappa\left\|\frac{\phi*\nabla_x\eta}{\left(1+\left\|\phi*\nabla_x\eta\right\|^2\right)^{1/2}}\otimes\frac{\phi*\nabla_x^2\eta}{\left(1+\left\|\phi*\nabla_x\eta\right\|^2\right)^{1/2}}\frac{\phi*\nabla_x\eta}{\left(1+\left\|\phi*\nabla_x\eta\right\|^2\right)^{1/2}}\right\|_{L^\infty}\\&\le\kappa\left\|\phi*\nabla_x^2\eta\right\|_{L^\infty}+\kappa\left\|\frac{\phi*\nabla_x\eta}{\left(1+\left\|\phi*\nabla_x\eta\right\|^2\right)^{1/2}}\right\|_{L^\infty}\left\|\phi*\nabla_x^2\eta\right\|_{L^\infty}\left\|\frac{\phi*\nabla_x\eta}{\left(1+\left\|\phi*\nabla_x\eta\right\|^2\right)^{1/2}}\right\|_{L^\infty}\\&\le2\kappa\left\|\phi*\nabla_x^2\eta\right\|_{L^\infty}\le2\kappa\left\|\nabla_x^2\eta\right\|_{L^\infty}\left\|\phi\right\|_{L^1(\mathbb{R}^2;\mathbb{R})}.\end{aligned}$$

(3.1.18). We compute gradient of (3.2.49)

$$\nabla_x\mathrm{div}_x\left(\nu(\phi)\right)=\kappa\frac{\phi*\nabla\Delta_x\eta}{\left(1+\left\|\phi*\nabla_x\eta\right\|^2\right)^{3/2}}-3\kappa(\phi*\Delta_x\eta)\frac{\phi*\nabla_x^2\eta}{\left(1+\left\|\phi*\nabla_x\eta\right\|^2\right)^2}\frac{\phi*\nabla_x\eta}{\left(1+\left\|\phi*\nabla_x\eta\right\|^2\right)^{1/2}},$$

then

$$\begin{aligned}&\left\|\nabla_x\mathrm{div}_x\left(\nu(\phi)\right)\right\|_{L^2(\mathbb{R}^2;\mathbb{R}^2)}\\&\le\kappa\left\|\phi*\nabla\Delta_x\eta\right\|_{L^2(\mathbb{R}^2;\mathbb{R}^2)}+3\kappa\left\|\phi*\Delta_x\eta\right\|_{L^2(\mathbb{R}^2;\mathbb{R}^2)}\left\|\phi*\nabla_x^2\eta\right\|_{L^\infty(\mathbb{R}^2;\mathbb{R}^{2\times2})}\\&\le\kappa\left\|\phi\right\|_{L^1(\mathbb{R}^2;\mathbb{R})}\left(\left\|\nabla\Delta_x\eta\right\|_{L^2(\mathbb{R}^2;\mathbb{R}^2)}+3\left\|\Delta_x\eta\right\|_{L^2(\mathbb{R}^2;\mathbb{R})}\left\|\nabla_x^2\eta\right\|_{L^\infty(\mathbb{R}^2;\mathbb{R}^{2\times2})}\left\|\phi\right\|_{L^1(\mathbb{R}^2;\mathbb{R})}\right).\end{aligned}$$

(3.1.19). We have that

$$\begin{aligned}
&\operatorname{div}_x\left(v(\phi_1)-v(\phi_2)\right)\\
&\quad=\kappa\frac{(\phi_1-\phi_2)*\Delta_x\eta}{\left(1+\left\|\phi_1*\nabla_x\eta\right\|^2\right)^{3/2}}+\kappa(\phi_2*\Delta_x\eta)\left(\frac{1}{\left(1+\left\|\phi_1*\nabla_x\eta\right\|^2\right)^{3/2}}-\frac{1}{\left(1+\left\|\phi_2*\nabla_x\eta\right\|^2\right)^{3/2}}\right).
\end{aligned}$$

Using the inequality $|(1+x^2)^{-3/2}-(1+y^2)^{-3/2}|\leq\frac{48}{25\sqrt{5}}|x-y|$, we obtain

$$\begin{aligned}
&\left\|\operatorname{div}_x\left(v(\phi_1)-v(\phi_2)\right)\right\|_{L^2(\mathbb{R}^2;\mathbb{R})}\\
&\leq\kappa\left\|(\phi_1-\phi_2)*\Delta_x\eta\right\|_{L^2(\mathbb{R}^2;\mathbb{R})}+\frac{48}{25\sqrt{5}}\kappa\left\|\phi_2*\Delta_x\eta\right\|_{L^\infty(\mathbb{R}^2;\mathbb{R})}\left\|(\phi_1-\phi_2)*\nabla_x\eta\right\|_{L^2(\mathbb{R}^2;\mathbb{R}^2)}\\
&\leq\kappa\left\|\phi_1-\phi_2\right\|_{L^1(\mathbb{R}^2,\mathbb{R})}\left(\left\|\Delta_x\eta\right\|_{L^2(\mathbb{R}^2;\mathbb{R})}+\frac{48}{25\sqrt{5}}\left\|\nabla_x\eta\right\|_{L^2(\mathbb{R}^2,\mathbb{R}^2)}\left\|\Delta_x\eta\right\|_{L^\infty(\mathbb{R}^2;\mathbb{R})}\left\|\phi_2\right\|_{L^1(\mathbb{R}^2,\mathbb{R})}\right).
\end{aligned}$$

□

Chapter 4

Numerical schemes for a vole population model in one-dimensional space

4.1 Finite volumes approximations of the model

Firstly, we recall the hyperbolic-parabolic model of voles

$$\begin{cases} \partial_t \rho + \partial_a \rho + \partial_x(\rho \chi_1(a)\mathbf{v}(x) Y_\theta(\phi - R)) = \mu \Delta_x \rho - \mathfrak{d}\rho, & (t,a,x) \in (0,T)\times(0,A_3)\times\Omega \\ \rho(t,0,x) = \mathscr{A}(\phi)\left(\displaystyle\int_{A_1}^{A_3} \rho(t,a,x)\,\mathrm{d}a\right)\omega(t,x), & (t,a,x) \in (0,T)\times(0,A_3)\times\Omega \\ \rho(0,a,x) = \rho_0(a,x), & (a,x) \in (0,A_3)\times\Omega, \end{cases} \tag{4.1.1}$$

where $t \in (0,T)$ is the time, $a \in (0,A_3)$ is the age, $x \in \Omega \subset \mathbb{R}$ is the space. The constants $0 < A_1 < A_2 < A_3$ are such that a vole is young if its age a is in $(0,A_1)$, juvenile if its age a is in (A_1,A_2) and adult if its age a is in (A_2,A_3). For the numerical simulations, we need to impose a boundary condition on the space domain. We choose here to impose a homogeneous Neumann boundary condition, i.e.

$$\partial_x \rho(t,\cdot) = 0, \qquad \text{on } \partial\Omega. \tag{4.1.2}$$

Given a finite time horizon $T > 0$, a suitable maximal age A_3, and a finite domain space $\Omega = [-d,d]$, we consider the computational domain $[0,T]\times[0,A_3]\times[-d,d]$ and let Δt, Δa and Δx be respectively the constant time, age and space steps.

We set $N_T = \lfloor T/\Delta t \rfloor$, $N_A = \lfloor A_3/\Delta a \rfloor$ and $N_X = \lfloor 2d/\Delta x \rfloor$. Then for any $0 \le h \le N_A$, we introduce the points $a_{h+1/2} = h\Delta a$ and, for any $1 \le h \le N_A$, the cells $K_h = [a_{h-1/2}, a_{h+1/2})$ and the cells centers $a_h = (h-1/2)\Delta a$. Without loss of generality we can always assume that $A_1 = \bar{h}\Delta a$ for a suitable index $\bar{h}$, and we have $A_2 = \alpha\bar{h}\Delta a$, where $\alpha > 1$.

Similarly, we define a mesh for space as follows: for any $0 \le i \le N_X$ we introduce the points $x_{i+1/2} = -d + i\Delta x$ and, for any $1 \le i \le N_X$, the cells $K_i = [x_{i-1/2}, x_{i+1/2}[$ and the cells centers

$$x_i = \frac{x_{i-1/2} + x_{i+1/2}}{2} = -d + (2i-1)\frac{\Delta x}{2}.$$

Finally, we define $t^n = n\Delta t$ for $0 \le n \le N_T$.

For $1 \le i \le N_X$, $1 \le h \le N_A$ and $0 \le n \le N_T$, we denote by ω_i^n, $\mathfrak{d}_{i,h}^n$ and $\rho_{i,h}^n$ the approximation of the averages of $\omega(t^n,\cdot)$, $\mathfrak{d}(t^n,\cdot,\cdot)$ and $\rho(t^n,\cdot,\cdot)$ on the cells K_i and $K_i \times K_h$, namely

$$\begin{aligned}
&\omega_i^n = \frac{1}{\Delta x}\int_{K_i} \omega(t^n,x)\mathrm{d}x, && \mathfrak{d}_{i,h}^n = \frac{1}{\Delta a\Delta x}\int_{K_h}\int_{K_i} \mathfrak{d}(t^n,a,x)\mathrm{d}a\,\mathrm{d}x,\\
&\rho_{i,h}^0 = \frac{1}{\Delta a\Delta x}\int_{K_h}\int_{K_i} \rho_0(a,x)\mathrm{d}a\,\mathrm{d}x \quad \text{and} && \rho_{i,h}^n \simeq \frac{1}{\Delta a\Delta x}\int_{K_h}\int_{K_i} \rho(t^n,a,x)\mathrm{d}a\,\mathrm{d}x, \quad n>0.
\end{aligned} \tag{4.1.3}$$

For each $i \in \{1,\dots,N_X\}$ and $n \in \{0,\dots,N_T\}$ the average of the total population of voles in cell i at time t^n is

$$\phi_i^n = \frac{1}{\Delta x}\int_{K_i} \phi_i(t^n,x)\,\mathrm{d}x,$$

that is

$$\begin{aligned}
\phi_i^n &= \frac{1}{\Delta x}\int_{K_i}\int_0^{A_3} \rho(t^n,a,x)\,\mathrm{d}a\,\mathrm{d}x\\
&= \frac{1}{\Delta x}\sum_{h=1}^{N_A}\int_{K_h}\int_{K_i} \rho(t^n,a,x)\mathrm{d}a\,\mathrm{d}x \simeq \Delta a\sum_{h=1}^{N_A}\rho_{i,h}^n.
\end{aligned}$$

From the Neumann condition in (4.1.2), we have

$$\begin{cases}
\rho_{0,h}^n = \rho_{1,h}^n, & 0 \le n \le N_T, \quad 1 \le h \le N_A,\\
\rho_{N_x,h}^n = \rho_{N_x+1,h}^n, & 0 \le n \le N_T, \quad 1 \le h \le N_A.
\end{cases}$$

We will use the upwind scheme to discretize the model (4.1.1), where for the diffusion term, we choose to use an implicit treatment, in order to keep the hyperbolic CFL condition, i.e.

$$\frac{\Delta t}{\Delta a} \le 1, \quad \text{and} \quad \|\mathbf{v}\|_{L^\infty}\frac{\Delta t}{\Delta x} \le 1.$$

Assume that $(\rho_{i,h}^n)$ are given. For $1 \le i \le N_X$, $1 \le h \le N_A$, and $0 \le n \le N_T$, we obtain the following scheme

$$\begin{cases}
(1+\Delta t d_{i,h}^{n+1})\rho_{i,h}^{n+1} - \dfrac{\mu\Delta t}{\Delta x^2}\left(\rho_{i+1,h}^{n+1} - 2\rho_{i,h}^{n+1} + \rho_{i-1,h}^{n+1}\right) = \left(1-\dfrac{\Delta t}{\Delta a}\right)\rho_{i,h}^n + \dfrac{\Delta t}{\Delta a}\rho_{i,h-1}^n\\
\qquad -\dfrac{\Delta t}{\Delta x}\Big[\underbrace{Y_\theta(\phi_{i+1/2}^n - R)\mathbf{v}(x_{i+1/2})\chi_1(a_h)\rho_{i+1/2,h}^n}_{\mathbf{F}_{i+1/2,h}^n} - \underbrace{Y_\theta(\phi_{i-1/2}^n - R)\mathbf{v}(x_{i-1/2})\chi_1(a_h)\rho_{i-1/2,h}^n}_{\mathbf{F}_{i-1/2,h}^n}\Big],\\
\rho_{i,0}^n = \mathscr{A}(\phi_i^n)\,\Delta a\sum_{h=\tilde{h}}^{N_A}\rho_{i,h}^n\omega_i^n,
\end{cases} \tag{4.1.4}$$

where in the flux, $\mathbf{F}$, we use the upwind scheme to define

$$\rho^n_{i+1/2,h} = \begin{cases} \rho^n_{i,h} & \text{if } \mathbf{v}(x_{i+1/2}) \geq 0, \quad 1 \leq h \leq N_A, \quad 0 \leq n \leq N_T, \\ \rho^n_{i+1,h} & \text{if } \mathbf{v}(x_{i+1/2}) < 0, \quad 1 \leq h \leq N_A, \quad 0 \leq n \leq N_T, \end{cases}$$

and we denote $\mathbf{F}^n_{+1/2,h}, \mathbf{F}^n_{-1/2,h} \in \mathbb{R}^{N_X}$ the vectors of flux for each pair of index $h \in \{1, ..., N_A\}$, and $n \in \{0, ..., N_T\}$.

We finally obtain the main linear system

$$A^{n+1}_h X^{n+1}_h = B^n_h,$$

for every $1 \leq h \leq N_A$, $0 \leq n \leq N_T$, where

$$A^{n+1}_h = \begin{pmatrix} 1+\Delta t\, \mathfrak{d}^{n+1}_{1,h} & 0 & \cdots & 0 \\ 0 & 1+\Delta t\, \mathfrak{d}^{n+1}_{2,h} & \cdots & 0 \\ \vdots & \cdots & \ddots & \vdots \\ 0 & \cdots & 0 & 1+\Delta t\, \mathfrak{d}^{n+1}_{N_X,h} \end{pmatrix} - \mu \frac{\Delta t}{\Delta x^2} \begin{pmatrix} -1 & 1 & 0 & \cdots & 0 \\ 1 & -2 & 1 & \cdots & 0 \\ 0 & \ddots & \ddots & \ddots & \vdots \\ \vdots & \cdots & 1 & -2 & 1 \\ 0 & \cdots & 0 & 1 & -1 \end{pmatrix},$$

$$X^{n+1}_h = \begin{pmatrix} \rho^{n+1}_{1,h} \\ \rho^{n+1}_{2,h} \\ \vdots \\ \rho^{n+1}_{N_X,h} \end{pmatrix},$$

and

$$B^n_h = \left(1 - \frac{\Delta t}{\Delta a}\right) \begin{pmatrix} \rho^n_{1,h} \\ \rho^n_{2,h} \\ \vdots \\ \rho^n_{N_X,h} \end{pmatrix} + \frac{\Delta t}{\Delta a} \begin{pmatrix} \rho^n_{1,h-1} \\ \rho^n_{2,h-1} \\ \vdots \\ \rho^n_{N_X,h-1} \end{pmatrix} - \frac{\Delta t}{\Delta x} \left(\mathbf{F}^n_{+1/2,h}[1:N_x] - \mathbf{F}^n_{-1/2,h}[1:N_x] \right).$$

4.2 Validation

In this part, we validate the implementation of the numerical scheme described above. The numerical solution is compared to the exact solution of the equation in the case where the total population of voles never exceeds R, at any point in the domain. Under these circumstances, the flux term of space will not contribute to the model (4.1.1).

Next, since computing an exact solution for the complete equation is impossible, we compare the numerical solution with a reference numerical solution, computed with the finest possible mesh. Also, we assume that $\Omega = (0, r)$ and $\mathscr{A} \equiv 1$.

We recall that the dispersal of juvenile voles in the flux term with respect to space will not appear if the total population is always less than the threshold value R. In order to have that, we choose the initial density of voles

$$\rho_0(a,x) = \frac{R}{(A_3+1-e^{-A_3})}(1+e^{-a})e^{\frac{2x^3-3rx^2}{6}}. \tag{4.2.5}$$

Then we have $\phi(t,x) < R$, for every $(t,x) \in (0,T)\times(0,r)$. Moreover, taking the mortality and reproduction rates respectively

$$\mathfrak{d}(t,a,x) = \frac{1+2e^{-a}}{1+e^{-a}} + \mu(2x-r) + \mu x^2(x-r)^2 \quad \text{and} \quad \omega(t,x) = \frac{2}{(A_3 - A_1 - e^{-A_3} + e^{-A_1})}, \tag{4.2.6}$$

we deduce that the system has an exact solution defined by

$$\rho(t,a,x) = \frac{R}{(A_3+1-e^{-A_3})}e^{-t}(1+e^{-a})e^{\frac{2x^3-3rx^2}{6}}. \tag{4.2.7}$$

Due to the computational cost, we have to take a small value for the finite time $T = 0.5$, and as a consequence, small values $A_1 = 0.5$, $A_2 = 1$, $A_3 = 1.5$, $r = 0.5$. Moreover, we set $R = 200$, $\mu = 1$ and the velocity function $\mathbf{v}(x) = x$ for the validation part.

Figure 4.1 compares the exact and numerical solution, representing the total population of voles, at the time $t = 0.5$, and their initial data at $t = 0$. We observe a good agreement between the two solutions, the numerical one was computed with $\Delta a = \Delta t = \Delta x = 0.00625$.

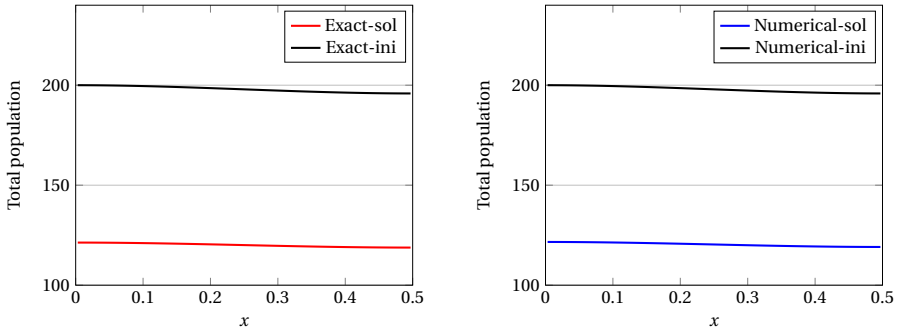

Figure 4.1 – Comparison of the total population of voles between the exact solution and the numerical solution at $t = 0.5$ and $t = 0$.

In the next part, we consider the whole equation in (4.1.1) and choose, as a reference solution, the numerical solution computed with $\Delta a = \Delta t = \Delta x = 0.0015625$. In this case, we investigate the different initial data, $\rho_0(a,x)$, $\rho_0^1(a,x)$, $\rho_0^2(a,x)$, knowing that the dispersal of juvenile voles takes place in the cases of $\rho_0^1(a,x)$ and $\rho_0^2(a,x)$.

Figures 4.2, 4.3, 4.4 show the comparison between the reference solution and numerical solution, which is computed with $\Delta a = \Delta t = \Delta x = 0.0046875$ and at time $t = 0.3$. In figures 4.4, the initial total population of voles is larger than the threshold value at every point of the domain, while in figures 4.3, the initial total population is larger than R in just a part of the domain. The difference between the values of the two solutions in all the considered cases is negligible.

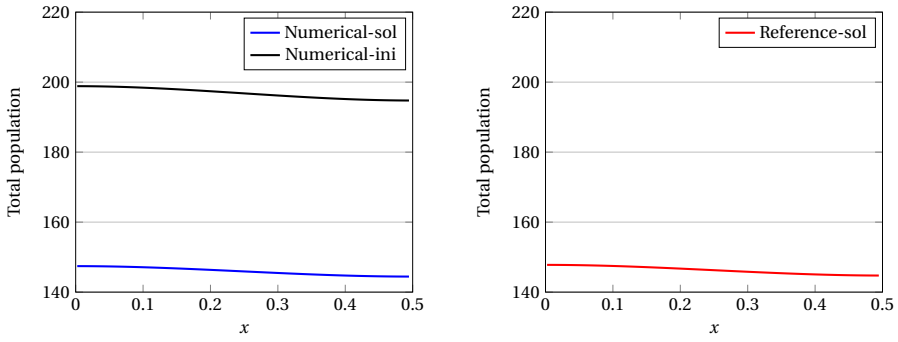

Figure 4.2 – Comparison of the total population of voles between the reference solution and the numerical solution with the initial datum $\rho_0(a,x)=\frac{R}{(A_3+1-e^{-A_3})}(1+e^{-a})e^{\frac{2x^3-3rx^2}{6}}$.

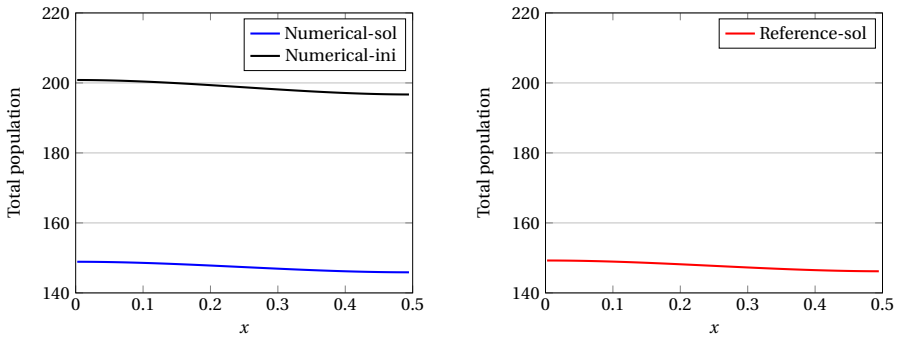

Figure 4.3 – Comparison of the total population of voles between the reference solution and the numerical solution with the initial datum $\rho_0^1(a,x)=\frac{202}{(A_3+1-e^{-A_3})}(1+e^{-a})e^{\frac{2x^3-3rx^2}{6}}$.

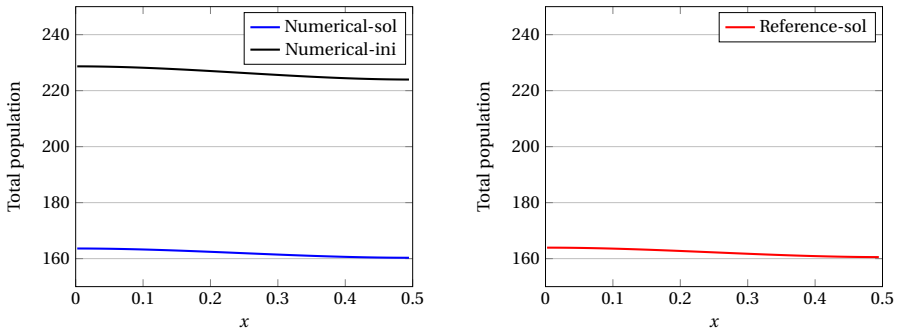

Figure 4.4 – Comparison of the total population of voles between the reference solution and the numerical solution with the initial datum $\rho_0^2(a,x)=\frac{230}{(A_3+1-e^{-A_3})}(1+e^{-a})e^{\frac{2x^3-3rx^2}{6}}$.

4.2.1 Numerical convergence

We introduce here the relative L^1-discrete error for the density at a given time t^n defined by

$$e^n_{L^1} = \frac{\sum_{1\le j\le N_a}\sum_{1\le i\le N_x} |\rho(t^n, a_j, x_i) - \rho^n_{i,j}|}{\sum_{1\le j\le N_a}\sum_{1\le i\le N_x} |\rho(t^n, a_j, x_i)|}, \tag{4.2.8}$$

where $\rho(t^n, a_j, x_i)$ is the exact solution evaluated at the point a_j, x_i and at time t^n.

In tables 4.1, we have reported the relative L^1-discrete errors for the model, that we obtain by comparing our numerical solution with the exact solution from the previous part, computed for different values of age, space and times steps at the time $t = 0.5$. The results suggest the convergence of the numerical scheme. Moreover, figures 4.5 indicate that the order of convergence of the scheme is approximately 1.

Δt	Δa	Δx	$e^{N_T}_{L^1}$
0.1	0.1	0.1	3.8×10^{-2}
0.05	0.05	0.05	1.99×10^{-2}
0.025	0.025	0.025	1.01×10^{-2}
0.0125	0.0125	0.0125	5.13×10^{-3}
0.00625	0.00625	0.00625	2.58×10^{-3}

Table 4.1 – L^1-discrete relative errors for the exact solution.

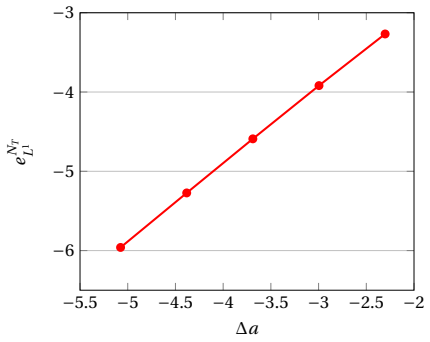

Figure 4.5 – L^1-discrete relative errors for the model in log/log scale at $t = 0.5$, comparing with the exact solution.

Remark 4.1. *In this result, we consider $\mu = 1$, but we have performed other comparisons with different values of μ and obtain similar results.*

Next, for the relative L^1-discrete error concerning the comparison with the reference solution, we use a similar formula in (4.2.8). More precisely, we redefine

$$e^n_{L^1} = \frac{\sum\limits_{1\le j\le N_a}\sum\limits_{1\le i\le N_x} |\tilde{\rho}^n_{i,j} - \rho^n_{i,j}|}{\sum\limits_{1\le j\le N_a}\sum\limits_{1\le i\le N_x} |\tilde{\rho}^n_{i,j}|}, \tag{4.2.9}$$

where $\tilde{\rho}^n_{i,j}$ is the reference solution computed on the cell $K_j \times K_i$ at time t^n.

In tables 4.2, we have reported the relative L^1-discrete errors of the whole model for three different initial data, computed for different values of age, space and times steps at the final time $t = 0.3$. The results again suggest the convergence of the numerical scheme. Moreover, figures 4.6 suggests that the order of convergence of the scheme is approximately 1.

Δt	Δa	Δx	$e^{N_T}_{L^1}, \rho_0$	$e^{N_T}_{L^1}, \rho^1_0$	$e^{N_T}_{L^1}, \rho^2_0$
0.1265625	0.1265625	0.1265625	8.95×10^{-2}	8.95×10^{-2}	1.06×10^{-1}
0.0421875	0.0421875	0.0421875	2.35×10^{-2}	2.35×10^{-2}	3.48×10^{-2}
0.0140625	0.0140625	0.0140625	6.72×10^{-3}	6.72×10^{-3}	9.58×10^{-3}
0.0046875	0.0046875	0.0046875	2.35×10^{-3}	2.34×10^{-3}	2.59×10^{-3}

Table 4.2 – L^1-discrete relative errors for the reference solution

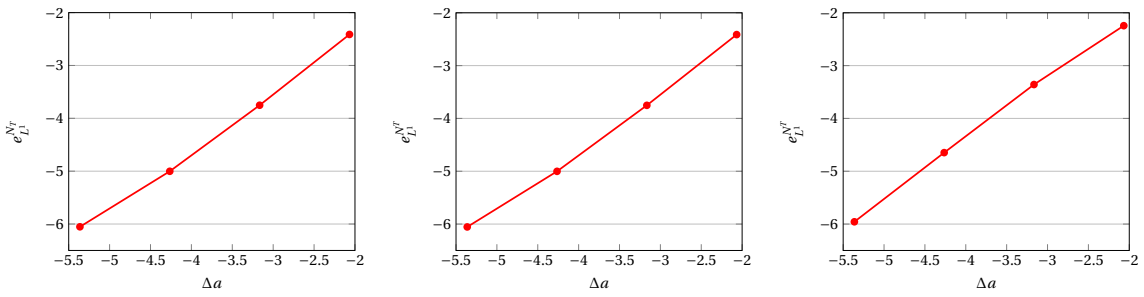

(a) ρ^1_0 (b) ρ^2_0 (c) ρ^3_0

Figure 4.6 – L^1-discrete relative errors for the whole model in log/log scale at $t = 0.3$, comparing with the reference solution.

Chapter 5

A Multi-Scale Epidemic Model of *Salmonella* infection with Heterogeneous Shedding

5.1 Mathematical models for a population structured by pathogen load

In this section, we will first present an ODE model which describes the evolution of pathogens in the gut for an individual. From this model, we will deduce a PDE for a population of individuals with pathogen loads, i.e. a drift-diffusion equation structured in pathogen load. We are able to prove the existence and uniqueness of the solution to this PDE and to compute explicitly the unique stationary state, which is reached asymptotically. This system is finally generalized by adding an ODE which takes into account the pathogens in the environment seen as a reservoir.

5.1.1 A simple model of the pathobiome dynamics

A simple way to model the pathobiome dynamics in the host gut is to consider two populations: the pathogen and its ecological competitors among the commensal gut bacteria. In order to build the equations, the following mechanisms are considered: the pathogens provoke an inflammatory response of the host, which affects the pathogens as well as the commensal bacteria. However, the inflammation causes an increase in the oxygen level near the gut epithelium, thus providing a competitive advantage to the pathogens. Indeed, the commensal microorganisms are mainly anaerobic, which means that they are highly sensitive to oxygen.

We now detail the model construction step-by-step. We start by assuming an antagonistic relationship between the pathogen and its ecological competitors, i.e. the fraction of microorganisms in the microbiota that share the same ecological niche. Let p and b be the concentrations of pathogens and antagonistic microbes in the host gut, and $K > 0$ be the carrying capacity of the niche, in the absence of any other limiting factor. The antagonism is modeled

by the equation

$$p + b = \mathrm{K} \tag{5.1.1}$$

Note that $p' = -b'$ at any time, so that when p increases, b decreases and vice versa, which is consistent with an antagonistic relationship. Note also that (5.1.1) allows the elimination of the unknown b in the equations describing the evolution of the system, however for the sake of clarity we will keep both variables until the end of the model description.

The pathogens and the antagonistic bacteria present in the intestine compete to conquer the niche, and the resident bacteria exert a barrier effect against the invasion, meaning that in the absence of any other phenomenon they eliminate the pathogens. Consequently, equation (5.1.1) is expanded into the following system of two differential equations:

$$\begin{aligned} p' &= -\mu_0 p b \\ b' &= \mu_0 p b \end{aligned}$$

where μ_0 is a positive coefficient accounting for the efficiency of b in the competition.

We now introduce, as mentioned above, a deleterious signal, such as oxygen, resulting from the inflammatory response to the pathogens. Let d be this signal, its evolution in time is modelled as

$$d' = \frac{1}{\tau}\left(-d + C_2 \frac{p^n}{p^n + {p_\star}^n}\right).$$

In this equation, the presence of the pathogens directly promotes the host inflammatory response and induces the production of d. This promotion is limited when the number of pathogens become very high; this is expressed through the sigmoid function $C_2 \dfrac{p^n}{p^n + {p_\star}^n}$ "centered" around the threshold value $p_\star \in [0, \mathrm{K}]$, with $n \in \mathbb{N}^*$ an exponent controlling the stiffness of the sigmoid. The parameter τ models a time delay between the evolution of the pathogens and the evolution of the signal d.

Two additional phenomena happen. First the deleterious signal d is more harmful to the antagonistic microbiota b than to the pathogens, thus favouring the pathogens in their fight to conquer the niche. Additionally, b undergoes a limitation in the efficiency of its competition with p related to the actual environment in the gut, such as the presence of other competitors of b or the basal immune system response, which we model by a self-inhibition term. These effects are taken into account by modifying the expression of the coefficient μ_0 according to

$$\mu_0 = \mu\left(1 - \frac{\alpha}{\mu} b - \frac{C_1}{\mu} d\right), \tag{5.1.2}$$

where μ, α and C_1 are positive. The term $1 - \dfrac{\alpha}{\mu} b$ represents the limitation related to the environment, and $-\dfrac{C_1}{\mu} d$ accounts for the influence of the deleterious signal d.

The evolution of b and p is therefore modeled by the following equations

$$\begin{aligned} b' &= bp\left(\mu - \alpha b - C_1 d\right) \\ p' &= -bp\left(\mu - \alpha b - C_1 d\right), \end{aligned}$$

in which the antagonistic relationship between b and p is now more complex than a simple competition where b wins and p loses, since asymptotically the introduction of (5.1.2) may modify the trade-off between b and p and allow for coexistence.

Using (5.1.1) to eliminate b and setting $A = \alpha \mathrm{K} - \mu$, the overall model is expressed as a system of two equations on p et d:

$$\begin{aligned} p' &= p(\mathrm{K}-p)\left(A - \alpha p + C_1 d\right), \\ d' &= \frac{1}{\tau}\left(-d + C_2 \frac{p^n}{p^n + {p_\star}^n}\right). \end{aligned}$$

Finally, we assume that the dynamics of d is very fast, that is $0 < \tau \ll 1$. Therefore, it is natural to assume that d is at quasi-steady state, and to simplify the model into a single equation

$$p' = p(\mathrm{K}-p)\left(A - \alpha p + C \frac{p^n}{p^n + {p_\star}^n}\right), \tag{5.1.3}$$

where $C = C_1 C_2$. We then get a monodimensional ODE on the pathogen only, that keeps track of the main drivers of Salmonella infection through its coefficients: 1) the parameter A sums up microbial ecology characteristics of the commensal by balancing its maximal efficiency coefficient μ with the environmental harshness αK, which is also taken into account by the parameter α; 2) the parameter C reflects the virulence of the host inflammatory response (the parameter C_2 describing the amount of deleterious signal produced during inflammation and C_1 its impact on commensals); 3) the host sensitivity to pathogens is shaped by the coefficients $p_\star$, that determines the amount of pathogen tolerated by the host, and the exponent n that represents the virulence of the inflammation (a higher n induces a sharper inflammatory response to the pathogen presence, beneficiary to the pathogen).

Depending on the values of A, α, C, n and $p_\star$, this ordinary differential equation can possess from two to five steady states in the interval $[0, \mathrm{K}]$, including 0 and K, alternatively stable or unstable. Discarding the trivial situation in which only two steady states (K is stable, 0 is unstable) exist, the stability of the equilibria in the case of 3, 4 or 5 steady states in $[0, \mathrm{K}]$ is summarized in Table 5.1, when A, α and C are positive. As mentioned in the introduction, we are interested in the biologically relevant situation of low and high-shedders, which corresponds to the co-existence of two stable steady states. The equilibria corresponding to 0 (no pathogen in the gut) or K (complete elimination of the antagonistic fraction of the microbiota) are not realistic in a livestock population context, where the contamination by the pathogen is certain and the commensal microbiota resistance is never totally suppressed. So the relevant situation on which we will focus is when there are two stable (p_1 and p_3) and three unstable (0, p_2 and K) steady states. The two stable steady states are interpreted as the concentrations of pathogens in low and high-shedders respectively.

Value	Stability		
	3 steady states	4 steady states	5 steady states
0	unstable	unstable	unstable
p_1	stable	stable	stable
p_2		unstable	unstable
p_3			stable
K	unstable	stable	unstable

Table 5.1 – Stability of the steady states $0 < p_1 < p_2 < p_3 < \mathrm{K}$ when A, α and C are positive.

5.1.2 A model derived from individual stochastic variability

From the previous ODE model, we obtain now an evolution equation for a whole population of individuals structured by pathogen loads.

Biological systems often exhibit intrinsic stochastic fluctuations in their dynamics. It therefore seems sensible to reformulate the model (5.1.3) as a stochastic differential equation (SDE)

$$d\,P = F(P)\,dt + \sigma\,dB, \tag{5.1.4}$$

where $P(t)$ is now a stochastic variable modeling the amount of pathogens in the gut, dB is a gaussian unitary white noise, $\sigma > 0$ is the instantaneous standard deviation of the stochastic fluctuations in the model and the function F is defined on $\mathbb{R}$ by

$$F(p) = \begin{cases} p(\mathrm{K}-p)\left(A - \alpha p + C\dfrac{p^n}{p^n + {p_\star}^n}\right), & \text{if } p \in [0,\mathrm{K}]\,, \\ 0, & \text{otherwise.} \end{cases} \tag{5.1.5}$$

It can be easily checked that F is uniformly Lipschitz on $\mathbb{R}$, and has linear growth. As σ is constant, we can use standard results from SDE theory (see e.g. [34]) to obtain the so-called forward Kolmogorov equation of (5.1.4)

$$\begin{aligned} &\partial_t u(t,p) = -\partial_p(F(p)\,u(t,p)) + \frac{\sigma^2}{2}\partial^2_{pp} u(t,p), \\ &u(0,\,\cdot\,) = u_{\mathrm{ini}}(\,\cdot\,); \end{aligned}$$

the solution $u(t,p)$, defined on $L^2(\mathbb{R}^+ \times \mathbb{R})$, is the probability density function of $p(t)$ at time t, conditionally on the probability density of the initial pathogen population density function u_{ini}.

However, this model is not quite satisfactory as brownian stochastic fluctuations make it possible to achieve realizations of $p(t)$ that are negative or greater than K. To avoid this, the SDE (5.1.4) has to be transformed into a SDE with reflecting boundary conditions which requires more sophisticated tools from stochastic process theory (see e.g. [39] for a quick

introduction). The resulting forward Kolmogorov equation is modified in such a way that the solution space is now $L^2\left(\mathbb{R}^+, L^2(0,\mathrm{K})\right)$ and its formulation is

$$\begin{aligned}
&\partial_t u(t,p) = -\partial_p(F(p)u(t,p)) + \frac{\sigma^2}{2}\partial^2_{pp}u(t,p),\\
&\partial_p u(\cdot,0) = \partial_p u(\cdot,\mathrm{K}) = 0,\\
&u(0,\cdot) = u_{\mathrm{ini}}(\cdot) \in L^2(0,K), \quad \int_0^{\mathrm{K}} u_{\mathrm{ini}}(p)dp = 1.
\end{aligned}$$

We now consider a very large population such that it can be described by a population density $s(t,p)$, meaning that $\int_a^b s(t,p)dp$ is the number of individuals with a pathogen load between a and b at time t. Define $s(t,p) = Nu(t,p)$ so that the total size of the population $N = \int_0^{\mathrm{K}} s(t,p)dp$ is constant. Then the population density s satisfies the following equations:

$$\partial_t s(t,p) = -\partial_p(F(p)s(t,p)) + \frac{\sigma^2}{2}\partial^2_{pp}s(t,p), \tag{5.1.6a}$$

$$\partial_p s(\,\cdot\,,0) = \partial_p s(\,\cdot\,,\mathrm{K}) = 0, \tag{5.1.6b}$$

$$s(0,\,\cdot\,) = s_{\mathrm{ini}}(\,\cdot\,) \in L^2(0,\mathrm{K}), \quad \int_0^{\mathrm{K}} s_{\mathrm{ini}}(p)dp = N, \tag{5.1.6c}$$

where F is defined at Eq.(5.1.5). This is a realistic population model, structured with respect to the pathogen load, in the absence of pathogen transmission.

5.1.3 Existence of solutions to Eq. (5.1.6) and convergence towards a stationary state

Let us now prove the existence and uniqueness of the solution to system (5.1.6).

Proposition 5.1. *For $s_{\mathrm{ini}} \in L_2(0,\mathrm{K})$, the PDE (5.1.6) has a unique solution in $C([0,T], L^2(0,\mathrm{K}))$.*

Proof. Consider the unbounded operator A with domain

$$\mathscr{D}(A) = \{w \in H^2(0,\mathrm{K}),\ w'(0) = 0,\ w'(\mathrm{K}) = 0\},$$

such that for all $w \in \mathscr{D}(A)$,

$$A(w) = -(Fw)' + \frac{\sigma^2}{2}w''.$$

Then $-A$ is a regular Sturm-Liouville operator. It follows from [15] that A generates a strongly continuous semigroup on $L^2(0,\mathrm{K})$, which proves the proposition. □

We now prove that system (5.1.6) possesses a unique stationary state.

Proposition 5.2. *The PDE (5.1.6) has a unique stationary state defined by*

$$s_\infty(p) = \lambda \exp\left(\frac{2}{\sigma^2}\int_0^p F(r)dr\right) \qquad \textit{with} \qquad \lambda = \frac{N}{\displaystyle\int_0^K \exp\left(\frac{2}{\sigma^2}\int_0^p F(r)dr\right)dp}, \tag{5.1.7}$$

where F is defined at Eq. (5.1.5).

Proof. The stationary states of model (5.1.6) are the solutions of the equation:

$$\partial_p\left(F(p)s_\infty(p) - \frac{\sigma^2}{2}\partial_p s_\infty(p)\right) = 0, \text{ with } \int_0^K s_\infty(p)dp = N.$$

Thanks to the definition of F and the boundary conditions, this leads to

$$F(p)s_\infty(p) - \frac{\sigma^2}{2}\partial_p s_\infty(p) = 0.$$

This simple ODE has a unique solution given by formula (5.1.7).

□

Finally, we can show that the solution reaches asymptotically this stationary state.

Proposition 5.3. *The solution of the PDE (5.1.6), defined at Prop.5.1, converges at exponential rate towards the steady state s_∞ defined in Prop. 5.2.*

Proof. We first consider solution $s(t,\cdot)$ of (5.1.6) with initial condition in $\mathscr{D}(A)$ as defined in proposition 5.1, and follow the method proposed by Bolley et al. in [5]. We consider the L^2 weighted norm

$$\|f\|^2_{\mathscr{L}^2(]0,\mathrm{K}[,1/s_\infty)} = \int_0^\mathrm{K} f(p)^2 \frac{dp}{s_\infty(p)}$$

and define the function

$$G(t) = \|s(t,\cdot) - s_\infty\|^2_{\mathscr{L}^2(]0,\mathrm{K}[,1/s_\infty)}.$$

As the initial condition is in $\mathscr{D}(A)$, $s(t,\cdot)$ is in $C^1((0,T),\mathscr{D}(A))$ and we can differentiate G with respect to t, which leads to

$$G'(t) = 2\int_0^\mathrm{K}\left(\frac{s(t,p)}{s_\infty(p)} - 1\right)\partial_t s(t,p)dp = \sigma^2\int_0^\mathrm{K}\left(\frac{s(t,p)}{s_\infty(p)} - 1\right)\partial_p\left[\partial_p s(t,p) - \frac{2}{\sigma^2}F(p)s(t,p)\right]dp.$$

Then, integrating by parts, using boundary conditions (5.1.6b) and the fact that $F(0) = F(K) = 0$, see Eq.(5.1.5), we find that

$$\begin{aligned} G'(t) &= -\sigma^2\int_0^\mathrm{K}\partial_p\left(\frac{s(t,p)}{s_\infty(p)} - 1\right)\left[\partial_p s(t,p) - \frac{2}{\sigma^2}F(p)s(t,p)\right]dp \\ &= -\sigma^2\int_0^\mathrm{K}\left|\partial_p\left(\frac{s(t,p)}{s_\infty(p)} - 1\right)\right|^2 s_\infty(p)dp. \end{aligned}$$

From Poincaré-Wirtinger's inequality for bounded domain with weighted norm (see [30, Lemme 3.3]) applied with $\|.\|_{\mathscr{L}^2(]0,\mathrm{K}[,s_\infty)}$, there exists a constant κ depending only on the domain $[0,K]$ and the weight s_∞, such that

$$\kappa \int_0^{\mathrm{K}} \left| \frac{s(t,p)}{s_\infty(p)} - 1 \right|^2 s_\infty(p)\,dp \leqslant \int_0^{\mathrm{K}} \left| \partial_p \left(\frac{s(t,p)}{s_\infty(p)} - 1 \right) \right|^2 s_\infty(p)\,dp.$$

Then, using the expression of G and G', we obtain that

$$G'(t) \leqslant -\kappa\sigma^2 G(t).$$

Finally, by a direct application of the differential form of Gronwall's lemma, one can deduce that for all initial condition in $\mathscr{D}(A)$, the solution $s(t,p)$ of (5.1.6) converges when time goes to infinity towards the steady state s_∞, in the sense of $\mathscr{L}^2\left(]0,K[, \frac{1}{s_\infty}\right)$, at rate $e^{-\sigma^2\kappa t}$.
From the density of $\mathscr{D}(A)$ in $L^2(0,K)$ it follows that for all initial condition in $L^2(0,K)$, the (mild) solution $s(t,p)$ of (5.1.6) also converges when time goes to infinity towards the steady state s_∞, in the sense of $\mathscr{L}^2\left(]0,K[, \frac{1}{s_\infty}\right)$, at rate $e^{-\sigma^2\kappa t}$.

□

5.1.4 Generalized model adding transmission through an external reservoir

Our aim in this subsection is to add some exchanges of pathogens between individuals through the environment. The salmonella pathogen can be released in the environment by the infected animals and can contaminate food sources, for example watering troughs. This mechanism creates an external reservoir of pathogens which varies according to the excretion and absorption of salmonella by individuals. Thus, it constitutes a major environmental factor in the spread of pathogens. In order to account for this mechanism, the model (5.1.6) is modified into

$$\partial_t s(t,p) = -\partial_p\Big(\big(F(p) + \beta_{\mathrm{in}}(p)r(t) - \beta_{\mathrm{ex}}(p)\big)s(t,p)\Big) + \frac{\sigma^2}{2}\partial^2_{pp}s(t,p), \tag{5.1.8a}$$

$$\frac{dr(t)}{dt} = -\left(\gamma + \int_0^{\mathrm{K}} s(t,p)\beta_{\mathrm{in}}(p)\,dp\right) r(t) + \int_0^{\mathrm{K}} s(t,p)\beta_{\mathrm{ex}}(p)\,dp, \tag{5.1.8b}$$

$$\frac{\sigma^2}{2}\partial_p s(t,\mathrm{K}) + \beta_{\mathrm{ex}}(\mathrm{K})s(t,\mathrm{K}) = \frac{\sigma^2}{2}\partial_p s(t,0) - \beta_{\mathrm{in}}(0)r(t)s(t,0) = 0, \tag{5.1.8c}$$

$$s(0,\cdot) = s_{\mathrm{ini}}(\cdot) \in H^1(0,\mathrm{K}), \quad \int_0^{\mathrm{K}} s_{\mathrm{ini}}(p)\,dp = N, \quad r(0) = r_{\mathrm{ini}} \in \mathbb{R}^+, \tag{5.1.8d}$$

where F is defined at Eq.(5.1.5).

Here the new variable r denotes the reservoir of pathogens in the environment. In PDE (5.1.8a), the term $\beta_{\mathrm{in}}(p)r$ represents the uptake of pathogens from the environment, while $\beta_{\mathrm{ex}}(p)$ stands for the pathogen excretion by individuals. Similarly, in the ODE (5.1.8b), the quantity $r(t)s(t,p)\beta_{\mathrm{in}}(p)dp$ indicates the uptake of pathogens from the environment by individuals with pathogen load p and the last term $s(t,p)\beta_{\mathrm{ex}}(p)dp$ describes the increase of the

pathogen reservoir induced by individuals with pathogen load p. We set $\beta_{\text{in}}(p) = \beta_{\text{in}}\left(\text{K} - p\right)$ and $\beta_{\text{ex}}(p) = \beta_{\text{ex}} p$, with $\beta_{\text{in}}, \beta_{\text{ex}} > 0$, so that the contamination from the reservoir decreases with the pathogen load whereas the excretion increases with the pathogen load. The positive parameter γ is the natural decay rate of the pathogen reservoir. Finally, boundary conditions are modified into Robin boundary conditions in order to ensure the conservation of the total population.

5.2 Numerical results for models (5.1.6) without transmission and model (5.1.8) with transmission

Our goal in this section is to display and comment some numerical simulations of systems (5.1.6) and (5.1.8); we test different initial data and compare the solutions of the two models, with or without transmission.

The numerical scheme is based on upwind scheme for the transport term and the time-implicit centered three point scheme for the diffusion part. The simulations have been performed with Python 3 (using Numpy & Scipy) on a 500 cell mesh grid and with the parameters summarized in table (5.2).

In this theoretical analysis, in the absence of experimental calibration, the parameters A, α and C are set to values for which the deterministic model (5.1.3) has two well separated non trivial stable equilibria corresponding to the last column in Table 5.1, in order to obtain a bimodal equilibrium distribution in equation (5.1.6), describing the coexistence of high-shedder and low-shedder phenotypes in the population. The parameter K has been chosen arbitrarily, and could be rescaled to reflect another carrying capacity. The logistic threshold $p_\star$ has been tuned to trigger an inflammation into the host gut when the pathogen load is close to half the carrying capacity. The diffusion parameter σ was selected in the same order of magnitude than the transport process, meaning that the stochastic effects during the pathogen infection are not negligible and can impact the pathogen dynamics. The parameters β_{in} and β_{ex} provide a small inter-host infection rate.

Parameter	K	A	α	C	n	$p_\star$	σ	γ	β_{in}	β_{ex}
Value	5.0	0.1	0.35	1.2	50	2.15	1.75	1.0	1	0.2

Table 5.2 – Values of the parameters used to perform the simulations presented in section 5.2.

5.2.1 Structured population without transmission

Figure 5.1 represents some solutions of the population model (5.1.6) structured by pathogen load and without transmission through a reservoir, for the parameters given at Table 5.2. Three different initial data, shown in dotted blue line in Subfigures 5.1(a), 5.1(b) and 5.1(c)

are considered:

$$s_{\text{ini}}(p) = 0.2, \qquad s_{\text{ini}}(p) = \frac{e^{-(p_1-p)^2/4}}{\int_0^K e^{-(p_1-p)^2/4}dp}, \qquad s_{\text{ini}}(p) = \frac{e^{-(p_3-p)^2/4}}{\int_0^K e^{-(p_3-p)^2/4}dp}, \tag{5.2.9}$$

where $p_1 \sim 0.285$ and $p_3 \sim 3.714$ are the two stable steady states. As expected, for each initial datum, the solution converges towards the theoretical stationary state computed at Eq. (5.1.7). This stationary state possesses two maximal values at $p = p_1$ and $p = p_3$, corresponding respectively to the low-shedder and the high-shedder groups and a minimal value at $p = p_2$, an unstable steady state of Eq.(5.1.3). However, we can observe some discrepancies in the transient behavior, as noticed on the plots of Subfigures 5.1(d), 5.1(e) and 5.1(f) representing the evolution with time and pathogen load of the density population s. Especially, depending on the initial datum, the steady state can be reached from above (p_3 neighborhood in Fig. 5.1(a), 5.1(c), p_1 neighborhood in Fig. 5.1(b)) or from below (p_1 neighborhood in Fig. 5.1(a), 5.1(c), p_3 neighborhood in Fig. 5.1(b)). Furthermore, the steady state is reached faster in Fig. 5.1(d) (around $t = 6$) than in Fig 5.1(e) (around $t = 9$) or 5.1(f) (around $t = 8$).

5.2.2 Structured population with transmission through a pathogen reservoir

Figure 5.2 represents the density population s, solution to the structured in pathogen load population system (5.1.8), with transmission through a pathogen reservoir. The initial datum used for this simulation is $s_{\text{ini}}(p) = 0.2$ and $r_{\text{ini}} = 0$.

The evolution of the population density $s(t,p)$ is plotted in Subfigure 5.2(a), together with levelsets. Numerical experiments show that $s(t,p)$ converges towards a stationary state. The time evolution of the reservoir variable r and of the total pathogen load within the population $\int_0^K ps(t,p)dp$ is displayed in Subfigure 5.2(b). Due to the pathogen excretion, the reservoir variable first increases until a maximal value of 0.123 at $t = 1.11$. Then in a second phase, it slightly decreases and tends to stabilize around 0.099. Subfigure 5.2(c) shows the comparison between the solution $s(t,p)$ for $t = 5$, in dashed green line, and $t = 10$ close to the stationary state (red line). To highlight the effect of the reservoir, we plot s_∞, i.e. the stationary state without reservoir (r^- control, black line), which differs notably from the stationary state with reservoir (red line). It can be observed that low and high shedder clusters are shifted and that their sizes are changed. Indeed, the low shedder cluster is centered around the steady state $p_1 \simeq 0.61$ for the model with the reservoir variable, whereas it is centered around the steady state $p_1 \simeq 0.28$ without the reservoir variable. In addition, the low shedder cluster is larger in the sense that it contains more individuals when accounting for the reservoir variable. For the high shedder cluster, the effect is the opposite. Indeed, in the model with the reservoir variable, the cluster is smaller (fewer individuals) and shifted towards a smaller value of pathogen load: $p_3 \simeq 3.43$ instead of $p_3 \simeq 3.71$ without reservoir variable. The increase of the low-shedder average pathogen load may reflect the higher exposure to environmental

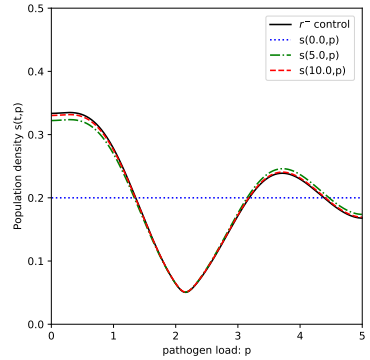

(a) Population distribution s as a function of pathogen load p for $s_{\text{ini}}(p) = 0.2$

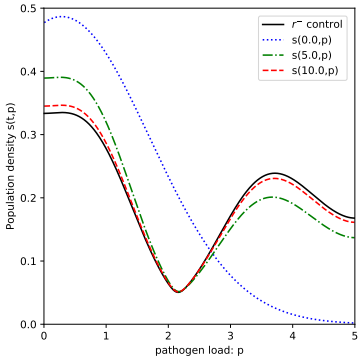

(b) Population distribution s as a function of pathogen load p for $s_{\text{ini}}(p) = \dfrac{e^{-(p_1-p)^2/4}}{\displaystyle\int_0^K e^{-(p_1-p)^2/4}}$

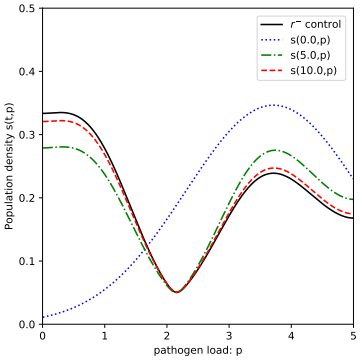

(c) Population distribution s as a function of pathogen load p for $s_{\text{ini}}(p) = \dfrac{e^{-(p_3-p)^2/4}}{\displaystyle\int_0^K e^{-(p_3-p)^2/4}}$

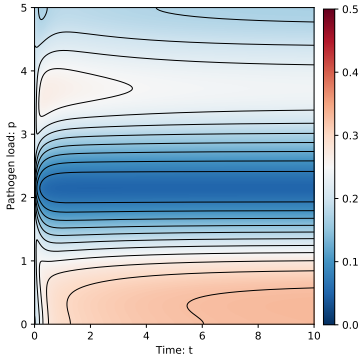

(d) Population density evolution, for $s_{\text{ini}}(p) = 0.2$

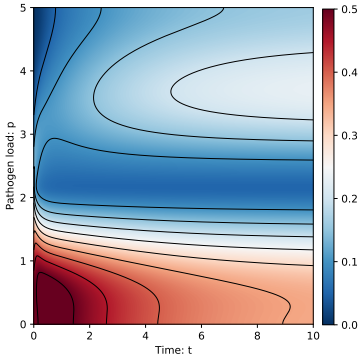

(e) Population density evolution, for $s_{\text{ini}}(p) = \dfrac{e^{-(p_1-p)^2/4}}{\displaystyle\int_0^K e^{-(p_1-p)^2/4}}$

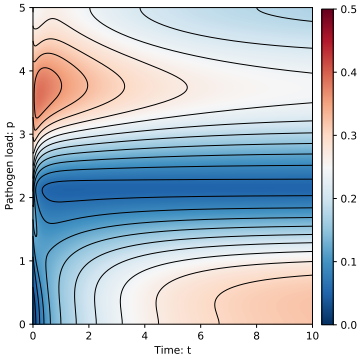

(f) Population density evolution, for $s_{\text{ini}}(p) = \dfrac{e^{-(p_3-p)^2/4}}{\displaystyle\int_0^K e^{-(p_3-p)^2/4}}$

Figure 5.1 – **Basal experiment:** Evolution of the population distribution when no transmission is considered (model (5.1.6)). Each column corresponds to the different initial data introduced in Eq. (5.2.9). Top row: population density is displayed at time $t = 0$ (blue dotted line), $t = 5$ (green dashed line) and $t = 10$ (red dashed line), compared to the stationary state without reservoir (r^- control, plain black line). Bottom row: Evolution of the population density, together with level sets, for the three different initial data.

pathogen, whereas the decrease of high shedder load may come from excretion. Indeed, the degradation of the pathogen in the environment makes the reservoir variable a sink source for intra-host pathogens and pulls the pathogen loads towards lower values.

For this model, stationary states can be computed thanks to some fixed-point technique. However, the proof of the asymptotic convergence towards a stationary state is much more difficult to handle than the proof of Prop.5.3, due to the coupling with the ODE.

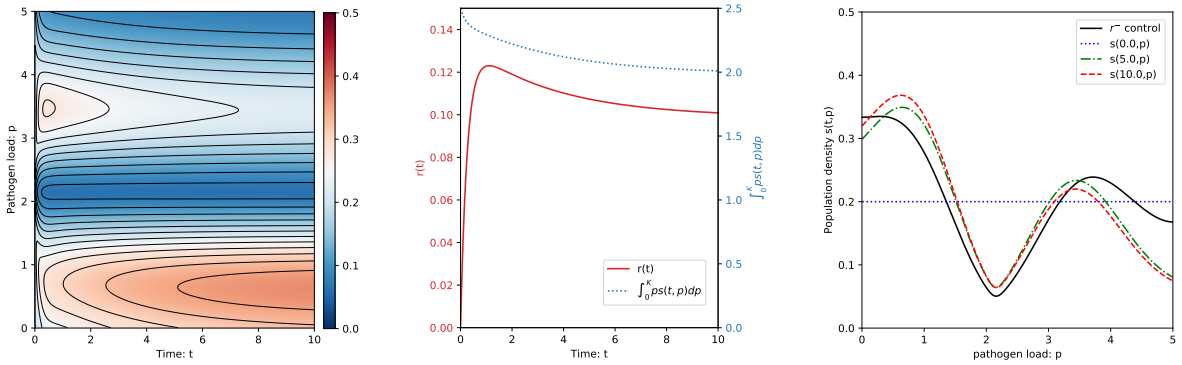

(a) Evolution of the population density s

(b) Evolution of the reservoir variable r and total pathogen load within the population

(c) Population density s at different times

Figure 5.2 – **Pathogen reservoir:** Evolution of the population density when contact with an environmental pathogen reservoir is added (model (5.1.8)). Initial data are $s_{\text{ini}}(p) = 0.2$ and $r_{\text{ini}} = 0$. (A) Population density dynamics together with level sets. (B) Evolution of the environmental pathogen reservoir r (red line) and total pathogen load within the population $\int_0^K ps(t,p)dp$ (blue dotted line). (C) Population densities s at times $t = 0$ (dotted blue line), $t = 5$ (green dash dotted line) and $t = 10$ (red dashed line), compared with the stationary state of the model without reservoir s_∞ ($r - control$, black line).

However, we can draw some first conclusions from numerical experiments: for the range of parameters we have tested for β_{in} and β_{ex}, the solution always converges towards a steady state. Moreover, whatever the initial datum s_{ini} chosen among those of Eq.(5.2.9) or Dirac masses and whatever r_{ini}, the population density s converges asymptotically towards the same stationary solution.

Consequently, we think that the PDE system (5.1.8) possesses only one stable stationary solution and that all solutions converge towards this steady state.

5.3 Study of various control strategies

Control strategies consist in external actions in order to limit the spread of pathogens within the population. Two types of control will be considered: on the one hand, the cleaning action limits the pathogen reservoir in the environment, by removing a certain amount of pathogens represented by the reservoir variable, and, on the other hand, drugs can be used to cure the population. A combination of these two treatments is also considered and a comparison between these three possibilities is performed.

Let us first describe how to model the two treatment strategies in the PDE system (5.1.8).

The cleaning action removes pathogens from the environment. It can be modeled by adding an extra term of the form $-C(t,r)$ in the right hand side of Equation (5.1.8b) for the

reservoir variable. As a first attempt to describe this mechanism, it is assumed that C is a linear function of r, meaning that the cleaning treatment removes a constant fraction of pathogen reservoir per time unit. Moreover, cleaning might start after a given time and/or might be periodic. Therefore, we assume that C takes the following form:

$$C(t,r) = \rho r \mathbb{1}_{t\in \mathrm{I}_C},$$

where $\rho \in \mathbb{R}^+$ is the cleaning rate and I_C the time interval(s) during which the cleaning is applied.

On the contrary, the treatment with drugs decreases the pathogen load of the individuals. Therefore this mechanism is modeled by adding an extra term $-T(t,p)s(t,p)$ in the drift term of the population mass balance equation (5.1.8a). It is assumed that the treatment removes a constant fraction of the pathogen load of an individual per time unit and that it also depends on time. So, we write the term T accounting for drug treatment as

$$T(t,p) = \theta p \mathbb{1}_{t\in \mathrm{I}_T},$$

where the rate $\theta \in \mathbb{R}^+$ models the treatment efficiency and I_T the time interval(s) during which the treatment is administrated.

Taking into account cleaning and drug treatment, the system (5.1.8) becomes

$$\partial_t s(t,p) = -\partial_p\Big(\big(F(p) + \beta_{\mathrm{in}}(p)r - \beta_{\mathrm{ex}}(p) - T(t,p)\big)s(t,p)\Big) + \frac{\sigma^2}{2}\partial^2_{pp}s(t,p), \tag{5.3.10a}$$

$$\frac{d\,r(t)}{dt} = -\left(\gamma + \int_0^{\mathrm{K}} s(t,p)\beta_{\mathrm{in}}(p)dp\right)r(t) + \int_0^{\mathrm{K}} s(t,p)\beta_{\mathrm{ex}}(p)dp - C(t,r), \tag{5.3.10b}$$

$$\frac{\sigma^2}{2}\partial_p s(t,\mathrm{K}) + \big(\beta_{\mathrm{ex}}(K) + T(t,K)\big)s(t,\mathrm{K}) = \frac{\sigma^2}{2}\partial_p s(t,0) + \big(T(t,0) - \beta_{\mathrm{in}}(0)r(t)\big)s(t,0) = 0, \tag{5.3.10c}$$

$$s(0,\cdot) = s_{\mathrm{ini}}(\cdot) \in H^1(0,\mathrm{K}), \quad \int_0^{\mathrm{K}} s_{\mathrm{ini}}(p)dp = N, \quad r(0) = r_{\mathrm{ini}} \in \mathbb{R}^+. \tag{5.3.10d}$$

The simulations presented in the following subsections are performed with the parameters of Table 5.2. We also take $\rho = 5$ for the cleaning rate and $\theta = 0.25$ for the drug treatment rate.

5.3.1 Cleaning strategy

Let us begin with the study of the cleaning strategy.

Figures 5.3 and 5.4 represent two simulations of system (5.3.10) with cleaning only, i.e. $T(t,p) = 0$. For the simulation displayed in Figure 5.3, the cleaning is activated during the whole simulation, namely $\mathrm{I}_C = \mathbb{R}_+$, whereas in the simulation displayed in Figure 5.4 the cleaning is only activated on the time interval $\mathrm{I}_C = [10,20]$.

The results presented in Figure 5.3 are comparable to the simulation presented in Subsection 5.2.2. Indeed, in this case, system (5.3.10) reduces to system (5.1.8) in which the decay

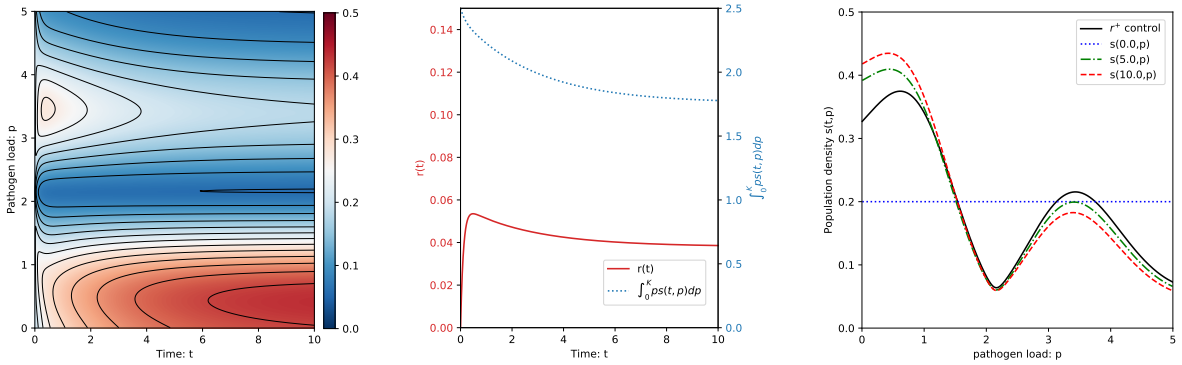

(a) Evolution of the population density s together with level sets

(b) Evolution of the reservoir variable r and total pathogen load within the population

(c) Population density s at different times

Figure 5.3 – **Reservoir, cleaning, no drug, stationary treatment:** Evolution of the population density when contact with an environmental pathogen reservoir is added and when cleaning and no drug are applied (model (5.3.10) with $T = 0$). Initial data are $s_{\text{ini}}(p) = 0.2$ and $r_{\text{ini}} = 0$. Cleaning is applied during the whole simulation ($\mathrm{I}_C = \mathbb{R}_+$). (A) Population density dynamics together with level sets. (B) Evolution of the environmental pathogen reservoir r (red line) and total pathogen load within the population $\int_0^{\mathrm{K}} ps(t,p)dp$ (blue dotted line). (C) Population densities s at times $t = 0$ (blue dotted line), $t = 5$ (green dash dotted line) and $t = 10$ (red dashed line), compared with the stationary state of the model with reservoir but no cleaning and no drug treatment ($r + control$, black line).

rate for the pathogen reservoir γ has been shifted to $\tilde{\gamma} = \gamma + \rho$. As in Section 5.2.2, the system seems to converge towards a stationary state. However, the features previously observed are enhanced. First, we can notice that the population density s affected by cleaning contains more low shedder individuals and less high shedder individuals than the population density without cleaning. In addition, the reservoir variable takes lower values in the case of cleaning; for example, we observe that at time $t = 10$, $r(10) \simeq 0.038$ with cleaning and $r(10) \simeq 0.118$ without cleaning. Similarly, the total pathogen load in the whole population takes lower values, for example, at time $t = 10$, $\int_0^{\mathrm{K}} ps(10,p)dp \simeq 2.0$ without cleaning and $\int_0^{\mathrm{K}} ps(10,p)dp \simeq 1.77$ with cleaning. Finally, the pathogen loads corresponding to low and high shedder individuals are changed ($p_1 \simeq 0.42$ and $p_3 \simeq 3.39$) compared to the model without cleaning ($p_1 \simeq 0.61$ and $p_3 \simeq 3.43$).

Figure 5.4 displays the results of a simulation where the cleaning is applied only during a range of time $\mathrm{I}_C = [10,20]$, which allows to study the dynamic response of the system. In Subfigures 5.4(a) and 5.4(b) , we can notice three different periods of time. The first one corresponds to the time range $t \in [0,10]$, when the system evolves without cleaning. During this time interval, the system behaves like system (5.1.8) (see Section 5.2.2). The second period corresponds to $t \in \mathrm{I}_C = [10,20]$, when the cleaning is applied; according to Figure 5.4(b), the pathogen reservoir rapidly drops off to a range of values similar to those found in the simula-

tion where the cleaning is applied from the beginning, see Figure 5.3(b). On the opposite, the dynamic adaptation of the population is slower. Indeed, as it can be observed in Figure 5.4(b), the total pathogen load $\int_0^K ps(t,p)dp$, plotted in blue dashed line, also decreases but takes a longer time to stabilize. In the last period, which corresponds to $t > 20$, cleaning is removed. Here again, the dynamic adaptation of the pathogen reservoir variable occurs very quickly, whereas the adaptation of the population is slower.

As a conclusion, the cleaning action does not change the global dynamics of the system, but leads to smaller reservoir pathogen levels and lower average pathogen load in the population. Moreover, we can observe that the population dynamics response to cleaning takes more time than the pathogen reservoir dynamics response. Furthermore, when cleaning is stopped, the pathogen distribution rapidly turns back to the distribution observed when no cleaning is applied, showing that cleaning should be applied at a period smaller than this relaxation time scale to be efficient as a control strategy.

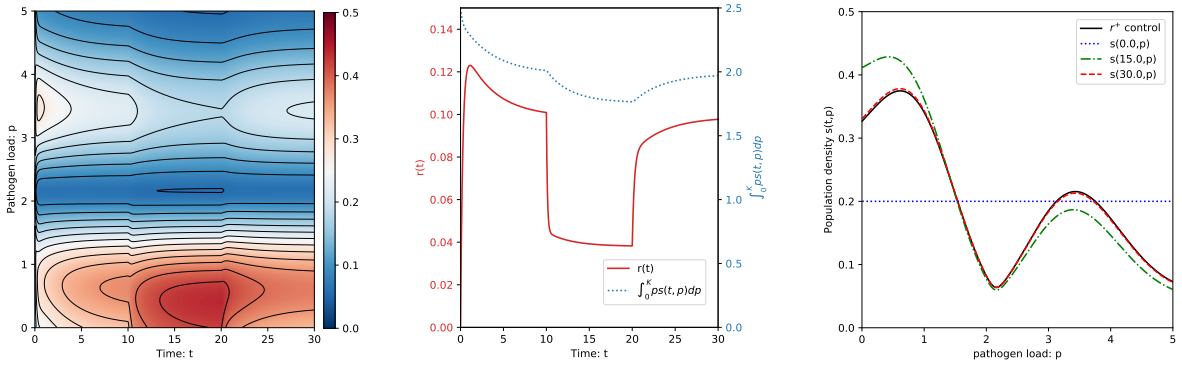

(a) Evolution of the population density s together with level sets

(b) Evolution of the reservoir variable r and total pathogen load within the population

(c) Population density s at different times

Figure 5.4 – **Reservoir, cleaning, no drug, transient treatment:** Evolution of the population density when contact with an environmental pathogen reservoir is added and when cleaning and no drug are applied (model (5.3.10) with $T = 0$). Initial data are $s_{\text{ini}}(p) = 0.2$ and $r_{\text{ini}} = 0$. Cleaning is applied on the time interval $\text{I}_C = [10,20]$. (A) Population density dynamics together with level sets. (B) Evolution of the environmental pathogen reservoir r (red line) and total pathogen load within the population $\int_0^K ps(t,p)dp$ (blue dotted line). (C) Population densities s at times $t = 0$ (blue dotted line), $t = 5$ (green dash dotted line) and $t = 10$ (red dashed line), compared with the stationary state of the model with reservoir but no cleaning and no drug treatment ($r + control$, black line).

5.3.2 Drug treatment strategy

In this subsection, we now consider the effect of a drug treatment and we neglect the cleaning, i.e. $C(t,r) = 0$ in Eq. (5.3.10). Two different scenarios of treatment are discussed

below.

Figure 5.5 represents the first scenario in which the treatment is applied for all time, namely $I_T = \mathbb{R}_+$. According to Figure 5.5(a) displaying the population dynamics and Figure 5.5(b) representing the pathogen reservoir, the system seems to converge towards a stationary state. The effect of the treatment can be estimated by comparing this simulation with the results obtained in Section 5.2.2, that is to say the same system without treatment. In Figure 5.5(b), it can be observed that the pathogen reservoir takes lower values in the case with treatment than without, for example $r(10) = 0.053$ with treatment and $r(10) = 0.10$ without. As expected, the total pathogen load in the population is smaller, meaning that the population is less infected by the pathogen when a treatment is administrated. This observation is enforced by comparing the size of the low and high shedder groups in Figure 5.5(c) with the ones in Figure 5.2(c). Indeed, with a drug treatment, a large part of the population concentrates around the low shedder pathogen load value p_1 and the high shedder group, i.e. individuals with a pathogen load around p_3, is smaller. Moreover, the treatment shifts towards lower values the pathogen loads corresponding to low and high shedder individuals, namely $(p_1, p_3) = (0.39, 3.09)$ with the treatment, whereas $(p_1, p_3) = (0.61, 3.43)$ without.

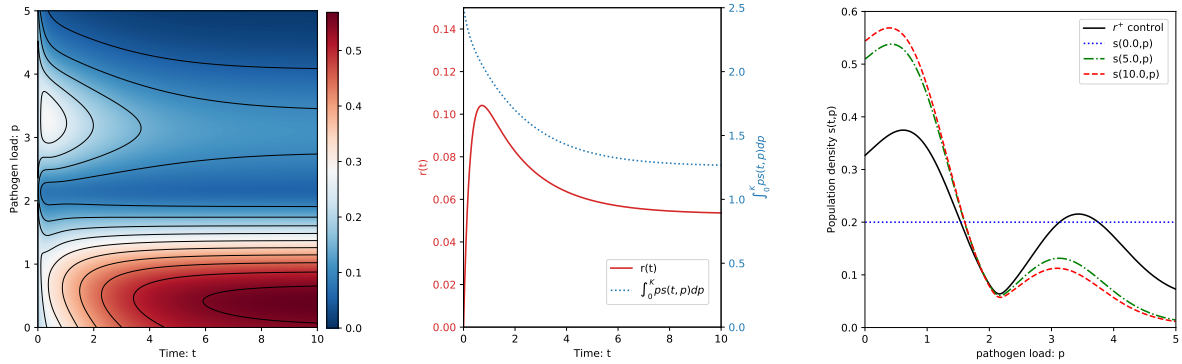

(a) Evolution of the population density s together with level sets

(b) Evolution of the reservoir variable r and total pathogen load within the population

(c) Population density s at different times

Figure 5.5 – **Reservoir, no cleaning,drug, stationnary treatment:** Evolution of the population density when contact with an environmental pathogen reservoir is added and when no cleaning but drug treatment is applied (model (5.3.10), with $C = 0$). Initial data are $s_{\text{ini}}(p) = 0.2$ and $r_{\text{ini}} = 0$. Cleaning is applied on the time interval $I_T = \mathbb{R}_+$. (A) Population density dynamics together with level sets. (B) Evolution of the environmental pathogen reservoir r (red line) and total pathogen load within the population $\int_0^K ps(t,p)dp$ (blue dotted line). (C) Population densities s at times $t = 0$ (blue dotted line), $t = 5$ (green dash dotted line) and $t = 10$ (red dashed line), compared with the stationary state of the model with reservoir but no cleaning and no drug treatment ($r + control$, black line).

In the simulation represented in Figure 5.6, drug treatment is only applied during the time

interval $I_T = [10,20]$. As for the cleaning case, this simulation allows to study the dynamic response of the system to the drug treatment and the evolution of the solution in Subfigures 5.6(a) and 5.6(b) can also be divided into three periods. The first one corresponds to the time range $t \in [0,10]$ with no cleaning. In this first phase, the system behaves like System (5.1.8), see Section 5.2.2 for the corresponding numerical results. The second time period corresponds to $t \in I_C = [10,20]$. During this period, according to Figure 5.6(b), the total pathogen load of the population, plotted in blue dashed line, and the pathogen reservoir decrease exponentially. Remark that, here, both the pathogen reservoir and the total pathogen load within the population decrease with the same exponential rate, unlike what was observed for the cleaning case. In the last period, which corresponds to $t > 20$, the treatment is removed and, as expected, the pathogen reservoir and the total pathogen load increase. Here again, the dynamic adaptation of the pathogen reservoir and the average pathogen load follow an exponential dynamics with a comparable rate. After the end of the therapy, the system recovers its original dynamics, showing again that the administration periodicity is important for a durable effect.

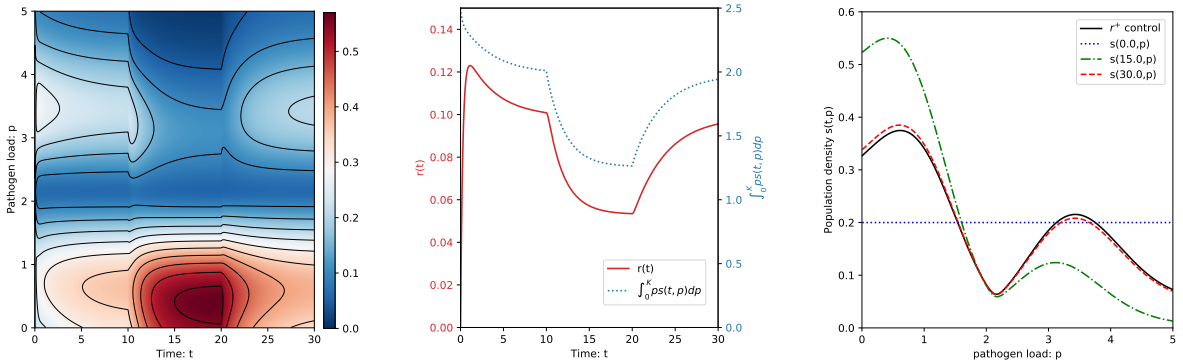

(a) Evolution of the population density s together with level sets

(b) Evolution of the reservoir variable r and total pathogen load within the population

(c) Population density s at different times

Figure 5.6 – **Reservoir, no cleaning, drug, transient treatment:** Evolution of the population density when contact with an environmental pathogen reservoir is added and when no cleaning but drug treatment is applied (model (5.3.10), with $C = 0$). Initial data are $s_{\text{ini}}(p) = 0.2$ and $r_{\text{ini}} = 0$. Cleaning is applied on the time interval $I_T = [10,20]$. (A) Population density dynamics together with level sets. (B) Evolution of the environmental pathogen reservoir r (red line) and total pathogen load within the population $\int_0^K ps(t,p)dp$ (blue dotted line). (C) Population densities s at times $t = 0$ (blue dotted line), $t = 5$ (green dash dotted line) and $t = 10$ (red dashed line), compared with the stationary state of the model with reservoir but no cleaning and no drug treatment ($r + control$, black line).

5.3.3 Combination of cleaning and drug treatment

We now consider the case when cleaning and drug treatment are combined in order to decrease the pathogen load. A simulation of System (5.3.10) with both terms $C(t,r)$ and $T(t,r)$ is displayed at Figure 5.7. In this simulation, cleaning and treatment are activated during the whole time, namely $\mathrm{I}_C = \mathrm{I}_T = \mathbb{R}_+$. The values for the cleaning rate and the treatment rate are the same as in the previous subsections and, as expected, both effects accumulate. Indeed, by comparing Figure 5.7(b) with Figures 5.3(b) and 5.5(b), it can be observed that the pathogen reservoir and the total pathogen load remain lower than in the cleaning or the drug treatment cases. Here again, it seems that the system converges towards a stationary state, according to Figure 5.7(a).

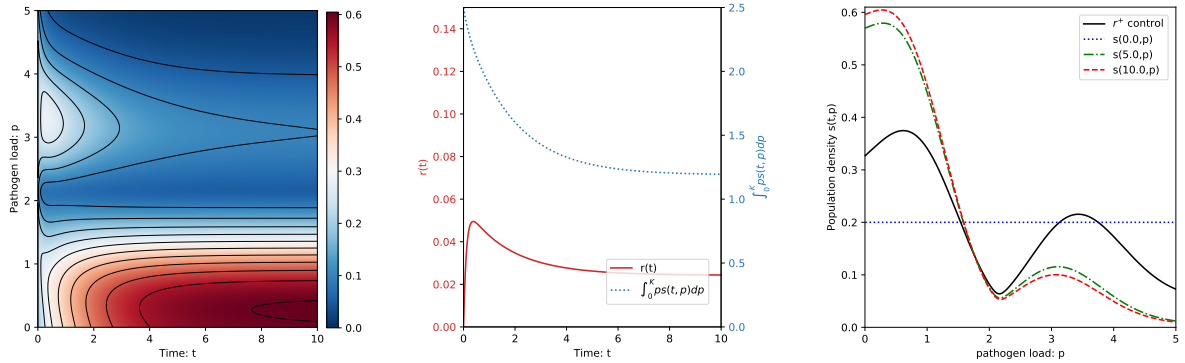

(a) Evolution of the population density s together with level sets

(b) Evolution of the reservoir variable r and total pathogen load within the population

(c) Population density s at different times

Figure 5.7 – **Reservoir, cleaning, drug, stationary treatment:** Evolution of the population density when contact with an environmental pathogen reservoir is added and when cleaning and drug treatment are applied (model (5.3.10)). Initial data are $s_{\mathrm{ini}}(p) = 0.2$ and $r_{\mathrm{ini}} = 0$. Cleaning and drug treatment are applied on $\mathbb{R}^+$. (A) Population density dynamics together with level sets. (B) Evolution of the environmental pathogen reservoir r (red line) and total pathogen load within the population $\int_0^K ps(t,p)dp$ (blue dotted line). (C) Population densities s at times $t = 0$ (blue dotted line), $t = 5$ (green dash dotted line) and $t = 10$ (red dashed line), compared with the stationary state of the model with reservoir but no cleaning and no drug treatment ($r + control$, black line).

5.3.4 Comparison of the various control strategies

According to the simulations presented in the previous subsections, the cleaning strategy does not allow to decrease efficiently the pathogen load. On the opposite, the drug treatment seems much more efficient and leads to a substantial reduction of the pathogen load in the population. Indeed, cleaning reduces the environmental pathogen load which decreases the

positive drift term $\beta_{\text{in}}(p)r$ in Eq. (5.3.10a): the impact of cleaning on the pathogen distribution is then driven by the excretion represented by the negative drift $\beta_{\text{ex}}(p)$ which is no longer balanced by the pathogen absorption. The same behavior occurs during drug treatment: the environmental pathogen load is decreased consecutively to the reduction of the high-shedding, and the negative drift β_{ex} also nearly fully applies. However, it is supplemented in that case by the treatment negative drift $T(t,p)$, inducing a stronger impact on the pathogen distribution. Depending on the parameters, the high shedder can be eliminated. However, these conclusions are highly dependent on the chosen parameter values and the modeling of the control strategies is highly simplified. Finally, the combination of cleaning and treatment seems to be, in any case, the most efficient strategy.

5.4 Generalization to a compartment model with transfers

In this section, we generalize the model (5.1.8) introduced in Sec. 5.1.4 by considering compartments. In particular, the compartments can represent different cages (or farms), between which there exist exchanges of animal or/and of the pathogens present in the environment, for example pathogens carried by farming tools.

Let us define $d \in \mathbb{N}^*$ as the number of compartments. From now on,

$$s(t,p) = \big(s_1(t,p), \quad s_2(t,p), \quad \dots, \quad s_d(t,p)\big) \in \mathbb{R}^d$$

will be a vector gathering the populations of the various compartments, structured by pathogen. Similarly, $r(t) = \big(r_1(t), \quad r_2(t), \quad \dots, \quad r_d(t)\big) \in \mathbb{R}^d$ is now the vector gathering the reservoir variables in all the compartments. Moreover, let A, respectively B, be the transfer matrix in $\mathscr{M}_d(\mathbb{R})$ representing the exchanges between compartments for the individuals, respectively for the salmonella pathogen reservoirs. Indeed, for $1 \leqslant i, j \leqslant d$ and $i \neq j$, the coefficient $\mathrm{A}_{i,j} \geqslant 0$ (resp. $\mathrm{B}_{i,j} \geqslant 0$) corresponds to the transfer rate from compartment j to compartment i. Because the total population of animals (resp. pathogens in the reservoir) has to be conserved by the transfers between compartments, the diagonal coefficient $\mathrm{A}_{i,i}$, which corresponds to the total amount leaving the compartment i, satisfies $\mathrm{A}_{i,i} = -\sum_{k\neq i} \mathrm{A}_{k,i}$ (resp. $\mathrm{B}_{i,i} = -\sum_{k\neq i} \mathrm{B}_{k,i}$). With these notations, the model writes as

$$\partial_t s(t,p) = -\partial_p\Big(\big(F(p) + \beta_{\text{in}}(p)r - \beta_{\text{ex}}(p)\big)s(t,p)\Big) + \frac{\sigma^2}{2}\partial^2_{pp} s(t,p) + \mathrm{A}s(t,p), \tag{5.4.11a}$$

$$\frac{d\,r(t)}{dt} = -\left(\gamma + \int_0^{\mathrm{K}} s(t,p)\beta_{\text{in}}(p)\,dp\right) r + \int_0^{\mathrm{K}} s(t,p)\beta_{\text{ex}}(p)\,dp + \mathrm{B}r(t), \tag{5.4.11b}$$

$$\frac{\sigma^2}{2}\partial_p s(t,\mathrm{K}) + \beta_{\text{ex}}(K)s(t,\mathrm{K}) = \frac{\sigma^2}{2}\partial_p s(t,0) - \beta_{\text{in}}(0)r(t)s(t,0) = 0, \tag{5.4.11c}$$

$$s(0,\cdot) = s_{\text{ini}}(\cdot) \in H^1(0,\mathrm{K}), \quad \int_0^{\mathrm{K}} s_{\text{ini}}(p)\,dp = N, \quad r(0) = r_{\text{ini}} \in \mathbb{R}^+. \tag{5.4.11d}$$

Let $N(t) = \displaystyle\int_0^{\mathrm{K}} s(t,p)\,dp$ be the vector of the total population in each compartment. By integrating (5.4.11a), one can deduce that N satisfies the ODE $N'(t) = \mathrm{A}N(t)$. Therefore,

using Eq.(5.4.11d), the population sizes in all compartments are explicitly given by $N(t) = \exp(t\mathrm{A})\,N$, where $N(0) = N = \int_0^{\mathrm{K}} s_{\mathrm{ini}}(p)\,dp$ is the vector of the initial total populations in the cages. We also remark that the overall total population remains constant since $\left(\sum_i N_i\right)' = \sum_i \left(AN\right)_i = \sum_j (\sum_i A_{i,j}) N_j = 0$.

5.4.1 Numerical simulations for multiple compartments (cages/farms)

In the following, we consider the case of 4 compartments and we perform some numerical simulations. We will first study the case of transfers of individuals without any transfer of reservoir pathogens, then the case of transfers of reservoir pathogens without any transfer of individuals.

Multiple compartments and transfers of individuals

Here, we investigate the case with no transfers for the reservoir pathogens r, that is to say $\mathrm{B} = 0$, and only transfers of individuals between the compartments. This situation may represent a farm where individuals of the same species will be exchanged between different cages or several farms with exchanges of individuals of the same species between them. Therefore, we make the assumption that the populations have the same characteristics in each compartment, i.e. F, β_{ex} and σ are identical. However, each compartment, cage or farm, may have its own properties and we use therefore different values for the intakes of pathogens from the reservoir β_{in} and for the reservoir decay rate γ according to the compartment. In addition, different initial distributions of the population in terms of pathogen load $s_{\mathrm{ini}}(p)$ and various initial conditions of reservoir pathogens r_{ini} are considered. The corresponding values are gathered in Table 5.3 and the transfers of individuals between compartments are given by the matrix

$$\mathrm{A} = \begin{pmatrix} -2.25 & 0.75 & 0.75 & 0.75 \\ 0.5 & -1.5 & 0.5 & 0.5. \\ 0.25 & 0.5 & -1.5 & 0.75 \\ 1.5 & 0.25 & 0.25 & -2 \end{pmatrix}. \tag{5.4.12}$$

Note that all the rows of A sum to 0 meaning that there is no loss or gain of individuals induced by transfers. Moreover, we choose s_{ini} such that $N = \begin{pmatrix} 1 & 1 & 1 & 1 \end{pmatrix}^T \in \mathrm{Ker}(\mathrm{A})$. Therefore, the repartition of livestock in each compartment remains constant over time. This particular choice has been made to be able to compare the results with the simulations without transfers.

The results of the simulation with these parameters are displayed in Figure 5.8. As it can be observed in Figures 5.8(a) and 5.8(b), the system seems to converge towards a stationary state. In Figure 5.8(b) the dashed curves represent the pathogen reservoirs in red and the pathogen population loads $\int_0^{\mathrm{K}} p s(t,p)\,dp$ in blue as a function of time when the transfers are neglected, whereas the plain curves correspond to the same quantities when the transfers are given by matrix A defined at Eq. (5.4.12). Similarly, in Fig. 5.8(c), the black curves correspond

Parameter	Compartment 1	Compartment 2	Compartment 3	Compartment 4
$s_{\text{ini}}(p)$	0.2	$\varphi_0(p)$	$\varphi_{0.5}(p)$	$\varphi_1(p)$
r_{ini}	0.1	0.125	0.15	0.175
β_{in}	1.6	1.3	1.0	0.7
γ	0.4	0.7	1.0	1.3
σ	2.45	1.4	1.75	2.1

Table 5.3 – Values of the intakes of pathogens from the reservoir β_{in}, reservoir decay rate γ, initial distributions of the population in terms of pathogen load $s_{\text{ini}}(p)$ and initial conditions of reservoir pathogens r_{ini} for the 4 different compartments, used in the simulation represented in Figure 5.8. The function $\varphi_\alpha(p)$ used to build the initial data is defined by $\varphi_\alpha(p) = \dfrac{e^{-(\alpha \mathrm{K}-p)^2/9}}{\int_0^{\mathrm{K}} e^{-(\alpha \mathrm{K}-p)^2/9} dp}$.

to the population distribution $s(t = 10, p)$ as a function of the pathogen load p at time $t = 10$ when the transfers are neglected; the solutions at different times when transfers are taken into account are displayed, namely $s(t = 0, p)$ in blue, $s(t = 5, p)$ in green, and $s(t = 10, p)$ in red. According to these simulations, the transfers of individuals modify the solution. For example, the pathogen reservoir and the total pathogen load for the population in the first compartment are lower than when transfers are accounted. On the opposite, in the second compartment, the pathogen reservoir and the total pathogen load for the population are higher when the transfers are activated. For the third compartment, the dynamics is almost unchanged. Finally, for the fourth compartment, the values at final time $t = 10$ for the pathogen reservoir and the total pathogen load of the population are similar but the transient dynamics is slowed down.

Multiple compartments and transfers between pathogen reservoirs

Now, we study the case with no transfers of individuals, that is to say $\mathrm{A} = 0$, and only transfers of reservoir pathogens between the compartments. Transfers of pathogen reservoirs between compartments correspond for example to transfers of pathogens induced by farming activities, for instance by using the same clothes or boots in different buildings on a farm. It can also represent the spread of the pathogen reservoir by environmental factors, e.g. wind, between farms or cages. In this case, all the parameters can be different from one compartment to another. However, in order to compare the effects of the transfers of the pathogen reservoirs with the transfers of individuals, the simulation presented in Figure 5.9 has been performed with the same parameters as in previous section, see Table 5.3. The transfers for

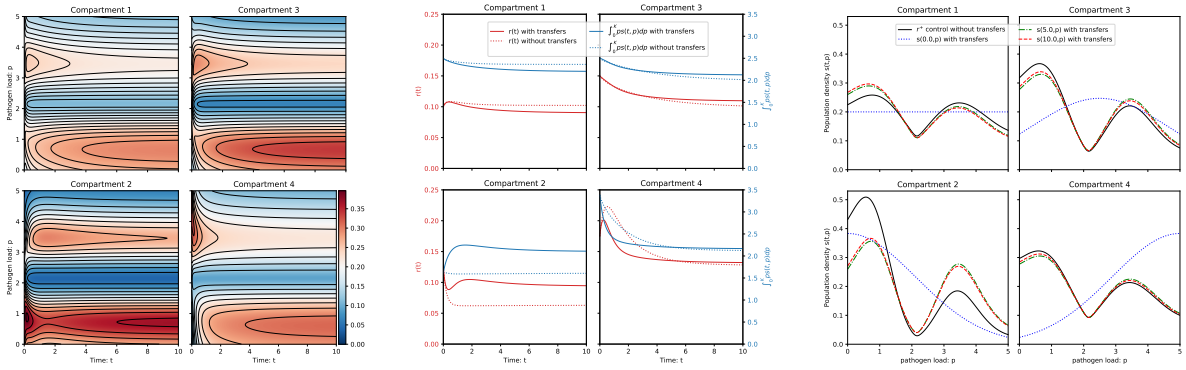

(a) Evolution of the population density s together with level sets in the 4 compartments.

(b) Evolution of the reservoir variable r and total pathogen load within the population in the 4 compartments.

(c) Population density s at different times in the 4 compartments.

Figure 5.8 – **4 compartments, animal transfer, no reservoir transfer:** Evolution of the population density in the 4 compartments when contact with an environmental pathogen reservoir is considered (model (5.4.11)). In the different compartment, no particular treatment is applied. Transfer of individuals between compartments is given by the matrix A in Eq. (5.4.12), but no transfer between compartment reservoir variables is added (B = 0). Initial data are different in each compartment (see parameter in Table 5.3)(A) Population density dynamics together with level sets. (B) Evolution of the environmental pathogen reservoir r (red line) and total pathogen load within the population $\int_0^K ps(t,p)dp$ (blue line), compared with a simulation with no inter-compartment transfer at all (A = 0, B = 0), in dotted lines. (C) Population densities s at times $t = 0$ (blue dotted line), $t = 5$ (green dash dotted line) and $t = 10$ (red dashed line). The solution is compared with the solutions $r^+control$ of system (5.1.8) at $t = 10$ computed with the parameters of Table 5.3. We note that consequently, $r^+control$ is different in each compartment and that this simulation represents a situation with no inter-compartment transfer (A = 0, B = 0).

the pathogen reservoirs are given by the matrix

$$\mathrm{B} = \begin{pmatrix} -6 & 0.25 & 0.5 & 0.25 \\ 2 & -1 & 2.5 & 0.5 \\ 1 & 0.25 & -6 & 0.25 \\ 3 & 0.5 & 3 & -1 \end{pmatrix}. \tag{5.4.13}$$

According to Figures 5.9(a) and 5.9(b), the solution seems to converge in time towards a stationary state. The main effect of transfers of the pathogen reservoirs between compartments can be observed in Figure 5.9(b), which compares the pathogen reservoir size and the total pathogen load in the population over time, in plain curves, with the same simulation without transfers, in dashed curves. With transfer matrix B given at Equation (5.4.13), we can notice the effects of the pathogen transfers, for example in compartment 4 or for the time

range [0,2] in compartment 1. However, within the range of parameters used in this analysis, the effect of pathogen reservoir transfers is very weak on the population. Indeed, we can remark that the total pathogen load – see Figure 5.9(b) – and the stationary states of the pathogen load distribution – see Figure 5.9(c) – with and without transfers for the reservoir pathogens are almost identical.

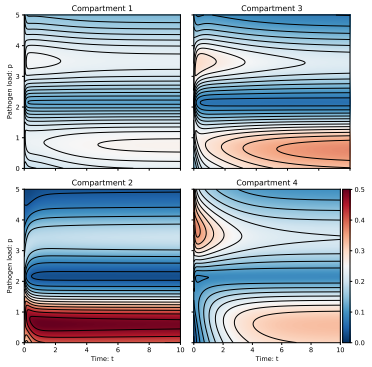

(a) Evolution of the population density s together with level sets in the 4 compartments.

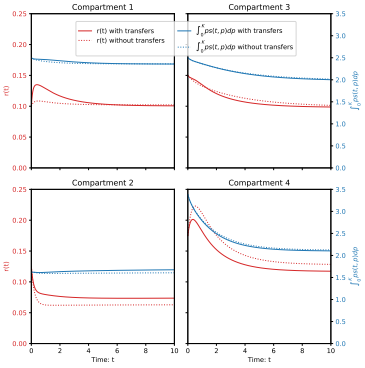

(b) Evolution of the reservoir variable r and total pathogen load within the population in the 4 compartments.

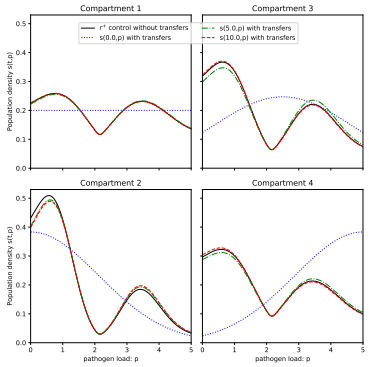

(c) Population density s at different times in the 4 compartments.

Figure 5.9 – **4 compartments, no animal transfer, reservoir transfer:** Evolution of the population density in the 4 compartments when contact with an environmental pathogen reservoir is considered (model (5.4.11)). In the different compartments, no particular treatment is applied. Transfer of individuals between compartments is discarded (A = 0) but transfer between compartment reservoir variables is added (B given by Eq. (5.4.13)). Initial data are different in each compartment (see parameter in Table 5.3) (A) Population density dynamics together with level sets. (B) Evolution of the environmental pathogen reservoir r (red line) and total pathogen load within the population $\int_0^K ps(t,p)dp$ (blue line), compared with a simulation with no inter-compartment transfer at all (A = 0, B = 0), in dotted lines. (C) Population densities s at times $t = 0$ (blue dotted line), $t = 5$ (green dash dotted line) and $t = 10$ (red dashed line). The solution is compared with the solutions $r^+control$ of system (5.1.8) at $t = 10$ computed with the parameters of Table 5.3. We note that consequently, $r^+control$ is different in each compartment and that this simulation represents a situation with no inter-compartment transfer (A = 0, B = 0).

Multiple compartments and spreading of pathogen load

Finally, we study a case with transfers of individuals and reservoir pathogens and we aim at exploring the spreading and contamination of pathogens from the first compartment to the

three other compartments. Initial data are therefore given by:

$$s_{ini,1}(p) = 0.2, \qquad s_{ini,k}(p) = \frac{\mathbb{1}_{p<0.25}}{\int_0^K \mathbb{1}_{p<0.25}(p)dp}, \quad k \in \{2,3,4\} \tag{5.4.14}$$

and we use the same parameters for all the compartments, that can be found in Table 5.2. The transfer matrices A and B are given by:

$$\mathrm{A} = \begin{pmatrix} -1 & 1 & 0 & 0 \\ 1 & -2 & 1 & 0 \\ 0 & 1 & -2 & 1 \\ 0 & 0 & 1 & -1 \end{pmatrix} \text{ and } \mathrm{B} = \begin{pmatrix} -1 & 1 & 0 & 0 \\ 1 & -2 & 1 & 0 \\ 0 & 1 & -2 & 1 \\ 0 & 0 & 1 & -1 \end{pmatrix}. \tag{5.4.15}$$

such that the first compartment contaminates the second, the second contaminates the third and the third contaminates the fourth.

The results are displayed in Fig. 5.10. As expected, the population densities converge to the same stationary state in the four compartments. With this parameter set, the propagation phenomenon is fast in comparison with the convergence time to stationary state in each compartment. We can observe, in particular in subfigure 5.10(b), that the pathogens reach the next compartment with a time delay, which propagates from one compartment to the other.

5.4.2 Towards a continuous model in space

By considering a large number of compartments and appropriate transfers between them, our model can be seen as a rough approximation of a continuous model in space. For example, the situation where the exchanges between compartments are induced by a diffusion process can be approximated by considering laplacian matrices with periodic boundary conditions for A and B, but with two different diffusion coefficients, namely

$$\mathrm{A} = 3\begin{pmatrix} -2 & 1 & 0 & 1 \\ 1 & -2 & 1 & 0 \\ 0 & 1 & -2 & 1 \\ 1 & 0 & 1 & -2 \end{pmatrix} \text{ and } \mathrm{B} = \begin{pmatrix} -2 & 1 & 0 & 1 \\ 1 & -2 & 1 & 0 \\ 0 & 1 & -2 & 1 \\ 1 & 0 & 1 & -2 \end{pmatrix}. \tag{5.4.16}$$

The parameter values and initial data remain the same as in the two previous subsections and are summarized in Table 5.3. Here again, we can see at Figure 5.11 that the solution seems to converge towards a stationary state. Due to the use of diffusion-like transfers, we can observe in Figure 5.11 that the repartitions of individuals in terms of pathogen loads tend to homogenize. The same kind of homogeneisation can be observed for the reservoir pathogen, its asymptotic values being close in each compartment.

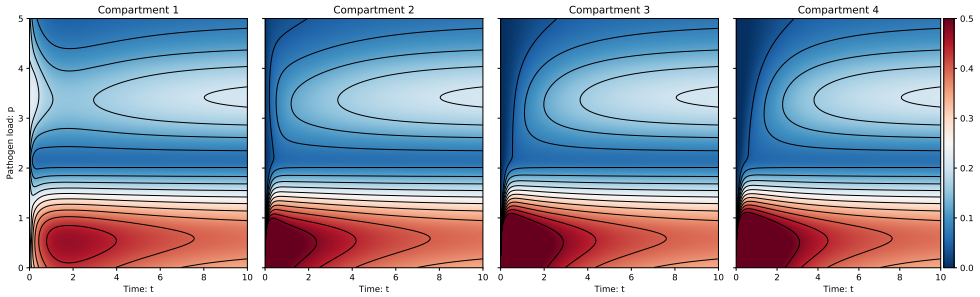

(a) Evolution of the population density s together with level sets in the 4 compartments.

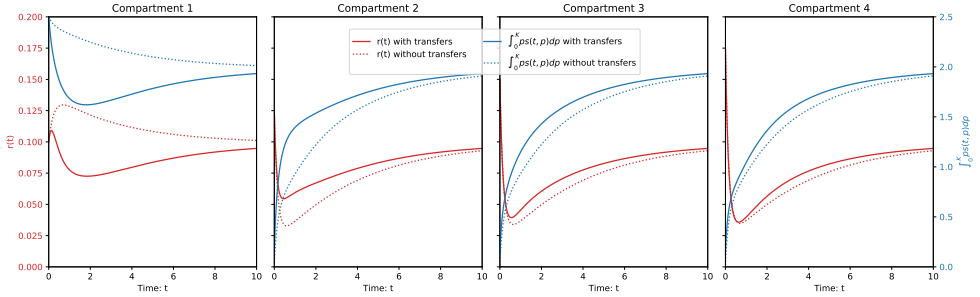

(b) Evolution of the reservoir variable r and total pathogen load within the population in the 4 compartments.

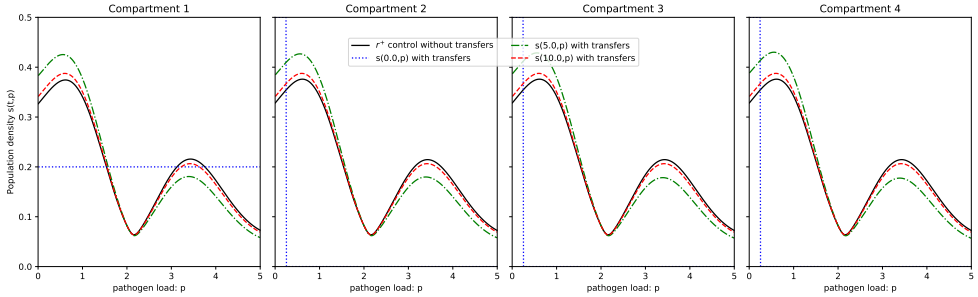

(c) Population density s at different times in the 4 compartments.

Figure 5.10 – **4 compartments, animal and reservoir transfers, initial pathogen load in the first compartment:** Evolution of the population density in the 4 compartments when contact with an environmental pathogen reservoir is considered (model (5.4.11)). In the different compartments, no particular treatment is applied. Transfer of individuals and reservoir variables between compartments are considered (A and B given by Eq.(5.4.15)). Initial data are given at Eq. (5.4.14) and the pathogen load is initially concentrated in the first compartment; the other parameters are independent of the compartments and can be found in Table 5.2. (A) Population density dynamics together with level sets. (B) Evolution of the environmental pathogen reservoir r (red line) and total pathogen load within the population $\int_0^K ps(t,p)dp$ (blue line), compared with a simulation with no inter-compartment transfer at all (A = 0, B = 0), in dotted lines. (C) Population densities s at times $t = 0$ (blue dotted line), $t = 5$ (green dash dotted line) and $t = 10$ (red dashed line). The solution is compared with the solutions $r^+control$ of system (5.1.8) at $t = 10$ computed with the parameters of Table 5.2 and no inter-compartment transfer (A = 0, B = 0).

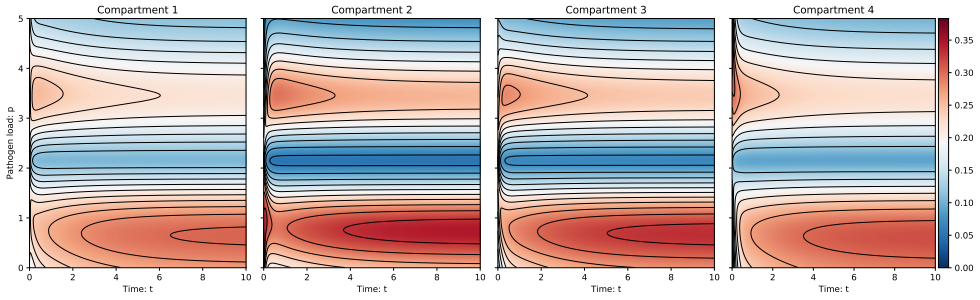

(a) Evolution of the population density s together with level sets in the 4 compartments.

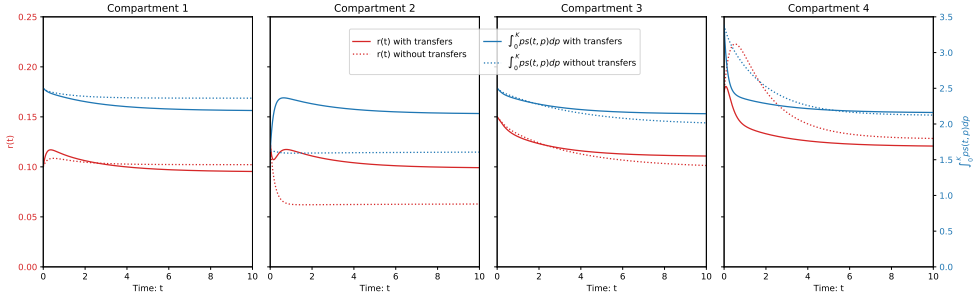

(b) Evolution of the reservoir variable r and total pathogen load within the population in the 4 compartments.

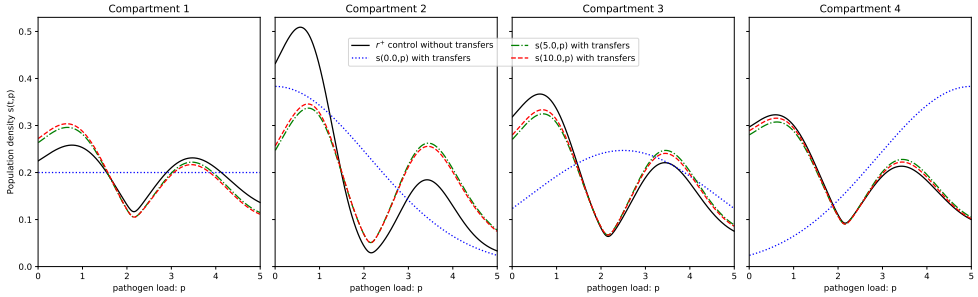

(c) Population density s at different times in the 4 compartments.

Figure 5.11 – **4 compartments, diffusive-like transfers:** Evolution of the population density in the 4 compartments when contact with an environmental pathogen reservoir is considered (model (5.4.11)). In the different compartments, no particular treatment is applied. Diffusive-like transfer of individuals and pathogen reservoir variables is added (A and B given by Eq. (5.4.16)). Initial data are different in each compartment (see parameter in Table 5.3)(A) Population density dynamics together with level sets. (B) Evolution of the environmental pathogen reservoir r (red line) and total pathogen load within the population $\int_0^K ps(t,p)dp$ (blue line), compared with a simulation with no inter-compartment transfer at all (A = 0, B = 0), in dotted lines. (C) Population densities s at times $t = 0$ (blue dotted line), $t = 5$ (green dash dotted line) and $t = 10$ (red dashed line). The solution is compared with the solutions $r^+control$ of system (5.1.8) at $t = 10$ computed with the parameters of Table 5.3. We note that consequently, $r^+control$ is different in each compartment and that this simulation represents a situation with no inter-compartment transfer (A = 0, B = 0).

List of Tables

List of Figures

Bibliography

[1] H. P. Andreassen, P. Glorvigen, A. Rémy, and R. A. Ims. New views on how population-intrinsic and community-extrinsic processes interact during the vole population cycles. *Oikos*, 122(4):507–515, 2013.

[2] C. Bardos, A. Y. le Roux, and J.-C. Nédélec. First order quasilinear equations with boundary conditions. *Comm. Partial Differential Equations*, 4(9):1017–1034, 1979.

[3] Virgile Baudrot, Antoine Perasso, Clémentine Fritsch, and Francis Raoul. Competence of hosts and complex foraging behavior are two cornerstones in the dynamics of trophically transmitted parasites. *Journal of Theoretical Biology*, 397:158–168, 2016.

[4] Karine Berthier, Sylvain Piry, Jean-François Cosson, Patrick Giraudoux, Jean-Christophe Foltête, Régis Defaut, Denis Truchetet, and Xavier Lambin. Dispersal, landscape and travelling waves in cyclic vole populations. *Ecology letters*, 17, 11 2013.

[5] F. Bolley, I. Gentil, and A. Guillin. Convergence to equilibrium in wasserstein distance for fokker–planck equations. *Journal of Functional Analysis*, 263(8):2430–2457, 2012.

[6] D. Cerqueira, B. De Sousa, C. Gabrion, P. Giraudoux, J.P. Quéré, and P. Delattre. Cyclic changes in the population structure and reproductive pattern of the water vole, arvicola terrestris linnaeus, 1758. *Mammalian Biology*, 71(4):193 – 202, 2006.

[7] G. M. Coclite and M. M. Coclite. Conservation laws with singular nonlocal sources. *J. Differential Equations*, 250(10):3831–3858, 2011.

[8] G. M. Coclite and L. di Ruvo. Well-posedness of the Ostrovsky-Hunter equation under the combined effects of dissipation and short-wave dispersion. *J. Evol. Equ.*, 16(2):365–389, 2016.

[9] G. M. Coclite, C. Donadello, and T. N. T. Nguyen. A PDE model for the spatial dynamics of a voles population structured in age. *Nonlinear Anal.*, 196:111805, 26, 2020.

[10] G. M. Coclite, H. Holden, and K. H. Karlsen. Wellposedness for a parabolic-elliptic system. *Discrete Contin. Dyn. Syst.*, 13(3):659–682, 2005.

[11] Giuseppe M. Coclite, Carlotta Donadello, and T. N. T. Nguyen. An hyperbolic-parabolic predator-prey model involving a vole population structured in age. 2020.

[12] G.M. Coclite and M. Garavello. Vanishing viscosity for mixed systems with moving boundaries. *Journal of Functional Analysis*, 264(7):1664 – 1710, 2013.

[13] R. M. Colombo and E Rossi. Hyperbolic predators vs. parabolic prey. *Communications in Mathematical Sciences*, 13(2):369 – 400, 2015.

[14] Rinaldo M. Colombo and Mauro Garavello. Stability and optimization in structured population models on graphs. *Mathematical Biosciences & Engineering*, 12:311–335, 2015.

[15] C. Delattre, D. Dochain, and J. Winkin. Sturm-liouville systems are riesz-spectral systems. *International Journal of Applied Mathematics and Computer Science*, 13(4):481–484, 2003.

[16] P. Delattre, B. De Sousa, and et *al* E. Fichet-Calvet. Vole outbreaks in a landscape context: evidence from a six year study of microtus arvalis. *Landscape Ecology*, 14:401–412, 1999.

[17] Pierre Delattre and Patrick Giraudoux. *Le campagnol terrestre: prévention et contrôle des populations*. QUAE, 2009.

[18] R.J. DiPerna. Convergence of approximate solutions to conservation laws. *Archive for Rational Mechanics and Analysis*, 82:27–70, 1983.

[19] Carlotta Donadello, Thi Nhu Thao Nguyen, and Ulrich Razafison. On the mathematical modeling of vole populations spatial dynamics via transport equations on a graph. working paper or preprint, July 2020.

[20] L. C. Evans. *Partial differential equations*, volume 19 of *Graduate Studies in Mathematics*. American Mathematical Society, Providence, RI, 1998.

[21] P. Giraudoux, P. Delattre, M. Habert, J. Quéré, S. Deblay, R. Duhamel R. Defaut, M. Moissenet, D. Salvi, and D. Truchetet. Population dynamics of fosserial water vole (arvicola terrestris scherman) : a land use and a landscape perspective. *Agriculture, Ecosystems and Environment*, 66(1):47–60, 1997.

[22] P. Giraudoux, P. Villette, J. Quéré, and et *al*. Weather influences m. arvalis reproduction but not population dynamics in a 17-year time series. *Sci Rep*, 9:13942, 2019.

[23] G. Halliez, F. Renault, E. Vannard, G. Farny, S. Lavorel, and P. Giraudoux. Historical agricultural changes and the expansion of a water vole population in an alpine valley. *Agriculture, Ecosystems and Environment*, 121:198–206, 2015.

[24] R. Ims and H. Andreassen. Spatial synchronization of vole population dynamics by predators birds. *Nature*, 408:194–196, 2000.

[25] D. M. Johnson, U. Büntgen, D. C. Frank, K. Kausrud, K. J. Haynes, A. M. Liebhold, J. Esper, and N. Chr. Stenseth. Climatic warming disrupts recurrent alpine insect outbreaks. *Proc. Natl. Acad. Sci.*, 107(47):20576–20581, 2010.

[26] C. Krebs. *Population fluctuations in rodents*. The University of Chicago Press, Chicago and London, 2013.

[27] Simon Labarthe, Béatrice Laroche, Thi Nhu Thao Nguyen, Bastien Polizzi, Florian Patout, and et al. A multi-scale epidemic model of salmonella infection with heterogeneous shedding. *ESAIM: Proceedings and Surveys, EDP Sciences*, 67:261–284, 2020.

[28] R. J. LeVeque. *Finite volume methods for hyperbolic problems*. Cambridge Texts in Applied Mathematics. Cambridge University Press, Cambridge, 2002.

[29] Nicolas Marilleau, Christophe Lang, and Patrick Giraudoux. Coupling agent-based with equation-based models to study spatially explicit megapopulation dynamics. *Ecological Modelling*, 384:34–42, 09 2018.

[30] S. MISCHLER. *Chapitre 1 - Inégalités de Poincaré et de Log-Sobolev*. Comportement remarquable d'EDP d'évolution issues de la biologie, 2013.

[31] F. Murat. L'injection du cône positif de H^{-1} dans $W^{-1,q}$ est compacte pour tout $q < 2$. *J. Math. Pures Appl. (9)*, 60(3):309–322, 1981.

[32] James D. Murray. *Mathematical Biology I. An Introduction*, volume 17 of *Interdisciplinary Applied Mathematics*. Springer, New York, 3 edition, 2002.

[33] J.D. Murray. *Mathematical Biology I, An introduction*. Interdisciplinary applied mathematics. Springer, third edition edition, 2004.

[34] B. Oksendal. *Stochastic differential equations*. Springer, 2003.

[35] E. Yu. Panov. Existence and strong pre-compactness properties for entropy solutions of a first-order quasilinear equation with discontinuous flux. *Archive for Rational Mechanics and Analysis*, 195(2):643–673, 2009.

[36] E. Yu. Panov. Erratum to: Existence and strong pre-compactness properties for entropy solutions of a first-order quasilinear equation with discontinuous flux. *Archive for Rational Mechanics and Analysis*, 196(3):1077–1078, 2010.

[37] M. Pascal and T. Boujard. Essai de typologie de paramètres démographiques et morphologiques de la fraction colonisatrice d'une population de campagnols terrestres (*Arvicola terrestris scherman*). *Terre et Vie*, 42:357–376, 1987.

[38] B. Perthame. *Transport equations in biology*. Birkhäuser, 2007.

[39] A. Pilipenko. *An introduction to stochastic differential equations with reflection (Vol. 1)*. Universitätsverlag Potsdam, 2014.

[40] J. Quéré and H. Le Louarn. *Les rongeurs de France*. Editions QUAE, Versailles, 2011.

[41] Francis Saucy and Schneiter Beat. Juvenile dispersal in the vole arvicola terrestris during rainy nights: A preliminary report. *Bulletin de la Societe Vaudoise des Sciences Naturelles*, 84:333–345, 12 1997.

[42] T. N. Sherratt, X. Lambin, S. J. Petty, J. L. Mackinnon, C.F. Coles, and C. J. Thomas. Use of coupled oscillator models to understand synchrony and travelling waves in populations of the field vole microtus agrestis in northern england. *J. Appl. Ecol.*, 37(s1):148–158, 2000.

[43] Eitan Tadmor, Michel Rascle, and Patrizia Bagnerini. Compensated compactness for 2d conservation laws. *Journal of Hyperbolic Differential Equations*, 2(3):697–712, 2005.

[44] L.C. Tartar. *Compensated compactness and applications to partial differential equations*. Nonlinear Analysis and Mechanics: Heriot-Watt Symposium, 1979.

[45] H. R. Thieme. *Mathematics in Population Biology*. Princeton Series in Theoretical and Computational Biology. Princeton, 2003.

[46] G. F. Webb. Population models structured by age, size, and spatial position. In *Structured population models in biology and epidemiology*, volume 1936 of *Lecture Notes in Math.*, pages 1–49. Springer, Berlin, 2008.

[47] G.F. Webb. Dynamics of populations structured by internal variables. *Math. Z.*, 189(3):319–335, 1985.

Résumé: L'objectif principal de la thèse est de proposer et d'analyser des modèles mathématiques basés sur des équations aux dérivées partielles (EDP) afin de décrire la dynamique spatiale de deux espèces de campagnols (Microtus arvalis et Arvicola terrestris), qui sont particulièrement surveillés dans l'est de la France. Les modèles que nous avons proposés reposent sur des EDP qui décrivent l'évolution de la densité de la population de campagnols en fonction du temps, de l'âge et de la position dans l'espace. Nous avons suivi deux approches complémentaires pour représenter la dynamique. Dans la première approche, nous avons proposé un premier modèle qui consiste en une EDP scalaire en structurée en temps, en âge, et en espace. Elle est complétée par une condition au bord non locale. Le flux est linéaire à coefficient constant dans la direction de l'âge mais contient un terme non local dans les directions de l'espace. De plus, l'équation contient un terme de second ordre par rapport aux variables spatiales. Nous avons démontré l'existence et la stabilité de solutions faibles entropiques pour le modèle en utilisant, la compacité par compensation établie par Panov et un argument du type doublement de variables. Dans la deuxième approche, nous nous sommes inspirés du modèle Multi Agents introduit par Marilleau-Lang-Giraudoux, où la dynamique spatiale des juvéniles est découplée de l'évolution locale dans chaque parcelle. Pour mettre en place ce deuxième modèle, nous avons introduit un graphe orienté dont les nœuds sont les parcelles (ou colonies). Dans chaque nœud, l'évolution de la colonie est décrite par une équation de transport structurée en temps et en âge, et les mouvements de dispersion dans l'espace sont représentés par les passages d'un nœud à un autre. Nous avons proposé une discrétisation du modèle, par des schéma volumes finis, et, grâce à des simulations numériques, nous avons pu illustrer le fait que le modèle est capable de reproduire certaines caractéristiques qualitatives de la dynamique spatiale observée dans la nature. Nous avons ensuite proposé un troisième modèle qui est un système proie-prédateur constitué d'une équation hyperbolique pour les prédateurs et d'une équation parabolique-hyperbolique pour les proies analogue à celle proposée dans le premier modèle. Le terme de force dans l'équation des prédateurs dépend de manière non localement de la densité des proies et les deux équations sont également couplées via des termes sources classiques de type Lotka-Volterra. Nous avons établi l'existence de solutions en appliquant la méthode de la viscosité évanescente, et nous avons établi un résultat de stabilité par un argument de type doublement de variables. Enfin nous avons proposé et validé un schéma de type volumes finis pour le premier modèle.

La dernière partie de mes travaux de recherche est dédiée à un projet auquel j'ai participé lors d'une école d'été CEMRACS. Il concerne un sujet de biomathématiques différent du thème principal de la thèse et porte sur un modèle épidémiologique pour la salmonellose. Nous avons proposé un nouveau cadre de modélisation générique multi-échelles de la transmission hétérogène d'agents pathogènes dans une population animale. Au niveau intra-hôte, le modèle décrit l'interaction entre le microbiote commensal, le pathogène et la réponse inflammatoire. Des fluctuations aléatoires de la dynamique écologique du microbiote individuel et de la transmission à l'échelle inter-hôte sont ajoutées pour obtenir un modèle EDP de la distribution des agents pathogènes au niveau de la population. Une extension du modèle a, par ailleurs, été développé pour représenter la transmission entre plusieurs populations. Le comportement asymptotique ainsi que l'impact des stratégies de contrôle, y compris le nettoyage et l'administration d'antimicrobiens, sont étudiés par des simulations numériques.
Mots-clés: Méthode des volumes finis, Équation parabolique – hyperbolique, Compacité par compensation, Problème aux limites non locales, Systèmes proie-prédateur, Équations de transport.

Abstract: The main objective of the thesis is to propose and analyze mathematical models based on partial differential equations (PDE) to describe the spatial dynamics of two species of voles (Microtus arvalis and Arvicola terrestris), which are particularly monitored in Eastern France. The models that we have proposed are based on PDE which describe the evolution of the density of the population of voles as a function of time, age and position in space. We have two complementary approaches to represent the dynamics. In the first approach, we propose a first model that consists of a scalar PDE depending on time, age, and space supplemented with a non-local boundary condition. The flux is linear with constant coefficient in the direction of age but contains a non-local term in the directions of space. Moreover, the equation contains a second order term in the spatial variables only. We have demonstrated the existence and stability of weak entropy solutions for the model by using, respectively, the Panov's theorem of the multidimensional compensated and a doubling of the variables type argument. In the second approach we were inspired by a Multi Agent model proposed by Marilleau-Lang-Giraudoux, where the spatial dynamics of juveniles is decoupled from local evolution in each plot. To apply this model, we have introduced a directed graph whose nodes are the plots. In each node, the evolution of the colony is described by a transport equation with two variables, time and age, and the movements of dispersion, in space, are represented by the passages from one node to the other. We have proposed a discretization of the model, by finite volume methods, and noticed that this approach manages to reproduce the qualitative characteristics of the spatial dynamics observed in nature. We also proposed to consider a predator-prey system consisting of a hyperbolic equation for predators and a parabolic-hyperbolic equation for preys, where the prey's equation is analogous to the first model of the vole populations. The drift term in the predators' equation depends nonlocally on the density of prey and the two equations are also coupled via classical source terms of Lotka-Volterra type. We establish existence of solutions by applying the vanishing viscosity method, and we prove stability by a doubling of variables type argument. Moreover, concerning the numerical simulation of the first model in one-dimensional space, we obtain a finite volume discretization by using the upwind scheme and then validate the numerical scheme.

The last part of my thesis work is a project in which I participated during a Summer school CEMRACS. The project was on a subject of biomathematics different from that of the thesis (an epidemiological model for salmonellosis). A new generic multi-scale modeling framework for heterogeneous transmission of pathogens in an animal population is suggested. At the intra-host level, the model describes the interaction between the commensal microbiota, the pathogen and the inflammatory response. Random fluctuations in the ecological dynamics of the individual microbiota and transmission at the inter-host scale are added to obtain a PDE model of drift-diffusion of pathogen distribution at the population level. The model is also extended to represent transmission between several populations. Asymptotic behavior as well as the impact of control strategies, including cleaning and administration of antimicrobials, are studied by numerical simulation.
Keywords: Finite volumes method, Parabolic–hyperbolic equation, Compensated compactness, Nonlocal Boundary value problem, Prey-predator systems, Transport equations.

2010 Mathematics subject classification: 35Q92, 92B05, 92D30, 65M08, 34B10.